

AD 727 023

AMRL-TR-71-12



**CREW COMPARTMENT VIBRATION ENVIRONMENT IN
THE B-52 AIRCRAFT DURING
LOW-ALTITUDE, HIGH-SPEED FLIGHT**

JERRY D. SPEAKMAN

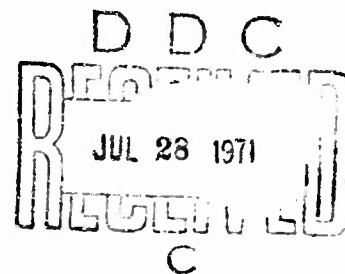
JUSTIS F. ROSE, JR., LT COL, USAF

MARCH 1971

This document has been approved for public
release and sale; its distribution is unlimited.

Reproduced by
NATIONAL TECHNICAL
INFORMATION SERVICE
Springfield, VA 2215

AEROSPACE MEDICAL RESEARCH LABORATORY
AEROSPACE MEDICAL DIVISION
AIR FORCE SYSTEMS COMMAND
WRIGHT-PATTERSON AIR FORCE BASE, OHIO



NOTICES

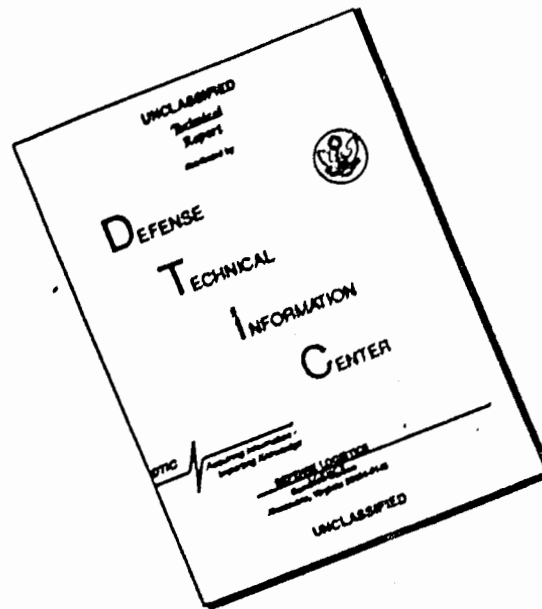
When US Government drawings, specifications, or other data are used for any purpose other than a definitely related Government procurement operation, the Government thereby incurs no responsibility nor any obligation whatsoever, and the fact that the Government may have formulated, furnished, or in any way supplied the said drawings, specifications, or other data, is not to be regarded by implication or otherwise, as in any manner licensing the holder or any other person or corporation, or conveying any rights or permission to manufacture, use, or sell any patented invention that may in any way be related thereto.

ADDRESSOR NO.		
OFFER	WRITE SECTION <input checked="" type="checkbox"/>	
RDS	COPY SECTION <input type="checkbox"/>	
TRANSMISSIONS	<input type="checkbox"/>	
JUSTIFICATION		
BY		
DISTRIBUTION/AVAILABILITY CODES		
DIST.	AVAIL. NO./BY	SPECIAL
A		

Organizations and individuals receiving announcements or reports via the Aerospace Medical Research Laboratory automatic mailing lists should submit the addressograph plate stamp on the report envelope or refer to the code number when corresponding about change of address or cancellation.

Do not return this copy. Retain or destroy.

DISCLAIMER NOTICE



THIS DOCUMENT IS BEST QUALITY AVAILABLE. THE COPY FURNISHED TO DTIC CONTAINED A SIGNIFICANT NUMBER OF PAGES WHICH DO NOT REPRODUCE LEGIBLY.

Security Classification

DOCUMENT CONTROL DATA - R & D

(Security classification of title, body of abstract and indexing annotation must be entered when the overall report is classified)

1. ORIGINATING ACTIVITY (Corporate author) Aerospace Medical Research Laboratory, Aerospace Medical Division, Air Force Systems Command, Wright-Patterson Air Force Base, Ohio 45433		2a. REPORT SECURITY CLASSIFICATION UNCLASSIFIED
		2b. GROUP N/A
3. REPORT TITLE CREW COMPARTMENT VIBRATION ENVIRONMENT IN THE B-52 AIRCRAFT DURING LOW-ALTITUDE, HIGH-SPEED FLIGHT		
4. DESCRIPTIVE NOTES (Type of report and inclusive dates) Final Report, August 66-December 1970		
5. AUTHOR(S) (First name, middle initial, last name) Jerry D. Speakman Justus F. Rose, Jr., Lt Col, USAF		
6. REPORT DATE March 1971	7a. TOTAL NO. OF PAGES 197	7b. NO. OF REFS 4
8a. CONTRACT OR GRANT NO.	8b. ORIGINATOR'S REPORT NUMBER(S) AMRL-TR-71-12	
b. PROJECT NO. 7231		
c. Task 723104		
d. Work Unit 723104020	8b. OTHER REPORT NO(S) (Any other numbers that may be assigned this report)	
10. DISTRIBUTION STATEMENT This document has been approved for public release and sale; its distribution is unlimited.		
11. SUPPLEMENTARY NOTES	12. SPONSORING MILITARY ACTIVITY Aerospace Medical Research Laboratory, Aerospace Medical Div., Air Force Systems Command, Wright-Patterson AFB, OH 45433	
13. ABSTRACT Measurements were made of the pilot station vibration environment experienced in the B-52 aircraft during low-altitude, high-speed flight. Data were obtained of the longitudinal, lateral and vertical linear accelerations and the roll axis angular velocities and accelerations. The terrain contour following flights at 500-900 feet above the flat to semi-mountainous regions of Louisiana and Arkansas were made at 350 knots true airspeed. Data analyses included probability density and distribution and the auto-power spectral density functions in addition to tests for stationarity, randomness and normality. The individual degree-of-freedom results are presented in graphical and tabular form and in general indicate that the pilot station vibration environment produced by the combination of gust response and maneuvering: (1) is stationary for up to 590 seconds; (2) is a random phenomena that does not satisfy the chi-square goodness-of-fit test for Gaussian distribution; (3) cannot be adequately simulated in the laboratory for human biomedical tolerance and/or psycho-physiological performance studies using only vertical axis motion; (4) is remarkably in agreement with those PSD's calculated for the lateral and vertical axes using an aircraft transfer function experimentally derived on another program and the Dryden gust input spectrum.		

DD FORM 1473
1 NOV 65

Security Classification

Security Classification

14. KEY WORDS	LINK A		LINK B		LINK C	
	ROLE	WT	ROLE	WT	ROLE	WT
Vibration Acceleration Angular Acceleration Random data analysis						

Security Classification

SUMMARY

PROBLEM

Terrain contour flying at low-altitude, high-speed as a radar defense penetration aid increases the vibration environment experienced in an aircraft. This additional stress can seriously compromise the ability of the crew members to satisfactorily perform their assigned duties. Before human biomedical tolerance and/or psycho-physiological performance criteria can be established by using laboratory simulation devices, it is necessary to first define the vibration environment typical of these military type flight operations. Since aircraft design characteristics primarily determine the frequency variations in the vibration environment experienced by the crew, the aircraft commonly used in Air Force operations have been categorized into the three major divisions of: (1) small, rigid fighters; (2) large, flexible bombers, (3) large, rigid bombers. This endeavor concludes the study undertaken to define the crew compartment vibration environment during low-altitude, high-speed flight in a present day, large, flexible bomber.

APPROACH

Appropriate instruments were installed in the pilot station of B-52E model aircraft to measure and record the vibration environment during six low-altitude, high-speed flights over flat to semi-mountainous terrain. Measurements were made of the linear accelerations in the longitudinal, lateral, and vertical axes and the roll axis angular velocities and accelerations. The acceleration time histories were analyzed to ascertain their amplitude probability and spectral (frequency) properties.

RESULTS

When analyzing random vibration data, it is common practice to assume the data is statistically stationary and exhibits a Gaussian or normal amplitude probability distribution. These data were stationary in all degrees-of-freedom for periods of 120-590 seconds, but did not meet the chi-square goodness-of-fit test for normality. Over the frequency range (0.4 - 20 Hz) that the human body reacts most unfavorably, power spectral density analyses revealed that all axes contribute significantly to the overall linear and angular acceleration environment present in the B-52 aircraft during low-altitude, high-speed flight.

CONCLUSIONS

Obtained accelerations induced by maneuvers greatly increase the overall intensity of the vibration environment and are probably why the time histories do not exhibit truly random amplitude probability density functions. The laboratory simulation of the LANS vibration environment for biomedical tolerance and/or psycho-physiological performance studies cannot be limited to only one degree-of-freedom.

FOREWORD

The measurement program and analyses reported herein were performed by the Biodynamics and Bionics Division, Aerospace Medical Research Laboratory, Wright-Patterson Air Force Base, Ohio. This program was initiated in 1966 to define the crew compartment vibration environment in a flexible-winged bomber-type aircraft during low-altitude, high-speed (LAHS) flight. Lt Col J. F. Rose, Jr., was responsible for program initiation, scheduling and data acquisition. Mr. J. D. Speakman was responsible for program technical direction, data analyses and report preparation. This work was accomplished under Project 7231, "Biomechanics of Aerospace Operations," and Task 723104, "Biodynamic Environment of Aerospace Flight Operations." Acknowledgement is made of the assistance of Mr. L. K. Kettler, University of Dayton Research Institute, who provided technical support for the instrumentation system during data acquisition. Research covered herein was accomplished from August 1966 to December 1970.

This technical report has been reviewed and is approved.

CLINTON L. HOLT, Colonel, USAF, MC
Commander
Aerospace Medical Research Laboratory

TABLE OF CONTENTS

<u>SECTION</u>	<u>PAGE</u>
I. INTRODUCTION	1
II. MEASUREMENT PROGRAM	2
A. INSTRUMENTATION	2
B. ROUTE DESCRIPTION	3
C. TEST FLIGHT IDENTIFICATION	3
III. DATA ANALYSES	8
A. PROBABILITY DENSITY AND DISTRIBUTION	8
B. POWER SPECTRAL DENSITY	10
IV. COMPARISON OF EXPERIMENTAL-HYPOTHETICAL POWER SPECTRAL DENSITIES	15
V. CONCLUSIONS	17
VI. REFERENCES	197

LIST OF TABLES

<u>TABLE NO.</u>	<u>TITLE</u>	<u>PAGE</u>
I.	FLIGHT IDENTIFICATION	7
II.	CREW STATION RMS ACCELERATION VALUES	11
III.	PSD ANALYSIS-MEASUREMENT ERROR AT 90% CONFIDENCE LEVEL	14

LIST OF FIGURES

<u>FIGURE NO.</u>		<u>PAGE NO.</u>
1	Equipment Location	23
2	Transducer Package	24
3 - 11	Terrain and B-52 Flight Profiles	25-33
12	Probability Scaling	34
13 - 72	Probability Functions (a. Density; b. Distribution)	35-154
73 - 87	Power Spectral Density Functions (a. X, Y and Z Axes; b. Roll Axis)	155-184
88	Composite X Axis PSD's	185
89	Composite Y Axis PSD's	186
90	Composite Z Axis PSD's	187
91	Composite Roll Axis Acceleration PSD's	188
92	Composite Roll Axis Velocity PSD's	189
93	Flight 1-2 Variation in X Axis PSD	190
94	Flight 1-2 Variation in Y Axis PSD	191
95	Flight 1-2 Variation in Z Axis PSD	192
96	Flight 1-2 Variation in Roll Axis Acceleration PSD	193
97	Flight 1-2 Variation in Roll Axis Velocity PSD	194
98	Comparison of Experimental-Hypothetical Y Axis PSD's	195
99	Comparison of Experimental-Hypothetical Z Axis PSD's	196

SECTION I

INTRODUCTION

The increasing importance being placed on low-altitude, high-speed (LAHS) missions in present and projected aircraft dictates that a realistic assessment be made of the crew station vibration environment experienced during such flights. Such an evaluation is necessary in order that valid crew member psycho-physiological performance and tolerance criteria can be established through the use of in-laboratory motion simulation testing. Since basic aircraft design characteristics primarily determine the vibration environment felt by the crew, military aircraft have been categorized into the three general divisions of: (1) small, rigid fighters; (2) large, flexible bombers; (3) large, rigid bombers. This report presents the results of measurements and analyses made of the crew compartment vibration environment produced by the response of a large, flexible bomber (B-52) to the combined stresses imposed by maneuvers and gusts during LAHS flight.

An in-flight measurement program was performed on the B-52 aircraft in August 1966, during which 1.6 hours of LAHS data was obtained on six flights conducted at 350 knots true airspeed at an altitude of 500-900 feet above slightly mountainous terrain. Linear accelerations in the longitudinal (X), lateral (Y) and vertical (Z) axes and angular velocities and accelerations in the roll, pitch and yaw axes were analog recorded as amplitude-time histories for subsequent statistical and spectral analysis in each axis. Because of instrumentation problems during data acquisition, no pitch or yaw axis information was obtained on any of the flights and only flights 1, 2, 4 and 6 yielded useable data in the other degrees-of-freedom.

SECTION II

MEASUREMENT PROGRAM

The aircraft used in this endeavor consisted of B-52E models operationally assigned to the Strategic Air Command that were pressed into service as test bed aircraft for a large-scale, low-level flight test program to evaluate target acquisition capability. The low-altitude, high-speed vibration data acquired on these flights were obtained as a "piggyback" effort to the primary mission of the flight test program. The aircraft were typical of the B-52 design with the exception that a 1 foot diameter and 6.7 foot long instrumentation pod was externally centerline mounted to the underside of the aircraft to accommodate the test equipment required for the primary mission test program. Comparison of the vibration measurements obtained during these tests with those previously made on another B-52 program indicates that the external instrumentation pod did not perceptibly alter the crew station vibration environment spectrum in either the lateral or vertical axis. The effect of the pod on the vibration spectrum in the other degrees of freedom is not known since comparable data in these axes were not available.

The vibration transducer assembly used in this program was rigidly mounted to the cockpit floor in front of the instructor's seat, i.e., the package was situated between and slightly behind the pilot and co-pilot seats. Figure 1 is a cut-away sketch of the B-52 showing the locations within the aircraft of the transducer assembly, tape recorder and monitor/control console.

INSTRUMENTATION

The crew station six degree of freedom vibration data acquisition system included a transducer package, individual data channel visual monitoring

and signal conditioning package and a 14 channel analog tape recorder with remote control capability. The transducer assembly contained a triaxial rate gyro device and three linear accelerometers orthogonally mounted in the configuration shown in figure 2 so as to align the respective axes with those of the aircraft. The pitch axis rate gyro was inoperative throughout the tests and the yaw axis data was always in the noise floor, therefore no useful data was obtained in these degrees of freedom. The roll rate gyro measured the angular velocity in the independent axis over the ranges of ± 100 degrees/sec. To supplement static calibrations performed with an ordinary rate table, the gyros were dynamically calibrated at the Army Inertial Guidance and Control Laboratory using a precision oscillating rate table. The linear accelerations were measured with servo type accelerometers having ranges of $\pm 1g$ in the X and Y axes and $\pm 5g$ in the Z axis. Calibration of these transducers was performed using a laboratory quality low frequency shake table.

To optimize the quasi-static, overall data signal to noise ratio that was being recorded at any given time, the analog tape recorder input sensitivity was adjusted to a very low level voltage. Each data channel included a 40 dB passive attenuator network that was adjustable in 10 dB increments. A trained in-flight operator used the visual monitoring system to determine when to make attenuator setting changes and thereby assured that the maximum overall data dynamic range was attained. In this manner, compensation was made whenever significant changes in the overall vibration environment was noted in any given axis. Such changes in the overall data signal can occur during LAHS flight over different types of terrain during a given sortie. However, this signal conditioning capability did not

alleviate the signal to noise ratio limitations imposed by the tape recorder on the instantaneous dynamic range of the data being recorded.

ROUTE DESCRIPTION

The test flights for this study were flown along a 400 nautical mile route extending from England Air Force Base in Louisiana to the Ouchita Mountains in the state of Arkansas. The portion of the route leading into the Ouchita Mountains is rather flat with the highest terrain being 535 feet above sea level and is made up of forests, meadows, rural roads and cultural features representative of small to medium population communities in the temperate zone worldwide. That part of the route within the Ouchita Mountains is primarily tree covered and rolling type terrain with the highest peak 2,830 feet above sea level. For navigational purposes the route was divided into an East Course and West Course with no discernable differences in the general topography covered by the two segments of the route. All flights were performed using the terrain following technique at less than 1,000 feet, i.e., the aircraft were flown 500-900 feet above the terrain. The test pilots were instructed to maintain as best they could their altitude above terrain, airspeed and position along the particular course being flown at that time.

TEST FLIGHT IDENTIFICATION

On each flight, data was recorded for a maximum of sixteen minutes or a distance of about 93 nautical miles along the route. This record time was fixed by the tape capacity and recording speed of the recorder. Reference 1 states that the properties of statistical stationarity and homogeneity of rather mild atmospheric turbulence might be expected for large scale regions of up to 85-90 nautical miles, but for cases of more

severe turbulence as can be encountered over mountainous terrain the distances over which the turbulence exhibits stationarity are usually somewhat smaller. Since most of the data acquired on these flights was over semi-mountainous terrain, before any spectral or amplitude probability analyses can be performed on the data it was necessary to sub-divide each flight record into segments that satisfied the statistical property of stationarity.

Reference 2 presents in rigorous terms the general concept of stationarity and the verification of time invariant statistical properties theoretically required for proof of stationarity. The reference shows such proof of stationarity is clearly not feasible in practical terms since it would require an infinite number of probable statistics. A practical test for stationarity is developed in the text based on the following assumptions: (1) proof of self stationarity for individual sample records can be accepted as proof of stationarity for the random process from which the time histories were obtained; (2) verification of weak stationarity, that is the mean value and autocorrelation function are not time dependent, will be acceptable for most practical types of analyses and applications; (3) the sample record lengths are very long compared to the random fluctuations of the data; (4) proof of stationarity of the mean square value can be accepted as proof of stationarity of the autocorrelation function. This last assumption is usually valid since the mean square value is equal to the autocorrelation function at $\tau = 0$ and it is highly unlikely that non-stationary data will have a time-varying autocorrelation function that does not also vary at $\tau = 0$. The test for stationarity consisted of merely applying the reverse arrangement or trend test to the mean and mean square values, obtained for

each consecutive ten second interval of the acceleration time history.

Each flight was first sub-divided whenever the in-flight operator made an attenuator setting change in the signal conditioning system during data acquisition. Each flight was then further subdivided when the test for stationarity failed in any axis at the 0.05 level of significance. Table I lists the flight segment identification, aircraft number, course designation and total time in seconds that the data satisfied the test for stationarity in all degrees of freedom. Figures 3-11 show the terrain and flight profiles above mean sea level.

TABLE I
FLIGHT IDENTIFICATION

IDENTIFICATION NUMBER	AIRCRAFT NUMBER	COURSE DESIGNATION	STATIONARY PERIOD (SEC)
1-1-1	640	WEST	230
1-1-2	640	WEST	130
1-1-3	640	WEST	130
1-2-1	640	WEST	140
1-2-2	640	WEST	140
1-2-3	640	WEST	120
2-1	640	EAST	120
2-2	640	EAST	230
2-3-1	640	EAST	140
2-4	640	EAST	330
4-2	127	WEST	280
4-3	127	WEST	380
4-4	127	WEST	170
6-2	634	EAST	590
6-3	634	EAST	230

SECTION III

DATA ANALYSES

To completely define any multiple degree of freedom vibration environment, it is necessary to determine the amplitude, frequency and phase characteristics of the data. Since the immediate application of this data is to use it as input for in-laboratory simulation of the environment for psycho-physiological human tolerance testing and the SIXMODE motion simulation device that will be used in such studies currently has an independent degree of freedom control capability, amplitude-time and frequency analyses were performed in each axis. Joint probability and cross-spectral analyses to obtain phase information were not warranted at this time.

PROBABILITY DENSITY AND DISTRIBUTION

Once it has been determined that the data is at least weakly self stationary, then a test to ascertain randomness is in order. Such tests usually involve analysis techniques that assume the data are random. The presence of periodic or near-periodic components can be detected by visual inspection of the autocorrelation, power spectral density and/or the amplitude probability density functions. Although not as powerful as the other two methods, use of the amplitude probability density function was chosen for the following reasons: (1) the autocorrelation function does not yield any additional information over that obtained from the power spectral density function since one is merely the Fourier transform or inverse transform of the other; (2) power spectral density analysis will be performed on the data any way since a measure of the frequency composition must be made to supplement any amplitude-time analysis performed; (3) an analysis of the amplitude-time distribution is of great value in itself in the description

of a given vibration environment.

Digital techniques were used to compute the normalized amplitude probability density and cumulative distribution functions in the X, Y, Z and roll axes for each flight segment that exhibited stationarity. Each acceleration time history was digitized at a sampling rate of 100 points per second and the number of points, N_i , that fell within each of 60 equal amplitudes, Δy , intervals was computed. Knowing the total number of data points, N , in the sample time history, the amplitude probability density function is defined as:

$$\text{Probability Density Function} = p_i(y) = \frac{N_i}{N \Delta y} \quad (1)$$

The probability density function defines the probability that the instantaneous value lies within the range of y and $(y + \Delta y)$. The probability that the instantaneous value is less than or equal to some specified value y is the cumulative probability distribution function, and it is defined as:

$$\text{Probability Distribution Function} = P_i(y) = \int_{-\infty}^y p_i(y) \quad (2)$$

The computer program used in this study computes the normalized probability density and distribution functions by dividing the instantaneous values by the standard deviation, σ . The standard deviation is the rms variation about the mean value and can be found from the variance which is defined by:

$$\text{Variance} = \sigma^2 = (\text{rms value})^2 - (\text{mean value})^2 \quad (3)$$

Since the computer program forces the mean value to zero, then it is seen from equation 3 that the standard deviation is equal to the rms value of the time history. Figure 12 shows the scaling used in all of the probability

density and distribution computations performed in this study. Figures 13-72 are the normalized probability density and distribution functions of the X, Y, Z and roll axis accelerations for each flight. The legend shown below each graph indicates the number of equal amplitude intervals used in the computations and the voltages corresponding to the root-mean-square and mean values. Table II gives for each flight-axis the root-mean-square acceleration value in g and $\text{radian}/(\text{sec})^2$ units after taking into account all transducer sensitivities and data acquisition and reduction correction factors.

POWER SPECTRAL DENSITY

Because of the biomedical considerations involved in the expected application of the LAHS data collected during this program, the frequency composition of the data is of utmost importance. Recent improvements have been made in the stability and reliability of analog devices designed to measure the power and cross power spectral density functions. Commercially available analog systems can now be used to perform such analyses as accurately as was previously available only by digital means. Historically speaking, swept spectrum analyses have received widespread acceptance for the frequency analysis of random, periodic, or mixed data samples that are either stationary or transient in nature. Their appeal has been mainly due to their versatility in being able to properly analyze a wide variety of data signals, especially acoustic and vibration environments at the higher frequencies. Numerous studies of the effects of sinusoidal and random vibrations on man have shown the human body reacts most unfavorably to those accelerations at frequencies less than 20 Hz. Primarily due to advancements in filter and detector design, frequency analyses can now be

TABLE II
CREW STATION RMS ACCELERATION VALUES

FLIGHT IDENTIFICATION	g UNITS			RAD/SEC ² UNITS
	X AXIS	Y AXIS	Z AXIS	ROLL AXIS
1-1-1	.03	.06	.15	.5
1-1-2	.02	.06	.16	.7
1-1-3	.02	.06	.17	.6
1-2-1	.03	.05	.14	.5
1-2-2	.04	.05	.13	.6
1-2-3	.02	.04	.12	.6
2-1	.02	.06	.17	1.5
2-2	.02	.06	.18	1.5
2-3-1	.02	.05	.16	1.4
2-3-2	.02	.05	.16	1.5
4-2	.02	.06	.16	.6
4-3	.05	.13	.18	.6
4-4	.05	.07	.22	.7
6-2	.03	.05	.15	.6
6-3	.07	.05	.16	.6

performed with swept spectrum analyzers at the low frequencies where the limiting factors in the analyses are certain, inviolate, underlying statistical principles and not the performance characteristics of the analyzer.

There is an error associated with any measurement or analysis effort dealing with random data since the data samples have a finite time duration and can only be described by statistical properties. In addition, most of these descriptive quantities are merely estimates or probabilities of occurrence rather than exact values. In general, the statistical number of degrees-of-freedom is a measure of the accuracy of the results obtained using a given frequency analysis procedure and is defined by:

$$n = 2 BT \quad (4)$$

where B is the effective bandwidth of the filter employed and T is the sample record length or integration time. The lengths of time that all axes exhibited stationarity as listed in Table I were used as the value of T for each flight of the B-52. From equation 4, once T has been established, some trade-off must be made between the desired filter bandwidths and the accuracy obtained for the analyses. To ascertain all major resonance and null regions present in the B-52 acceleration data were being defined, one data sample was analyzed using a 0.05 Hz filter. As a reasonable compromise between frequency resolution and measurement error, all of the power spectral density measurements were made using a 0.2 Hz filter. This means even with perfect instrumentation and careful calibration, there will be an uncertainty associated with these power spectral density results purely because of the statistical limitations involved when dealing with random data. Using

standard statistical procedures it is possible to specify the confidence level or percent probability a given measured value does lie within some specified accuracy limits. For example, considering flight 1-1-1 at the 90% confidence level with $n = 2 \text{ RT} = 2 \times 0.2 \times 230 = 92$ statistical degrees of freedom, one would find 90% of the time the measured power spectral density is within $\pm 23.6\%$ or $\pm 1.8 \text{ dB}$ of the actual value. In addition to this inaccuracy due to the limited number of degrees of freedom, one must also account for various data acquisition and reduction uncertainties present in the PSD analyses. Due to various instabilities in the total data acquisition system, these recorded acceleration time histories inherently have a $\pm 5\%$ error associated with them. An additional $\pm 2.5\%$ uncertainty in the PSD results stems from the accuracy limitations of the power detector used in the swept spectrum analyzer. Table III lists the total estimated accuracy limits at the 90% confidence level that can be expected of the PSD curves developed in this study.

The PSD curves shown in figures 73-87 were obtained with a fixed filter bandwidth of 0.2 Hz and time integration being applied to the power detector output over the entire sample record length.

Figures 88-92 show for each individual axis all of the crew station power spectral densities that were measured. The spread in the data shown in figures 88-92 was expected since it includes not only the variations due to gust input, but also those due to terrain, aircraft number, maneuvering, etc. For example, figures 93-97 show the variability in the power spectral density in each axis for various segments of Flight 1.

TABLE III

PSD ANALYSIS-MEASUREMENT ERROR AT 90% CONFIDENCE LEVEL

<u>FLIGHT NO.</u>	<u>DEGREES OF FREEDOM</u>	<u>\pm % ERROR</u>	<u>dB ERROR</u>
1-1-1	92	31.1	2.4
1-1-2	52	39.1	2.9
1-1-3	52	39.1	2.9
1-2-1	56	37.9	2.8
1-2-2	56	37.9	2.8
1-2-3	48	40.4	3.0
2-1	48	40.4	3.0
2-2	92	31.1	2.4
2-3-1	56	37.9	2.8
2-3-2	132	27.1	2.1
4-2	112	28.8	2.2
4-3	152	25.7	2.0
4-4	98	30.3	2.3
6-2	236	22.0	1.7
6-3	92	31.1	2.4

SECTION IV

COMPARISON OF EXPERIMENTAL-HYPOTHETICAL POWER SPECTRAL DENSITIES

The fundamental relationship between the input and response power spectral density for any constant parameter linear system is given by:

$$\text{PSD}_{\text{response}} = |T|^2 \times \text{PSD}_{\text{input}} \quad (5)$$

where $|T|^2$ is the gain factor or transfer function of the system or "black box" in question and is defined as $\sqrt{T_R^2 + T_I^2}$ where T_R and T_I are the real and imaginary components of the complex frequency response function.

From reference 3, experimentally derived Y and Z axis crew station transfer functions were extracted for a B-52 aircraft flying under test conditions very similar to those present during this data acquisition program. The aircraft gross weight and airspeed were nearly identical, but the flight altitude differed considerably. However, the flight altitude should primarily be reflected in the level of turbulence and response seen at the crew station, but it should not seriously affect the spectral characteristics of the transfer function.

To obtain a hypothetical power spectral density response function, the values for the crew station transfer function were multiplied on a point by point basis by the power spectral density of the gust input spectrum, which was empirically derived by Dryden as:

$$\text{PSD}_{\text{gust input}} = \frac{\sigma^2 L}{\pi V} \frac{1 + 3\left(\frac{\omega L}{V}\right)^2}{\left[1 + \left(\frac{\omega L}{V}\right)^2\right]^2} \quad (6)$$

where σ is the root mean square velocity of the gust input in ft/sec, ω is the frequency in radians/sec, L is the turbulence scale factor in feet and V is the true airspeed of the aircraft in ft/sec units. Reference 3 states that the same gust input expression can be used to realistically represent both the lateral and vertical turbulence spectra. This means that using $L = 500$ feet and $V = 591$ ft/sec, equation 6 can be multiplied at discrete frequencies by the appropriate transfer function value to obtain both the Y and Z axis normalized crew station response power spectral density. Figures 98 and 99 show the Y and Z axis power spectral densities measured on Flight 1-1-1 and those calculated using the experimental transfer functions from reference 3 and the Dryden gust input spectrum with $\sigma^2 = 19 \text{ (ft/sec)}^2$ for the lateral response and $\sigma^2 = 35 \text{ (ft/sec)}^2$ for the vertical response.

SECTION V

CONCLUSIONS

As shown in Table I, the vibration environment in the X, Y, Z and Roll axes exhibited the statistical property of stationarity for periods of 120-590 seconds. The distances flown during these periods of data stationarity varied from 13.5 to 63 miles. Reference 4 showed that an F-4C aircraft was able to travel 20-75 miles during periods of vibration data stationarity while also terrain contour flying over semi-mountainous regions but at much faster speeds than the B-52 used in this study. These distances flown during data stationarity are in excellent agreement with each other and are consistent with the maximum of 100 miles predicted in reference 1 for large scale regions where the properties of stationarity and homogeneity of turbulence might be expected to apply during non-storm conditions. They are quite less than the approximately 130 mile distances covered during data stationarity as mentioned in reference 3. However, special consideration should be given to the fact that during the B-52 flights conducted in reference 3, only light turbulence was encountered and the flights were made at 500-1000 feet above the highest terrain obstacle rather than terrain contour flying as was done in this study. Detailed examination of our B-52 acceleration time histories and route profiles revealed that the periods of data stationarity were generally terminated when the aircraft underwent a sustained maneuver or flew over terrain where the general characteristics changed considerably, e.g., from relatively flat terrain to semi-mountainous. Therefore, it is not surprising that the periods of stationarity in this study may be less than those experienced in other programs after it is recognized that aircraft maneuvers are prevalent during low-altitude, high-speed flight and that

regions of homogeneous turbulence are generally limited to covering terrain of similar characteristics.

Visual inspection of the probability density functions in figures 13-72 indicates the vibration time histories in any one axis are generally random in nature, but the vast majority of them contain one or more high probability components at specific amplitude intervals. The probability density function is a plot of the percentage of the total time spent at a given amplitude level. Obviously, maneuvers would tend to produce small amplitude changes over a long period of time compared to the length of time spent at a given level due to purely random fluctuations. The particular amplitude interval containing these accelerations produced by a maneuver would vary according to the maneuver characteristics, and would explain why the spikes seen in these probability density functions occur at various amplitude intervals. Since maneuvers while terrain contour flying are not performed periodically and the overall shapes of these probability density figures are not similar to those associated with mixed random and periodic phenomena, it is hypothesized that the extremely high and low amplitude intervals present in these data are the result of aircraft maneuvers.

When dealing with turbulence associated studies, it is common practice to assume the measured data exhibits a normal or Gaussian distribution. This is because the Central Limit Theorem suggests that any phenomenon that is the result of numerous random effects will tend to have a Gaussian distribution itself. However, strong nonlinear operations can produce deviations from the ideal Gaussian form. Negative results were obtained by applying the chi-square goodness-of-fit test for normality to the five probability density functions that appeared to most closely follow the

bell-shaped density function characteristic of Gaussian distributed phenomena. Based on these findings, the B-52 vibration environment experienced at the crew station during low-altitude, high-speed flight cannot be considered Gaussian in accordance with the statistical definition of the term.

From the viewpoint of in-laboratory simulation of the crew compartment low-altitude, high-speed in-flight vibration environment, the most significant conclusion drawn from this study can be readily derived from figures 73-87 showing the power spectral density in each individual axis. Most human biomedical tolerance and psychophysiological performance studies concerning the effects of such complex aircraft vibration environments that have been conducted in the past were limited to consideration of the vertical axis accelerations only. However, figures 73-87 unquestionably show that above 3 Hz the overall linear vibration environment measured in the crew compartment was not solely dependent upon the vertical axis accelerations, but that the lateral axis levels were equal to or greater than those in the Z axis. In addition, above approximately 10 Hz, the longitudinal axis levels were nearly equivalent to those seen in the lateral and vertical axes. As reported in reference 4, it was significant to ascertain that the linear accelerations in all axes must be considered during any research programs on human tolerance and/or performance criteria and the in-laboratory simulation of these complex vibration environments.

Excluding the very low frequency or phugoid vibrations, the following characterizations concerning the spectral content of the acceleration environment in each axis of the B-52 can be made from figures 88-92:

X axis - null regions located at 1.2, 1.8, 2.5 and 3.6 Hz separated by rather sharp resonances at 1.6, 2.0, 3.0 and 5.0 Hz followed by a mild 10 dB

decay to 15 Hz and then increasing to 20 Hz; Y axis - primary peak at 3.6 Hz with other resonances located at 1.3, 2.5 and 4.7 Hz followed by a 30 dB decay out to 20 Hz. These resonances are separated by narrow null regions located at 0.8, 2.0, 2.8 and 4.2 Hz; Z axis - null regions located at 1.2, 2.3, 3.5, 4.3 and 6.0 Hz separated by resonances at 1.9, 3.0, 3.8, 5.7 and 6.2 Hz followed by a 30 dB decay out to 20 Hz; Roll axis - null regions located at 1.0, 2.3, 3.3, 4.2 and 6.0 Hz separated by narrow resonances at 1.3, 2.8, 3.6 and 5.0 Hz with a broad resonance region located about 9.0 Hz followed by a mild 8 dB decay to 12 Hz and then deteriorating into a broadband signal out to 20 Hz with no discernable null or resonance regions. As expected, the roll axis angular velocity and acceleration environments exhibit identical resonant and nodal characteristics. Comparison of the roll axis spectra does show the angular acceleration levels increase with increasing frequency. This increase in amplitude with increasing frequency is inherent in the differentiation process.

As seen in figures 88-90, the linear acceleration PSD in the longitudinal, lateral or vertical axis only varied by about 5 dB for all flights. In view of the widely different terrain, gust input and pilot maneuver conditions under which the data was acquired, this spread in the PSD spectra was surprisingly small.

Figures 93-97 point out the even more astounding conclusion that the variability in the PSD spectra within a given flight is equal to the variations seen when comparing different aircraft flying over different terrains on different days. These data show the B-52 linear acceleration crew station environment experienced on one flight is probably no worse than 5 dB different than that experienced on any other flight made under the

same general flight profile conditions.

Figures 98 and 99 show the almost exact spectral agreement between our Flight 1-1-1 lateral and vertical PSD curves and those calculated using the experimental transfer functions from reference 3 and the empirically derived Dryden gust input spectrum. Since no measurement of the gust input intensity was made on any of the flights in this study, the values chosen for σ in figures 98 and 99 were selected to yield the best possible amplitude agreement with the Flight 1-1-1 curves. However, the σ values used are quite consistent with those expected during low-altitude, high-speed flight over semi-mountainous terrain. In addition, the σ value only controls the relative position of the PSD curve along the amplitude scale and in no way does the choice of the σ value affect the spectral characteristics of the PSD response function.

In summary, the more important conclusions drawn from this effort were:

- (1) The time periods over which all axes exhibited the statistical property of self-stationarity were limited to 120-590 seconds due to sustained aircraft maneuvers or large changes in the intensity of the gust input spectrum from flying over terrain with quite varied general landscape characteristics.
- (2) Sustained accelerations induced by maneuvers strongly contribute to the overall intensity of the vibration environment and are probably why the time histories do not exhibit truly random probability density functions.
- (3) The common assumption of Gaussian distribution does not seem warranted for these data since all cases evaluated by the chi-square goodness-of-fit test for normality failed at the 0.05 level of significance.
- (4) All axes contribute significantly to the total vibration environment

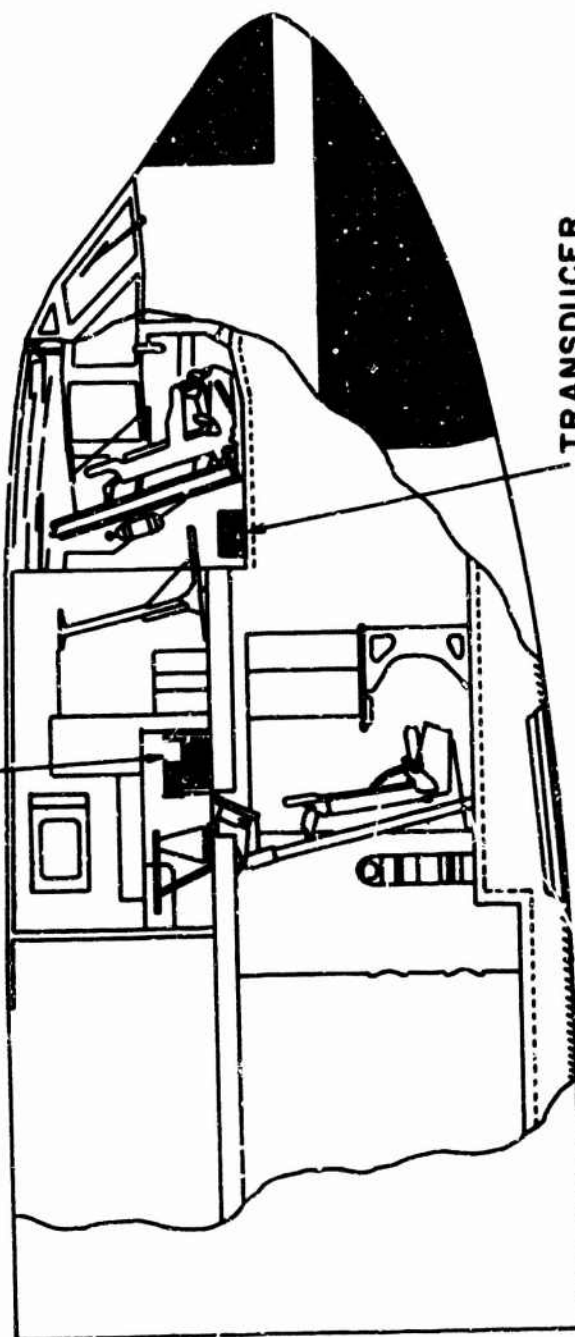
experienced by the crew of B-52 aircraft flying low-altitude, high-speed missions.

(5) In-laboratory simulation of the LAIS vibration environment for biomedical tolerance and/or psycho-physiological performance studies cannot be limited to motion in only one degree-of-freedom.

(6) variations in aircraft or terrain did not affect the pilot station PSD in the linear acceleration degrees-of-freedom by more than 5 dB for frequencies up to 20 Hz.

(7) These measured lateral and vertical axis PSD response functions are nearly identical in spectral content to those calculated using aircraft transfer functions experimentally derived under different flight conditions on another program and theoretical gust input spectra.

TAPE RECORDER, MONITOR CONSOLE,
AND CONTROL CONSOLE (IN RACK)



TRANSDUCER
ASSEMBLY

Figure 1. Equipment Location.

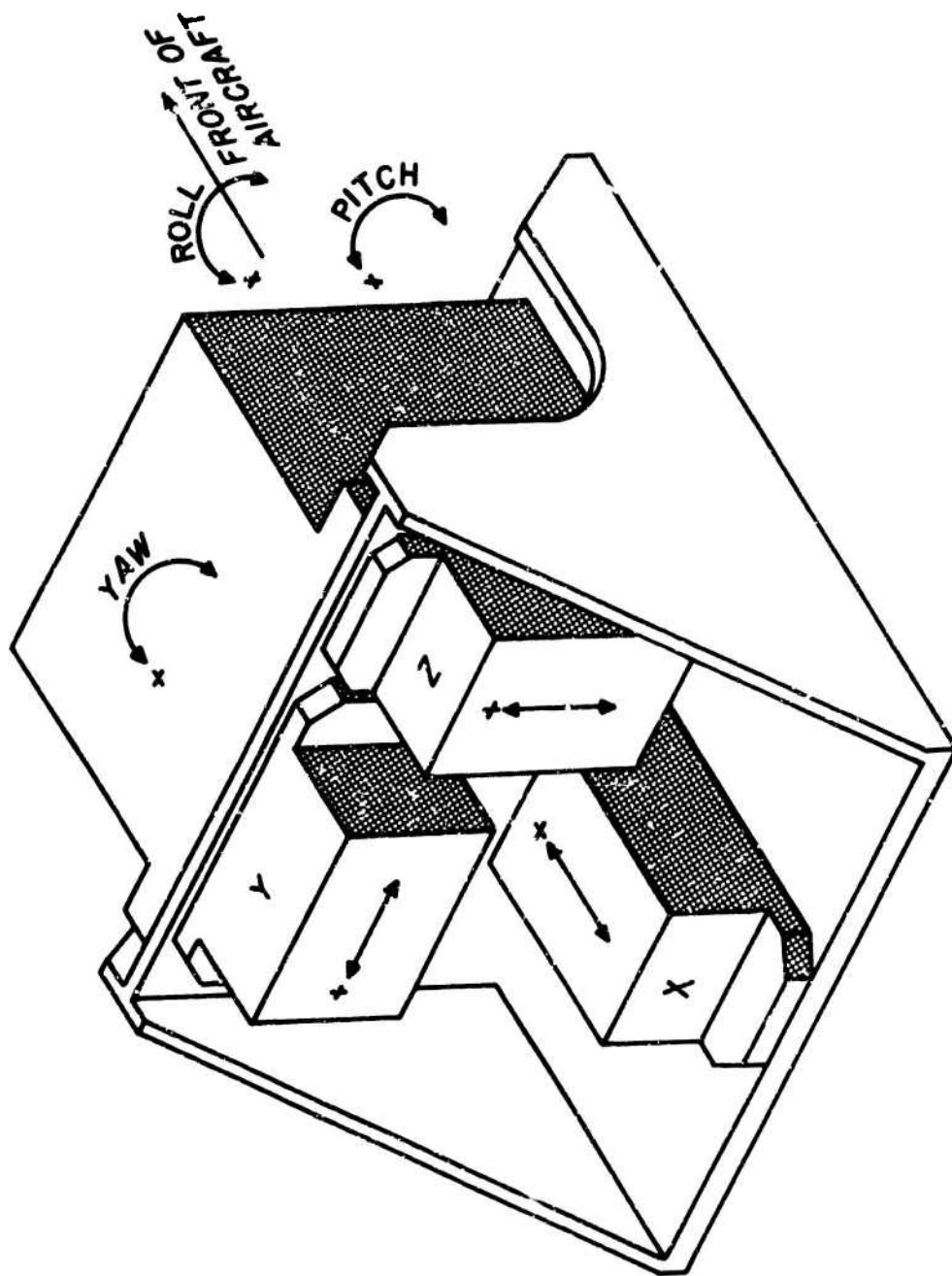
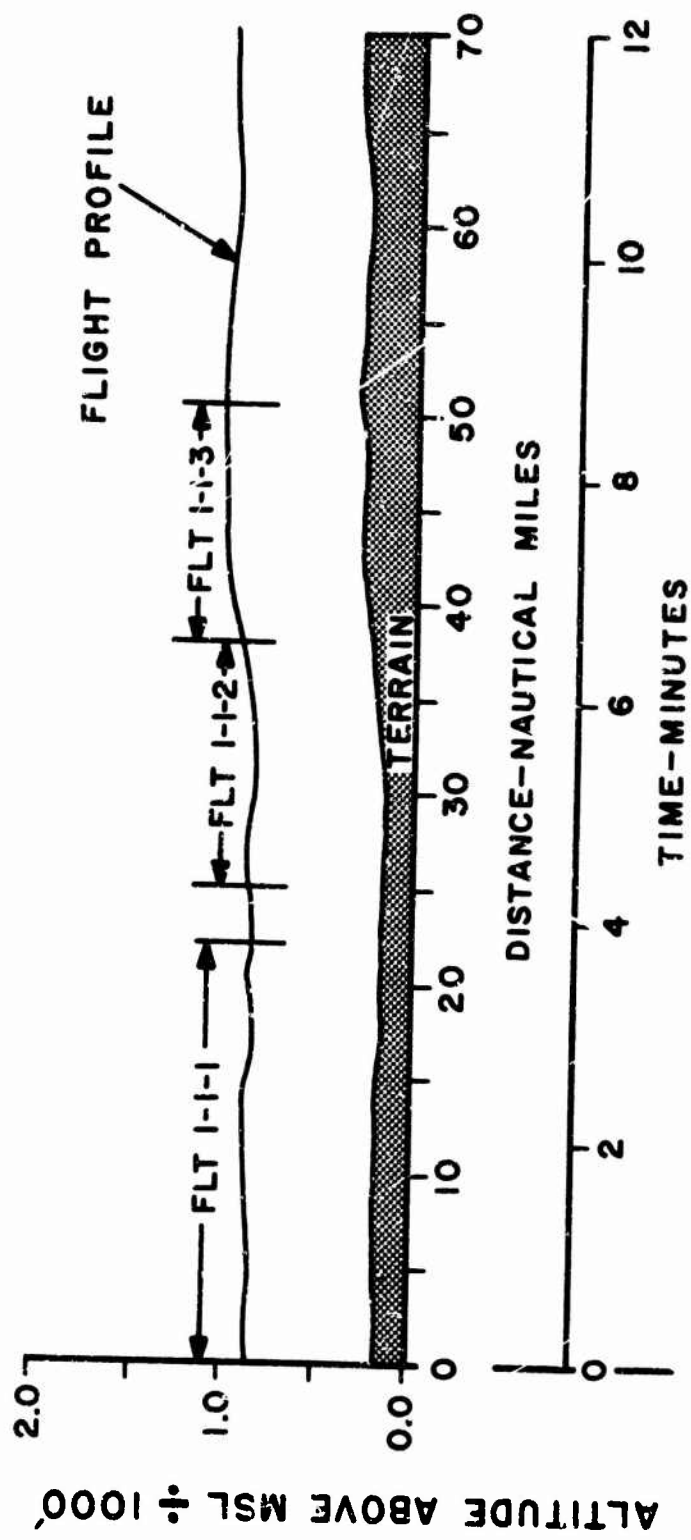
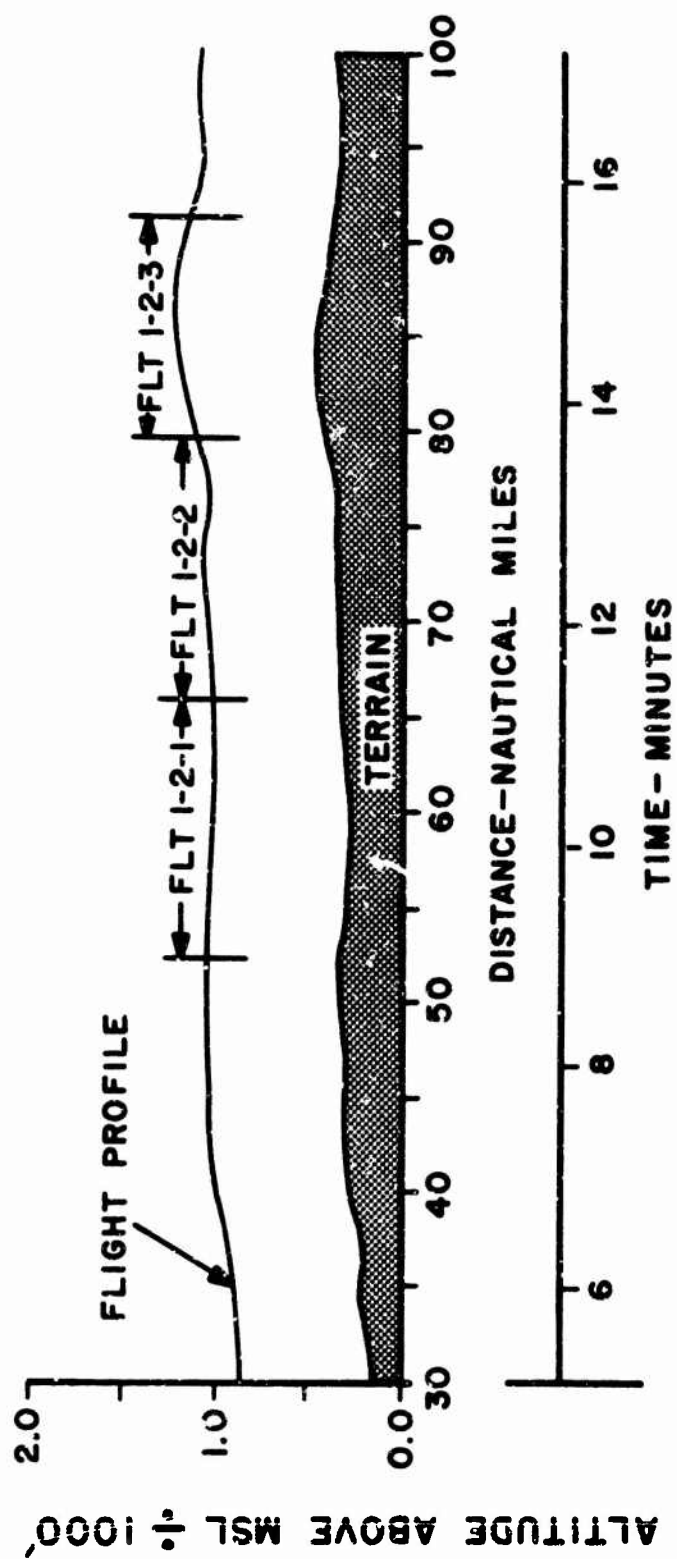


Figure 2. Transducer Package



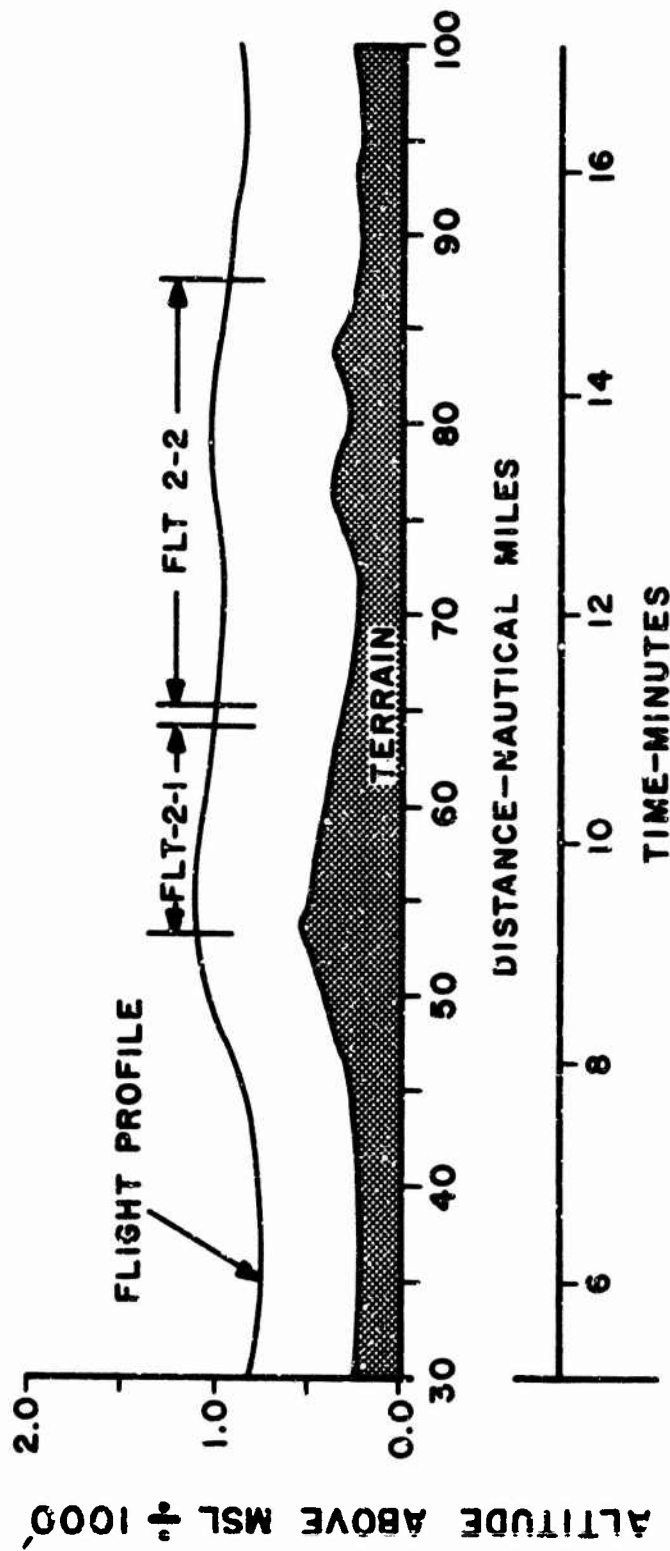
TERRAIN AND B-52 FLIGHT PROFILES—WEST COURSE

Figure 3. Flights 1-1-1, 1-1-2 and 1-1-3 Profiles



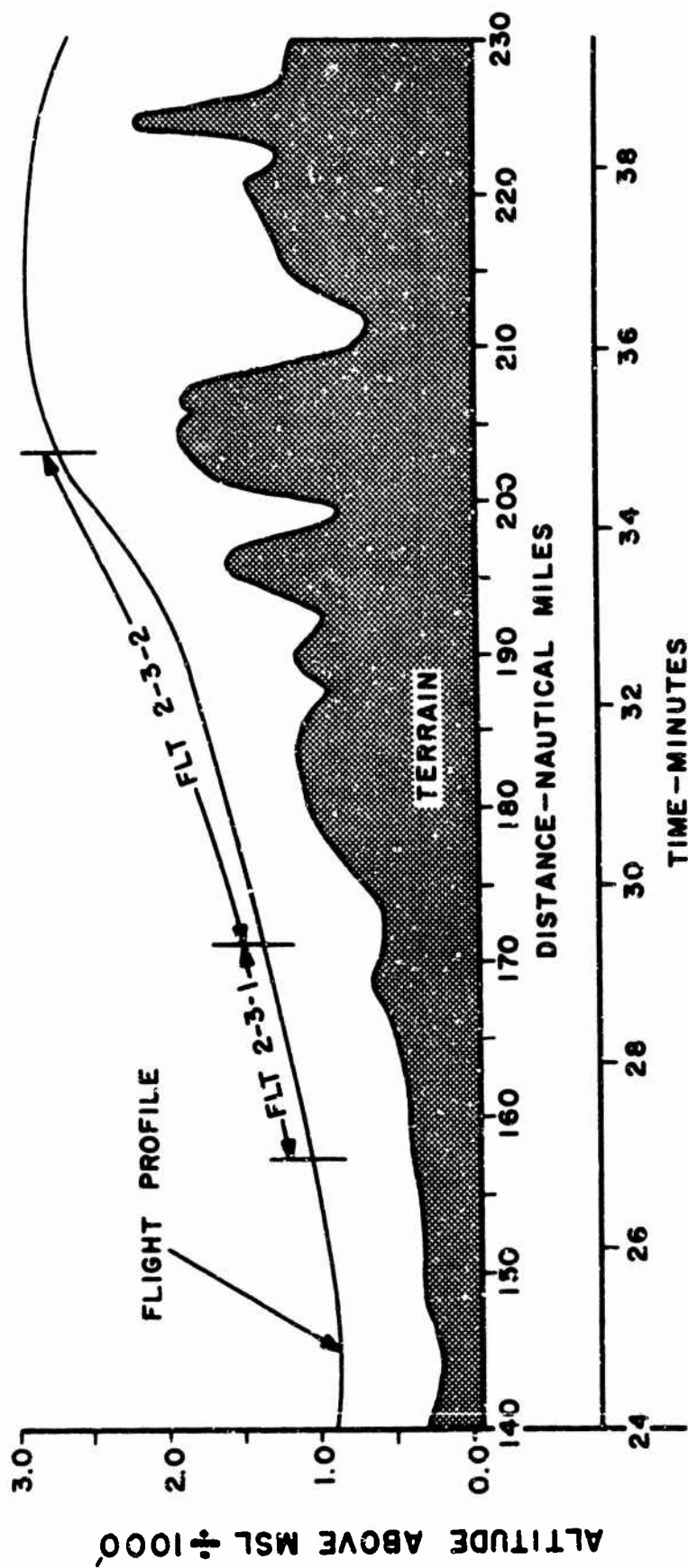
TERRAIN AND B-52 FLIGHT PROFILES-WEST COURSE

Figure 4. Flights 1-2-1, 1-2-2 and 1-2-3 Profiles



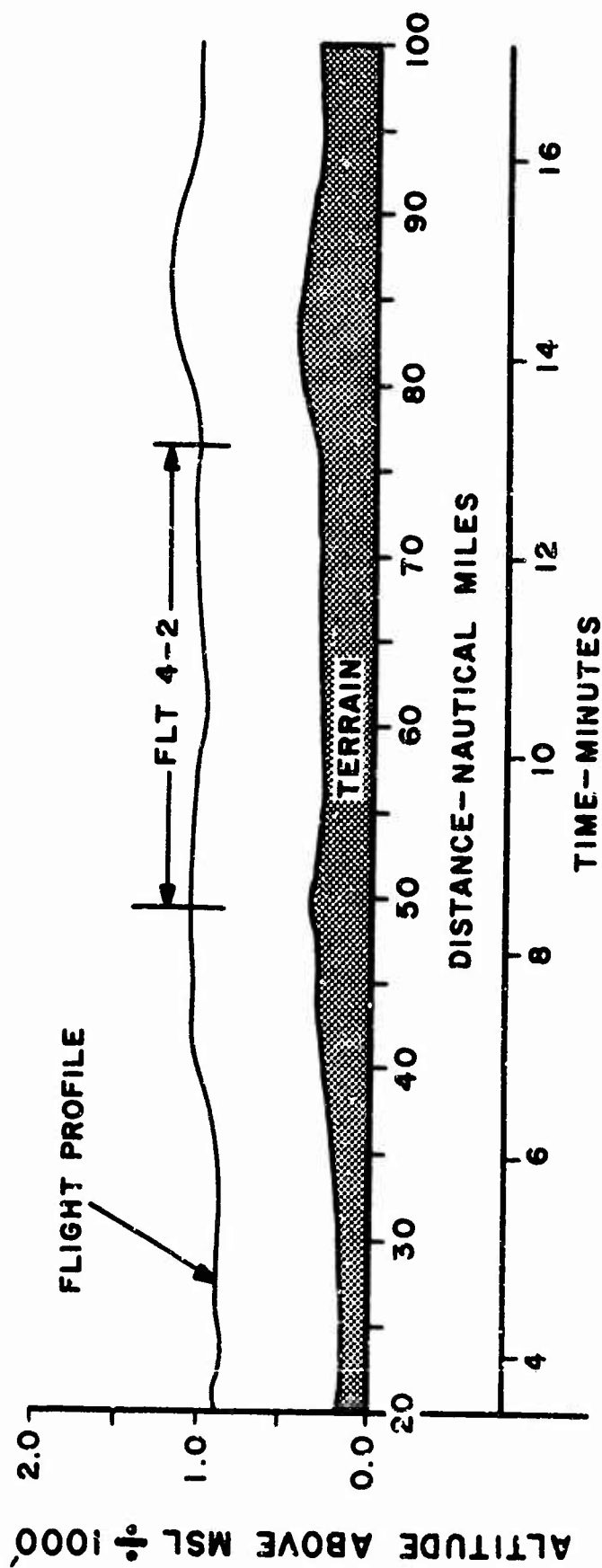
TERRAIN AND B-52 FLIGHT PROFILES-EAST COURSE

Figure 5. Flights 2-1 and 2-2 Profiles



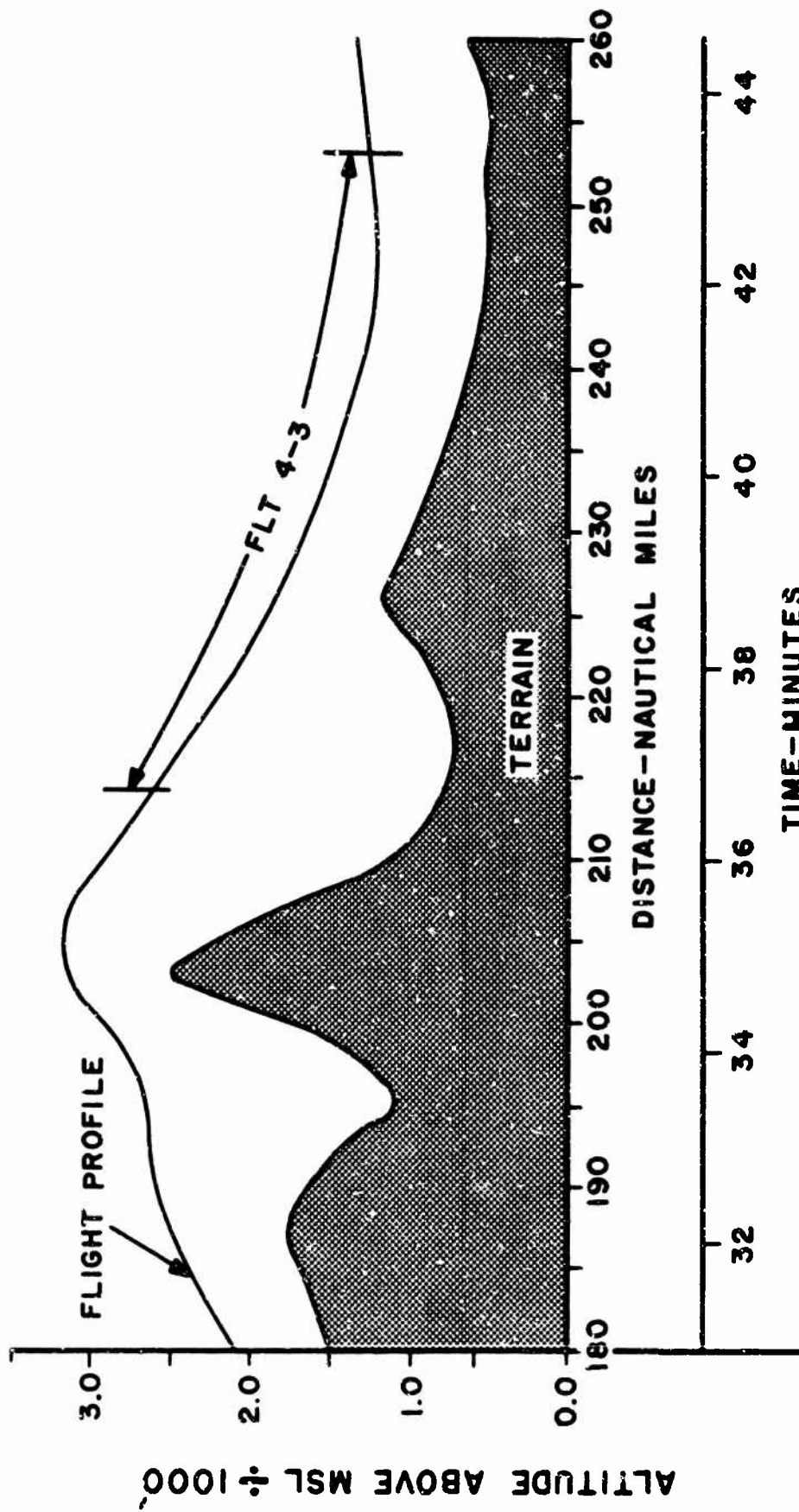
TERRAIN AND B-52 FLIGHT PROFILES-EAST COURSE

Figure 6. Flights 2-3-1 and 2-3-2 Profiles



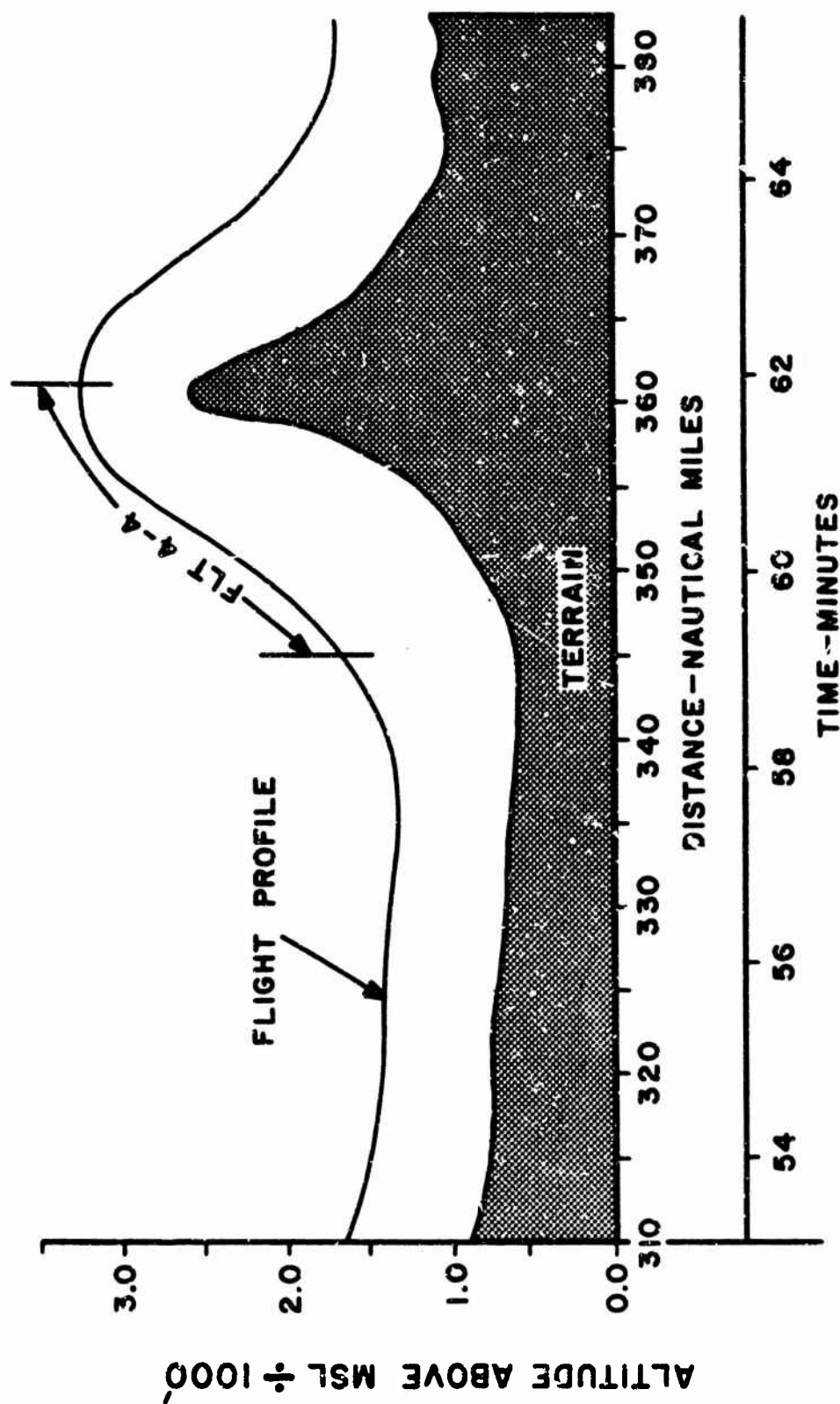
TERRAIN AND B-52 FLIGHT PROFILES--WEST COURSE

Figure 7. Flight 4-2 Profile



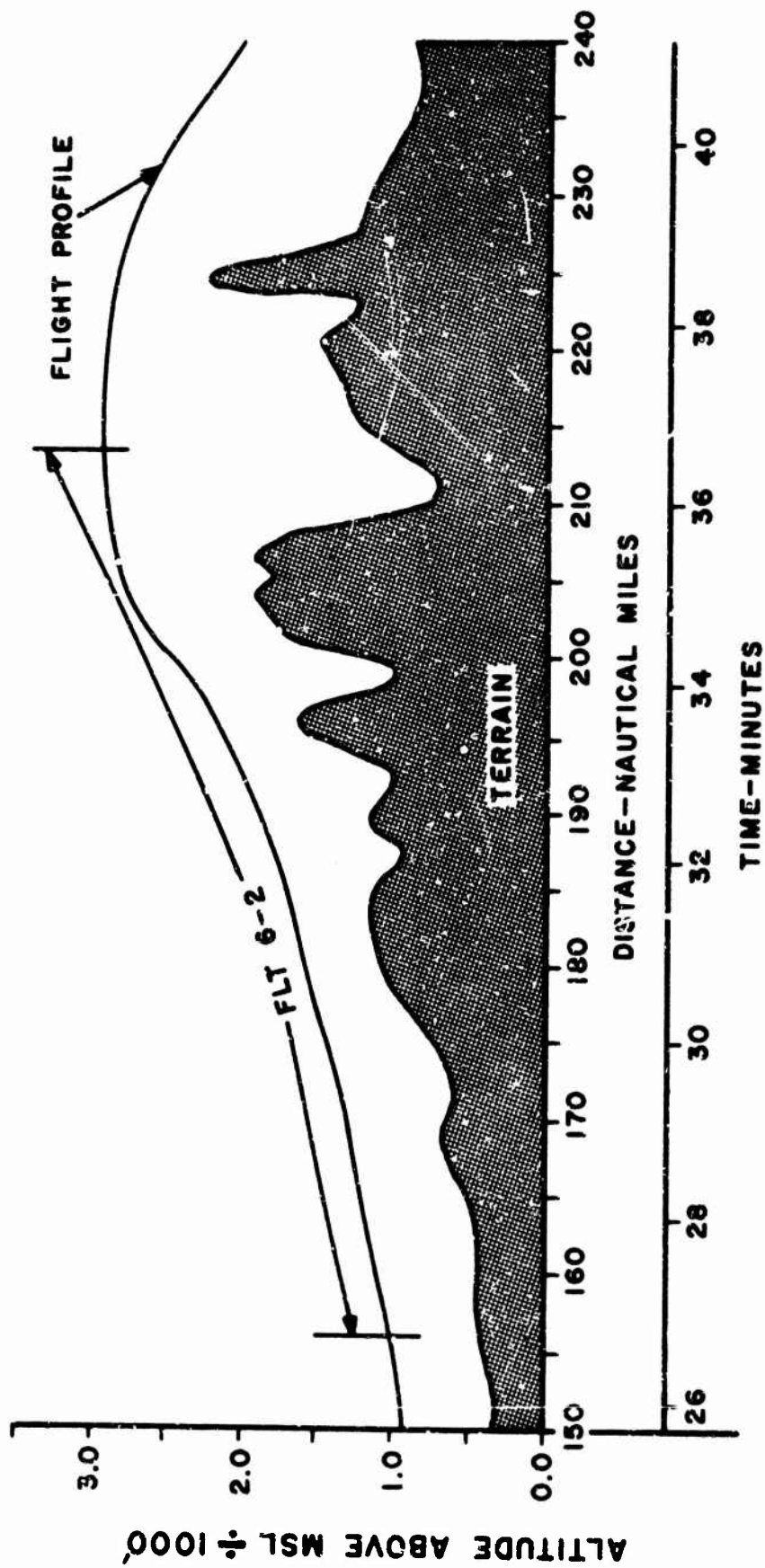
TERRAIN AND B-52 FLIGHT PROFILES-WEST COURSE

Figure 8. Flight 4-3 Profile



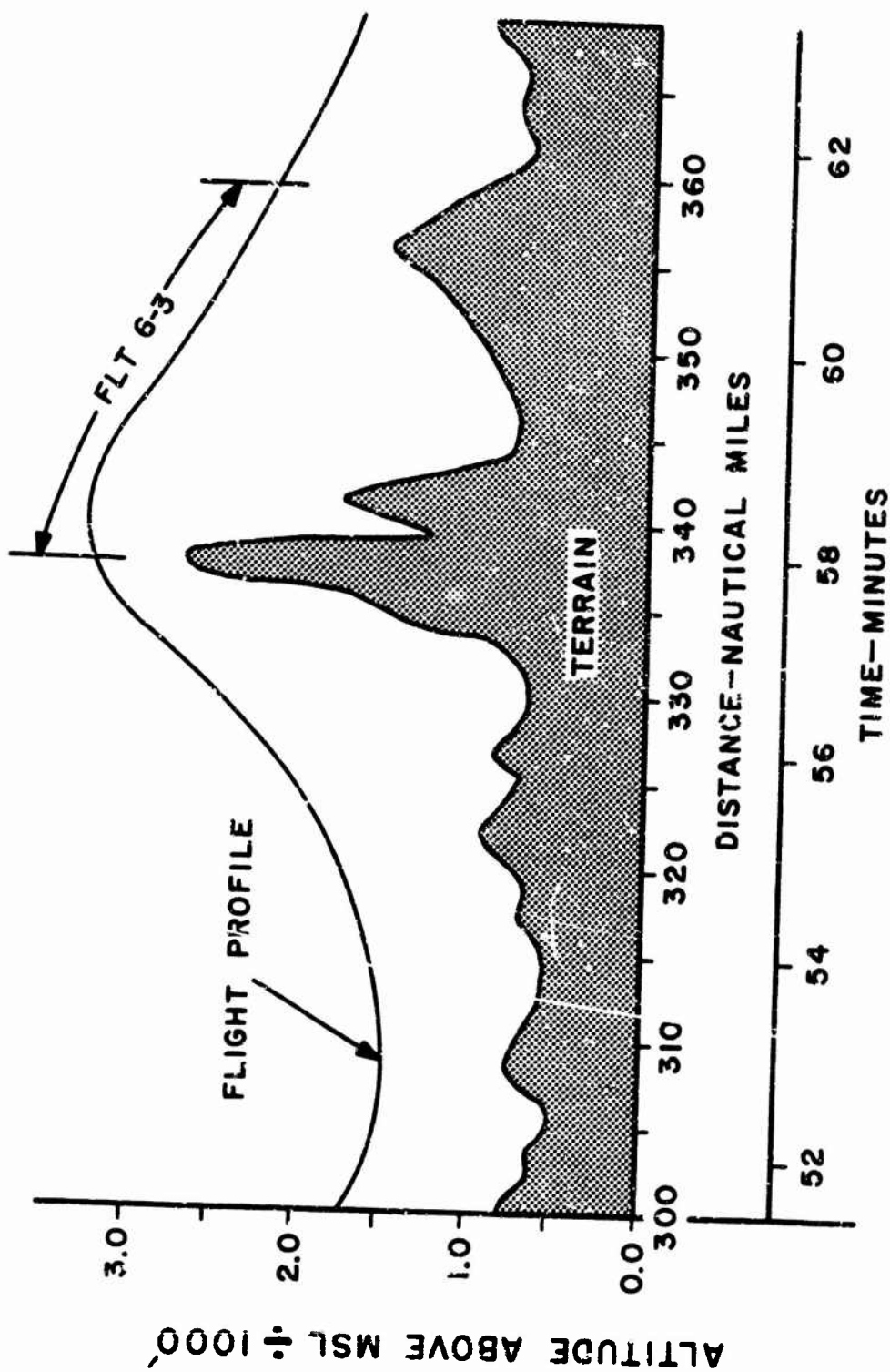
TERRAIN AND B-52 FLIGHT PROFILES--WEST COURSE

Figure 9. Flight 4-4 Profile



TERRAIN AND B-52 FLIGHT PROFILES-EAST COURSE

Figure 10. Flight 6-2 Profile



TERRAIN AND B-52 FLIGHT PROFILES-EAST COURSE

Figure 11. Flight 6-3 Profile

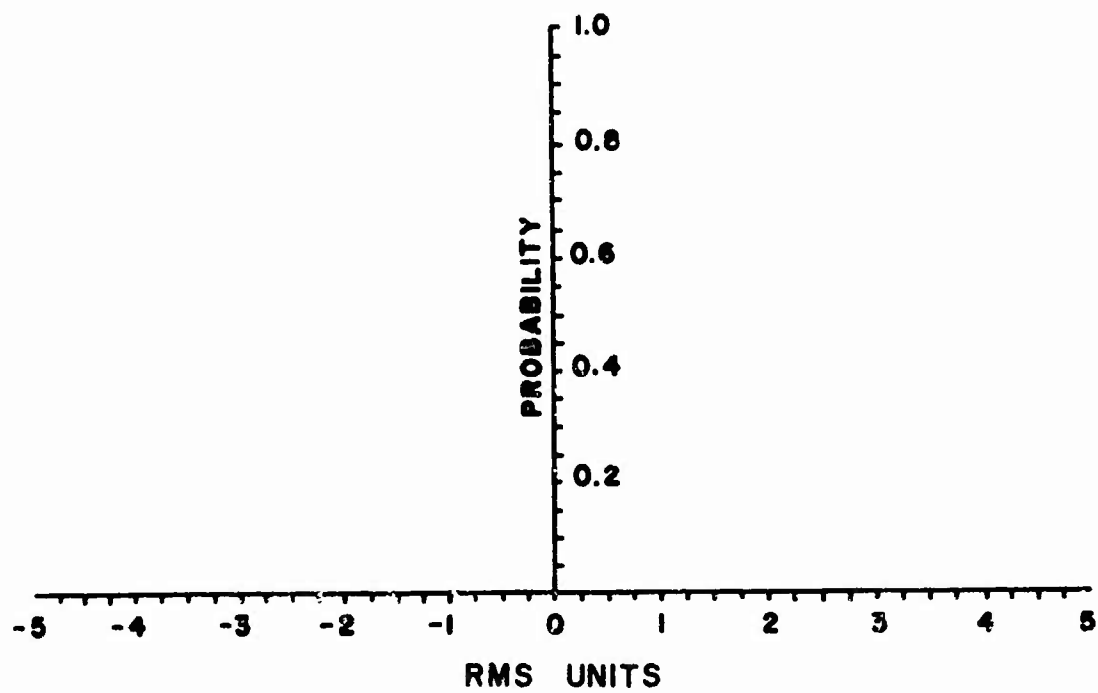


Figure 12. Probability Scaling

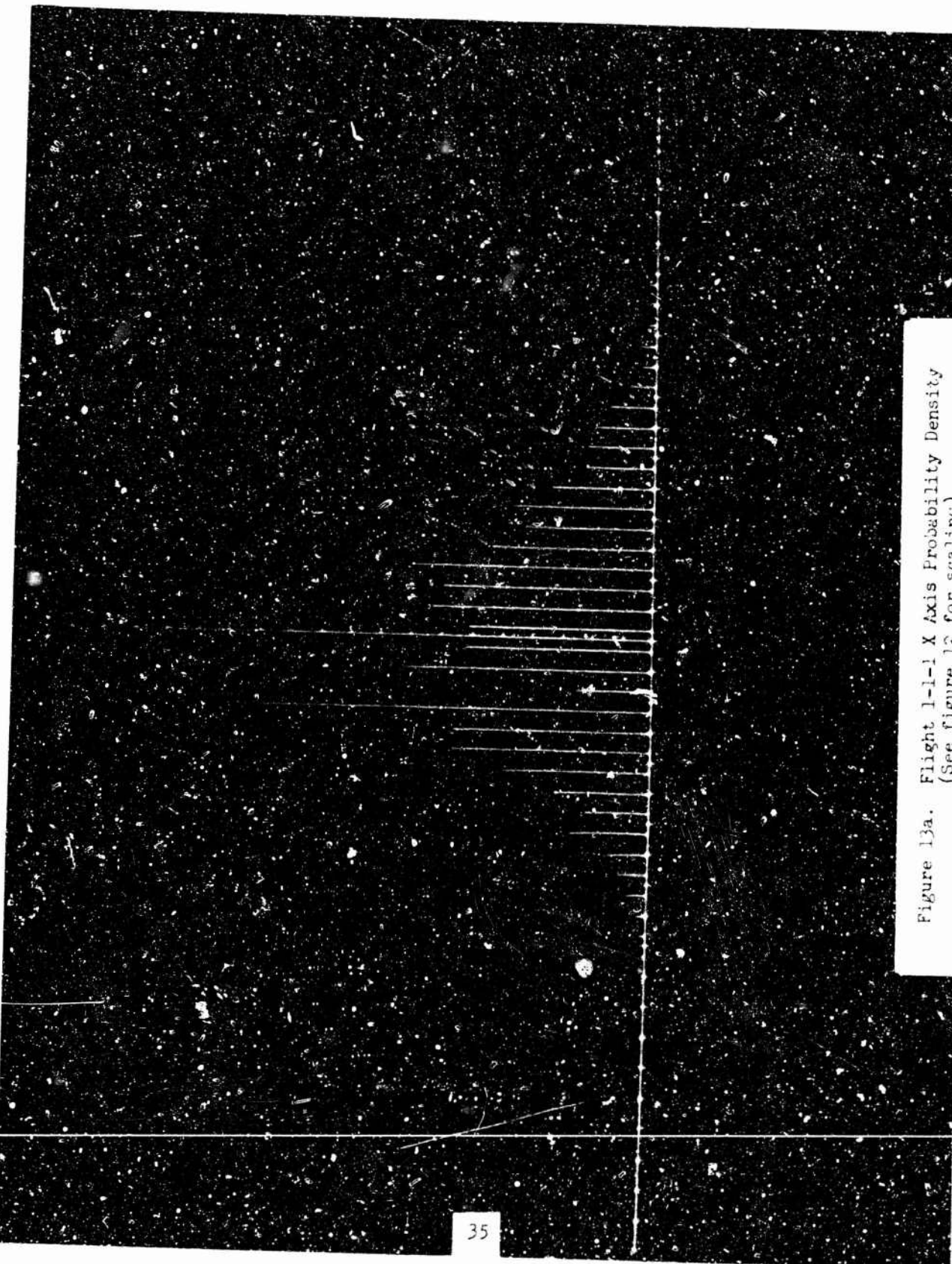


Figure 13a. Flight 1-1-1 X Axis Probability Density
(See figure 12 for scaling)

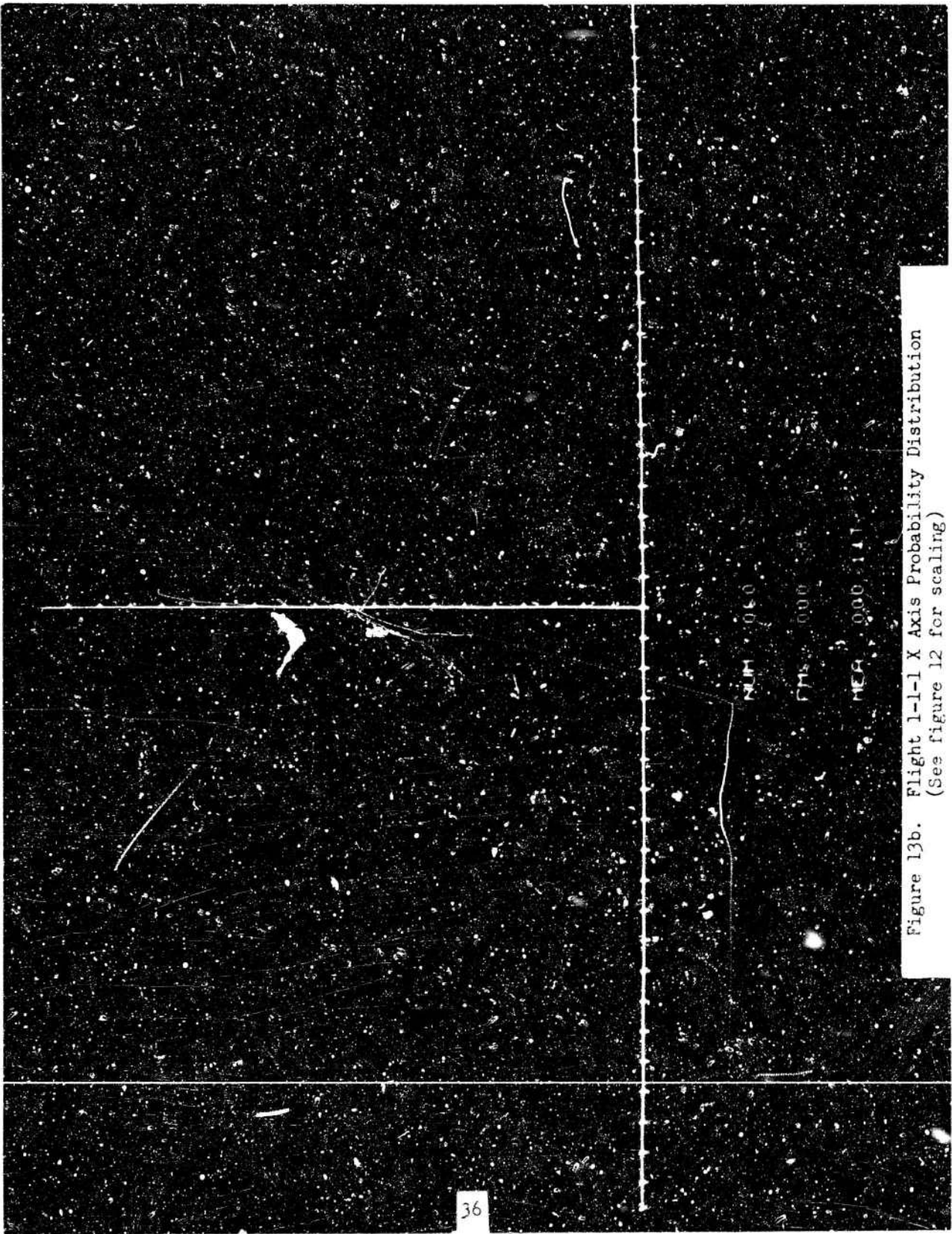


Figure 13b. Flight 1-1-1 X Axis Probability Distribution
(See figure 12 for scaling)

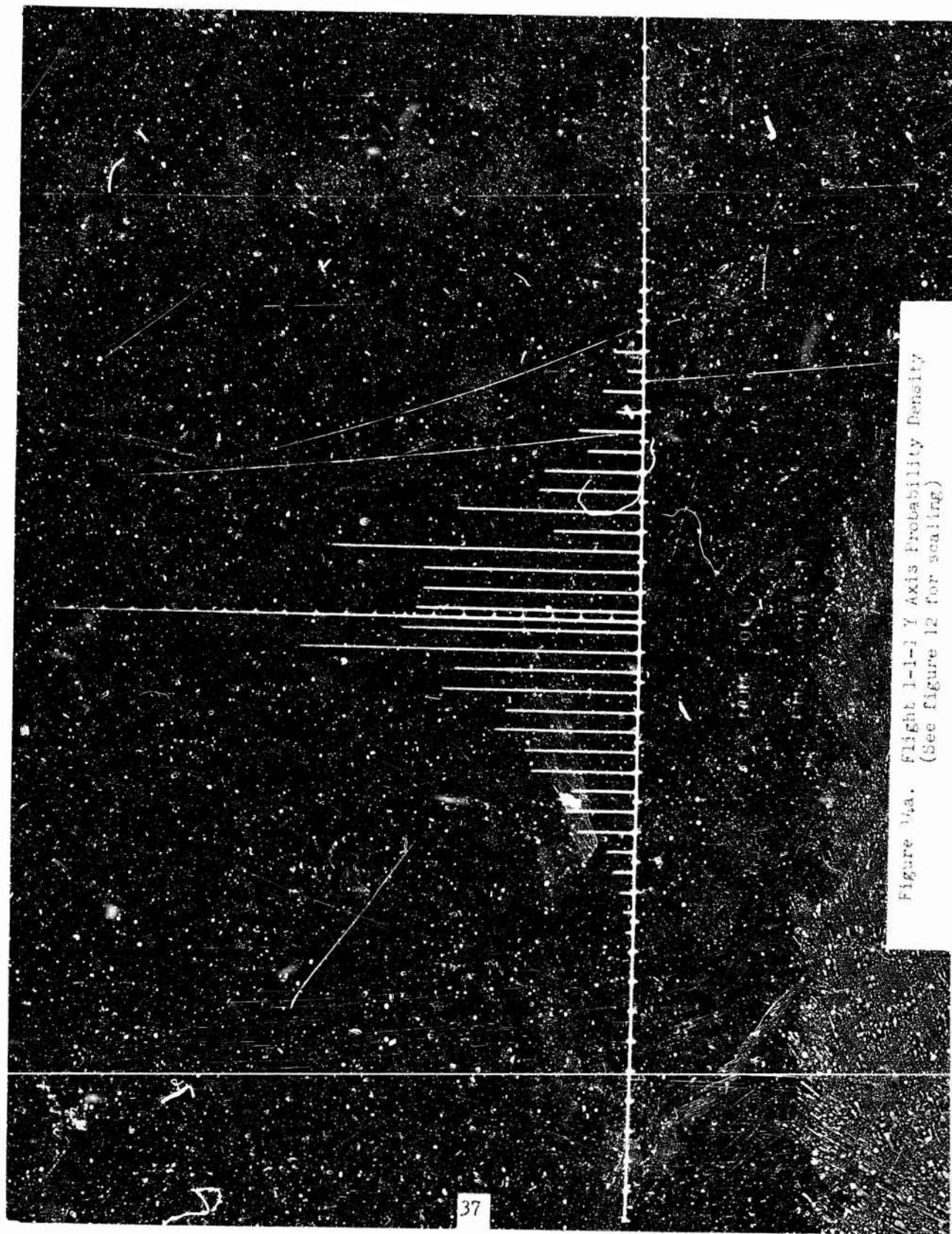
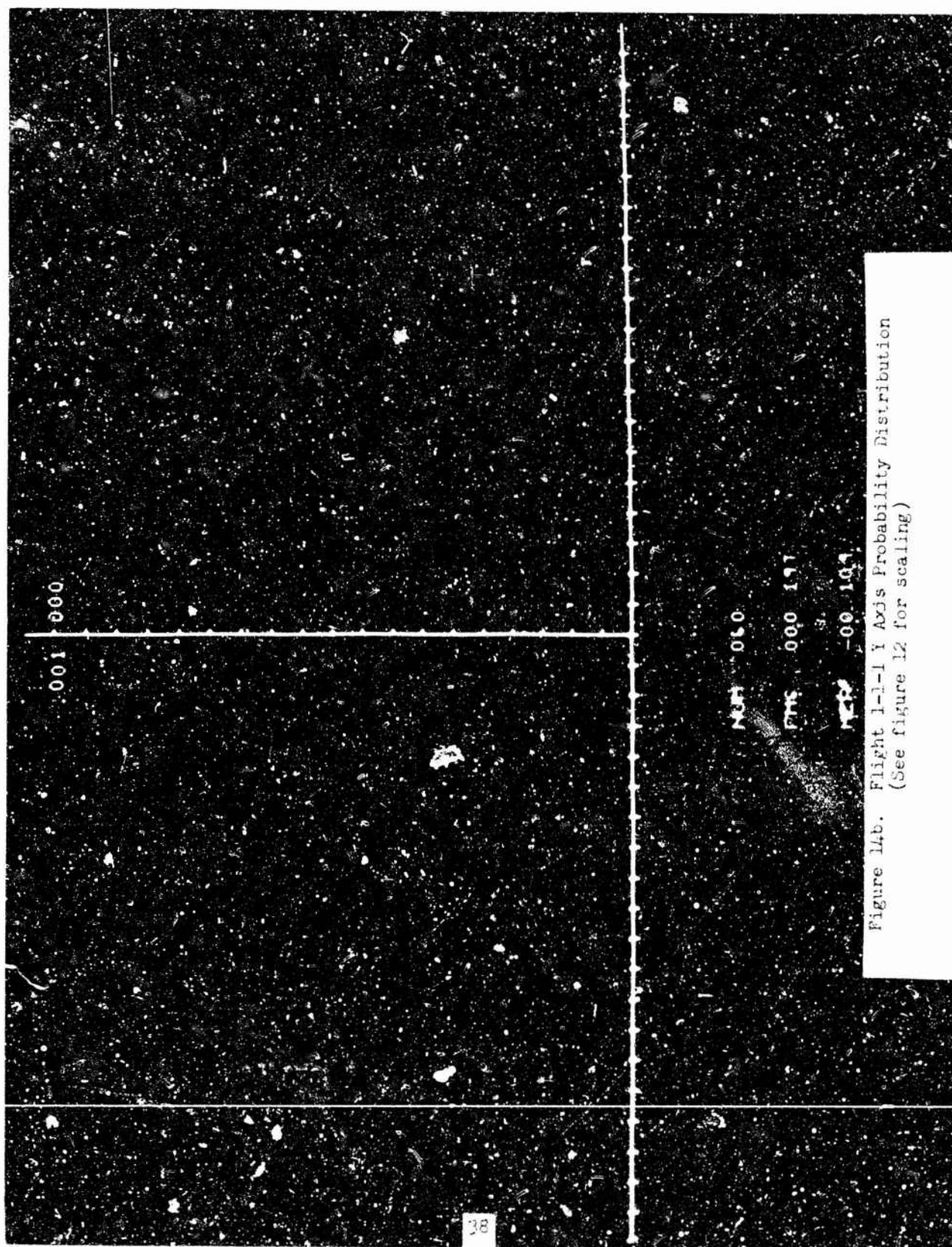
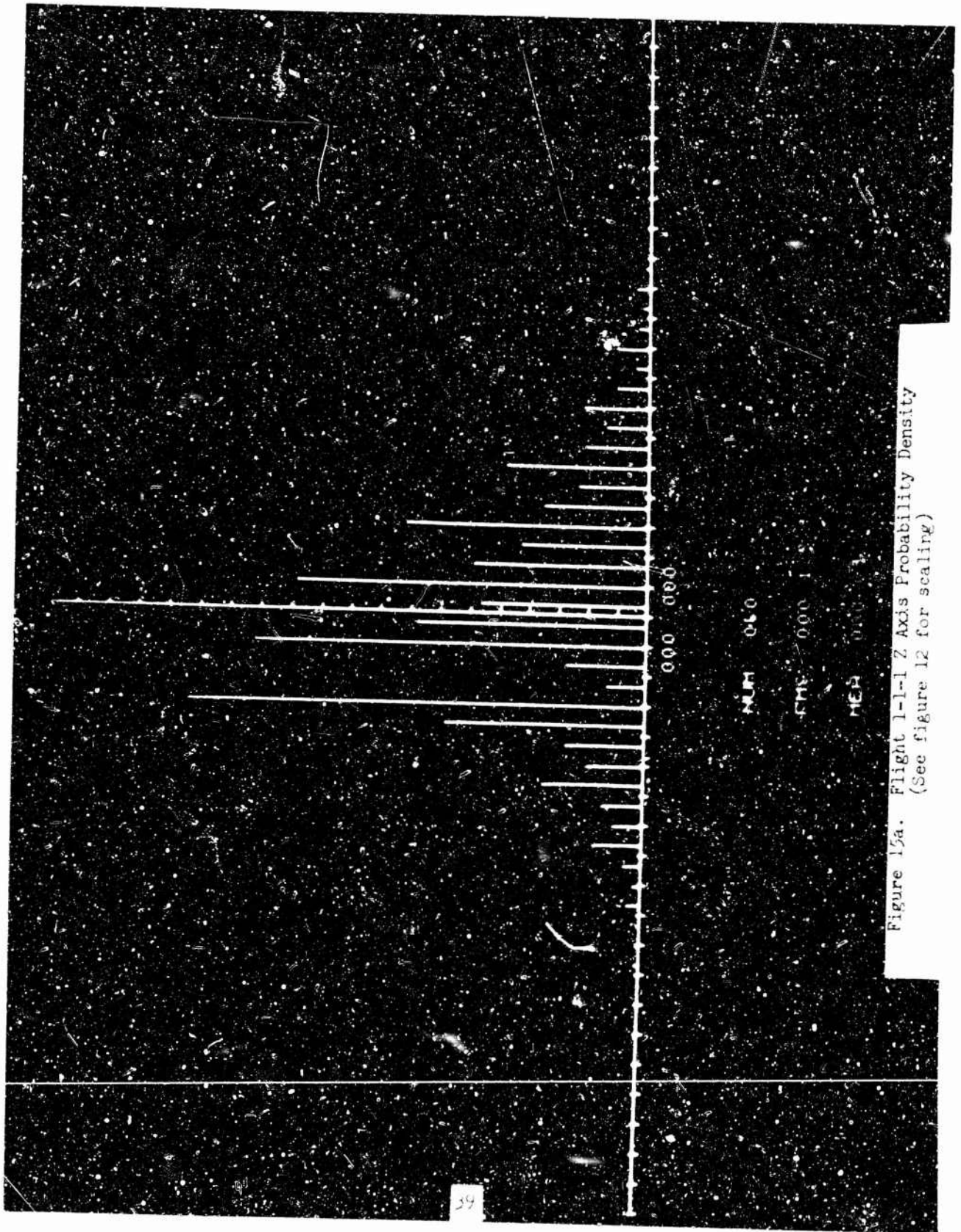
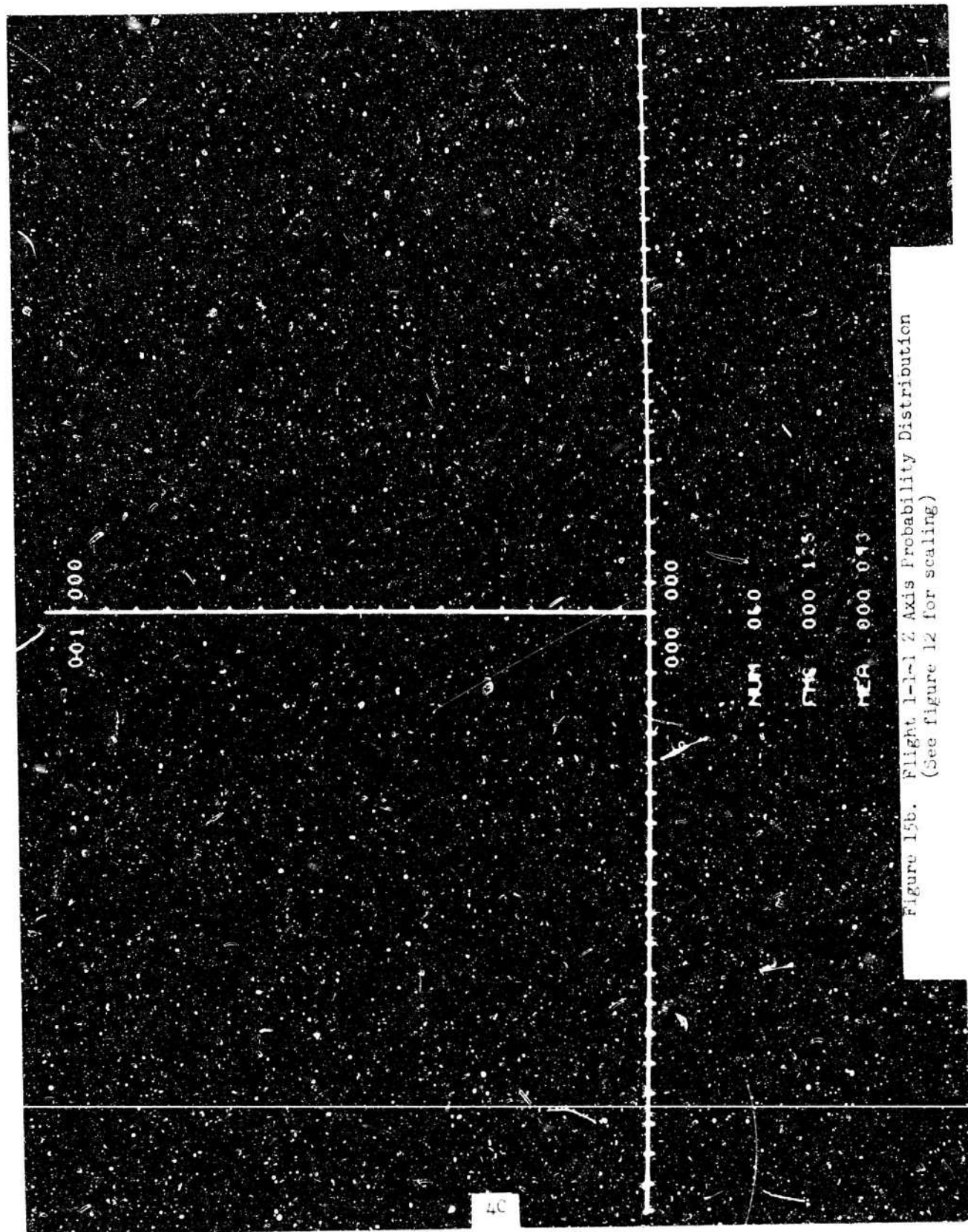


Figure 14a. Flight 1-1-1 Y Axis Probability Density
(See figure 12 for scaling)







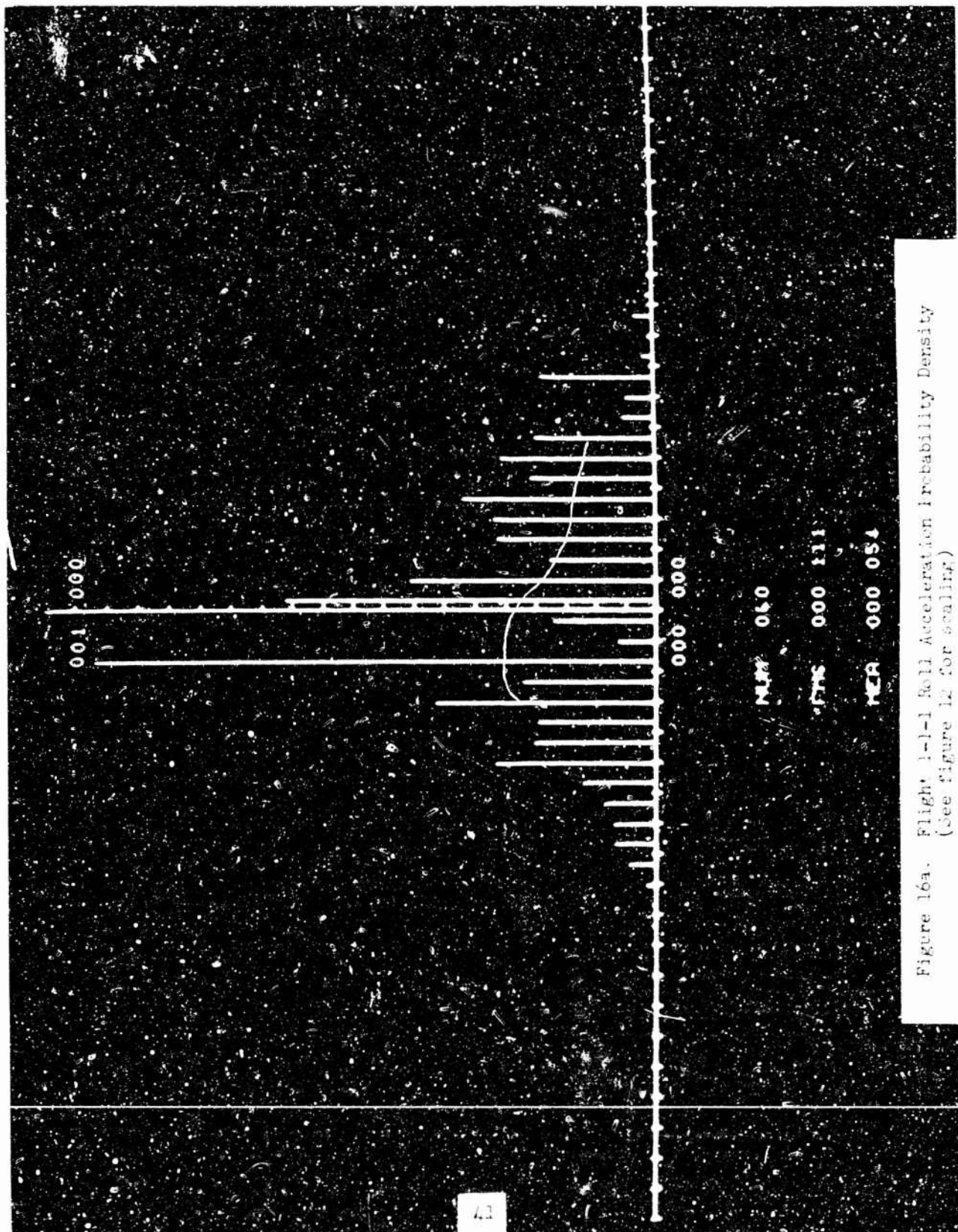
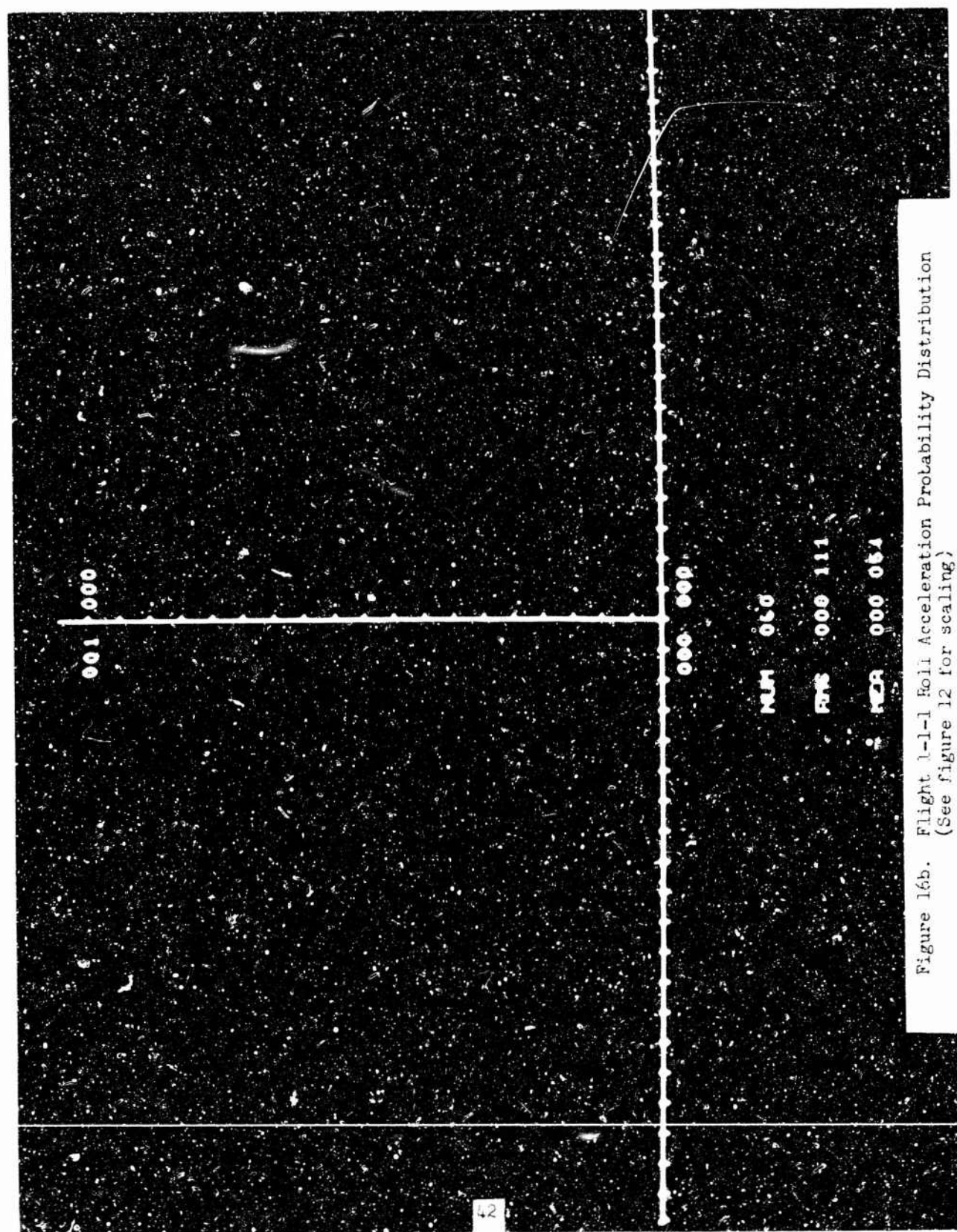


Figure 16a. Flight 1-1-1 Roll Acceleration Probability Density
(See figure 12 for scaling)



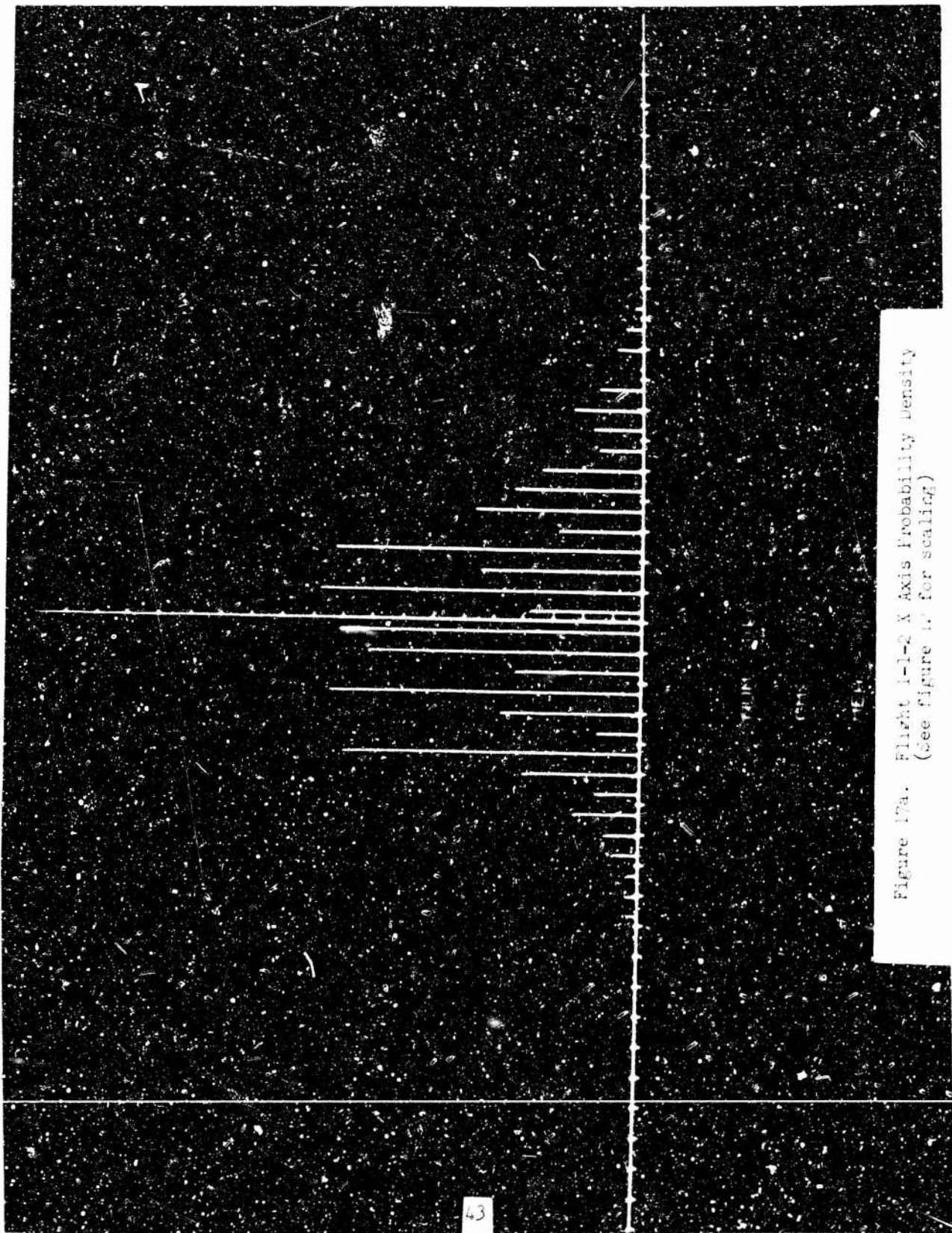


Figure 17a. Flight 1-1-2 X Axis Probability Density
(See figure 17 for scaling)

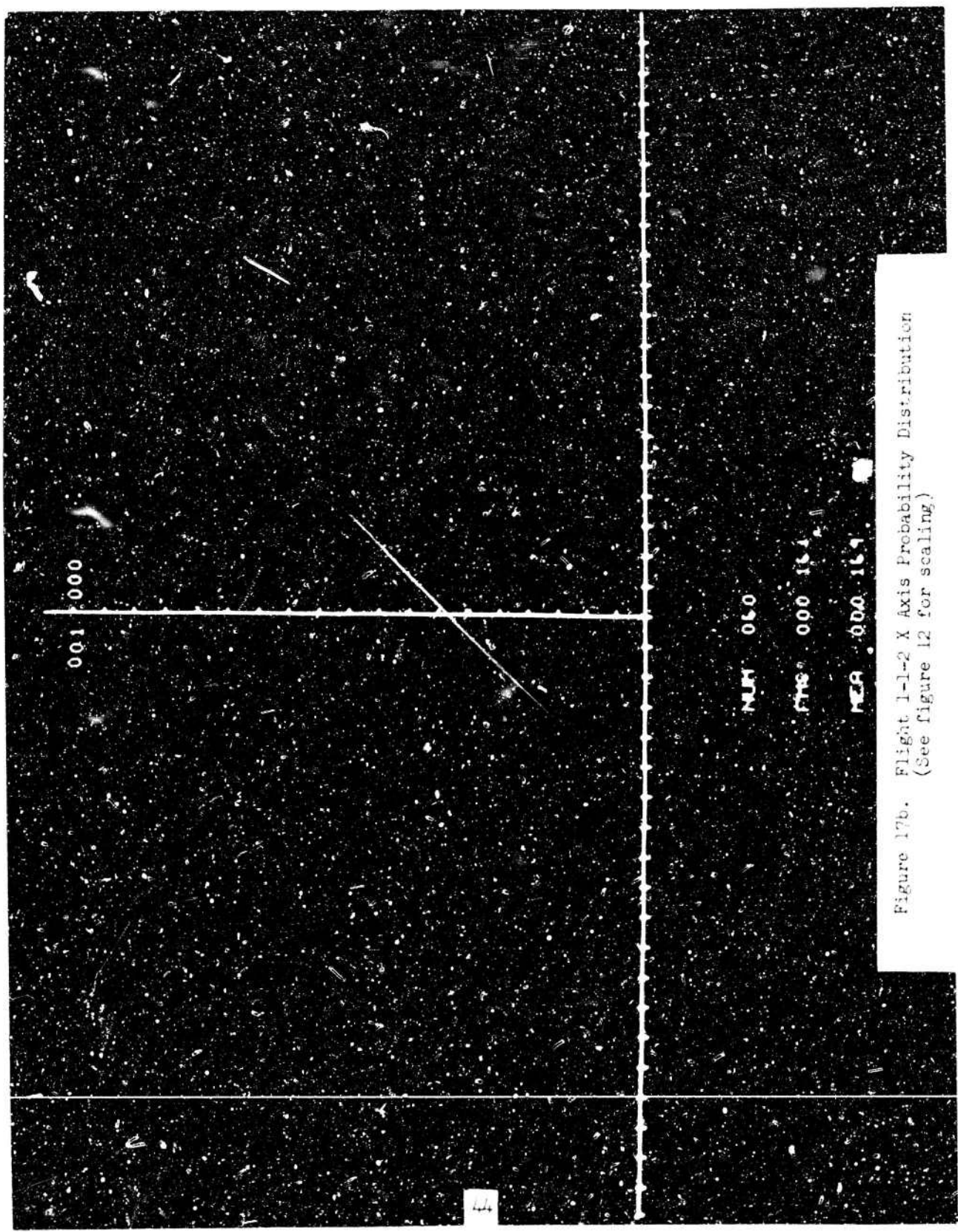


Figure 17b. Flight 1-1-2 X Axis Probability Distribution
(See figure 12 for scaling)

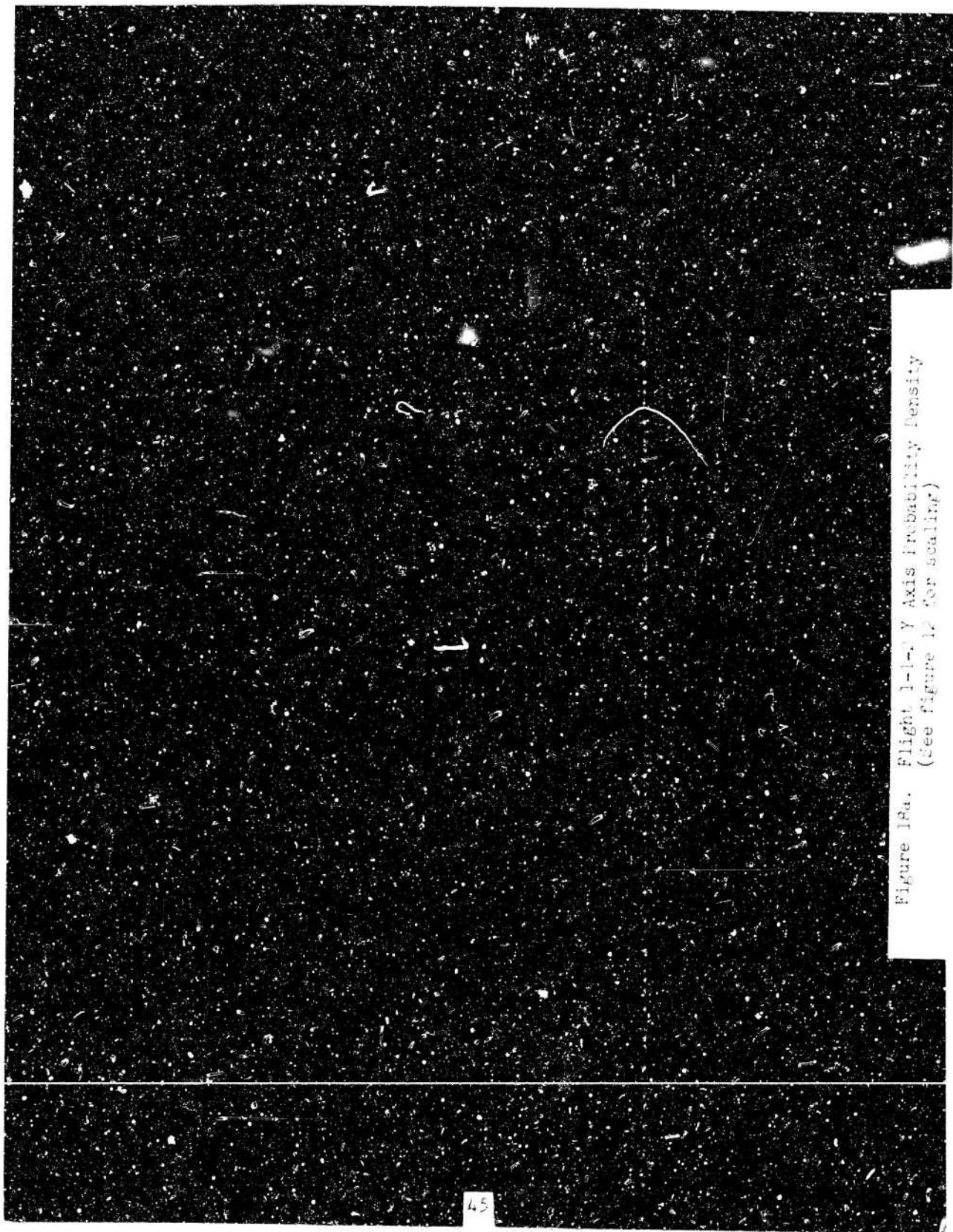


Figure 18a. Flight 1-1-77 Y Axis Probability Density
(See figure 17 for scaling)

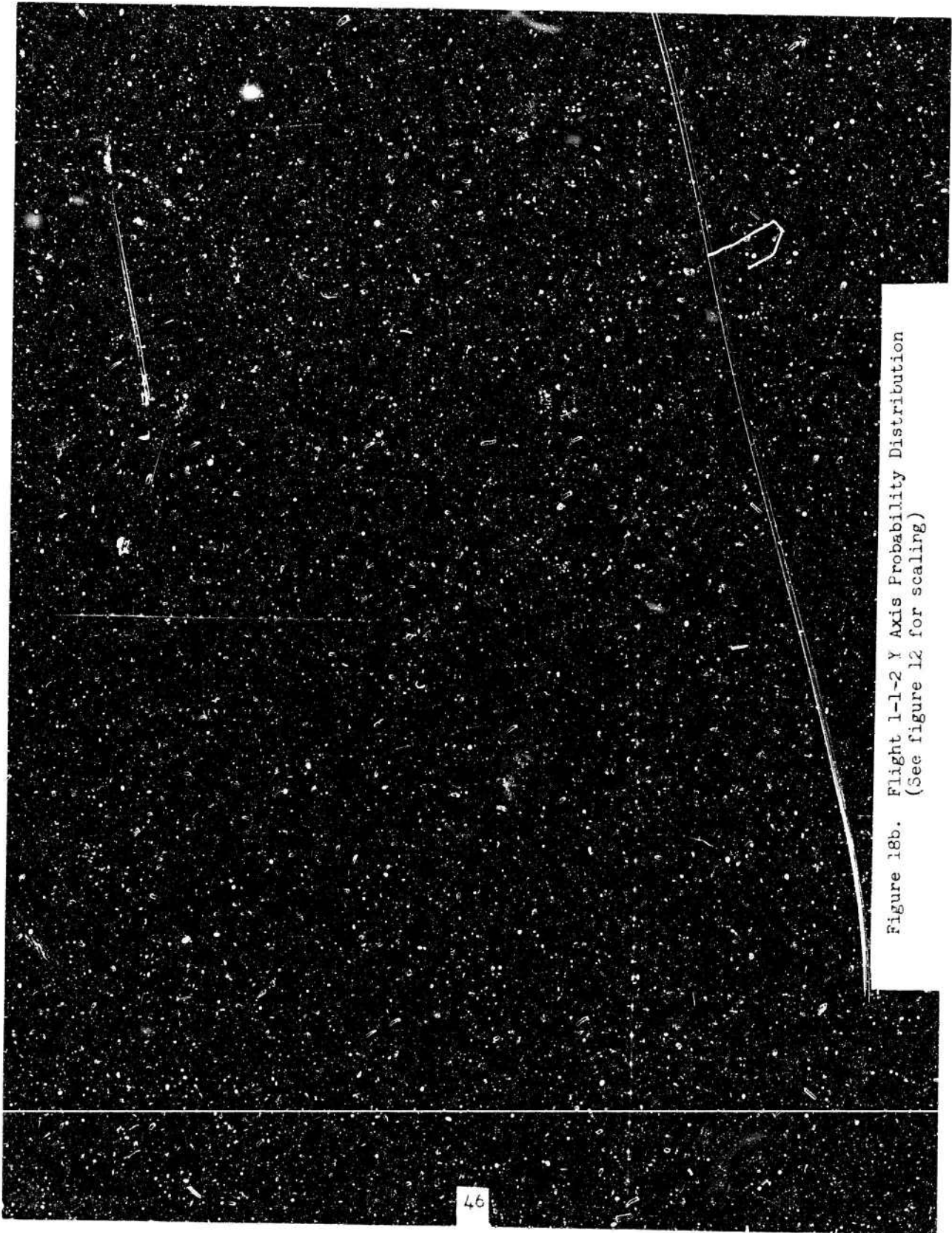


Figure 18b. Flight 1-1-2 Y Axis Probability Distribution
(See figure 12 for scaling)

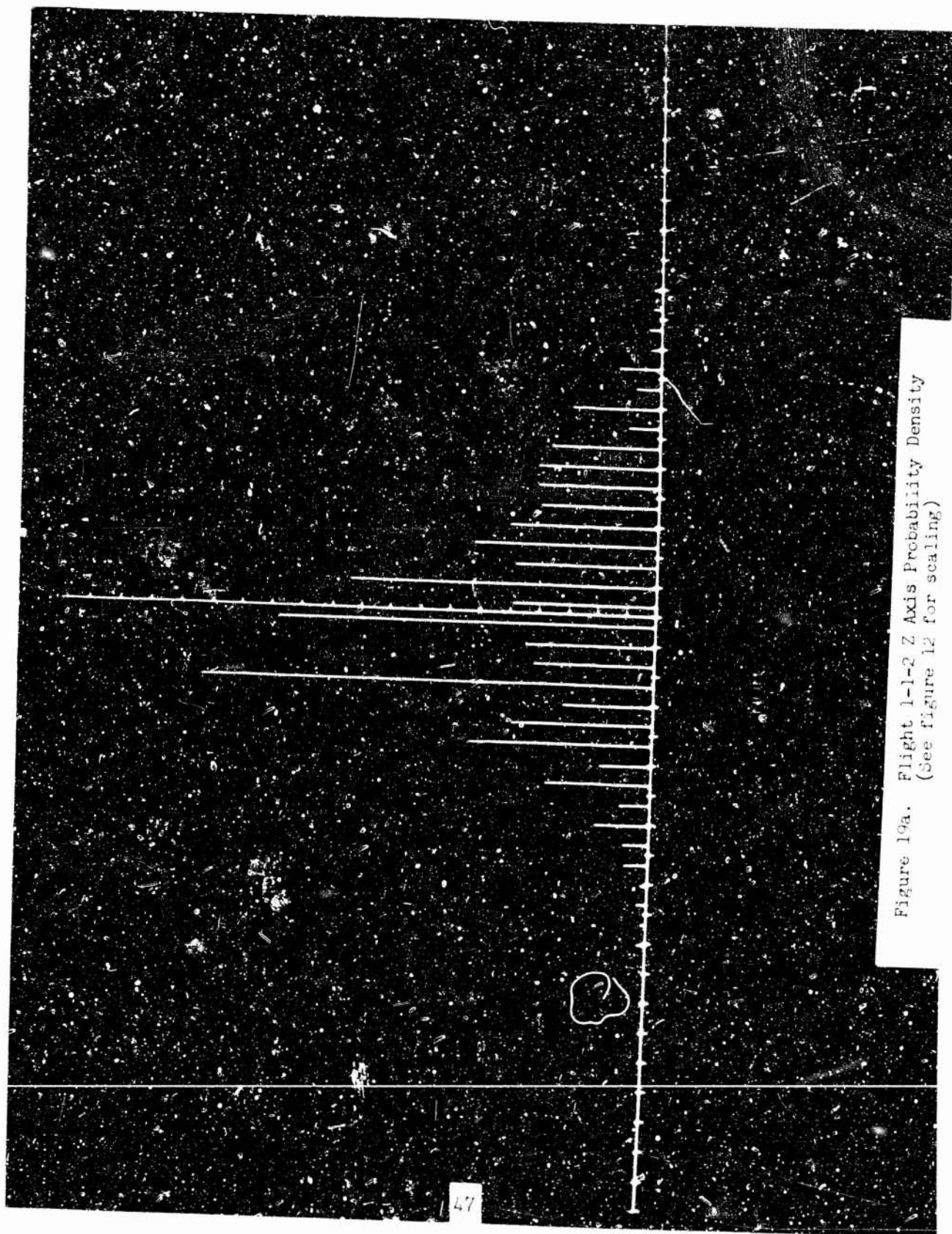


Figure 19a. Flight 1-1-2 Z Axis Probability Density
(See figure 12 for scaling)

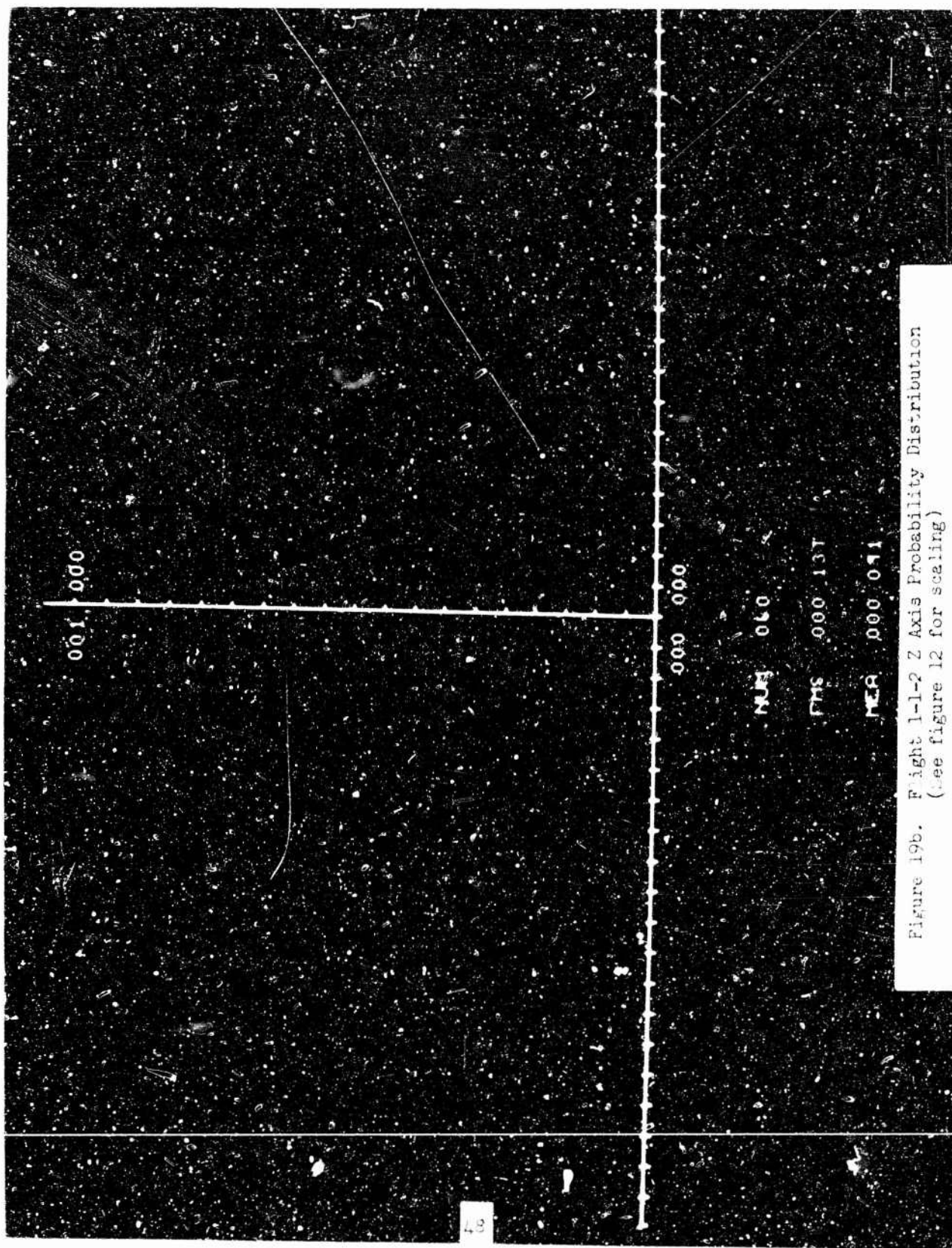
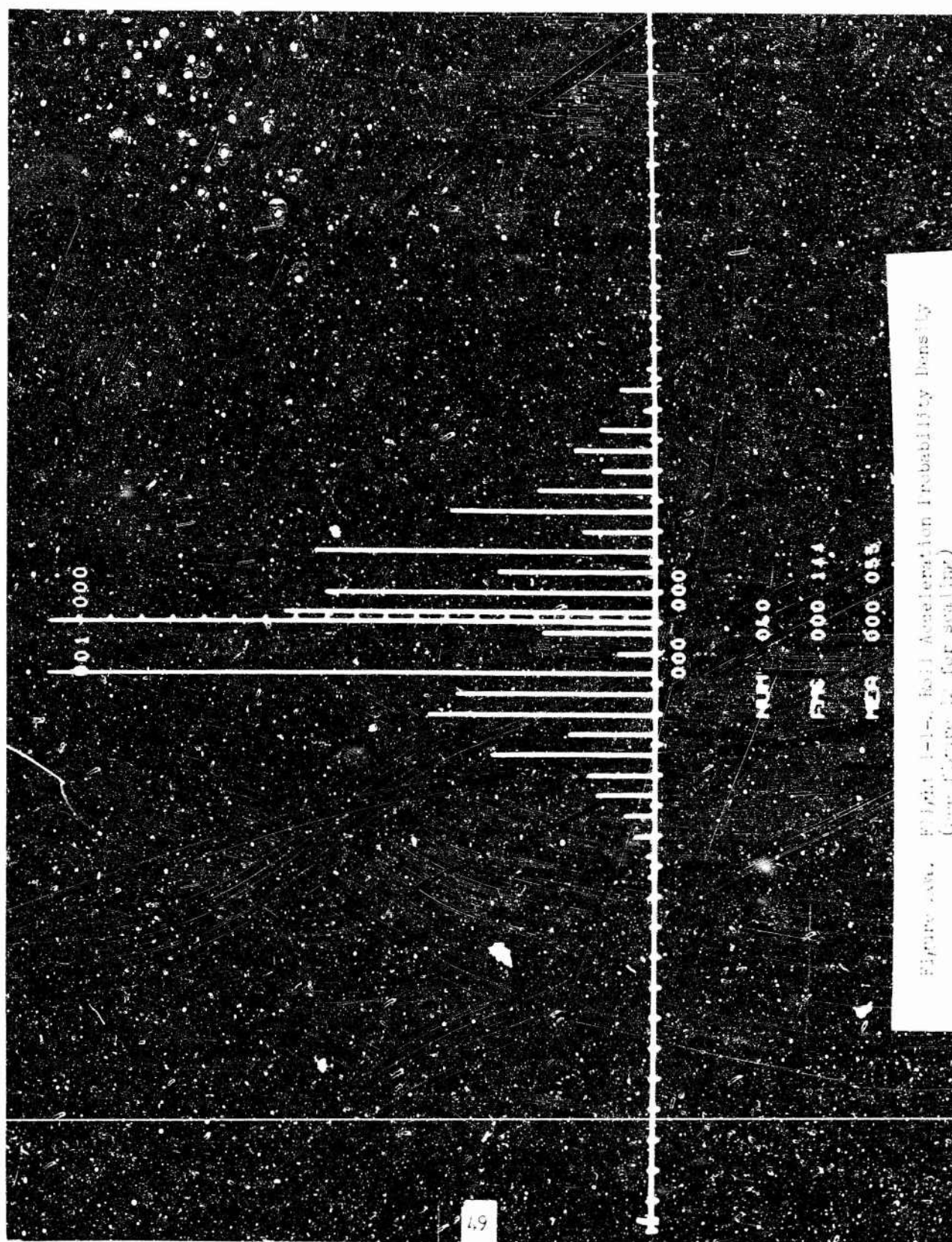
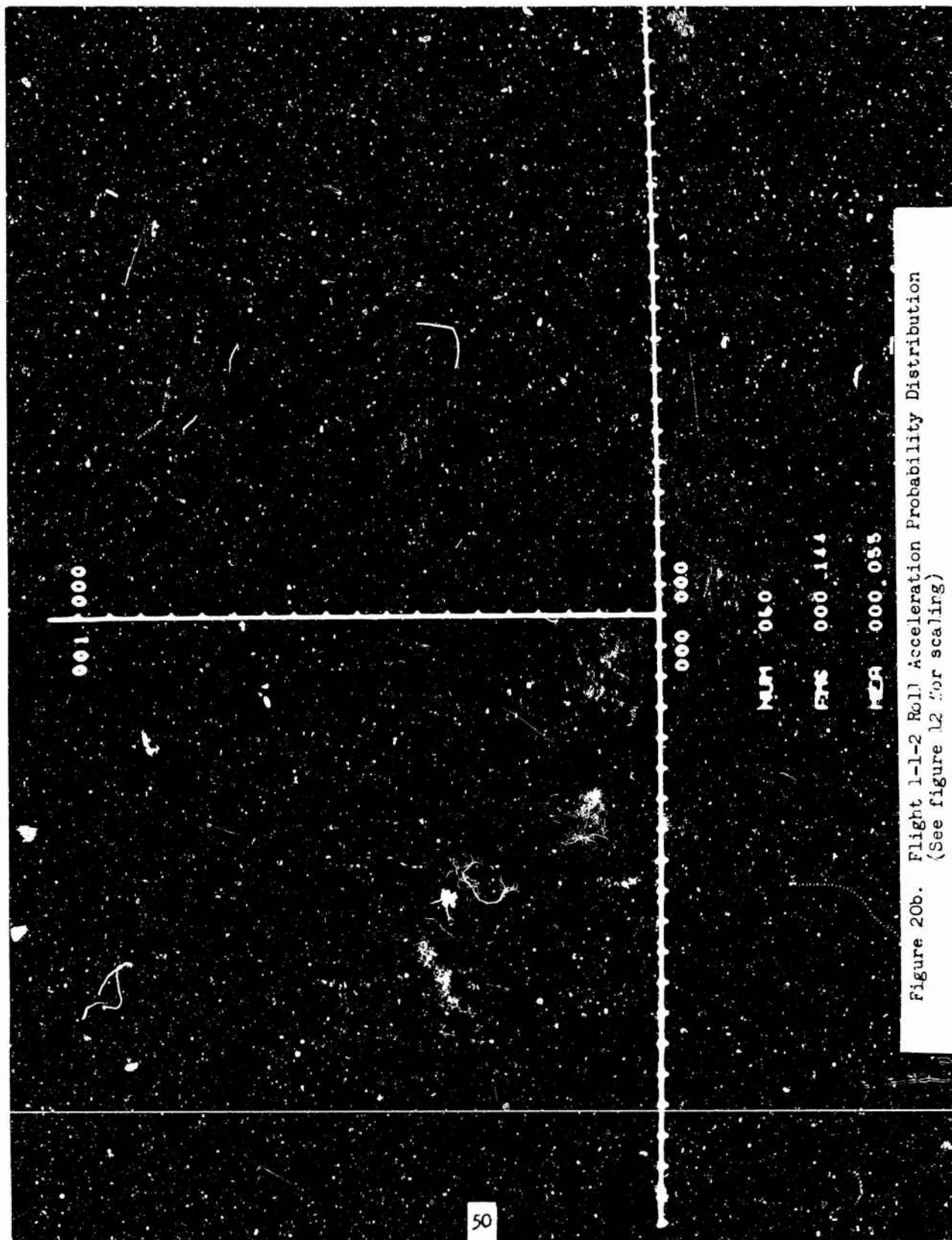


Figure 19b. Flight 1-1-2 Z Axis Probability Distribution
(see figure 12 for scaling)





001 000

000 000

MUM 060

ENS 000 144

MCA 000 055

Figure 20b. Flight 1-1-2 Roll Acceleration Probability Distribution
(See figure 12 for scaling)

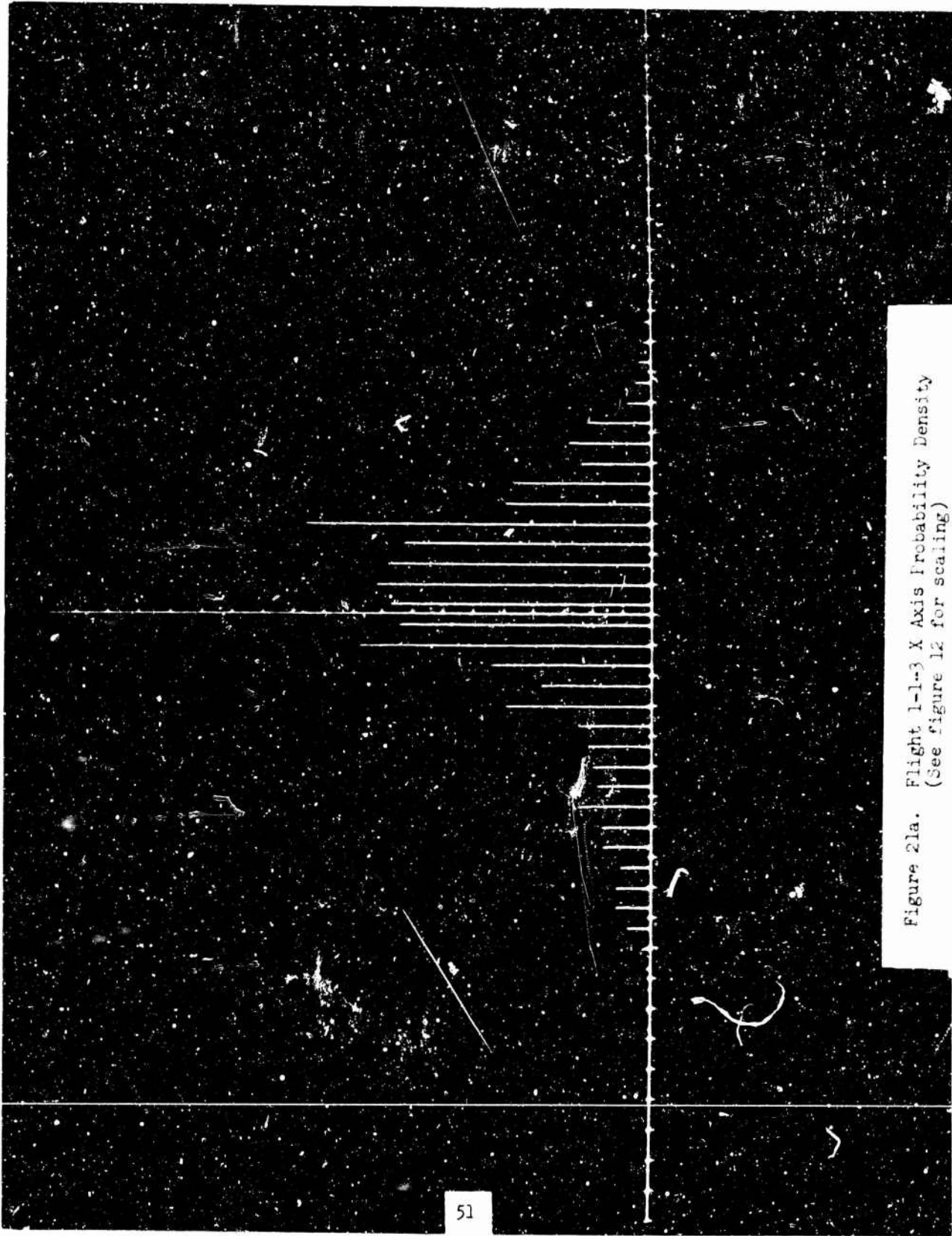


Figure 21a. Flight 1-1-3 X Axis Probability Density
(See figure 12 for scaling)

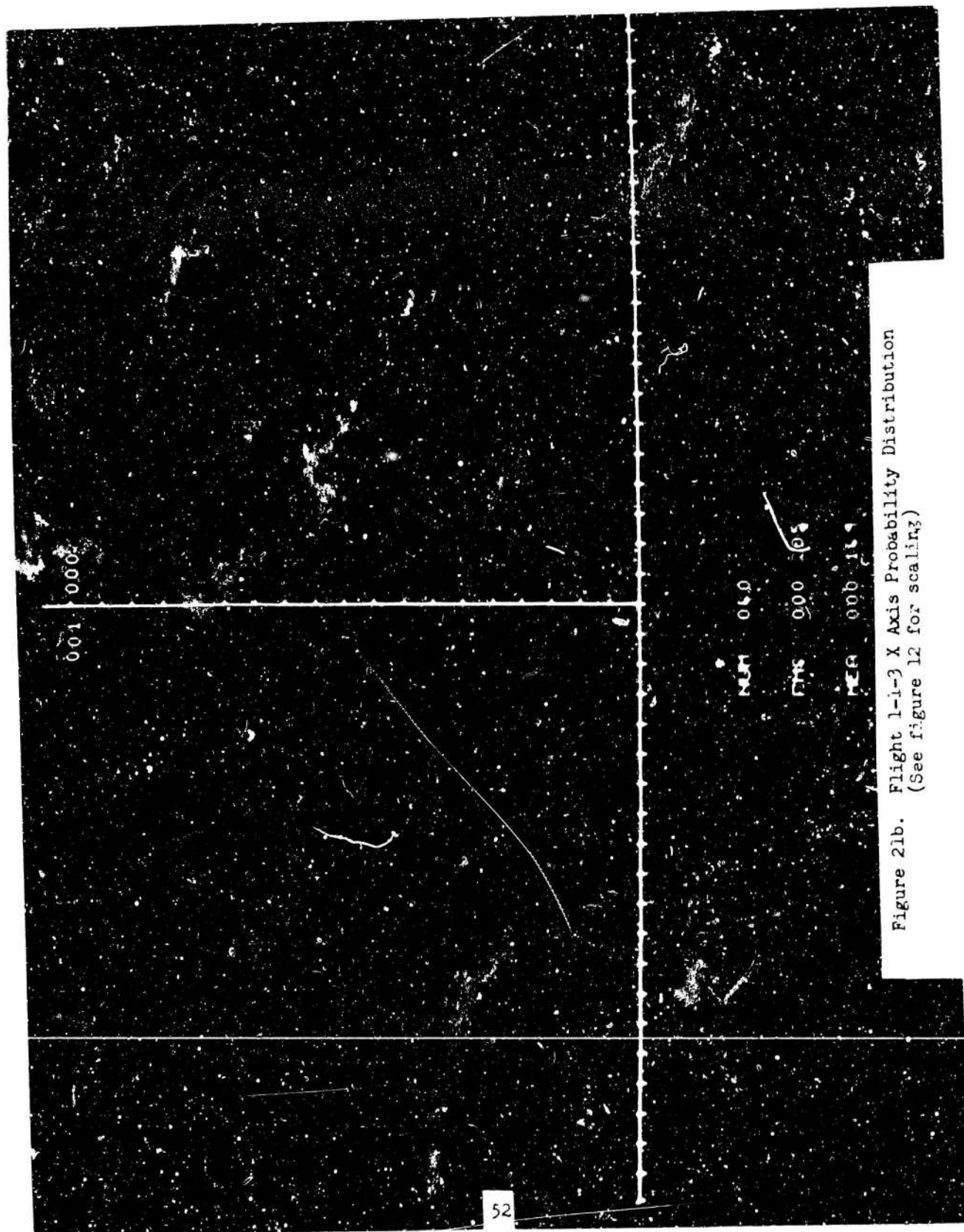


Figure 21b. Flight 1-i-3 X Axis Probability Distribution
(See figure 12 for scaling)

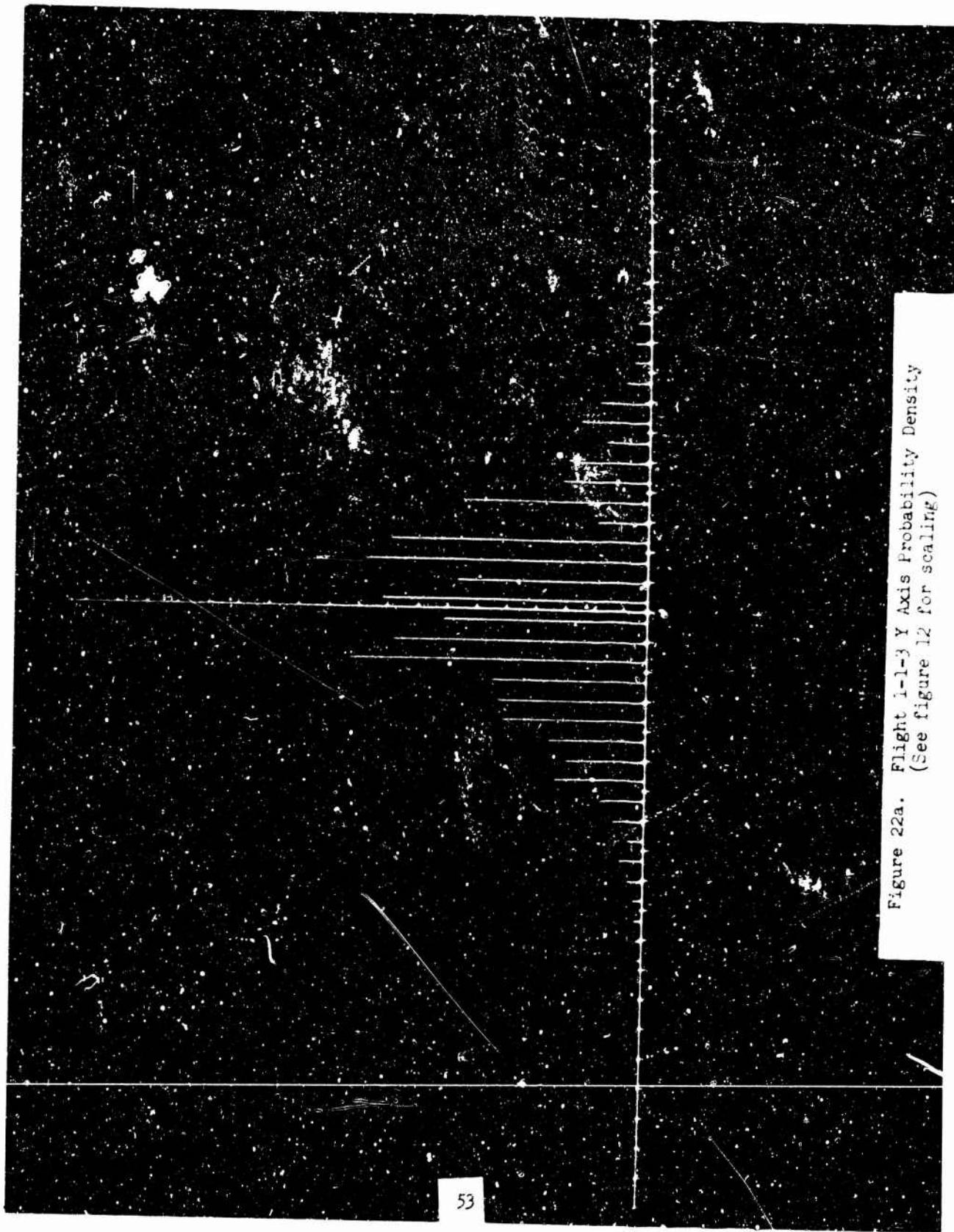


Figure 22a. Flight 1-1-3 Y Axis Probability Density
(See figure 12 for scaling)

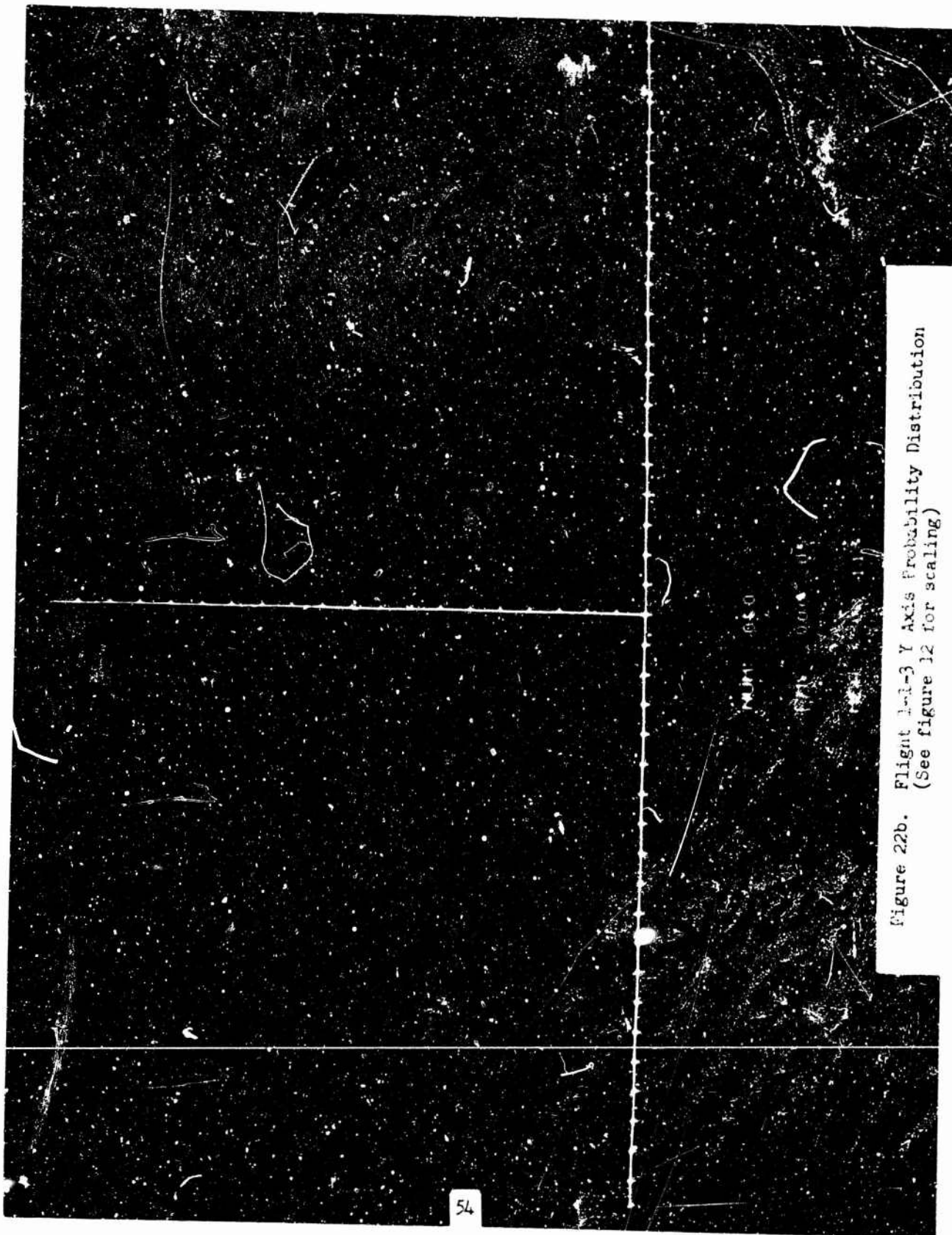


Figure 22b. Flight 1-1-3 Y Axis Probability Distribution
(See figure 12 for scaling)

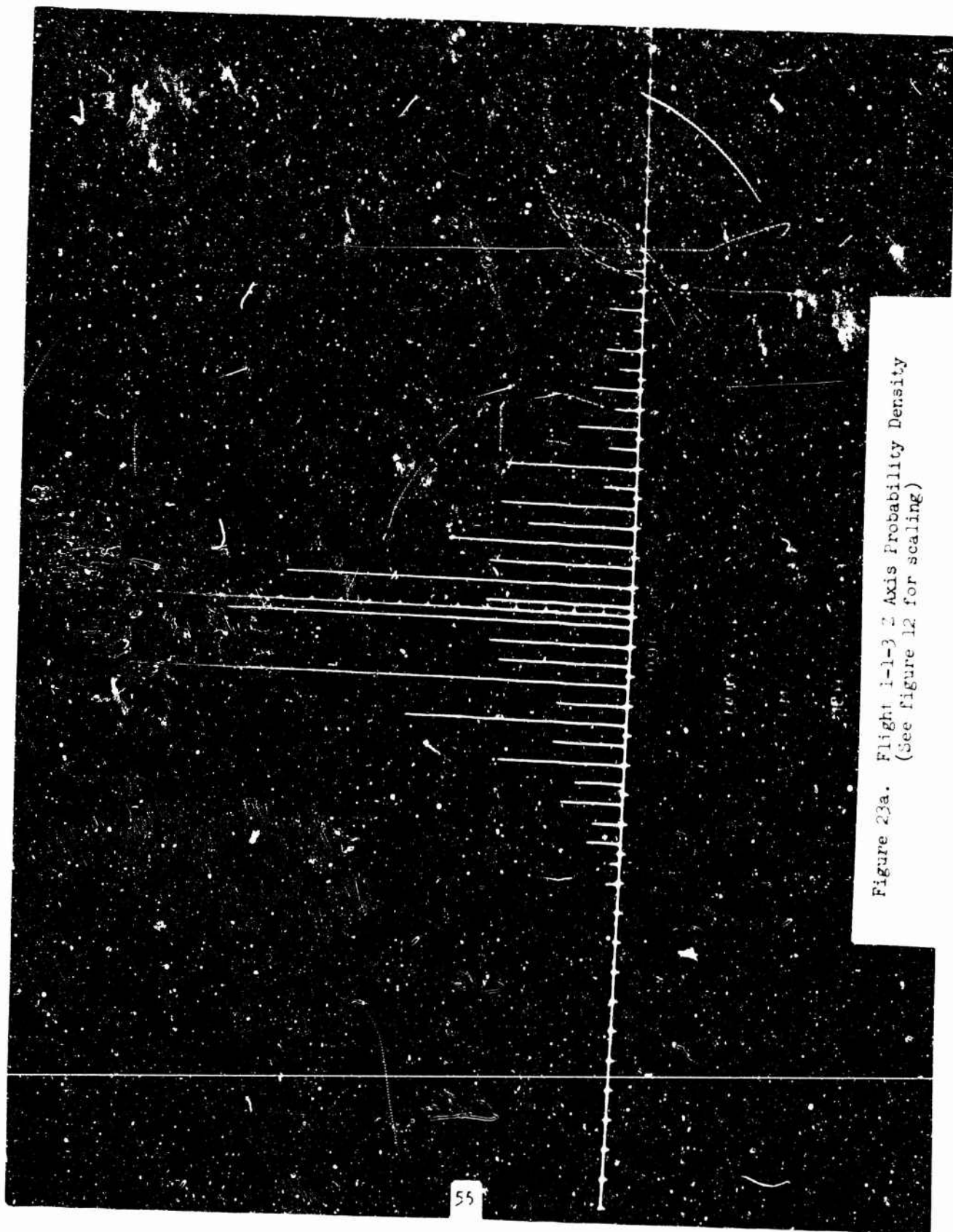


Figure 23a. Flight 1-1-3 Z Axis Probability Density
(See figure 12 for scaling)

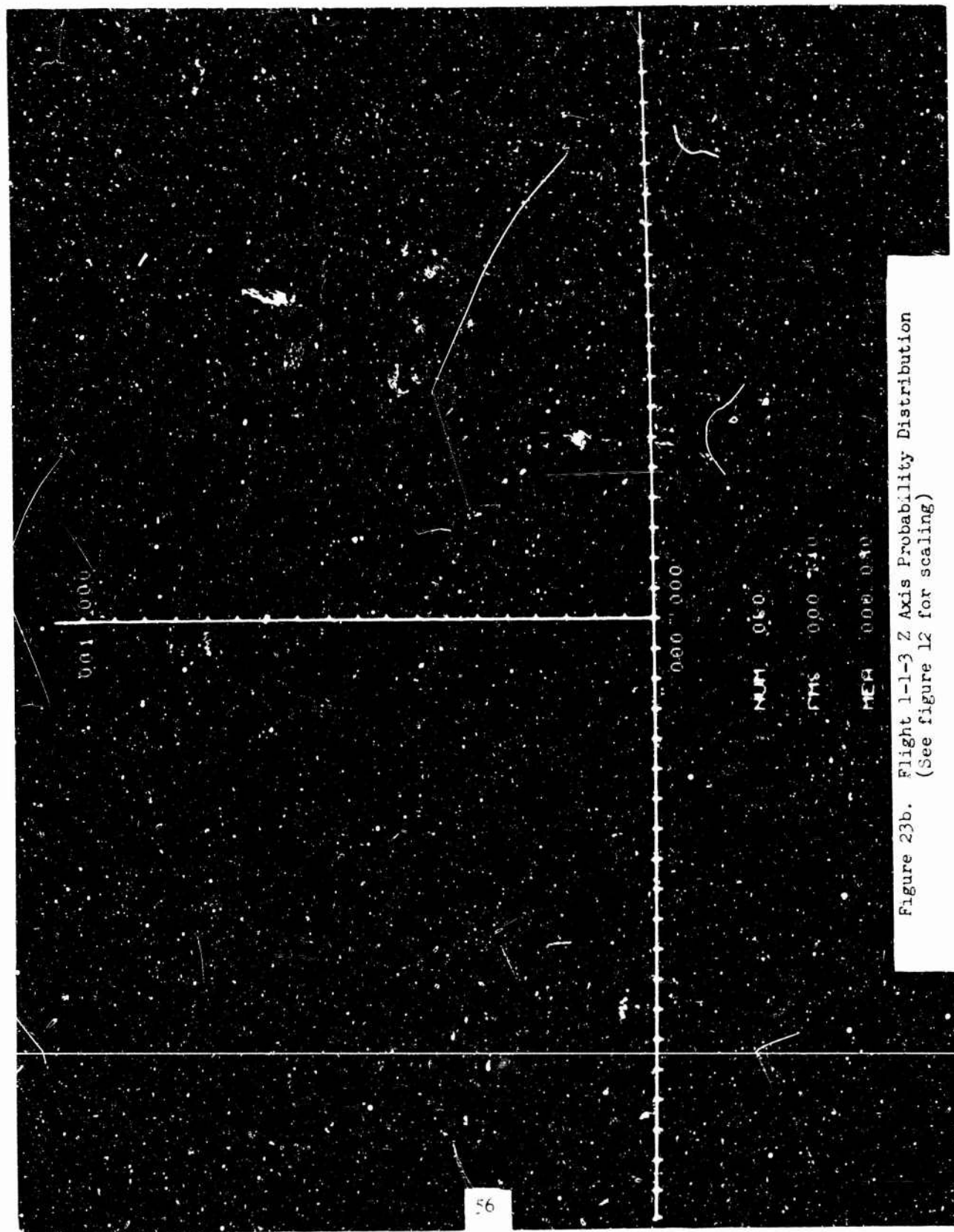
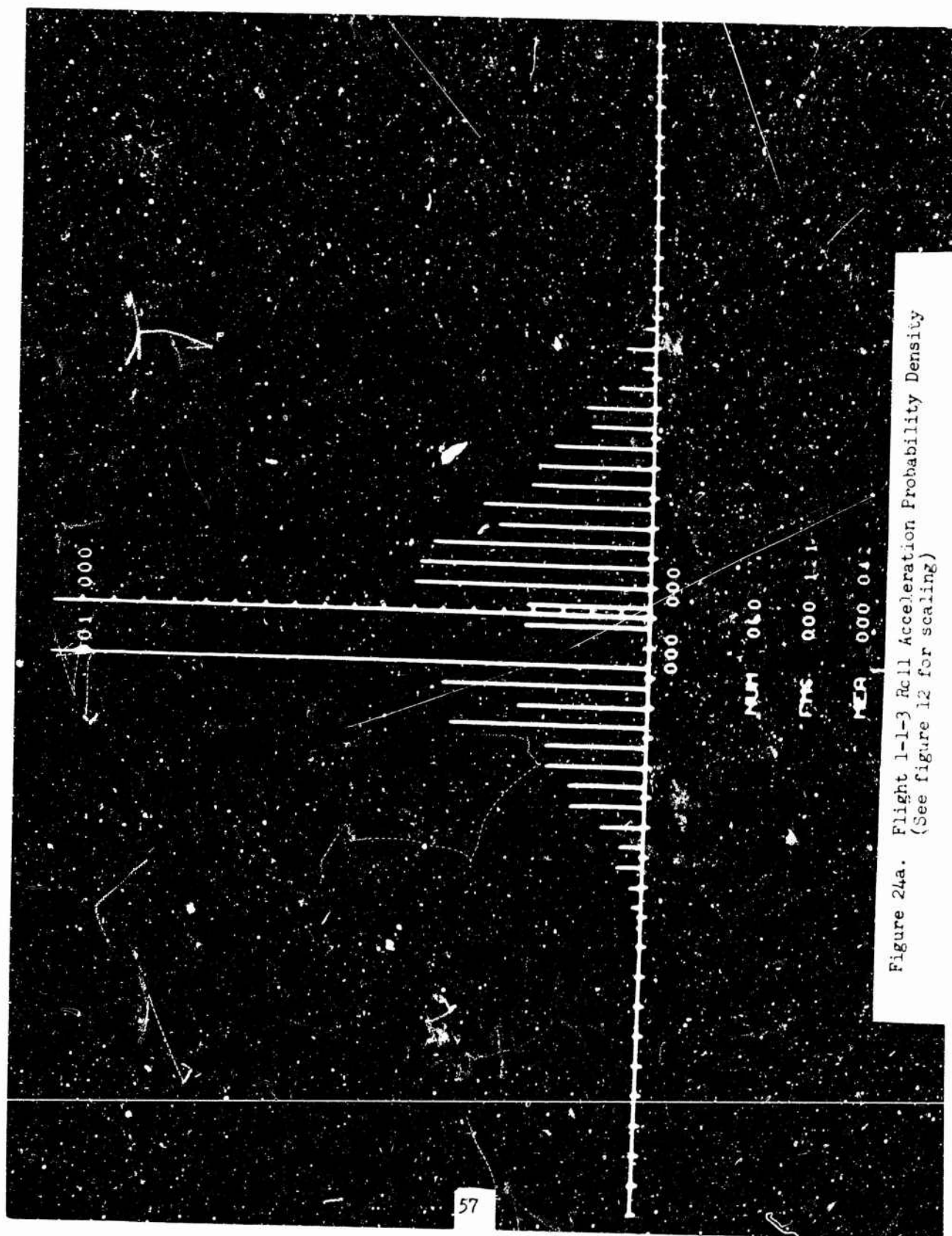


Figure 23b. Flight 1-1-3 Z Axis Probability Distribution
(See figure 12 for scaling)



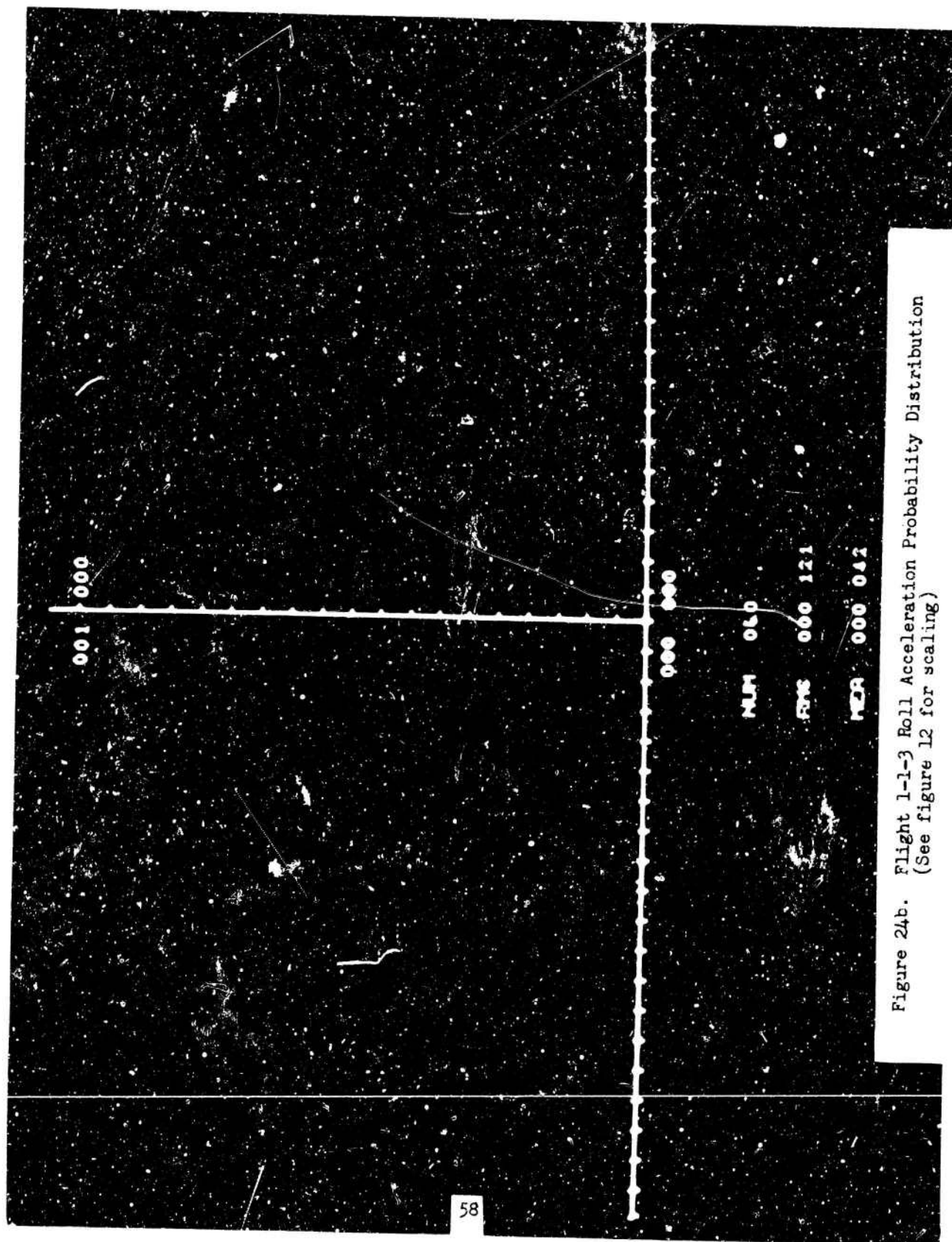


Figure 24b. Flight 1-1-3 Roll Acceleration Probability Distribution
(See figure 12 for scaling)

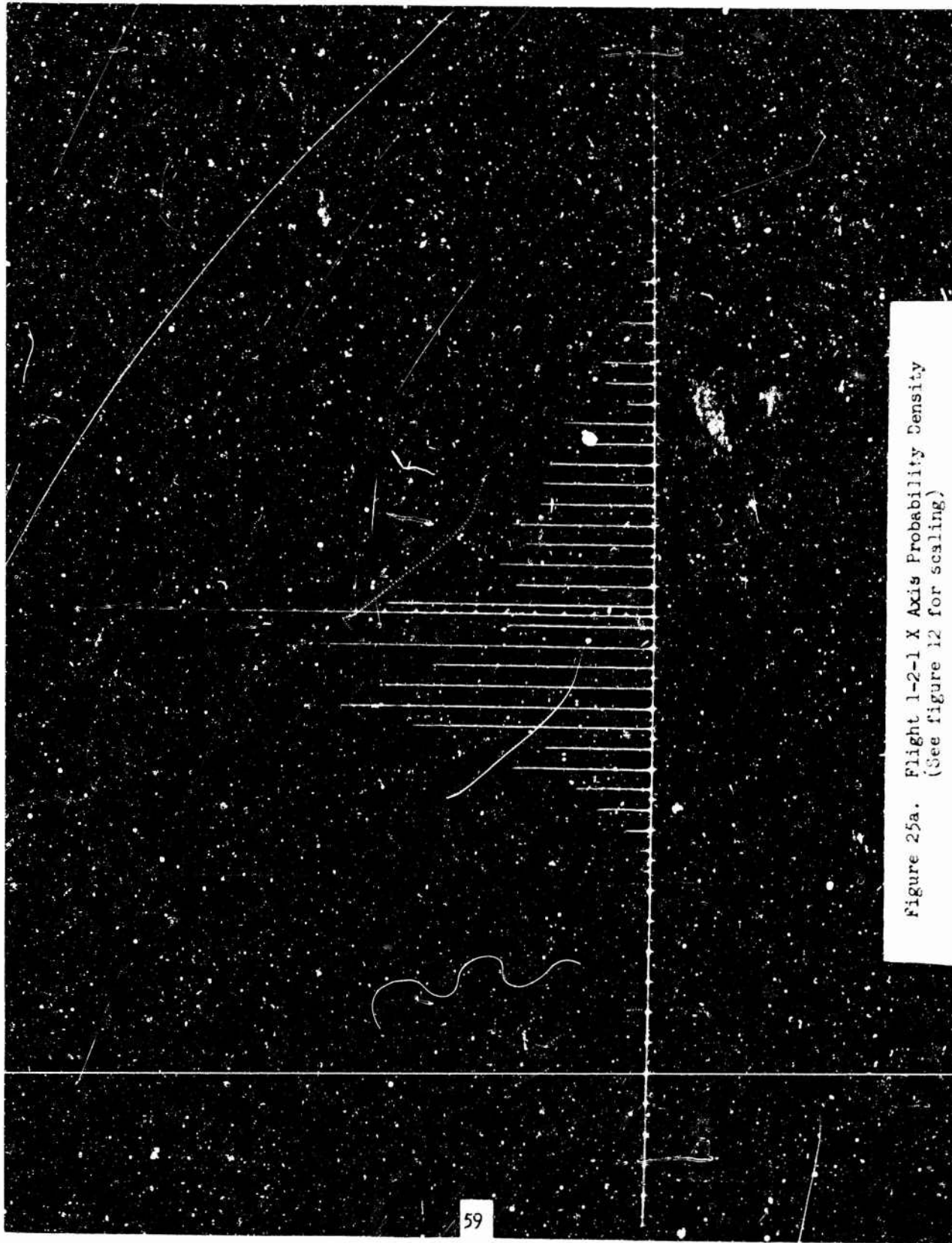


Figure 25a. Flight 1-2-1 X Axis Probability Density
(See figure 12 for scaling)

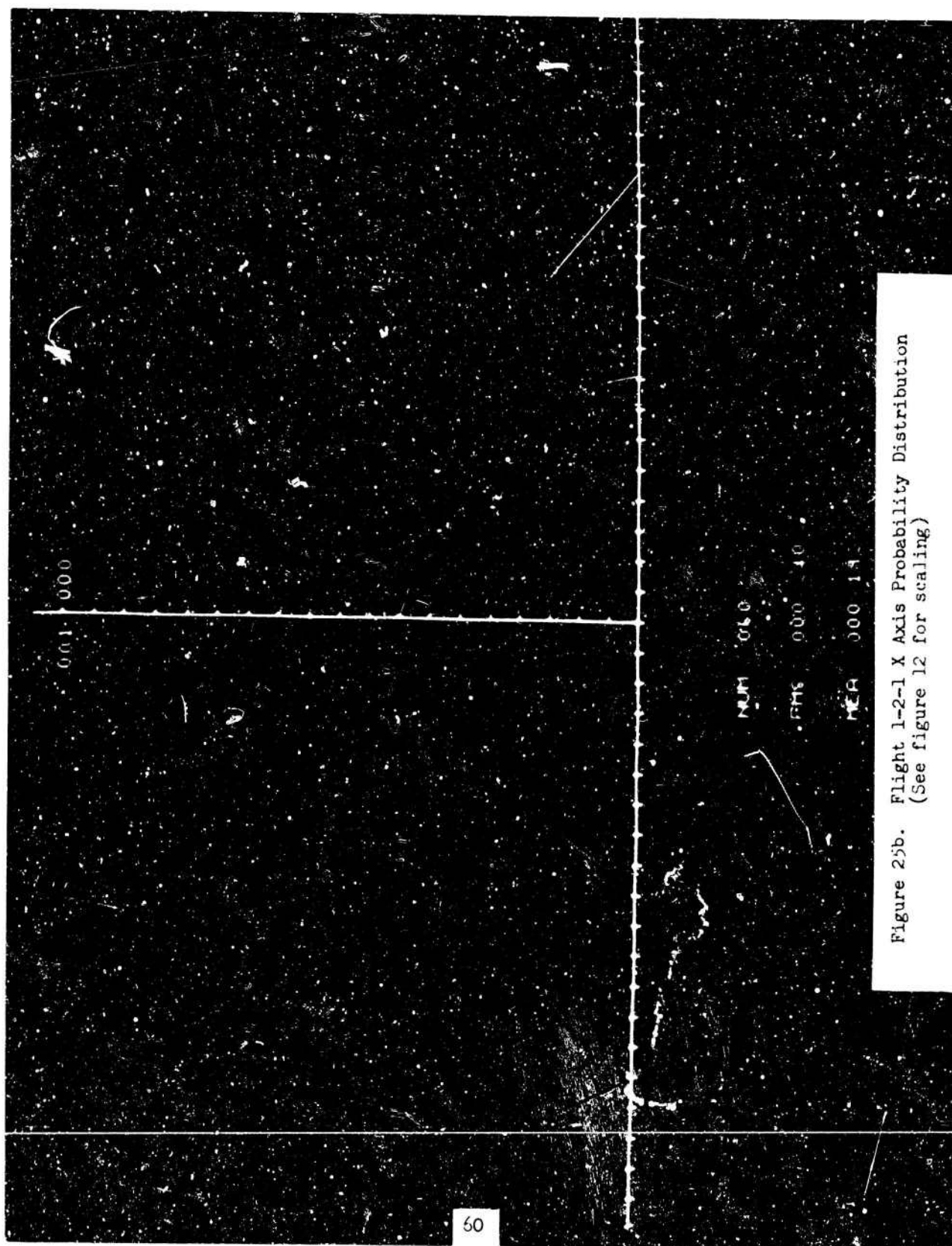


Figure 26a. Flight 1-2-1 Y Axis Probability Density
(See figure 12 for scaling)

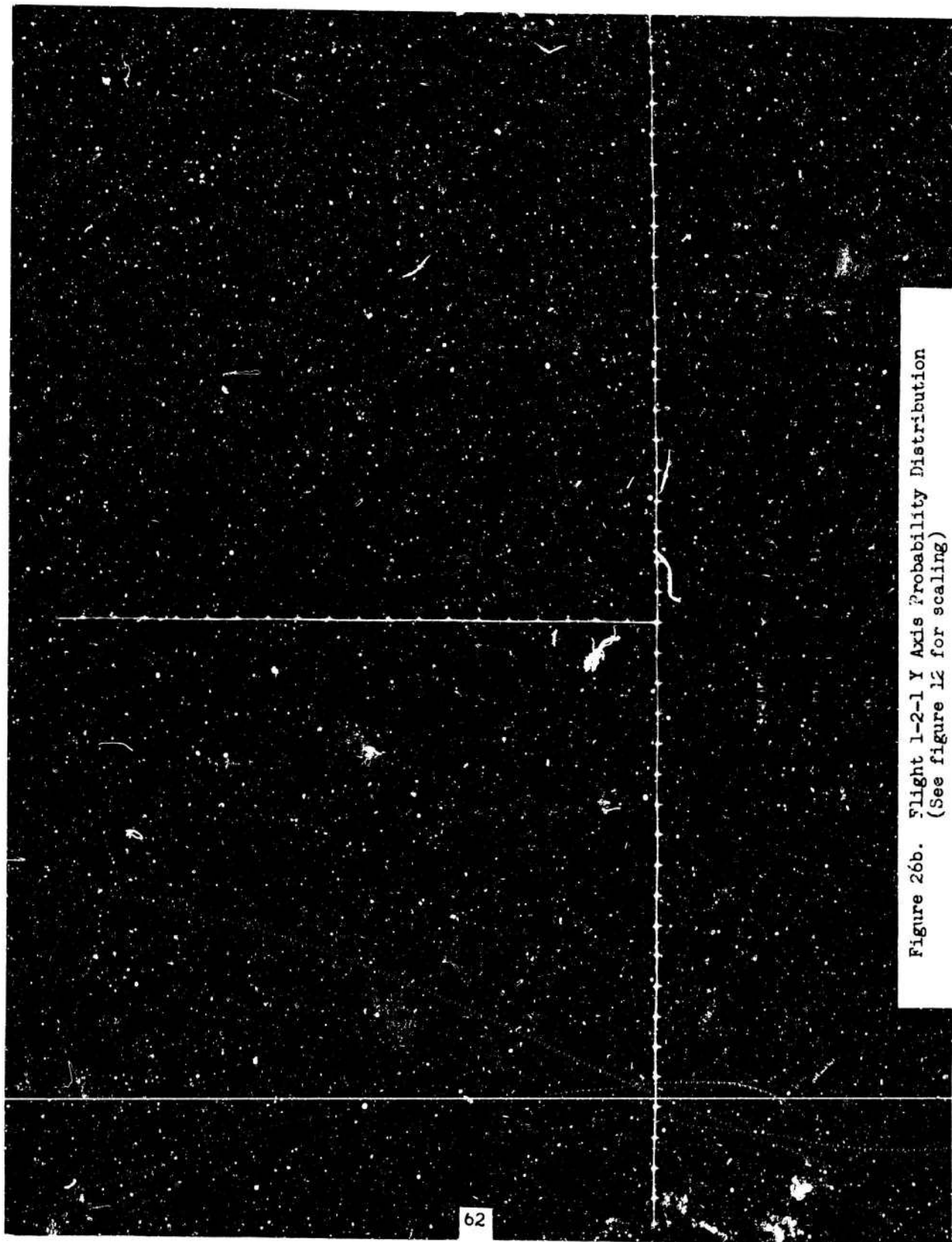


Figure 26b. Flight 1-2-1 Y Axis Probability Distribution
(See figure 12 for scaling)

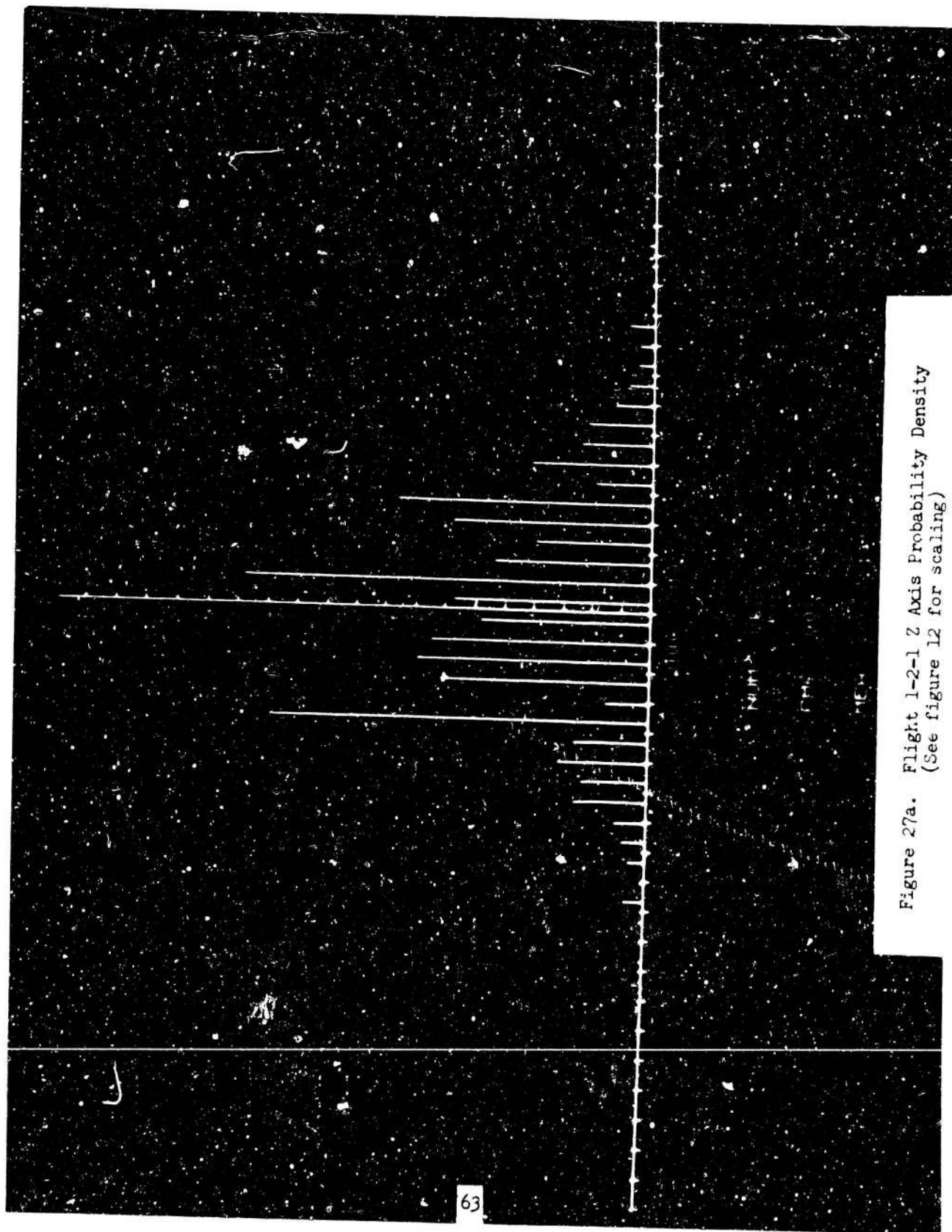


Figure 27a. Flight 1-2-1 Z Axis Probability Density
(See figure 12 for scaling)

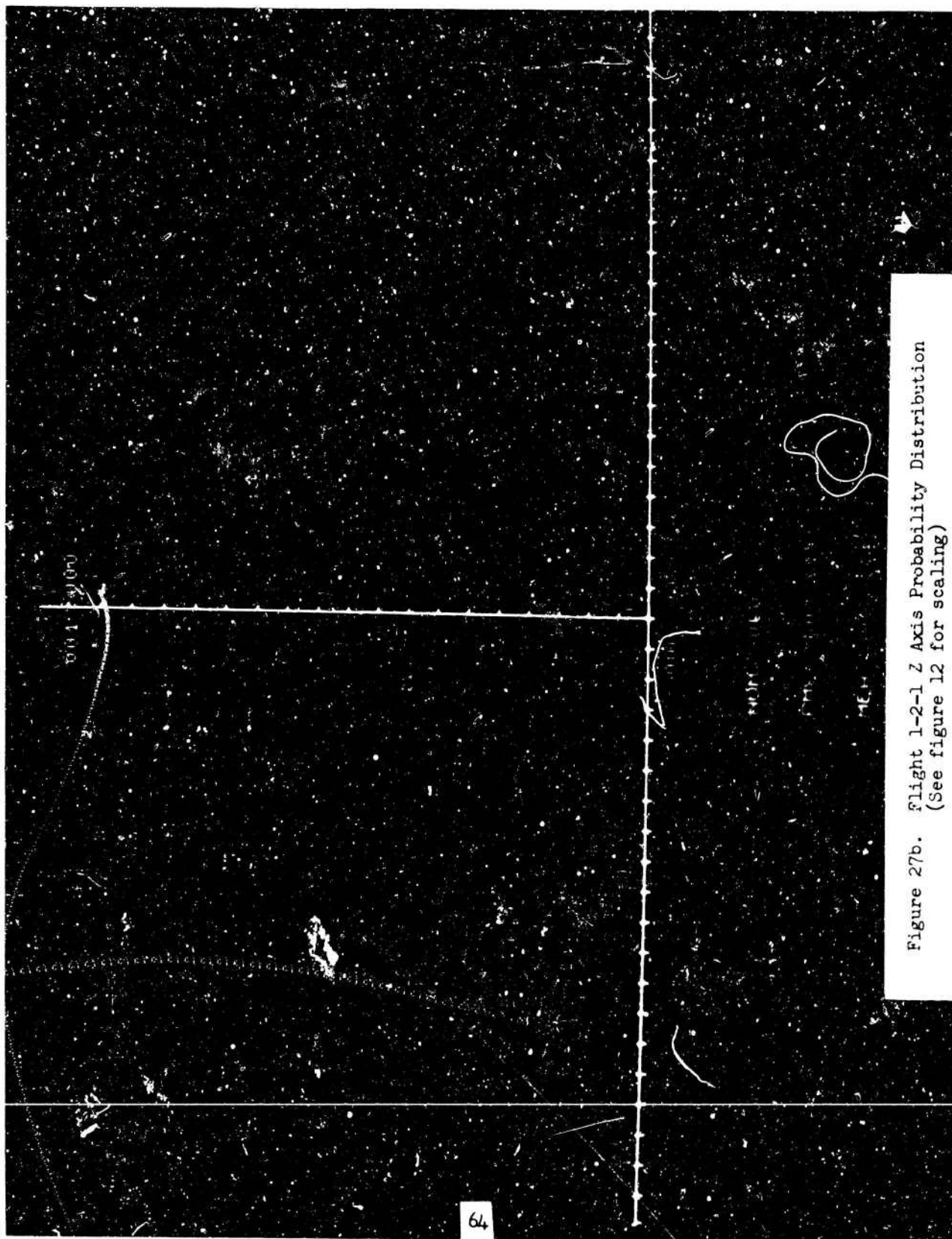


Figure 27b. Flight 1-2-1 Z Axis Probability Distribution
(See figure 12 for scaling)

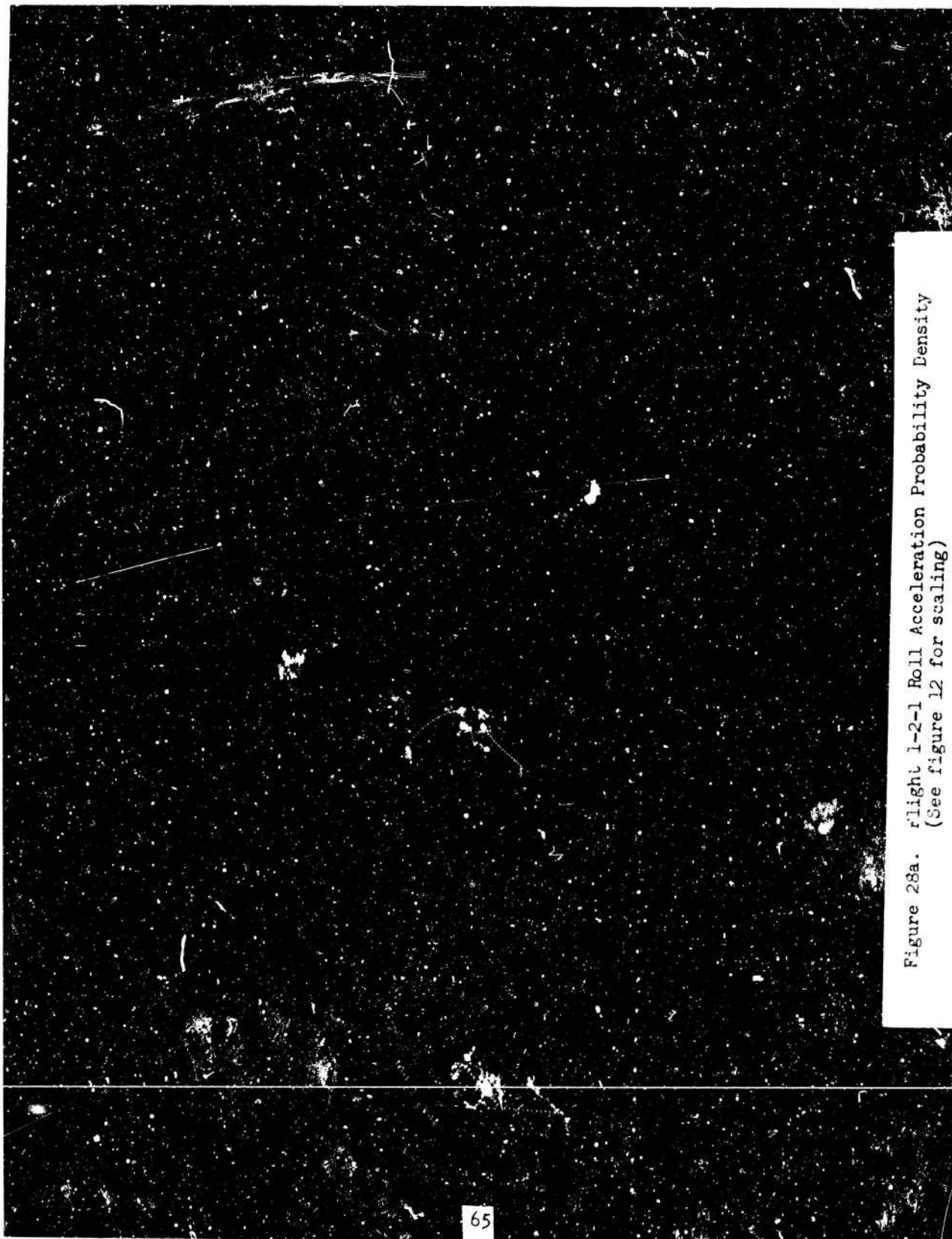


Figure 28a. Flight 1-2-1 Roll Acceleration Probability Density
(See figure 12 for scaling)

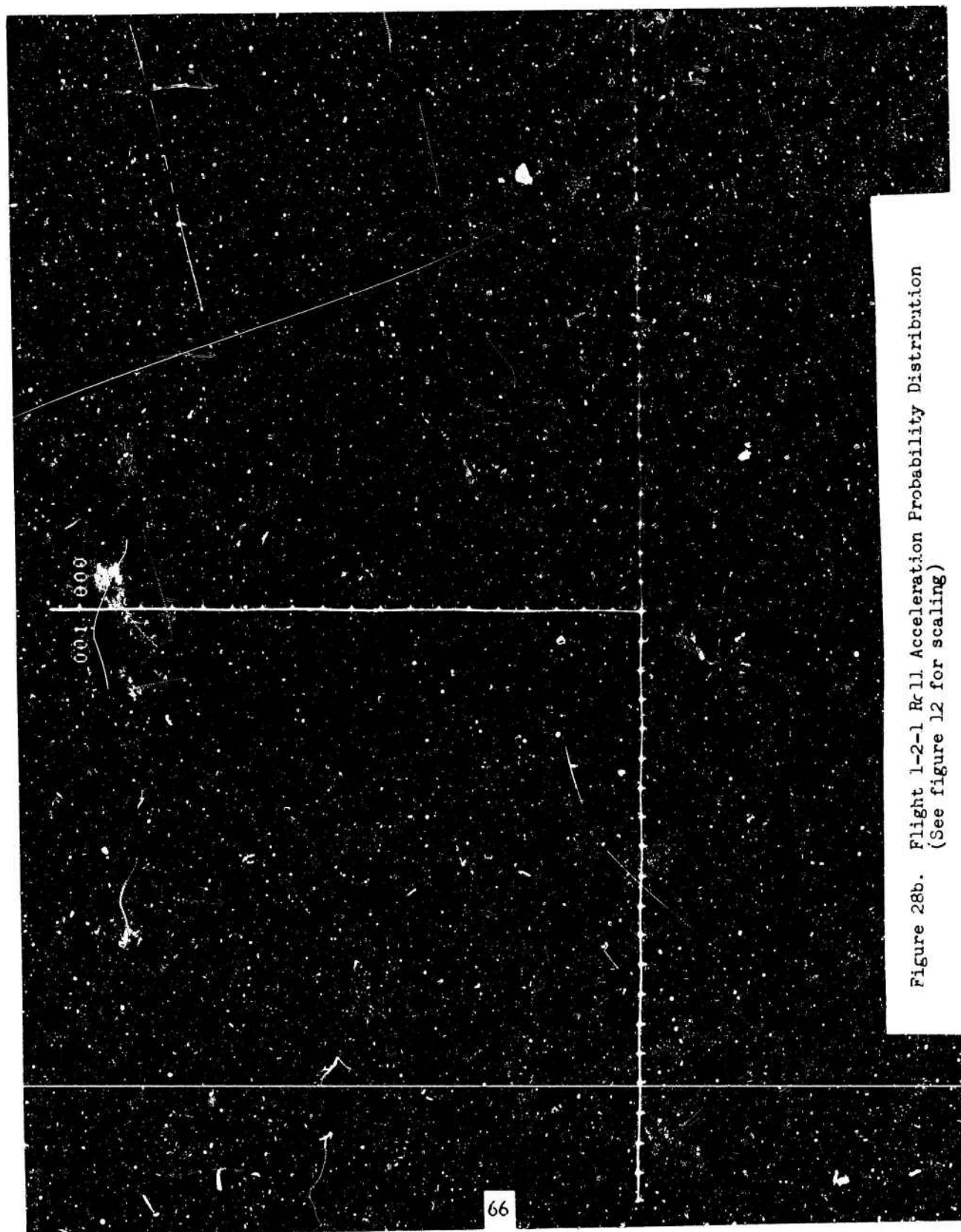


Figure 28b. Flight 1-2-1 Rcll Acceleration Probability Distribution
(See figure 12 for scaling)

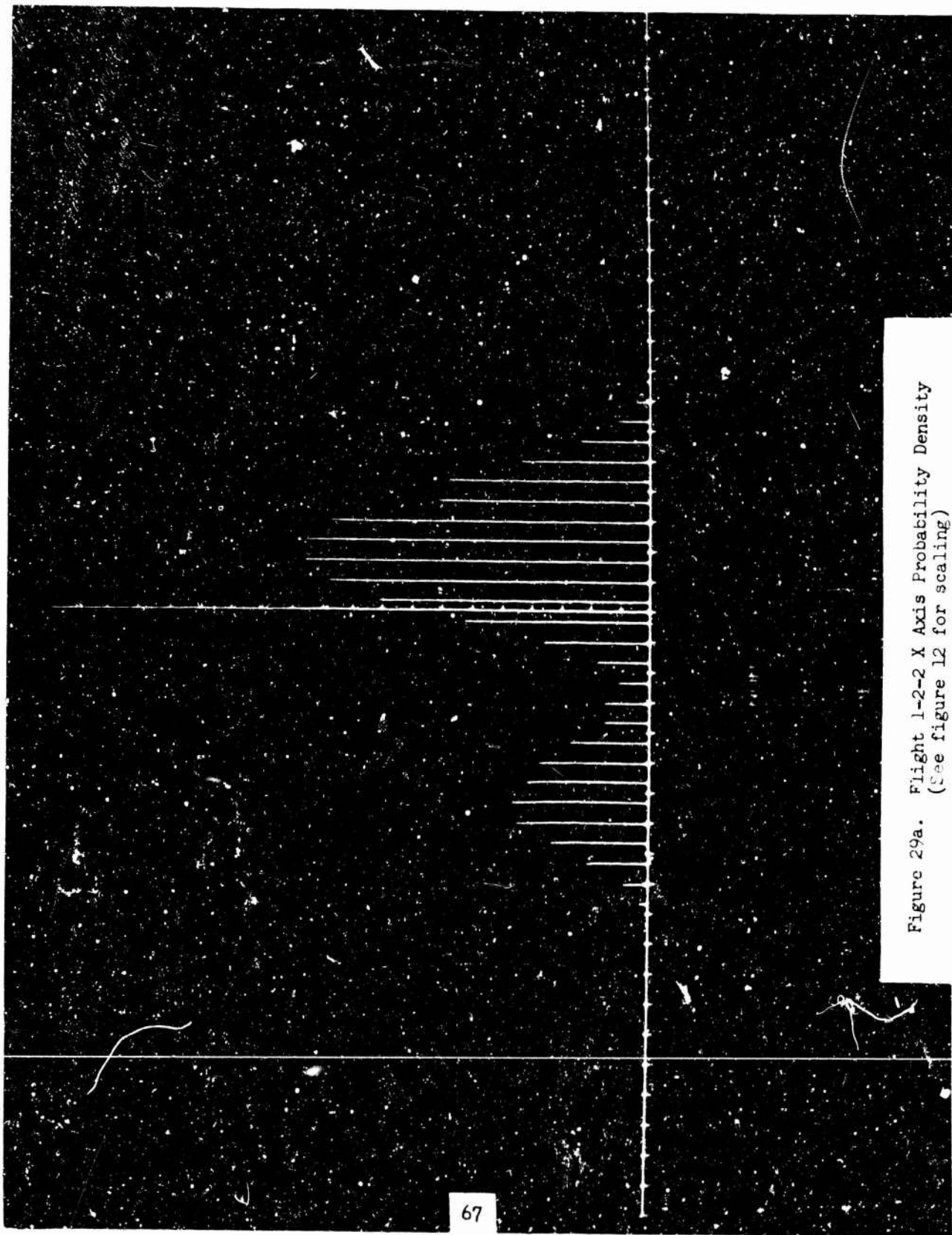


Figure 29a. Flight 1-2-2 X Axis Probability Density
(See figure 12 for scaling)

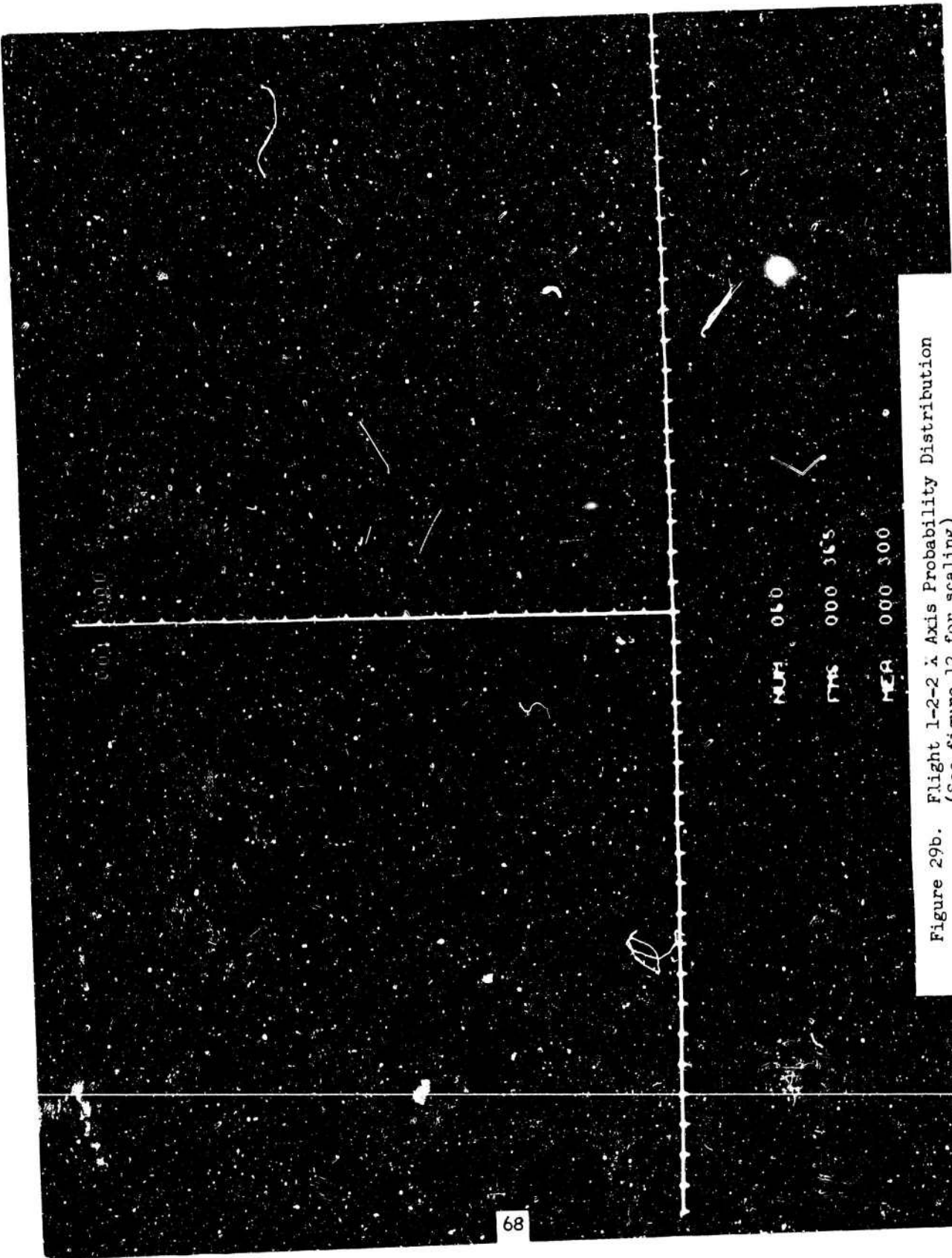


Figure 29b. Flight 1-2-2 X Axis Probability Distribution
(See figure 12 for scaling)

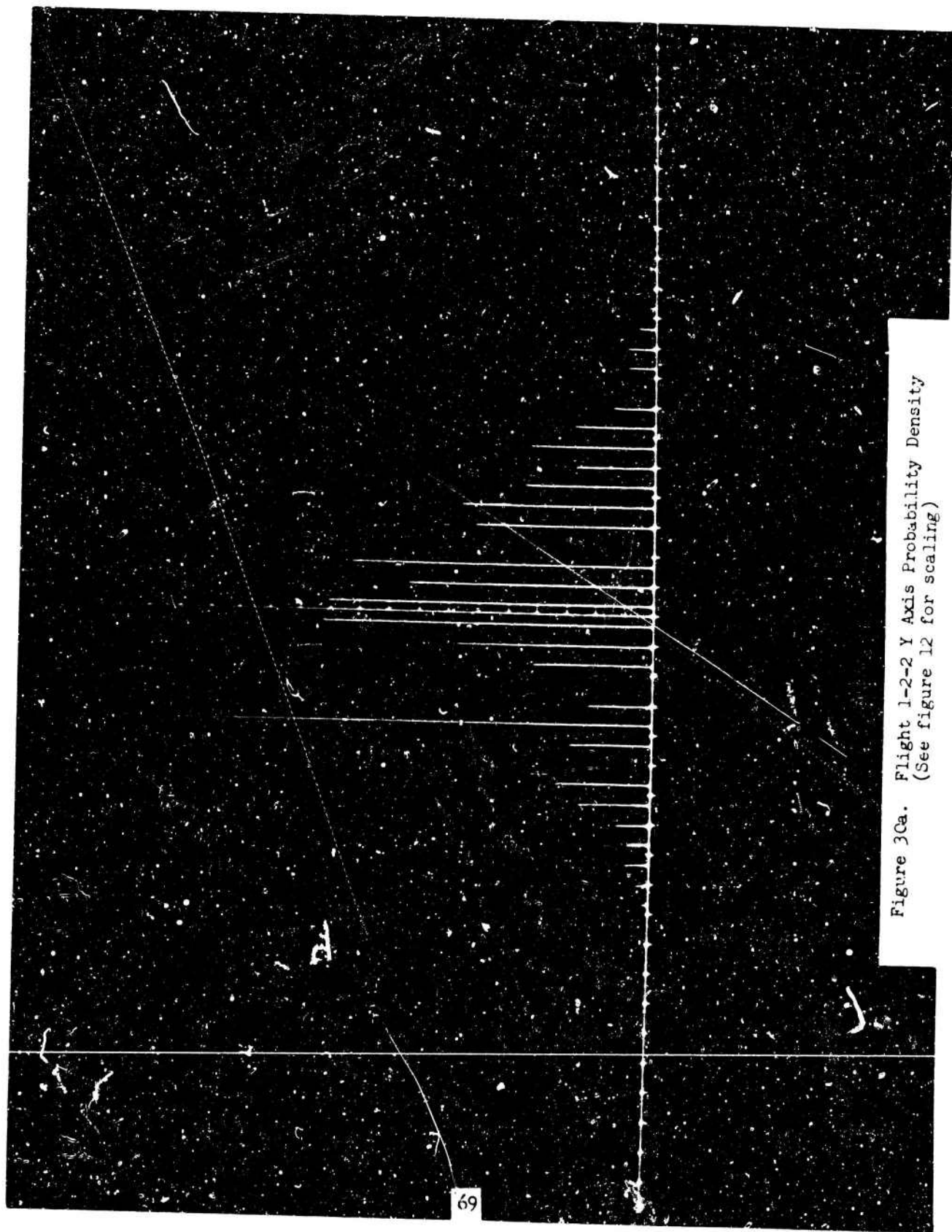


Figure 3Ca. Flight 1-2-2 Y Axis Probability Density
(See figure 12 for scaling)

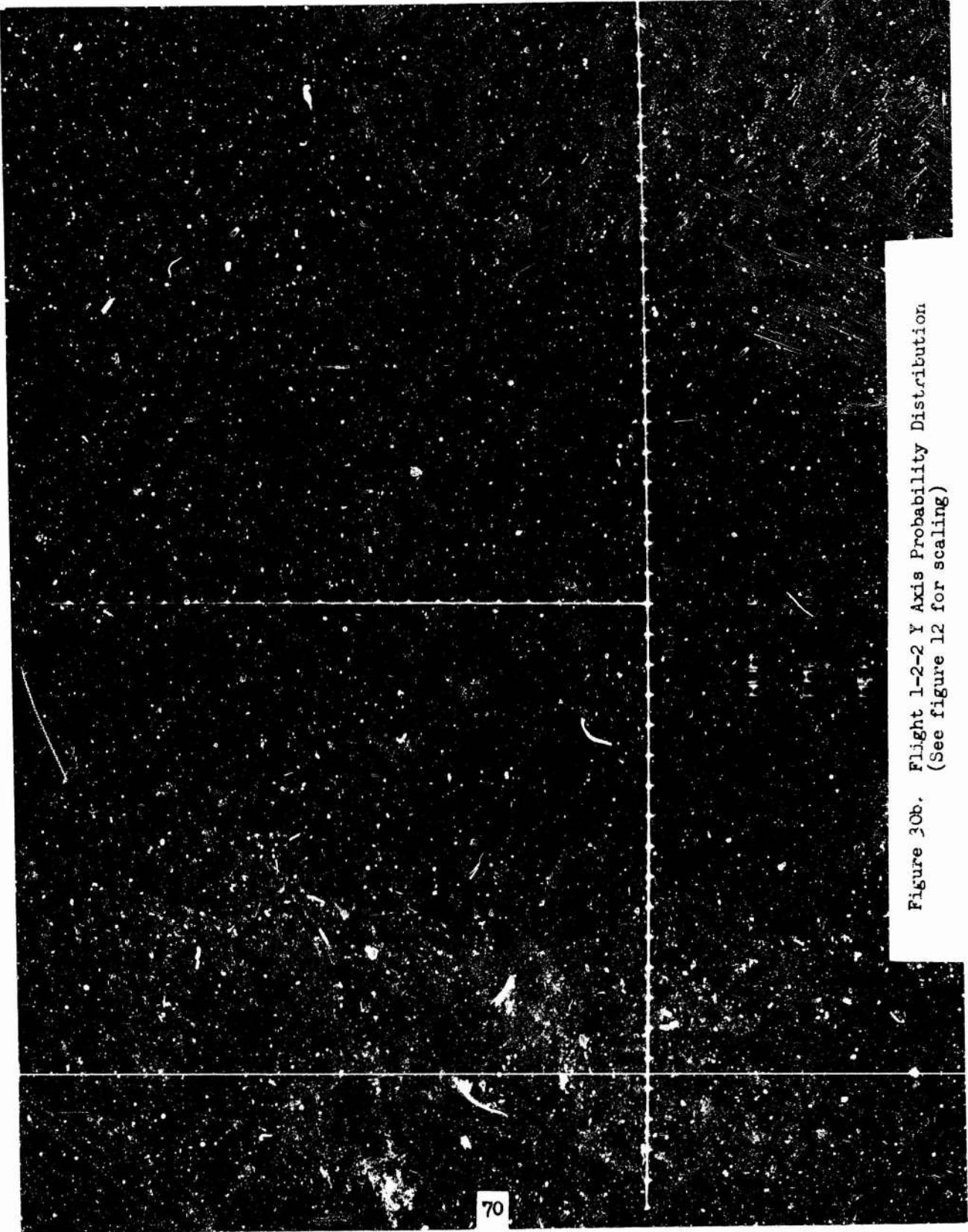
The image is a dark, high-contrast photograph of a probability distribution. A vertical line of small, bright white dots runs down the center of the frame. The background is black with a heavy grain and some scattered white specks. A horizontal line crosses the image about one-third of the way from the top. In the bottom right corner, there is a small white rectangular label with the number '70' inside.

Figure 30b. Flight 1-2-2 Y Axis Probability Distribution
(See figure 12 for scaling)

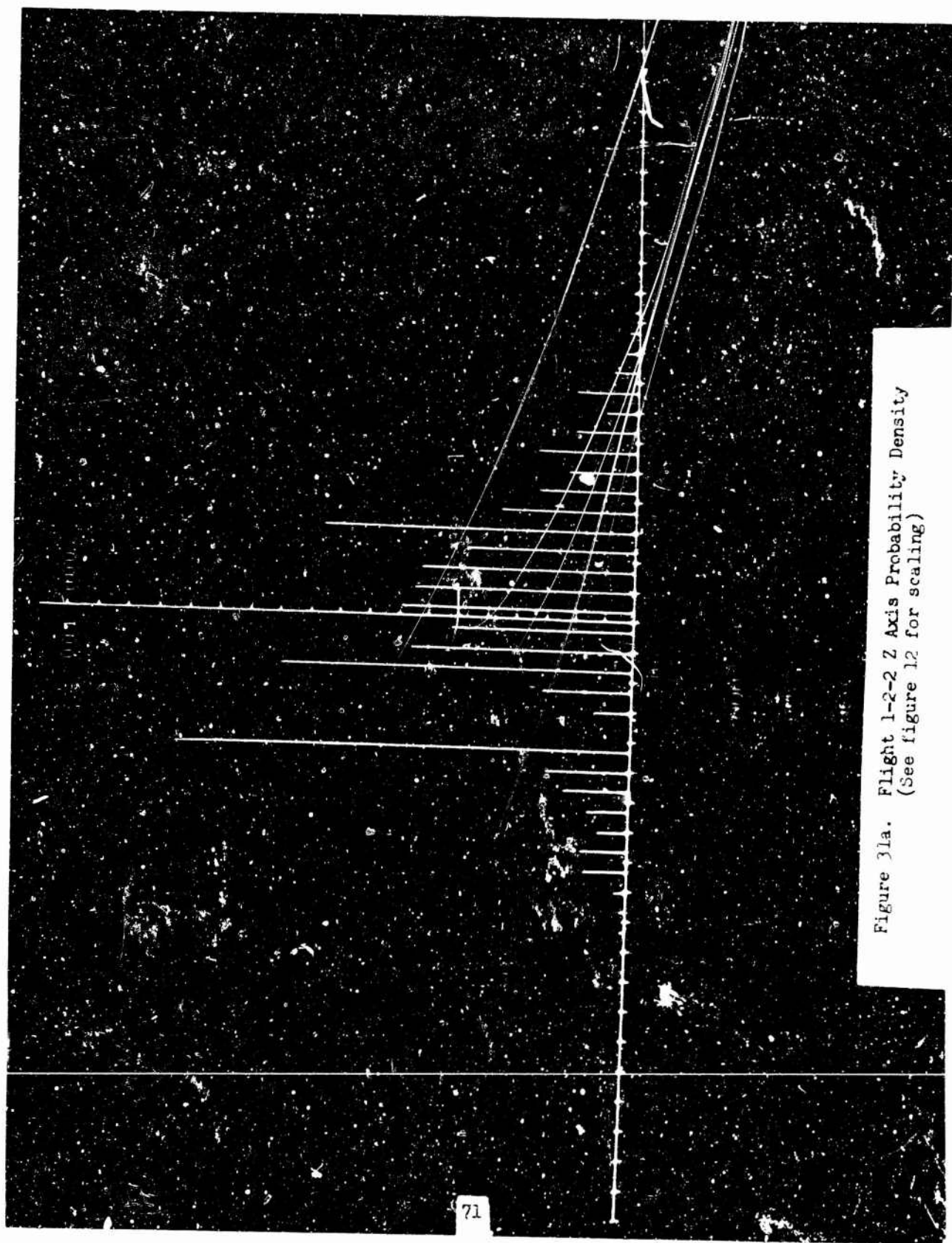
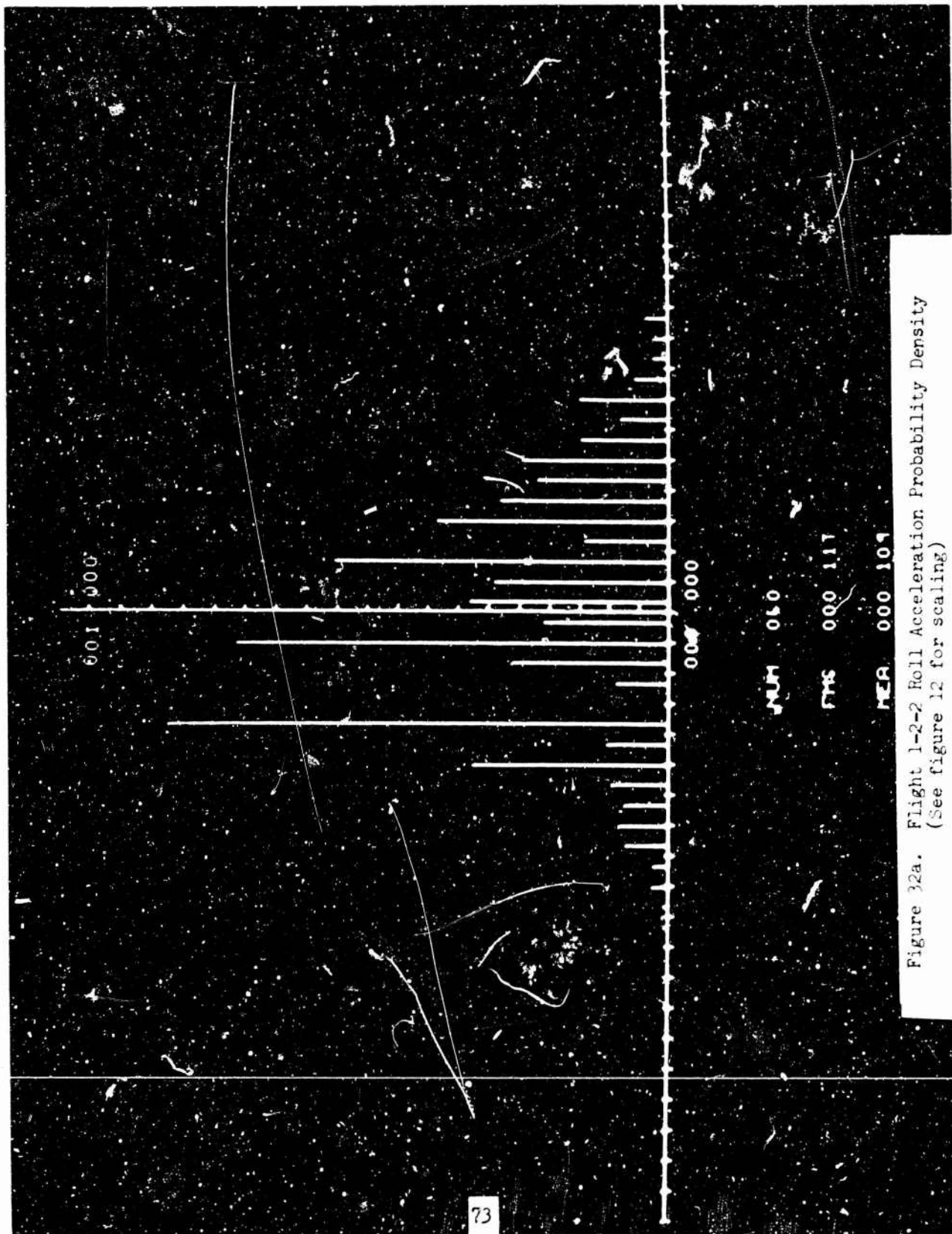


Figure 31b. Flight 1-2-2 Z Axis Probability Distribution
(See figure 12 for scaling)



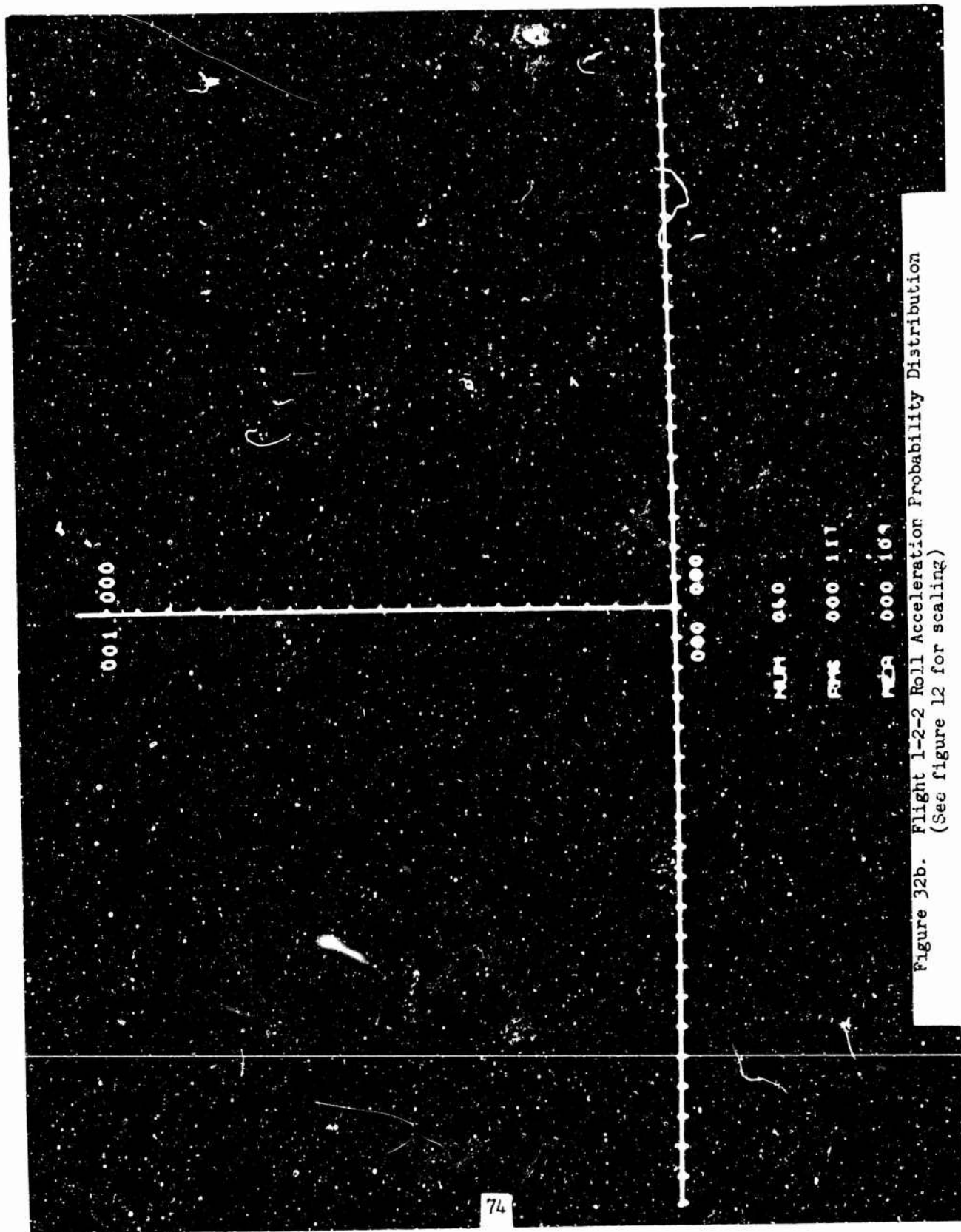


Figure 32b. Flight 1-2-2 Roll Acceleration Probability Distribution
(See figure 12 for scaling)

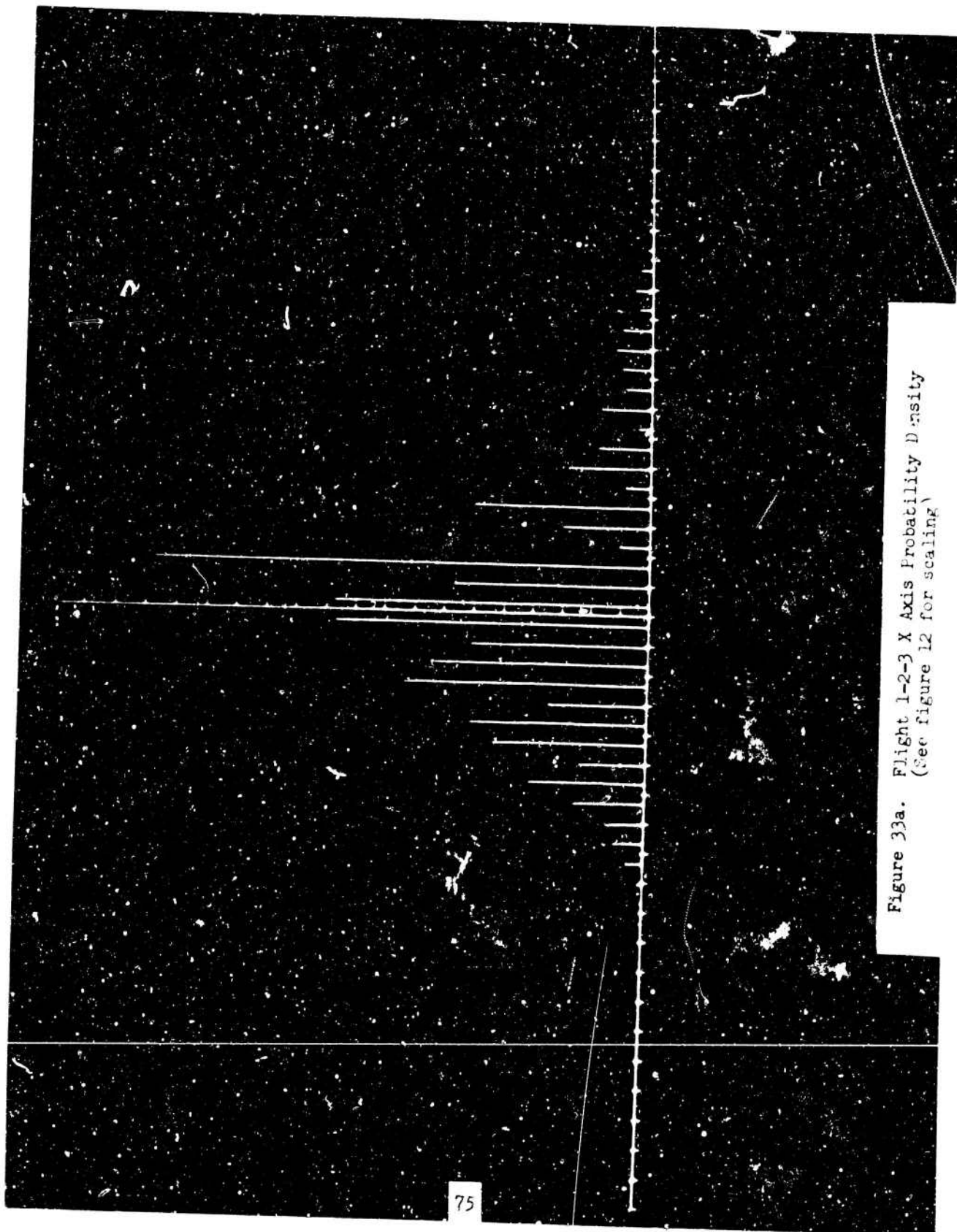


Figure 33a. Flight 1-2-3 X Axis Probability Density
(See figure 12 for scaling)

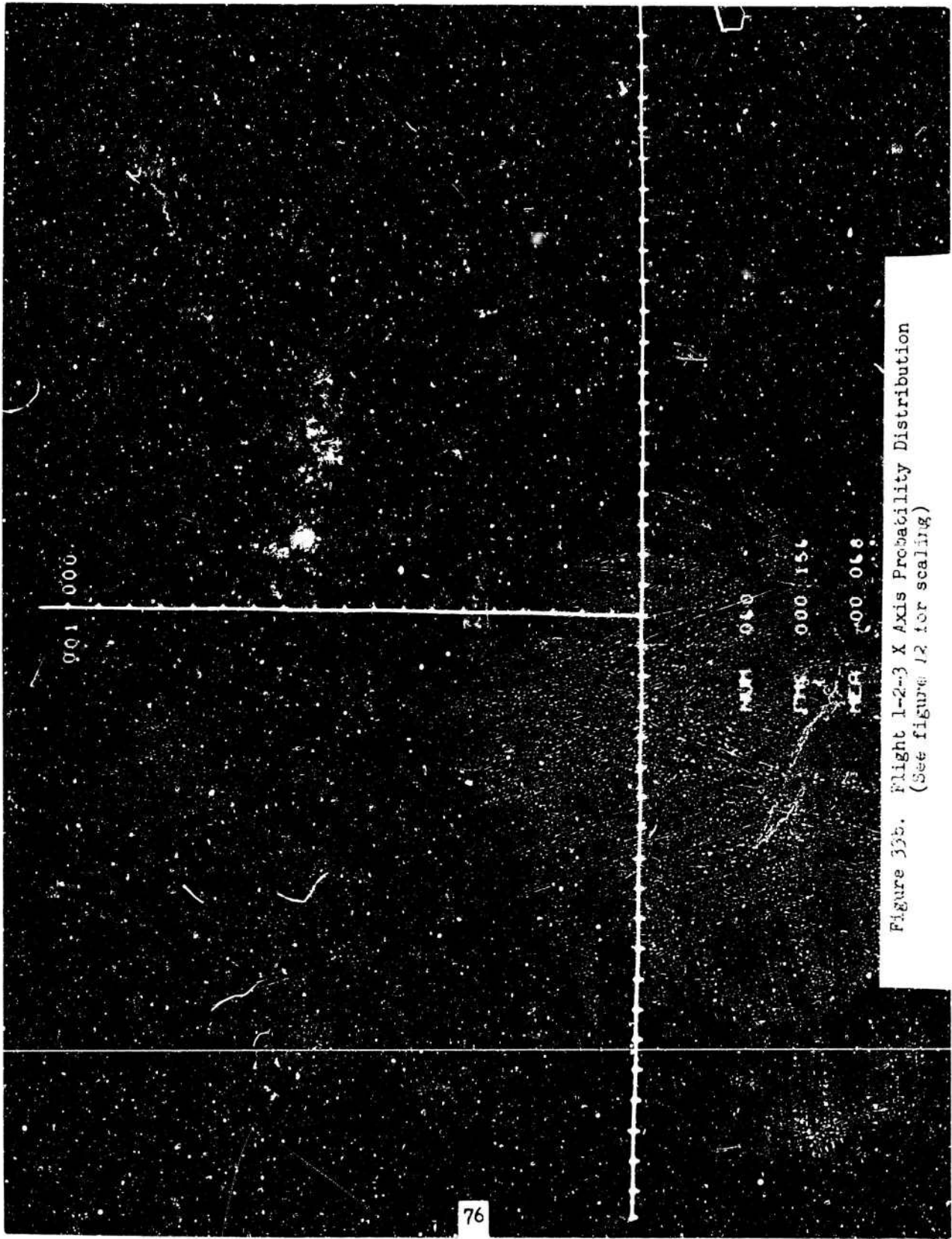


Figure 33b. Flight 1-2-3 X Axis Probability Distribution
(See figure 12 for scaling)

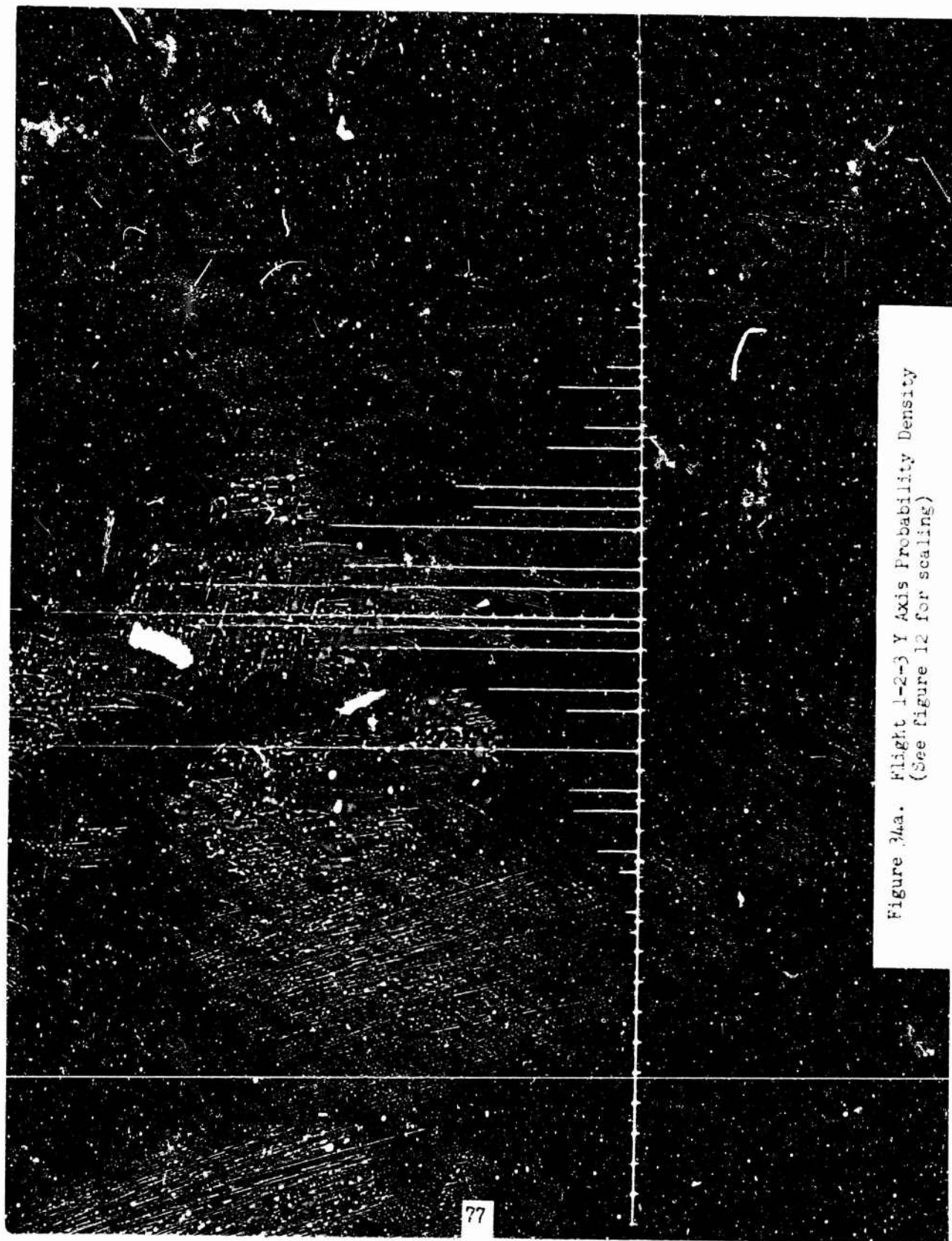
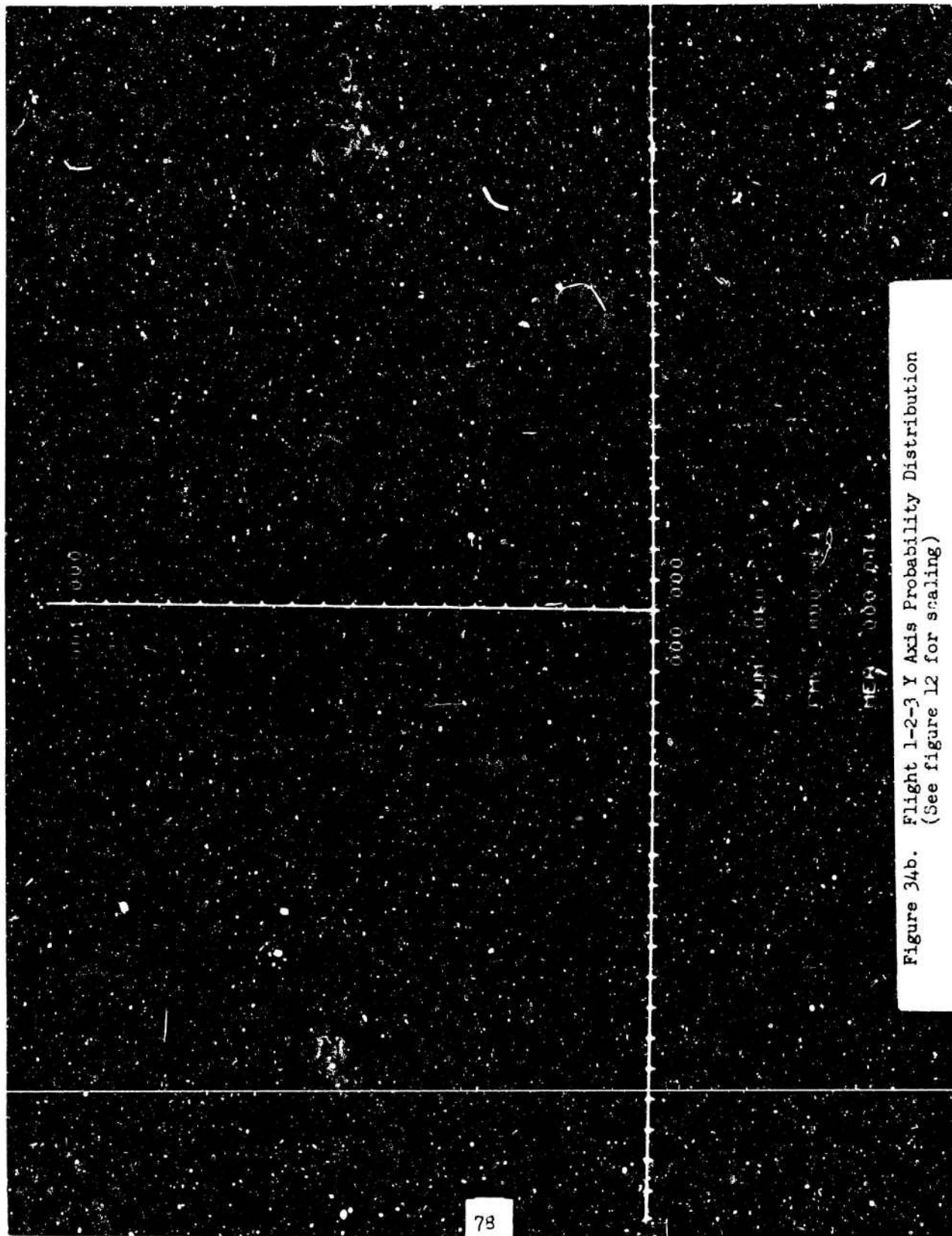


Figure 34a. Flight 1-2-3 Y Axis Probability Density
(See figure 12 for scaling)



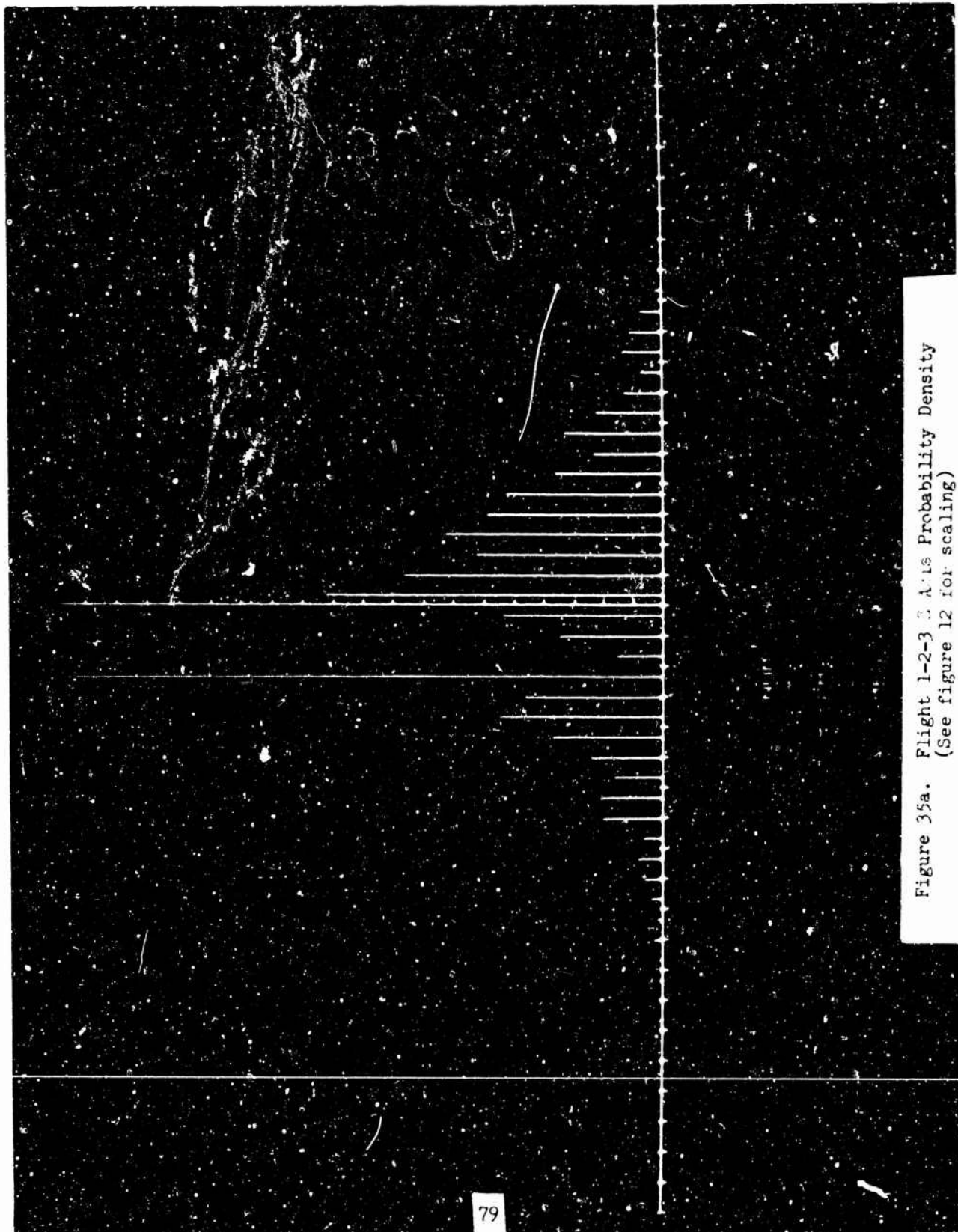


Figure 35a. Flight 1-2-3 Z Axis Probability Density
(See figure 12 for scaling)

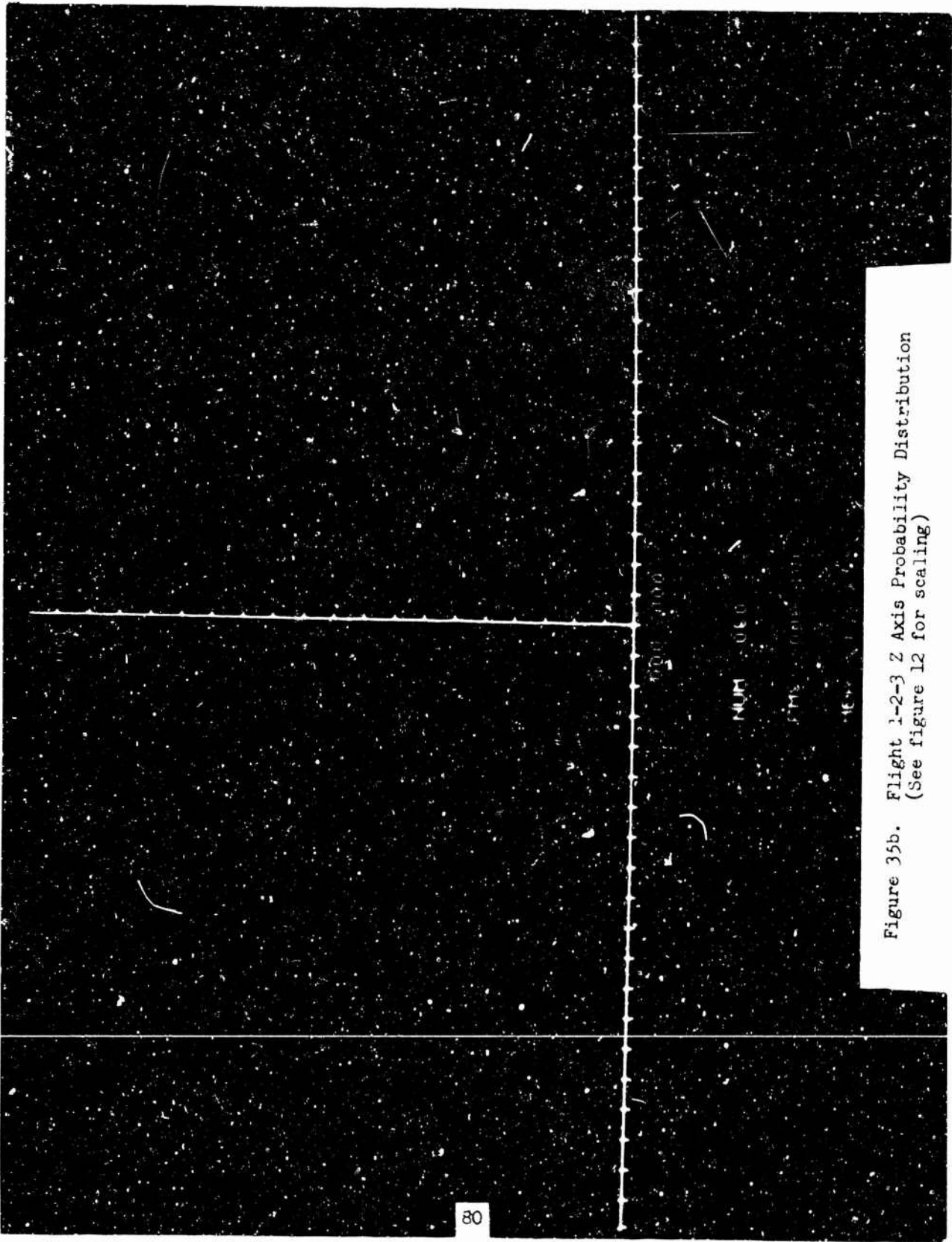
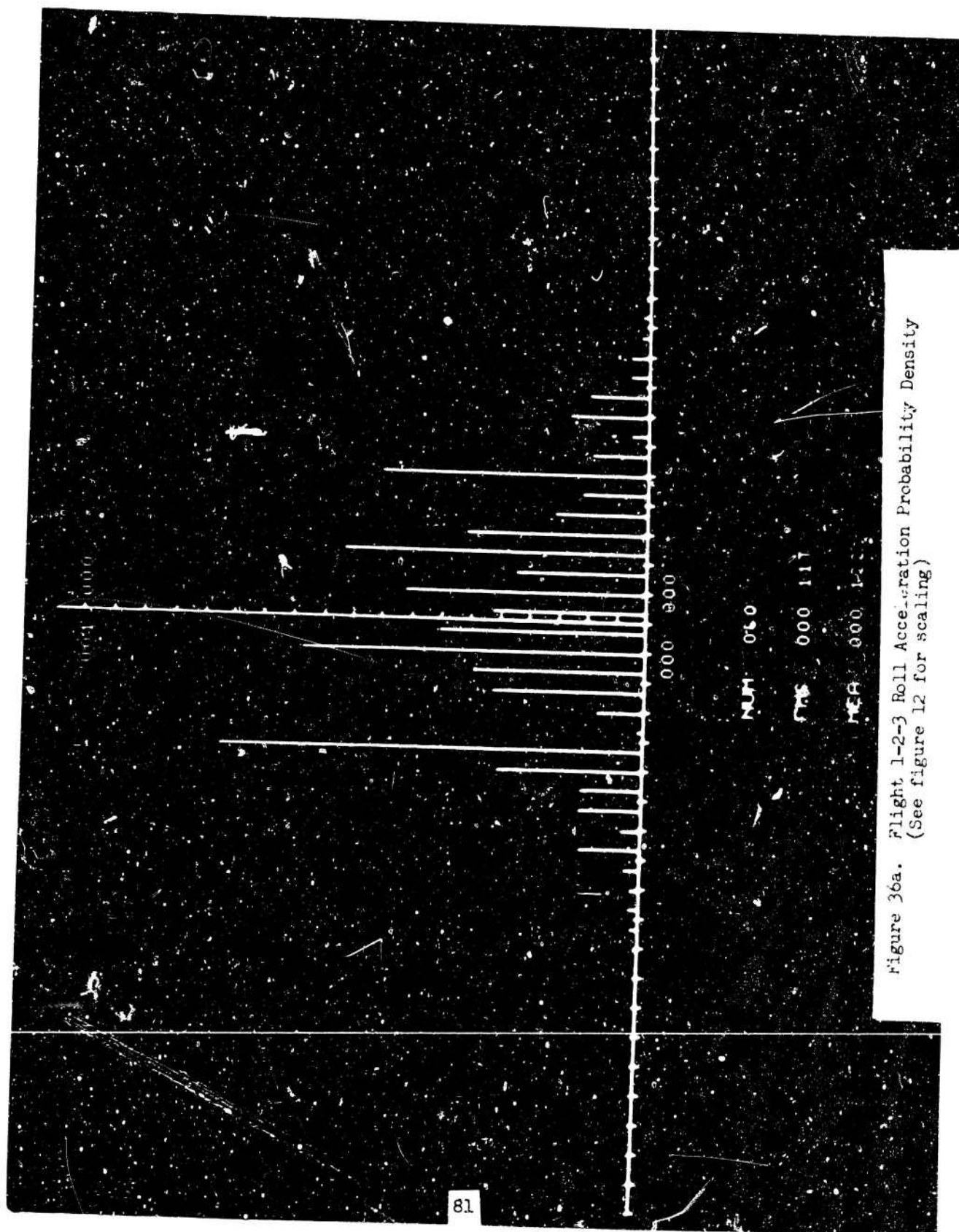


Figure 35b. Flight 1-2-3 Z Axis Probability Distribution
(See figure 12 for scaling)



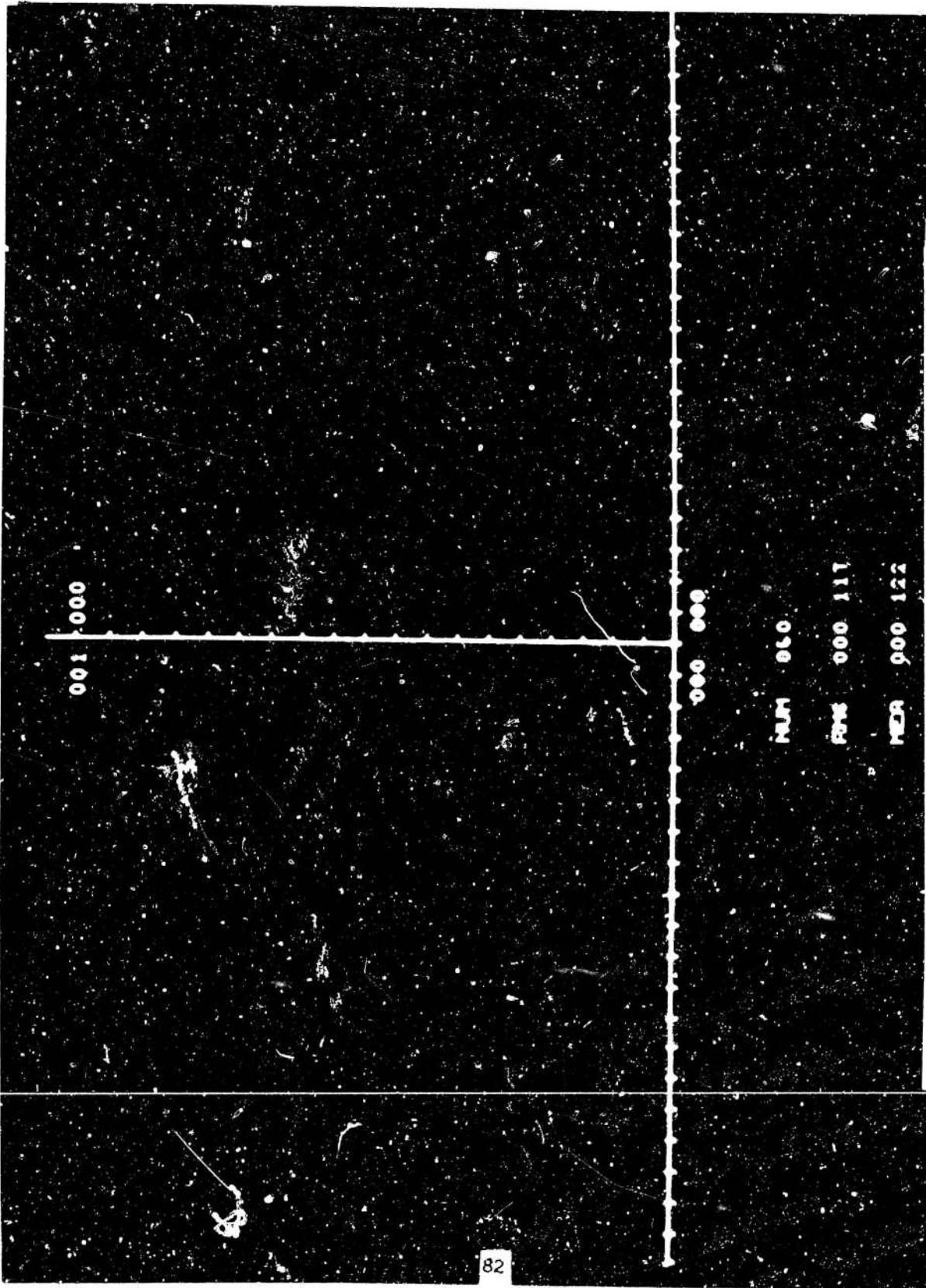


Figure 36b. Flight 1-2-3 Roll Acceleration Probability Distribution
(See figure 12 for scaling)

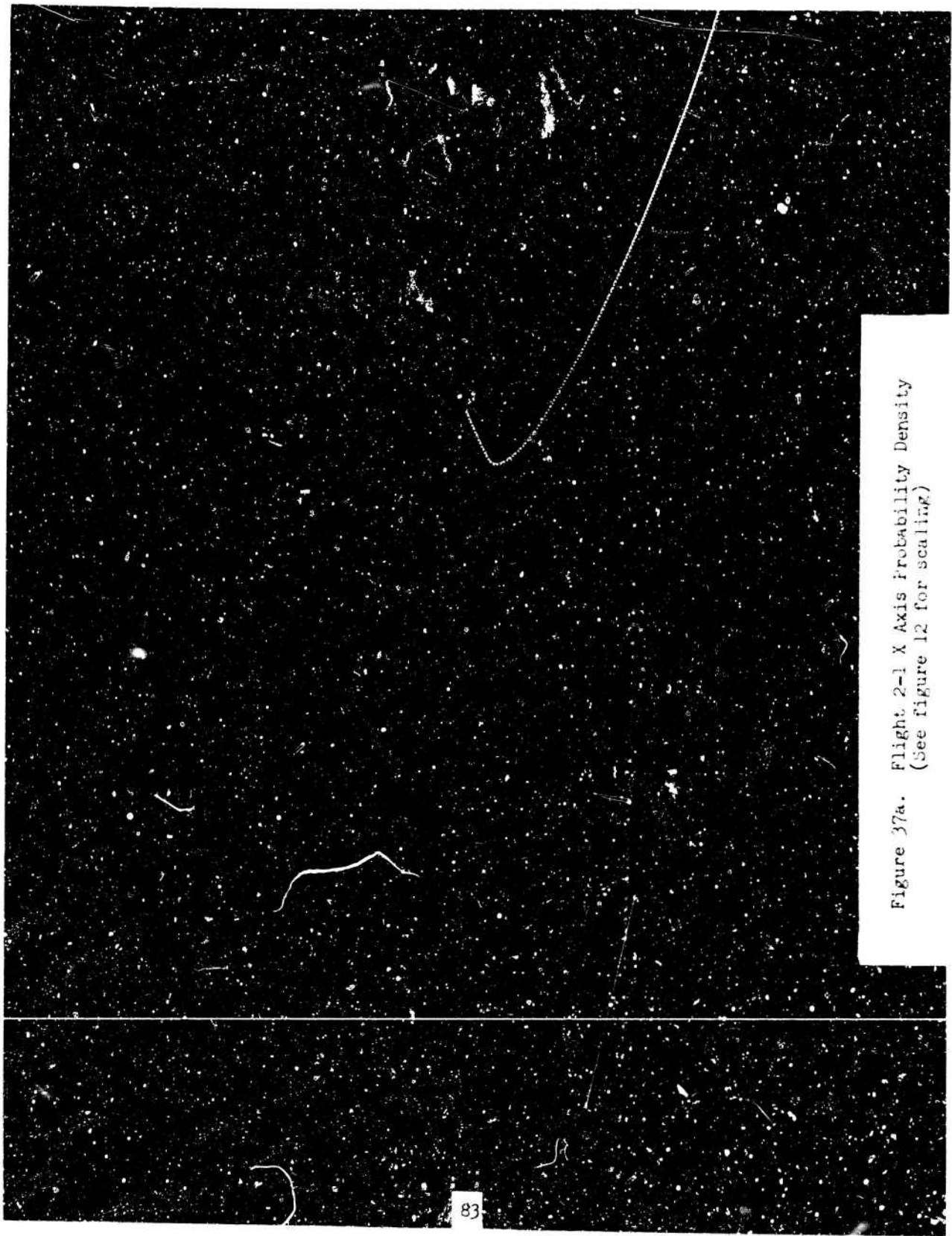


Figure 37a. Flight 2-1 X Axis Probability Density
(See figure 12 for scaling)

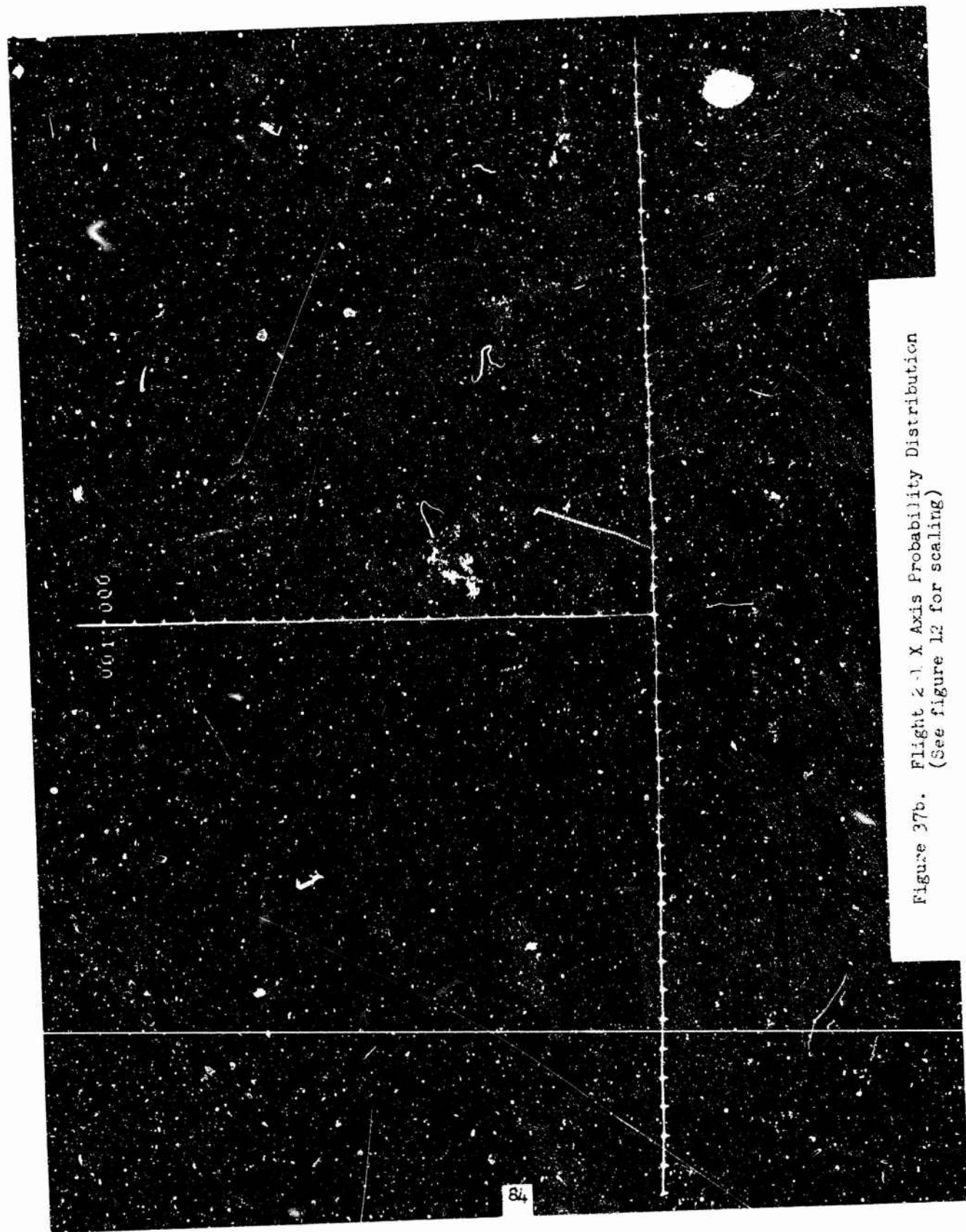


Figure 37b. Flight 2-1 X Axis Probability Distribution
(See figure 12 for scaling)

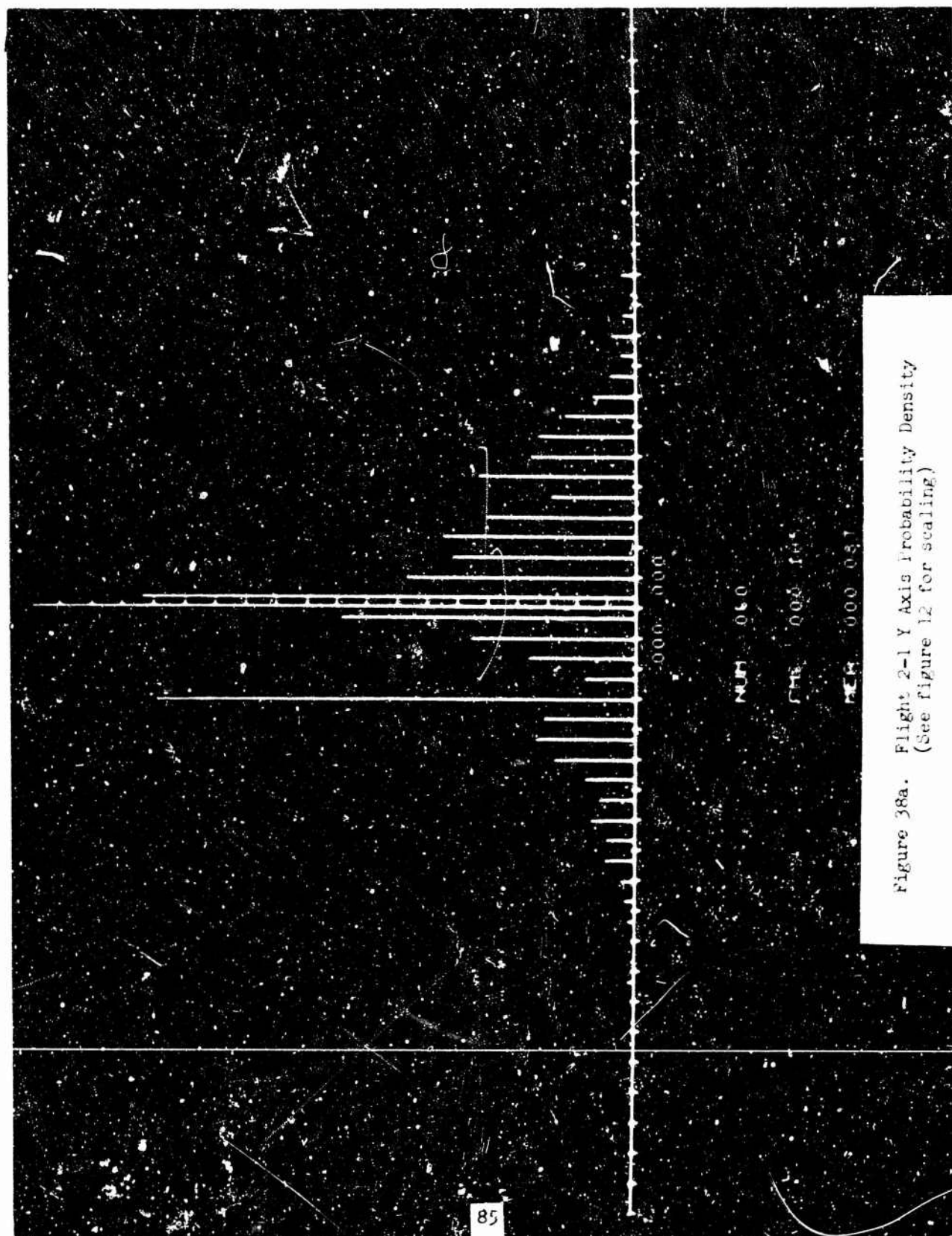


Figure 38a. Flight 2-1 Y Axis Probability Density
(See figure 12 for scaling.)

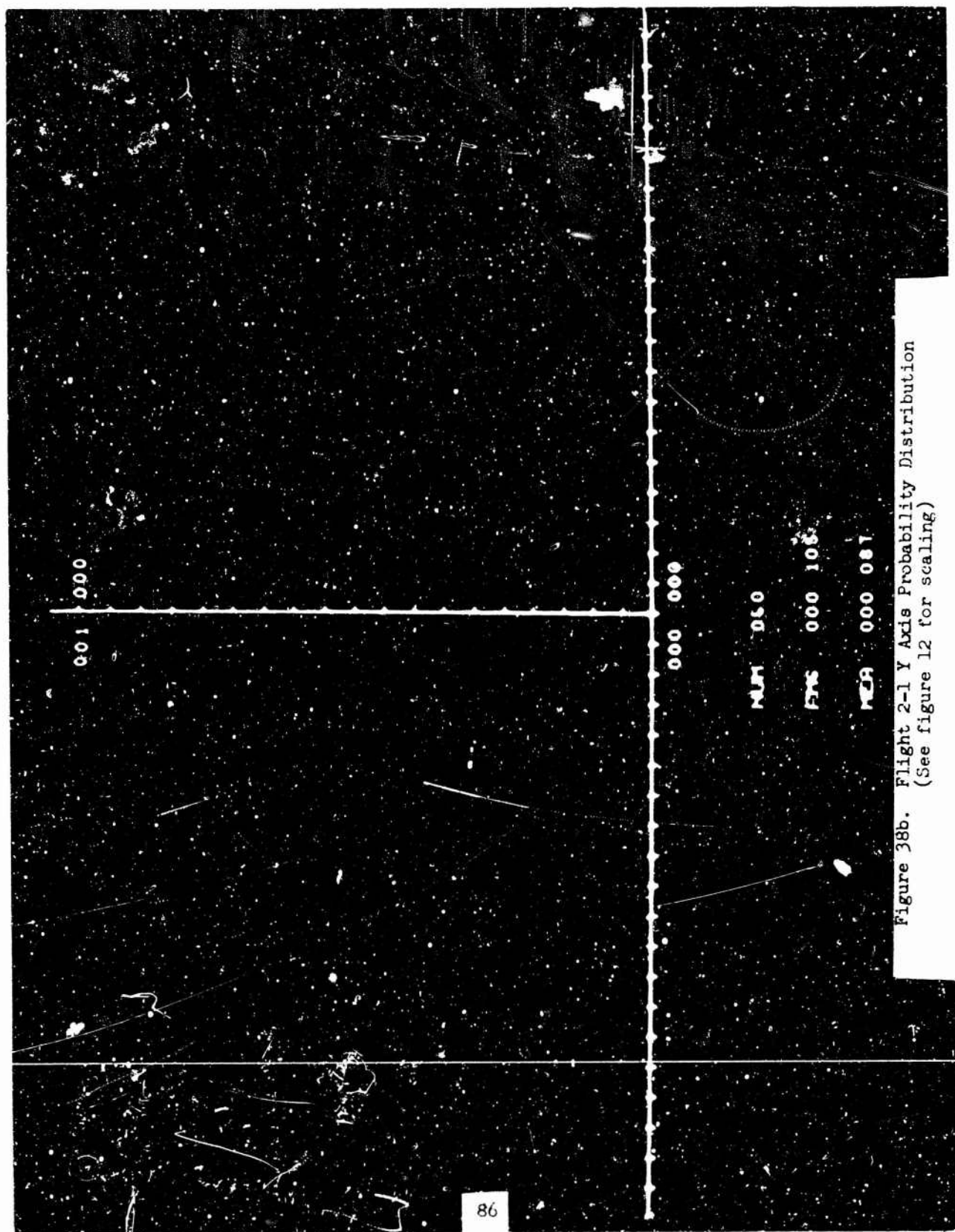


Figure 38b. Flight 2-1 Y Axis Probability Distribution
(See figure 12 for scaling)

MUM 010

FMS 000 106

MCA 000 087

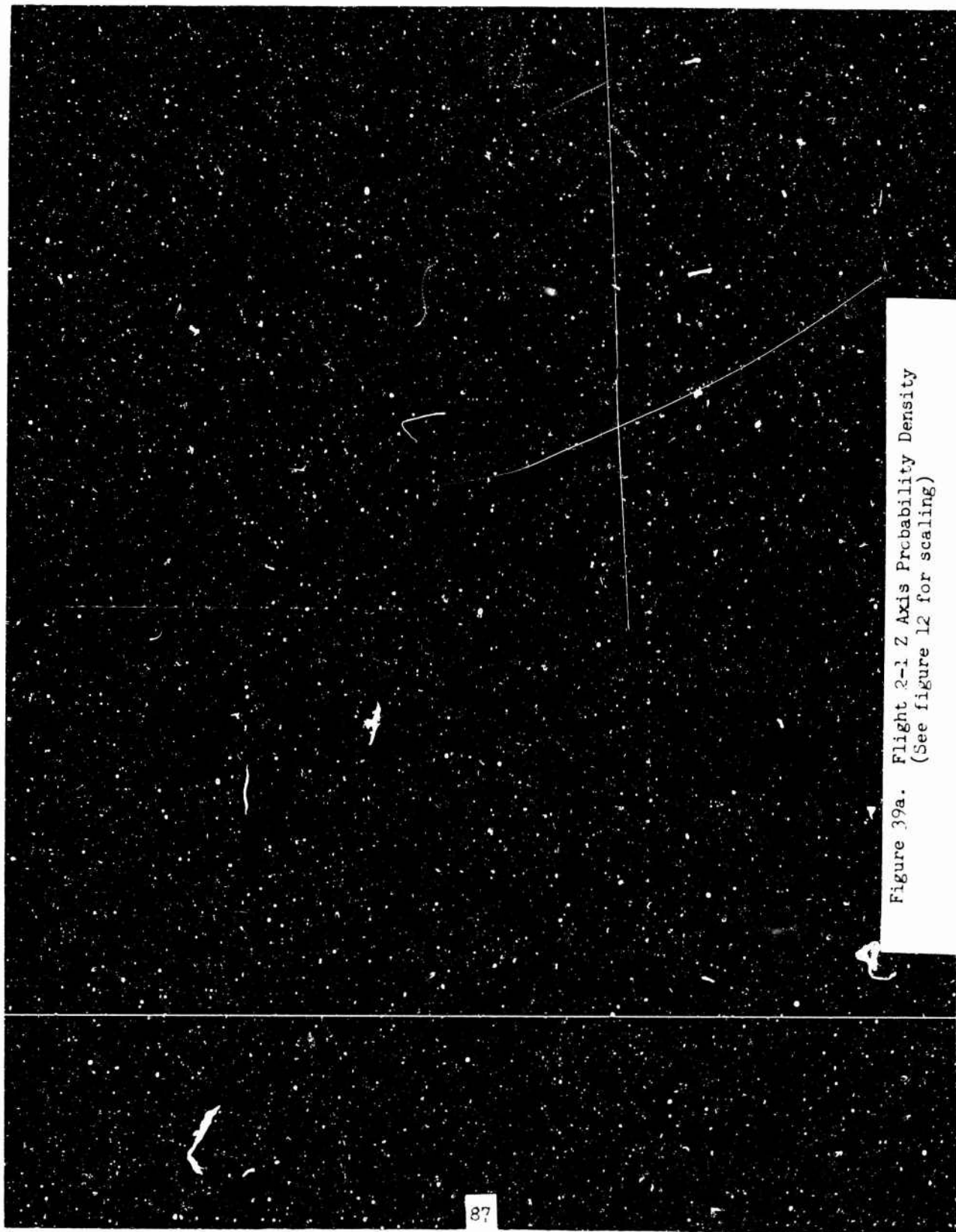


Figure 39a. Flight 2-1 Z Axis Probability Density
(See figure 12 for scaling)

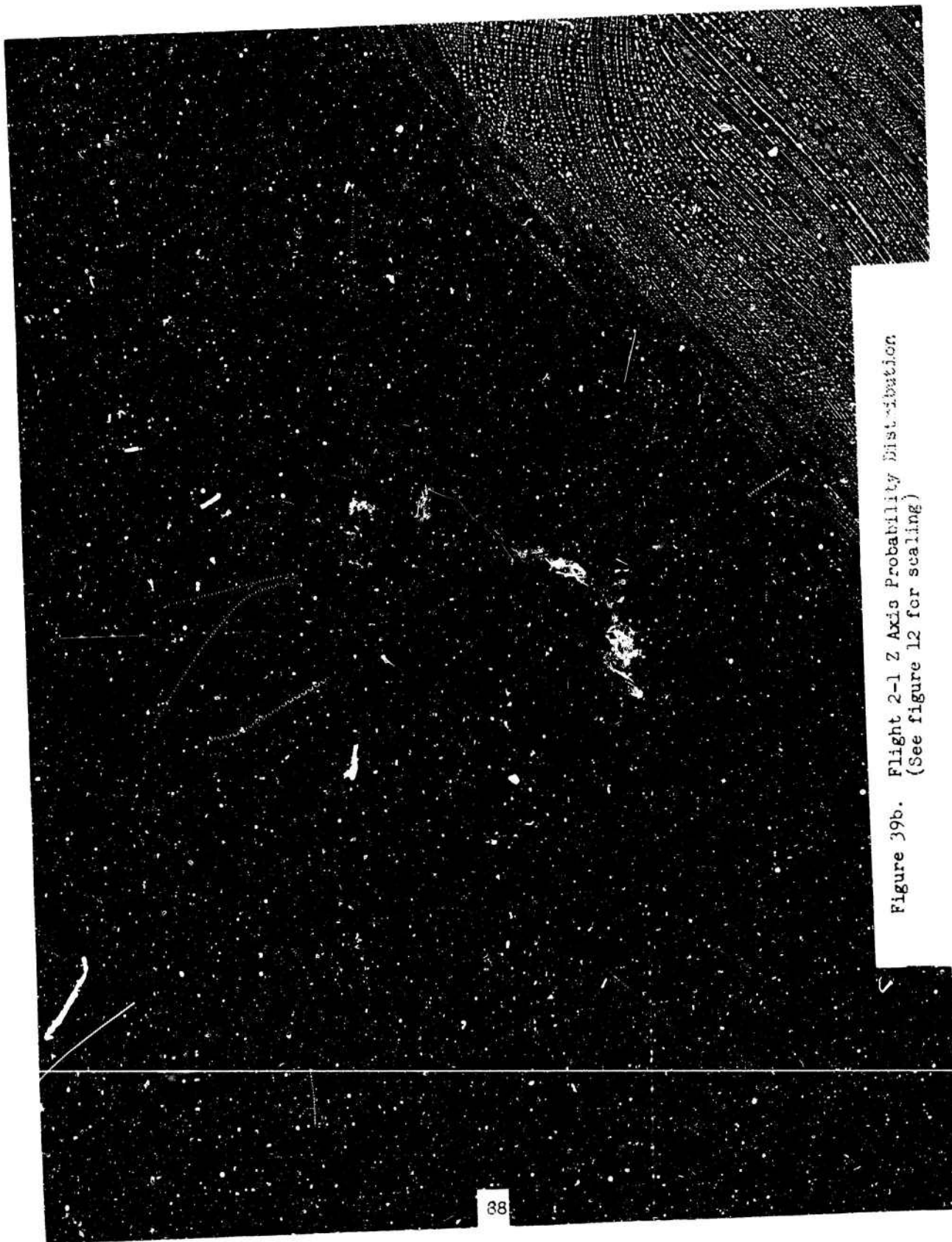
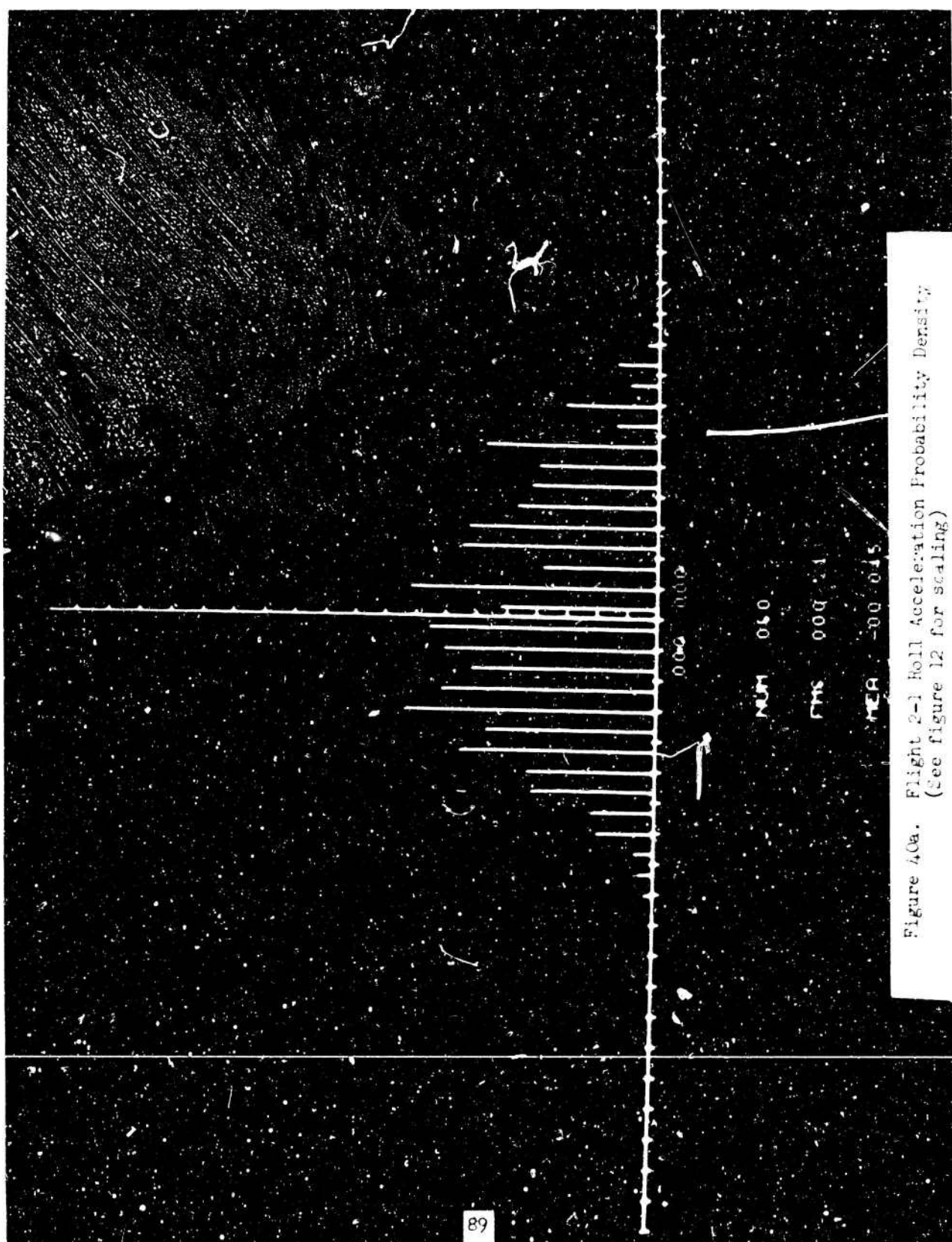


Figure 39b. Flight 2-1 Z Axis Probability Distribution
(See figure 12 for scaling)



001 000

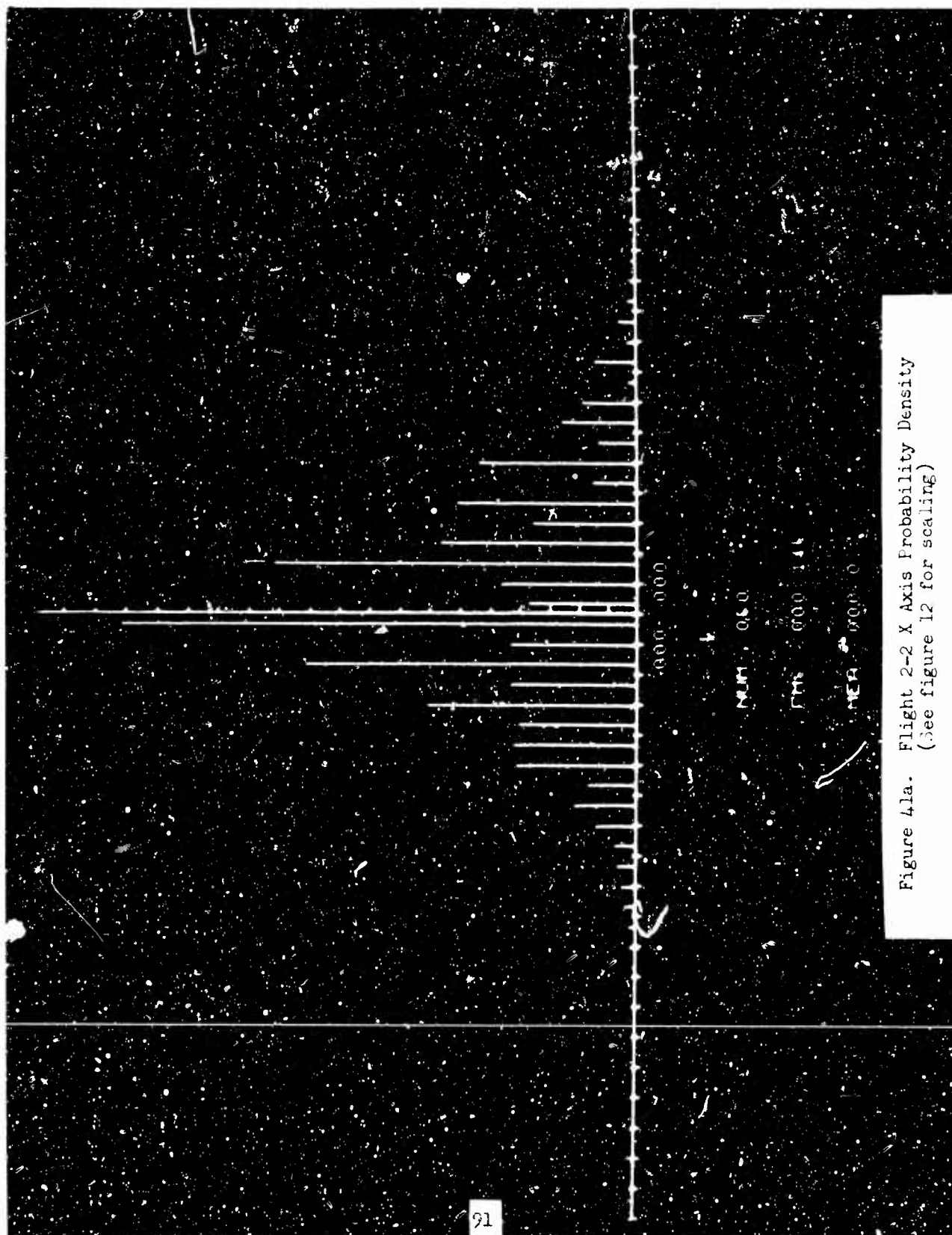
000 000

NUM 050

FMS 000 213

MEA -00 045

Figure 40h. Flight 2-1 Roll Acceleration Probability Distribution
(See figure 12 for scaling)



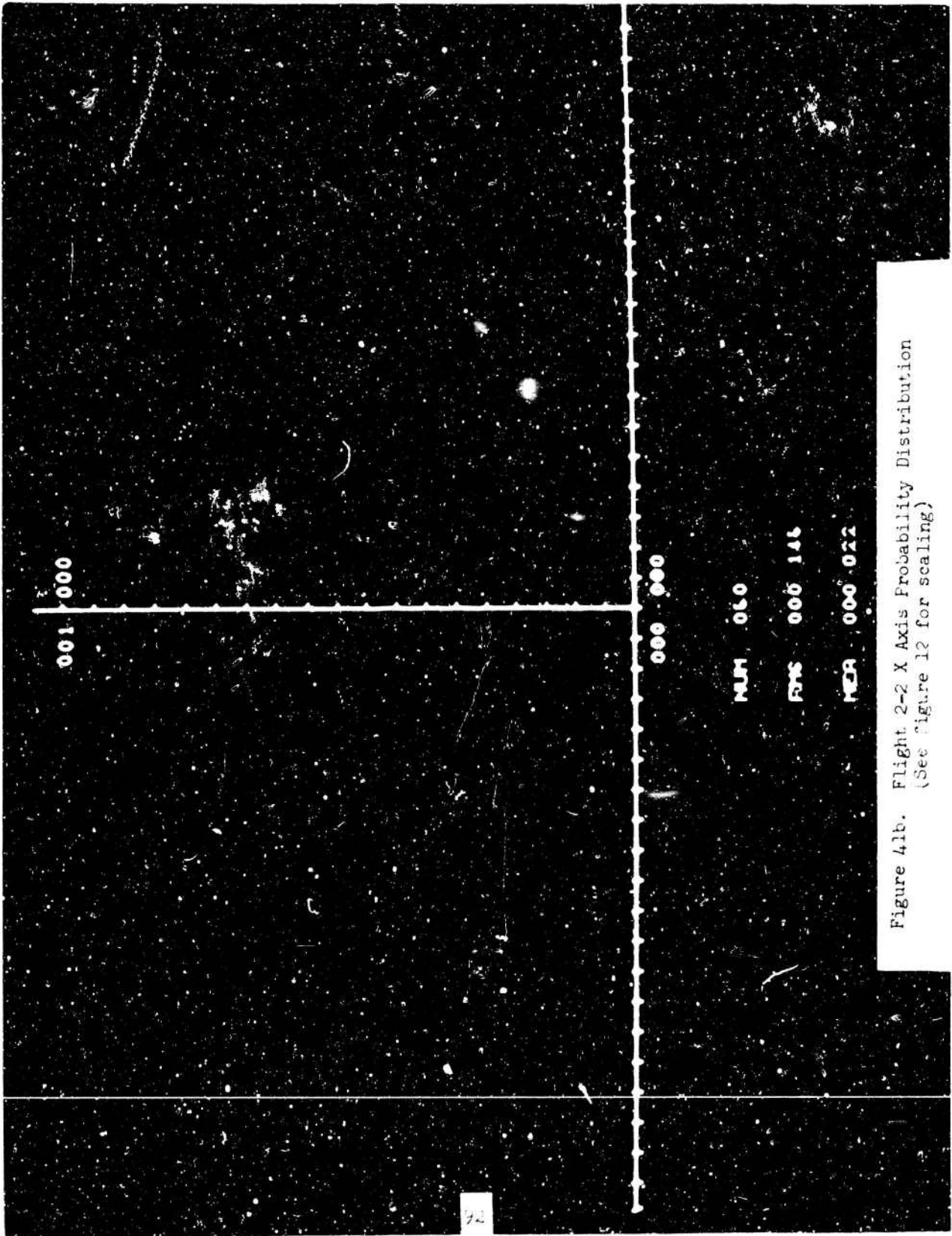
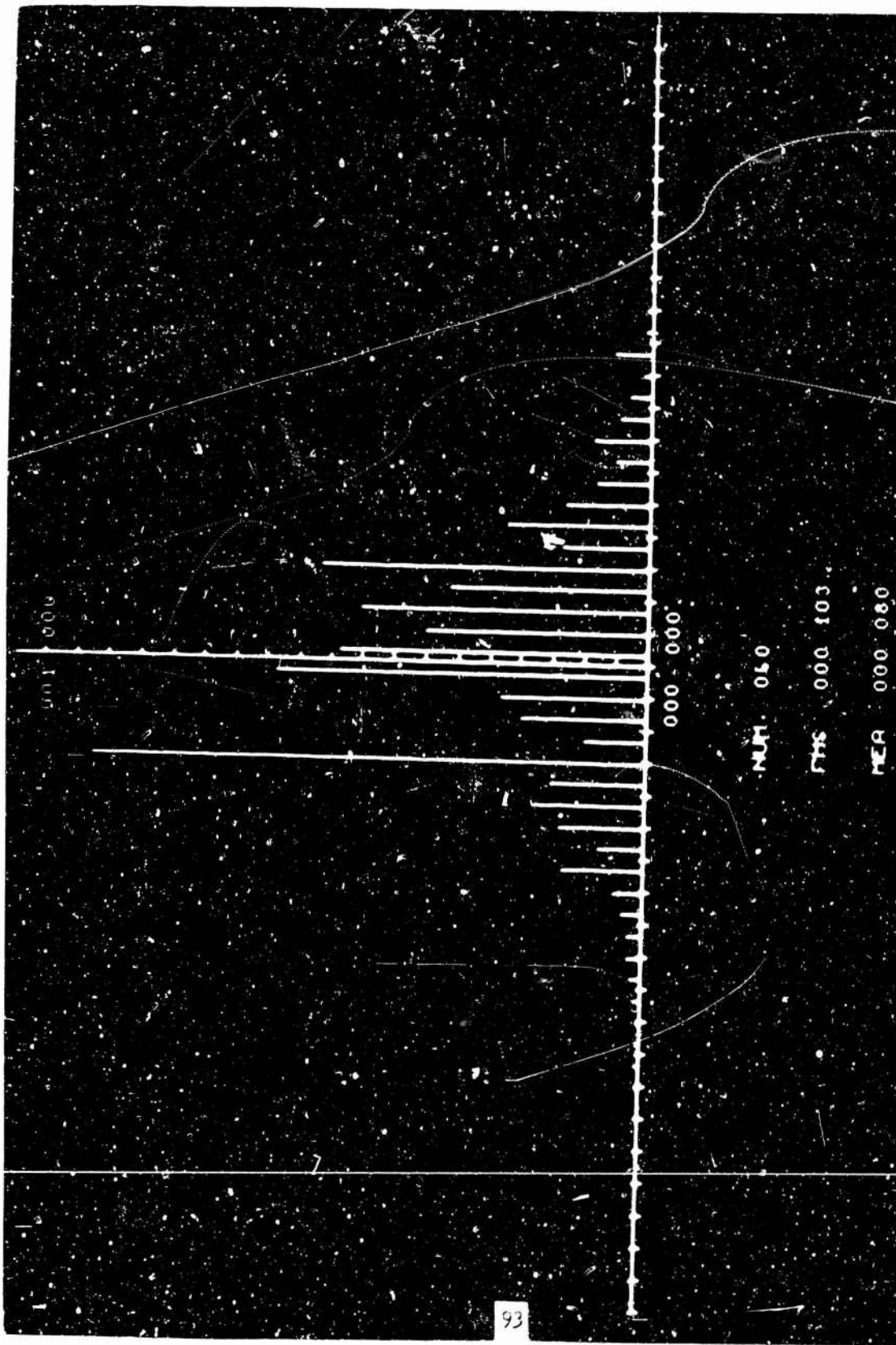
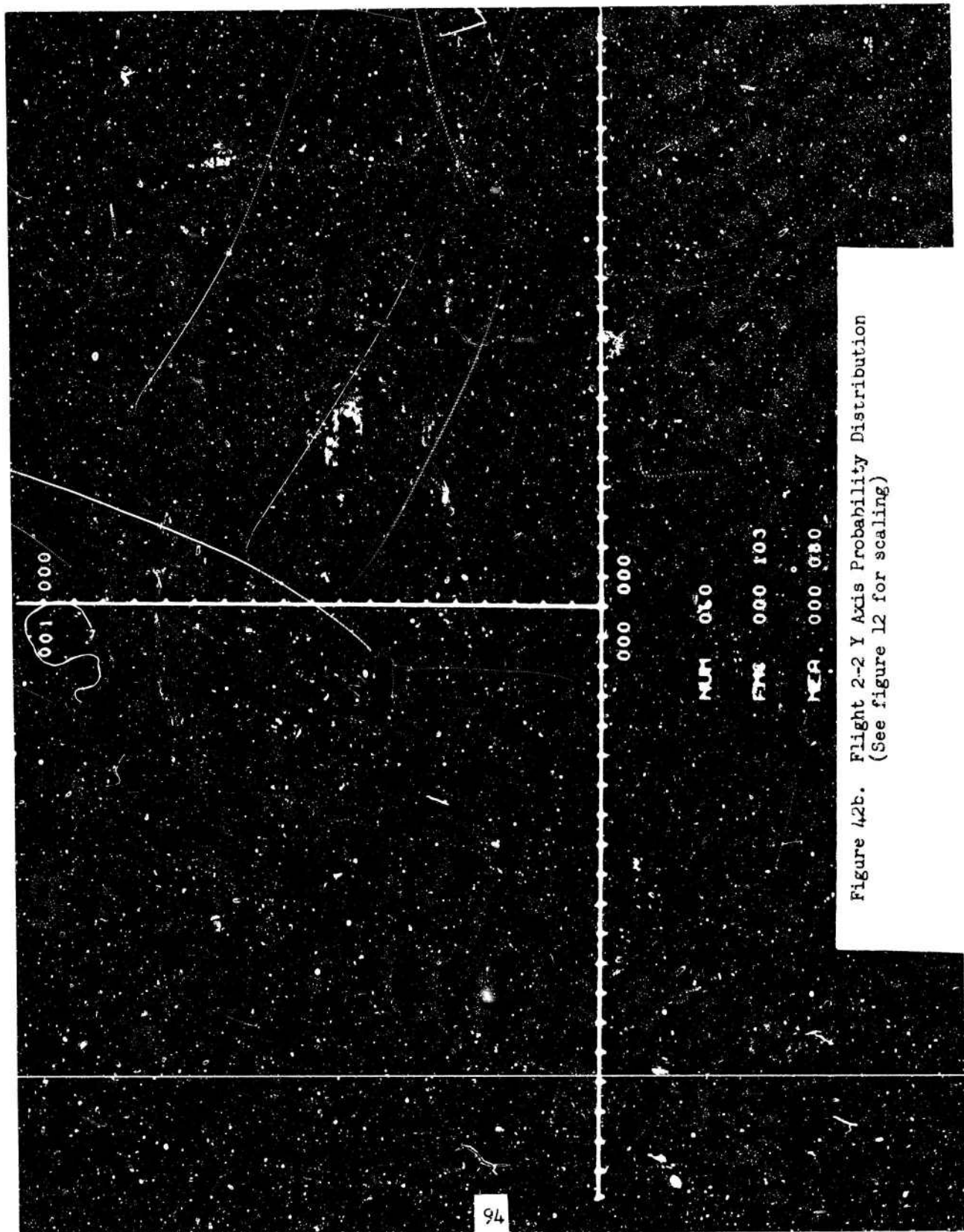


Figure 4lb. Flight 2-2 X Axis Probability Distribution
(See figure 12 for scaling)





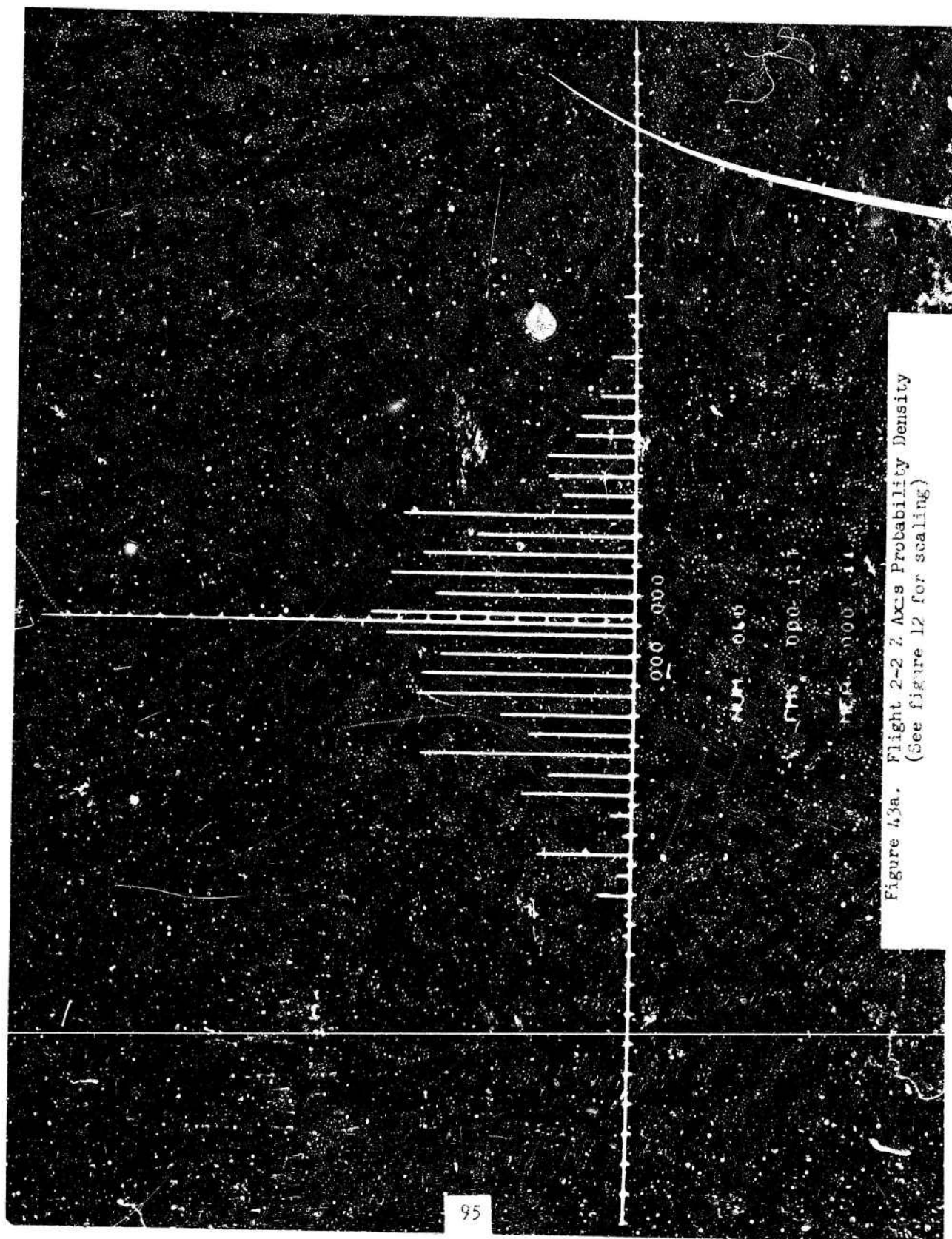
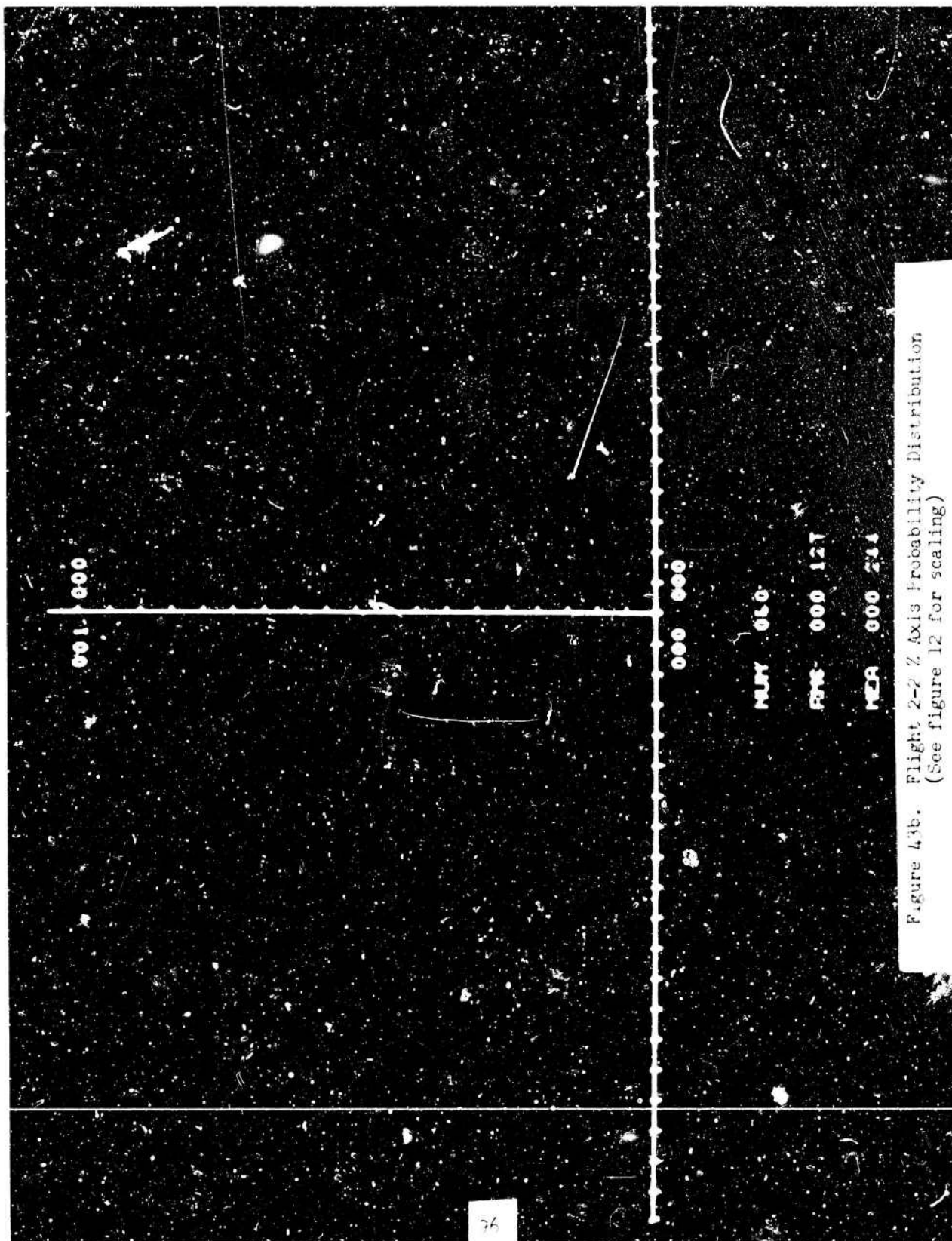


Figure 43a. Flight 2-2 Z Axis Probability Density
(See figure 12 for scaling)



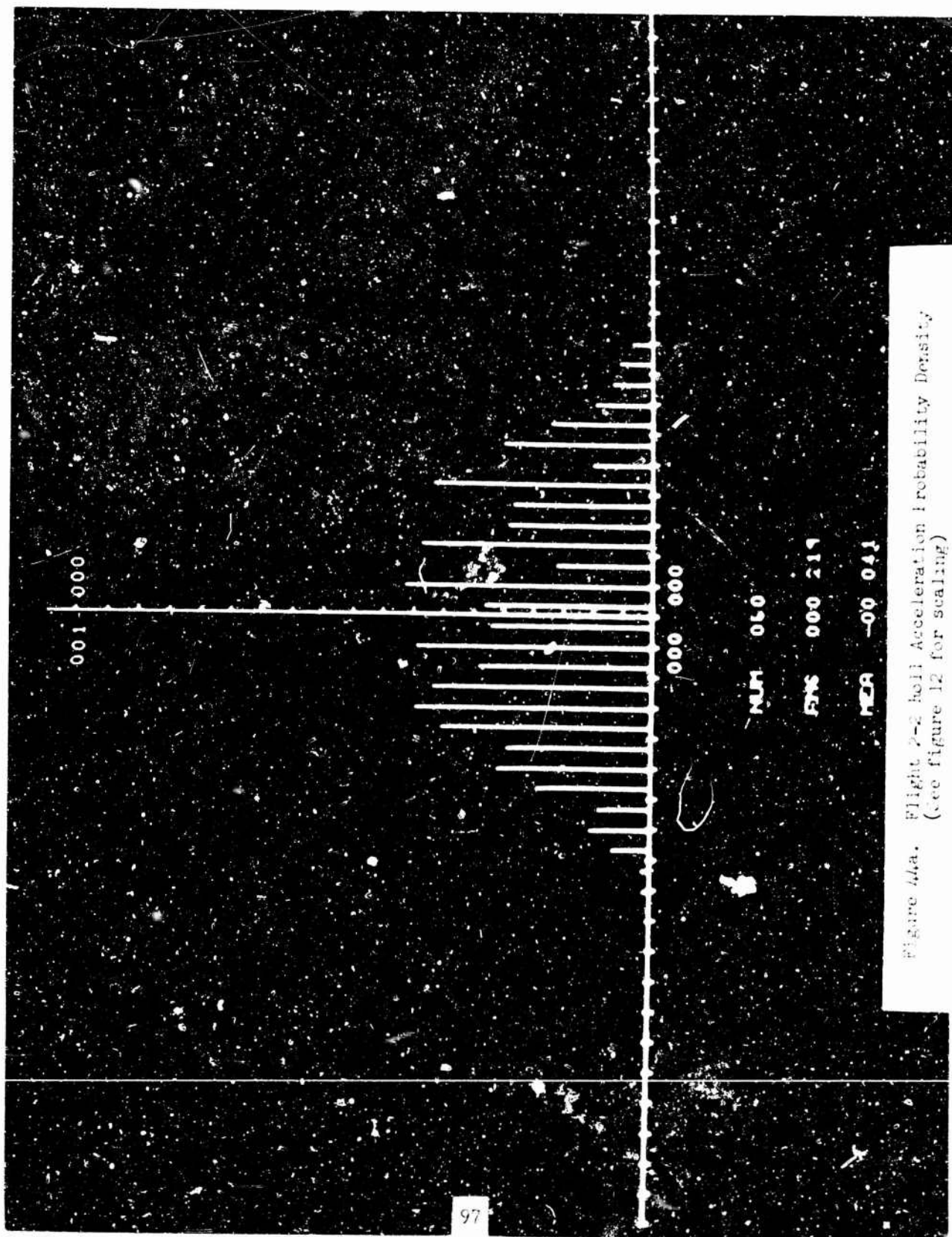


Figure 44a. Flight 2-2 roll Acceleration Probability Density
(see figure 12 for scaling)

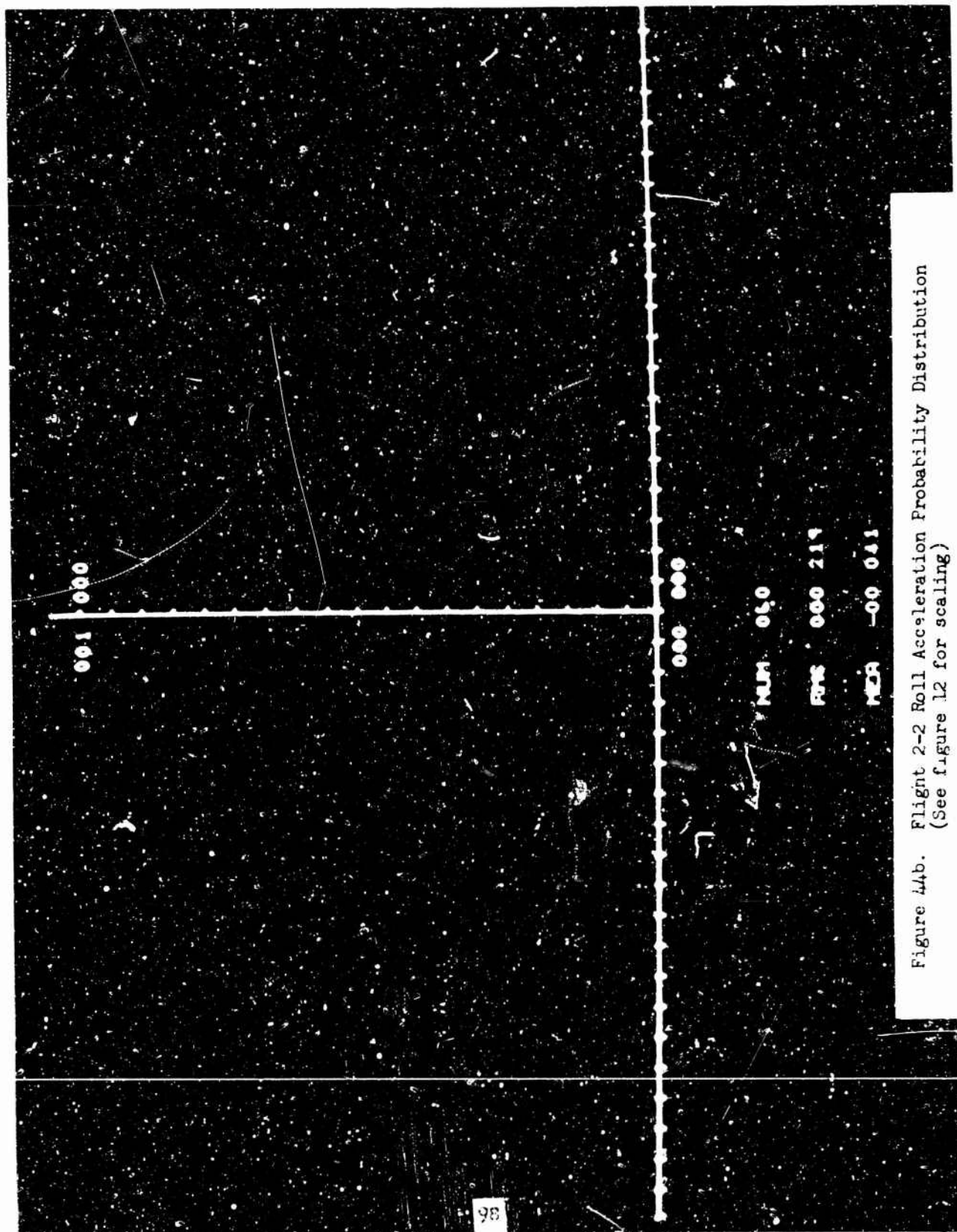


Figure 44b. Flight 2-2 Roll Acceleration Probability Distribution
(See figure 12 for scaling)

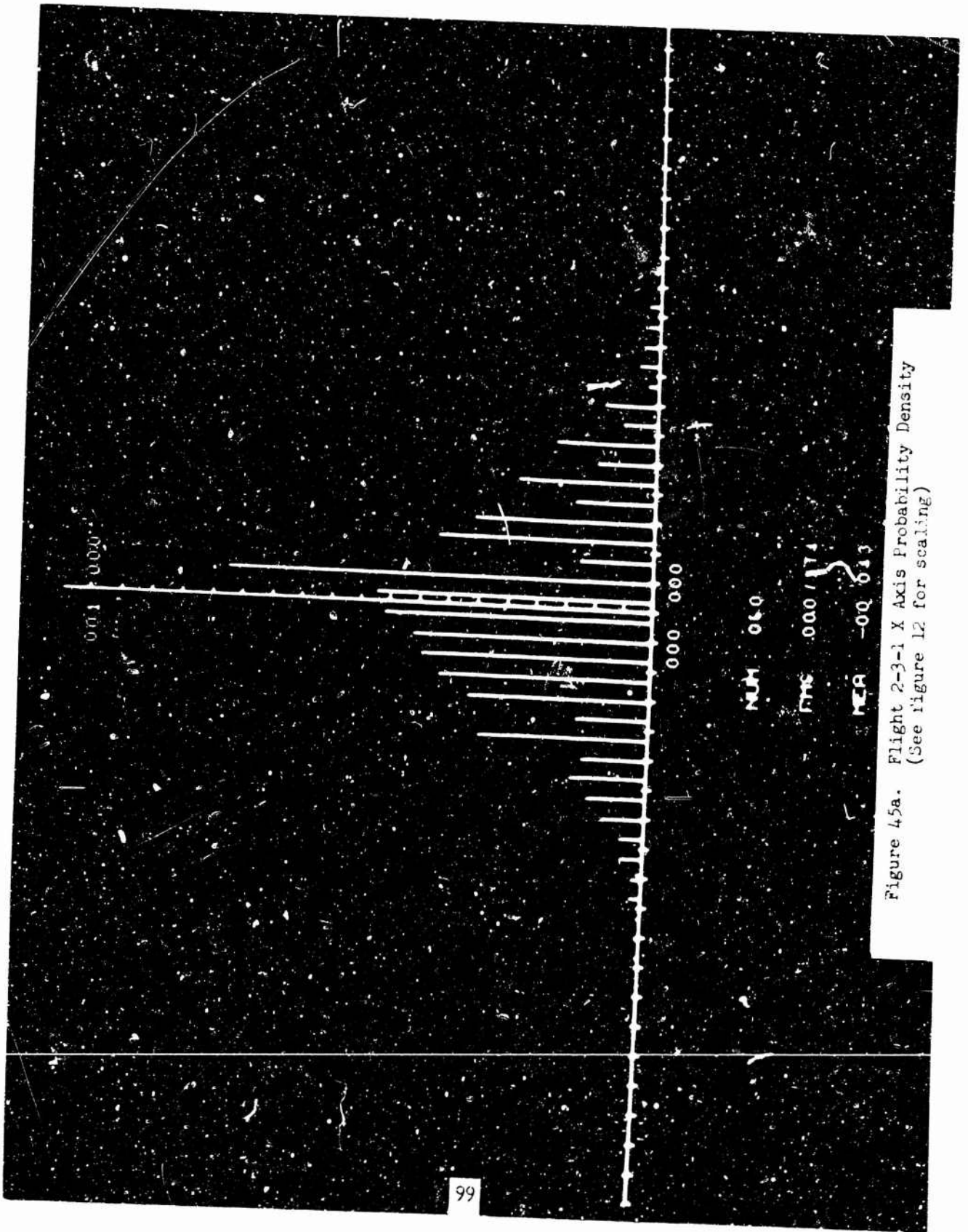
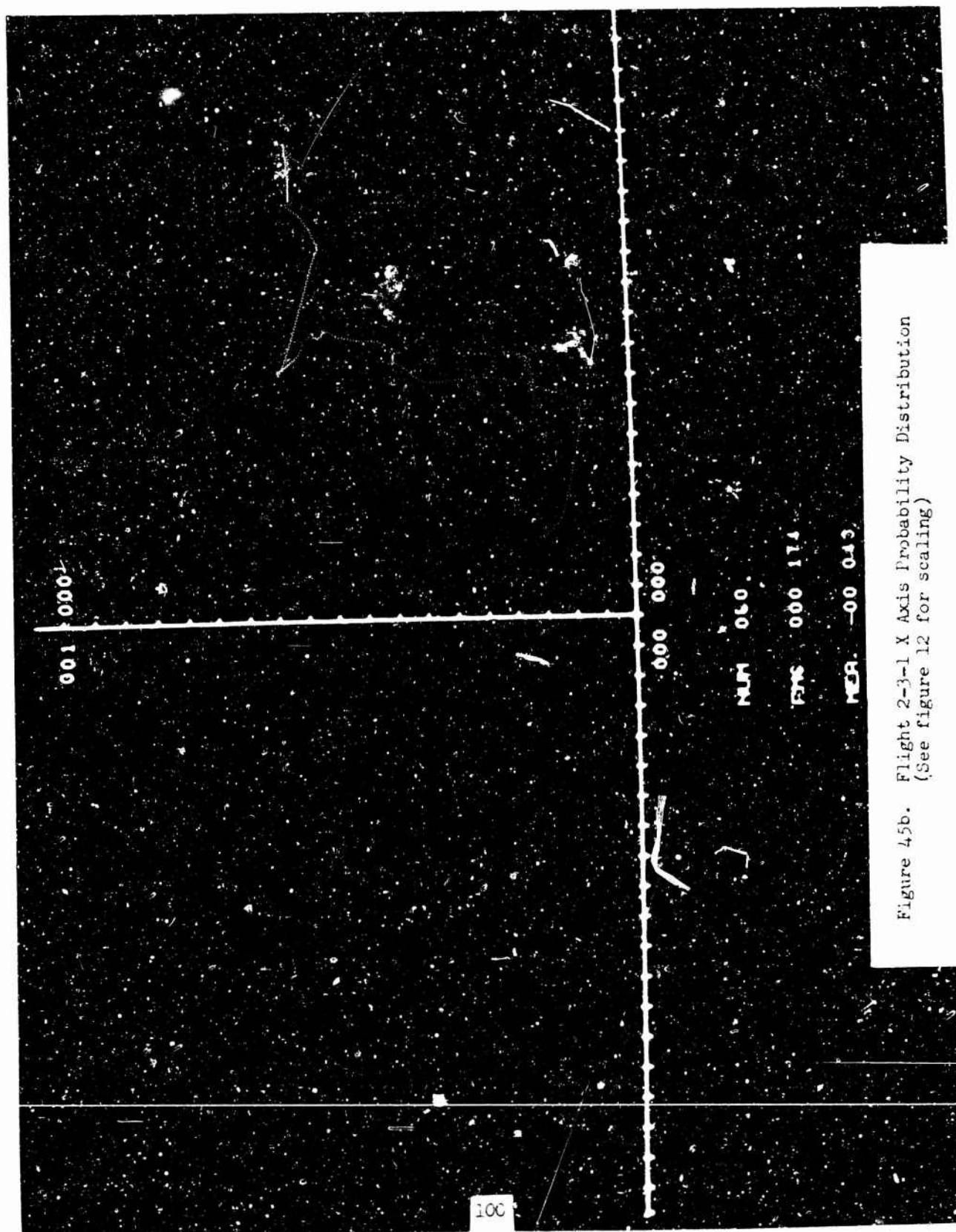


Figure 45a. Flight 2-3-1 X Axis Probability Density
(See figure 12 for scaling)



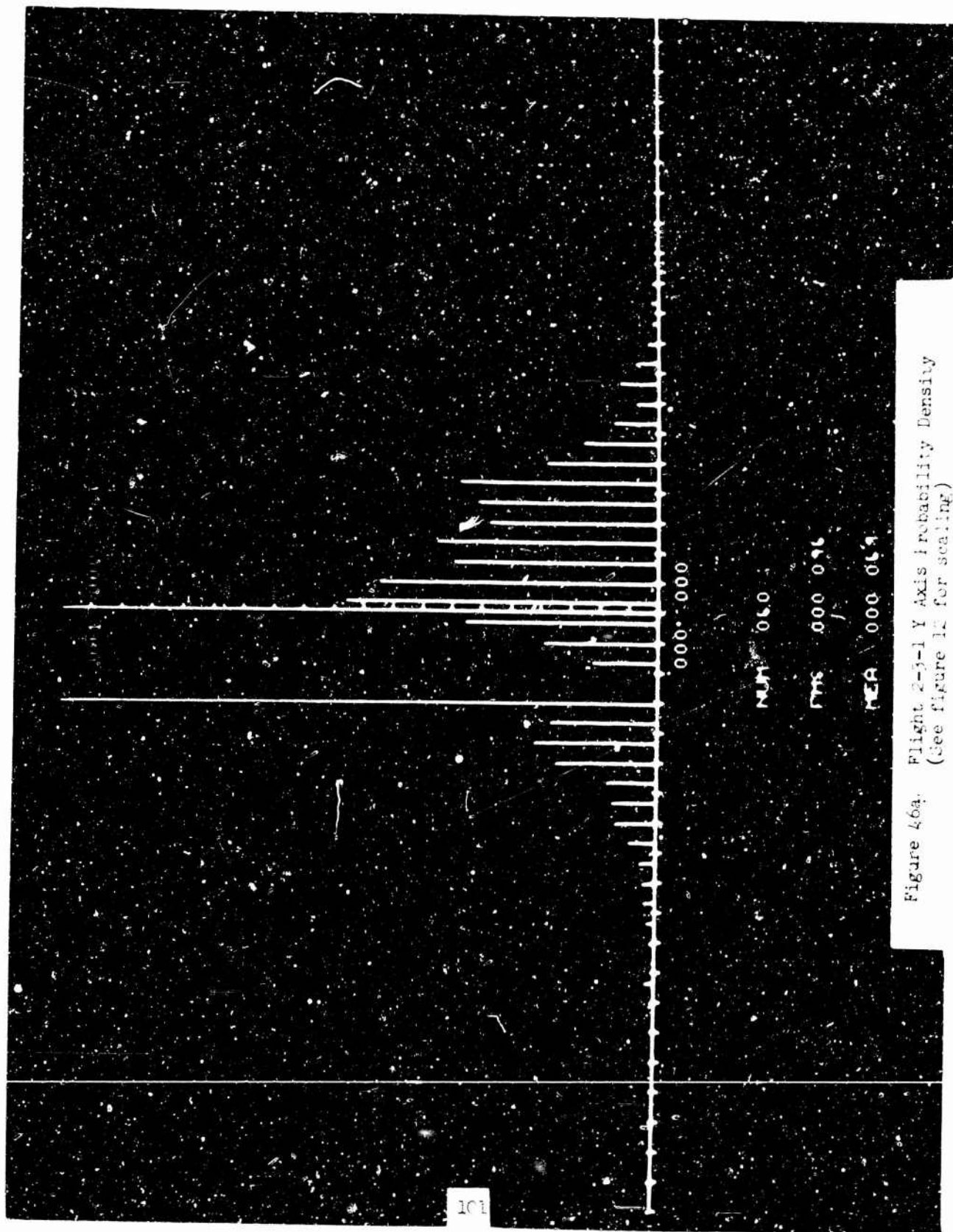


Figure 46a. Flight 2-3-1 Y Axis Probability Density
(See figure 12 for scaling)

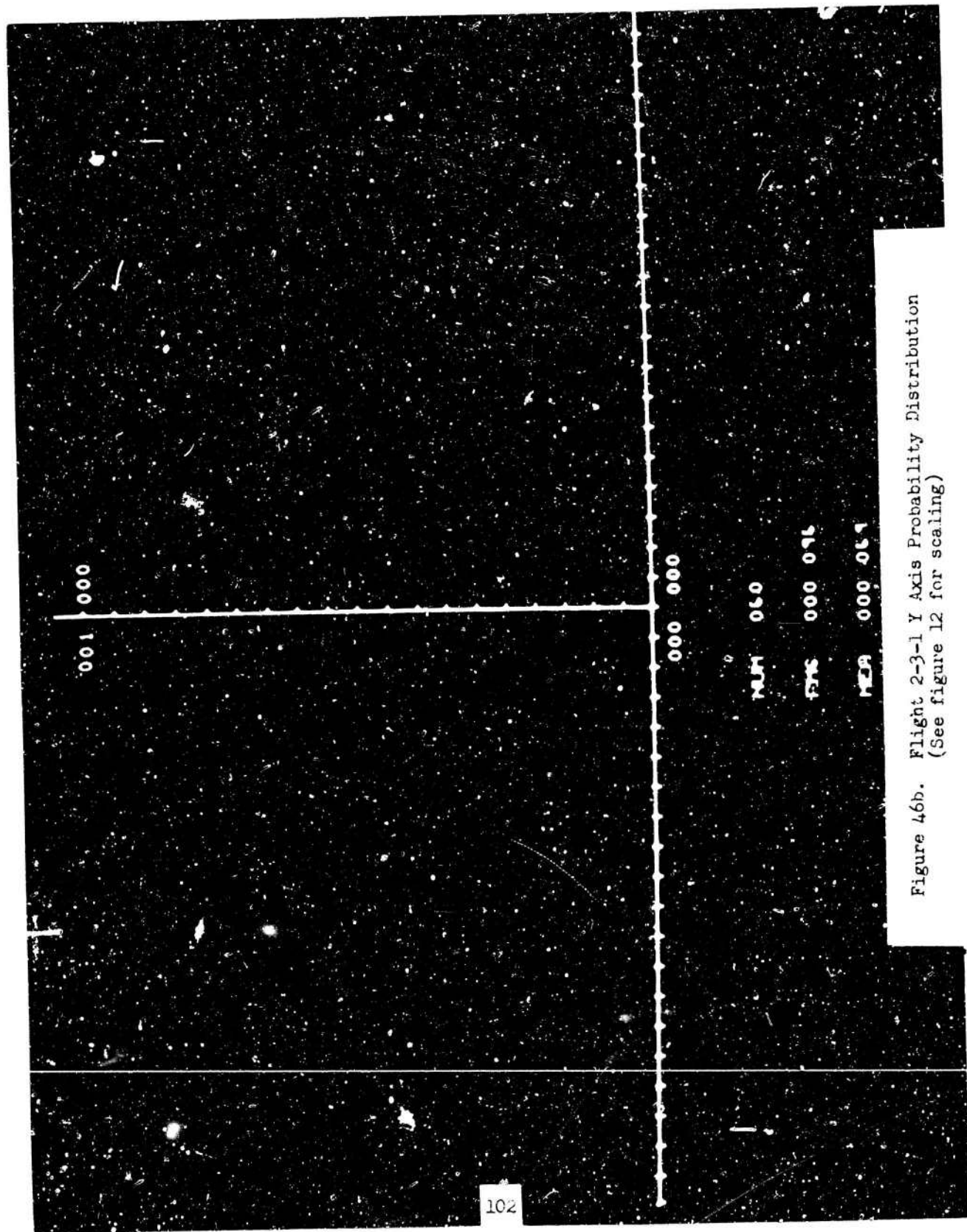


Figure 46b. Flight 2-3-1 Y Axis Probability Distribution
(See figure 12 for scaling)

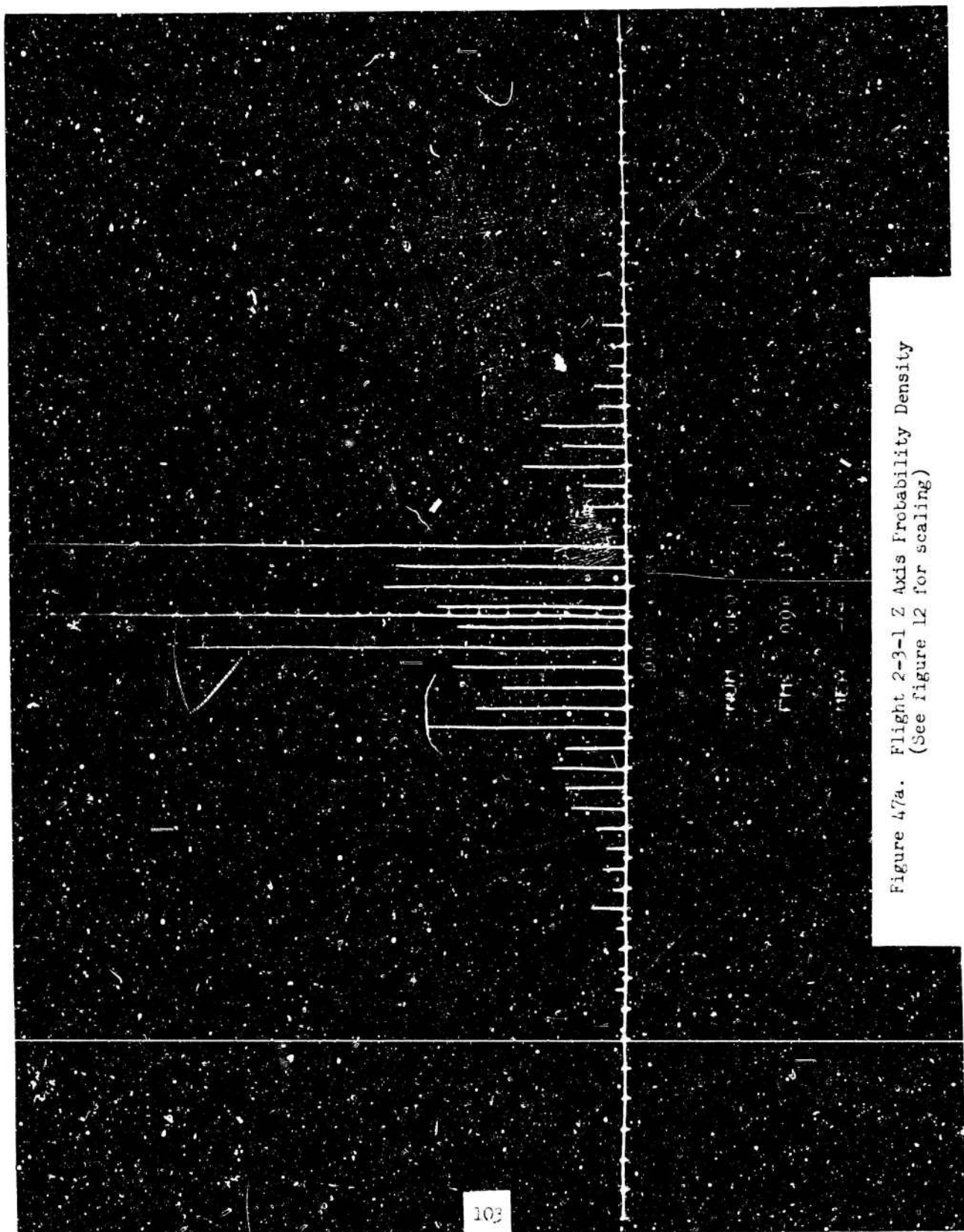


Figure 47a. Flight 2-3-1 Z Axis Probability Density
(See figure 12 for scaling)

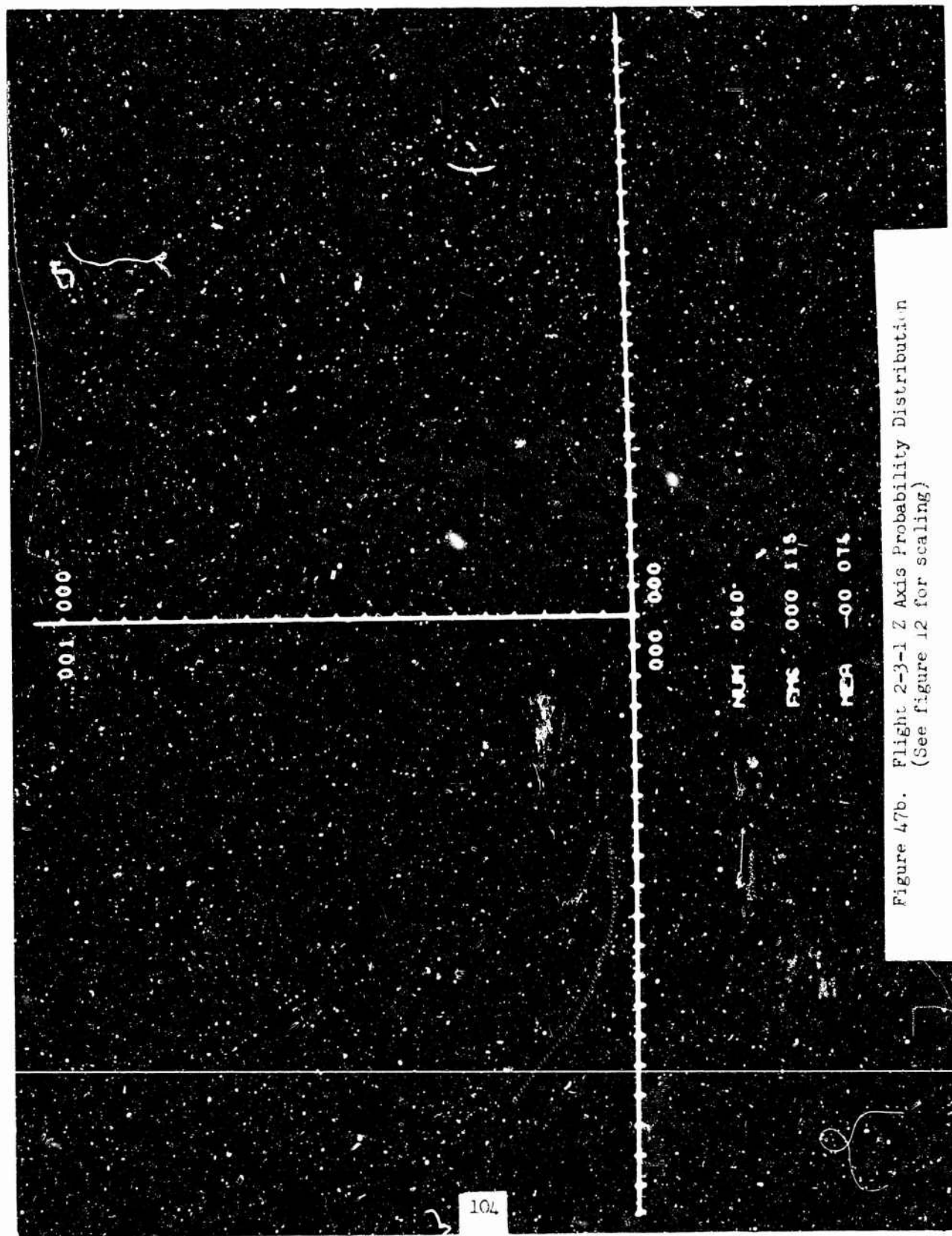


Figure 47b. Flight 2-3-1 Z Axis Probability Distribution
(See figure 12 for scaling)

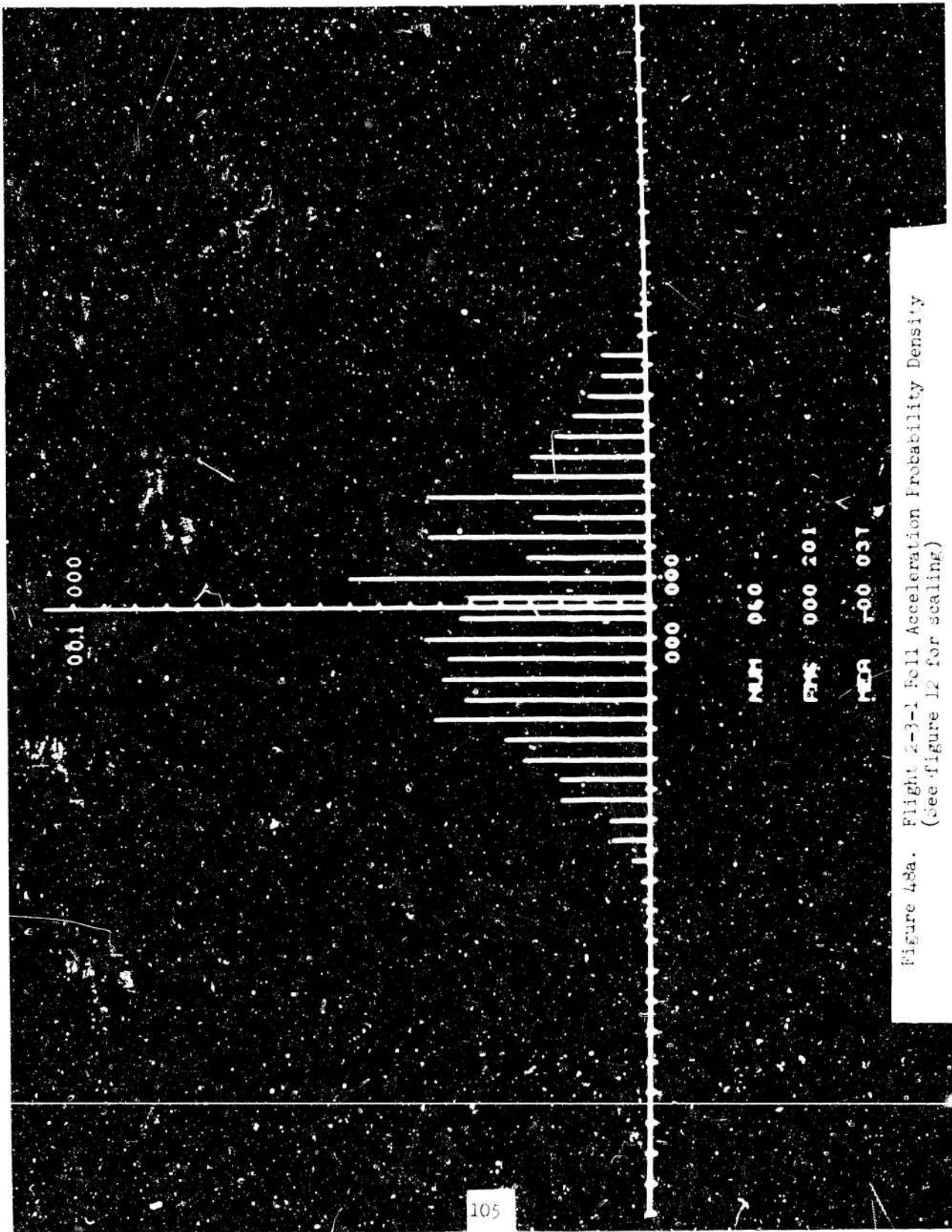
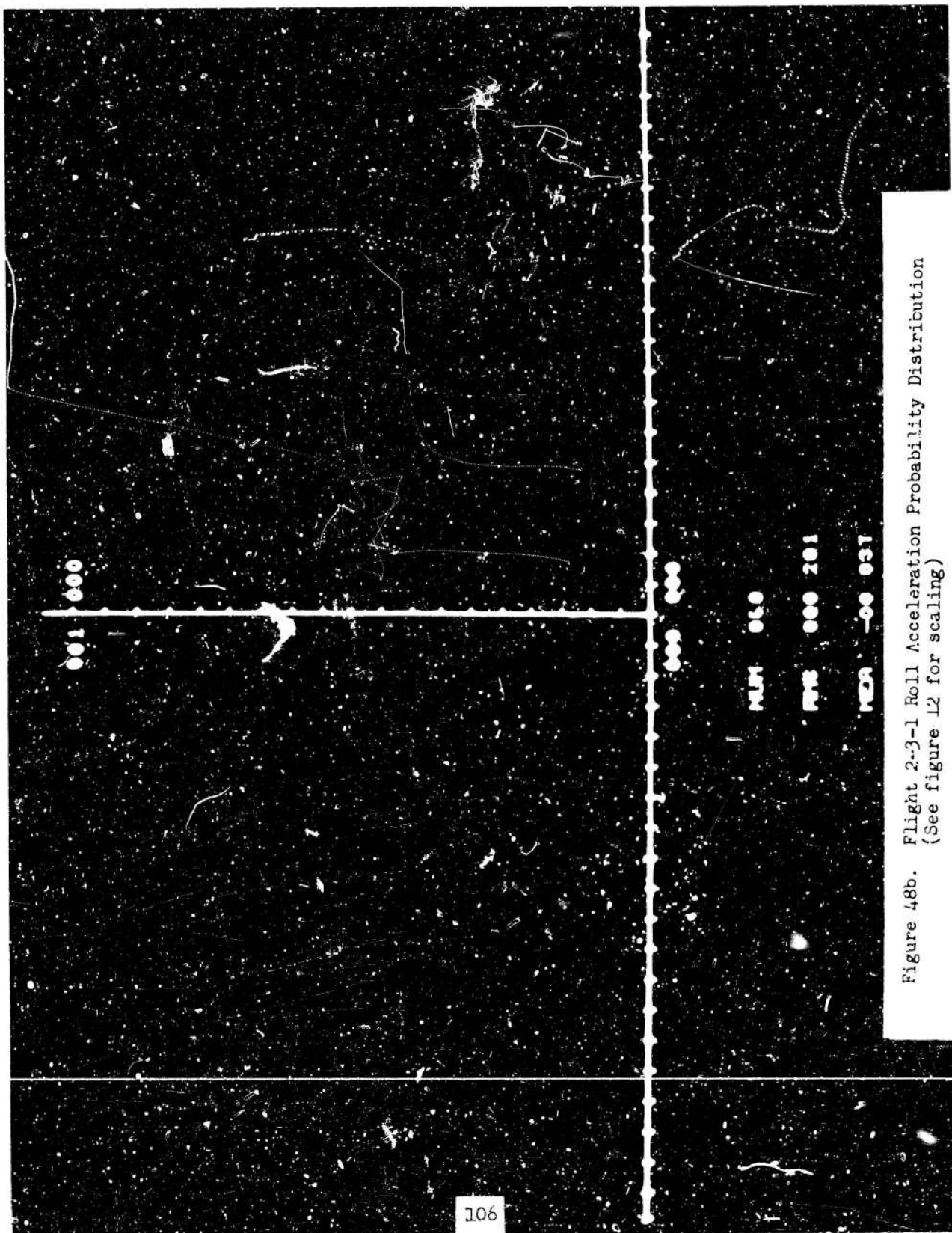


Figure 48a. Flight 2-3-1 Roll Acceleration Probability Density
(See figure 12 for scaling)



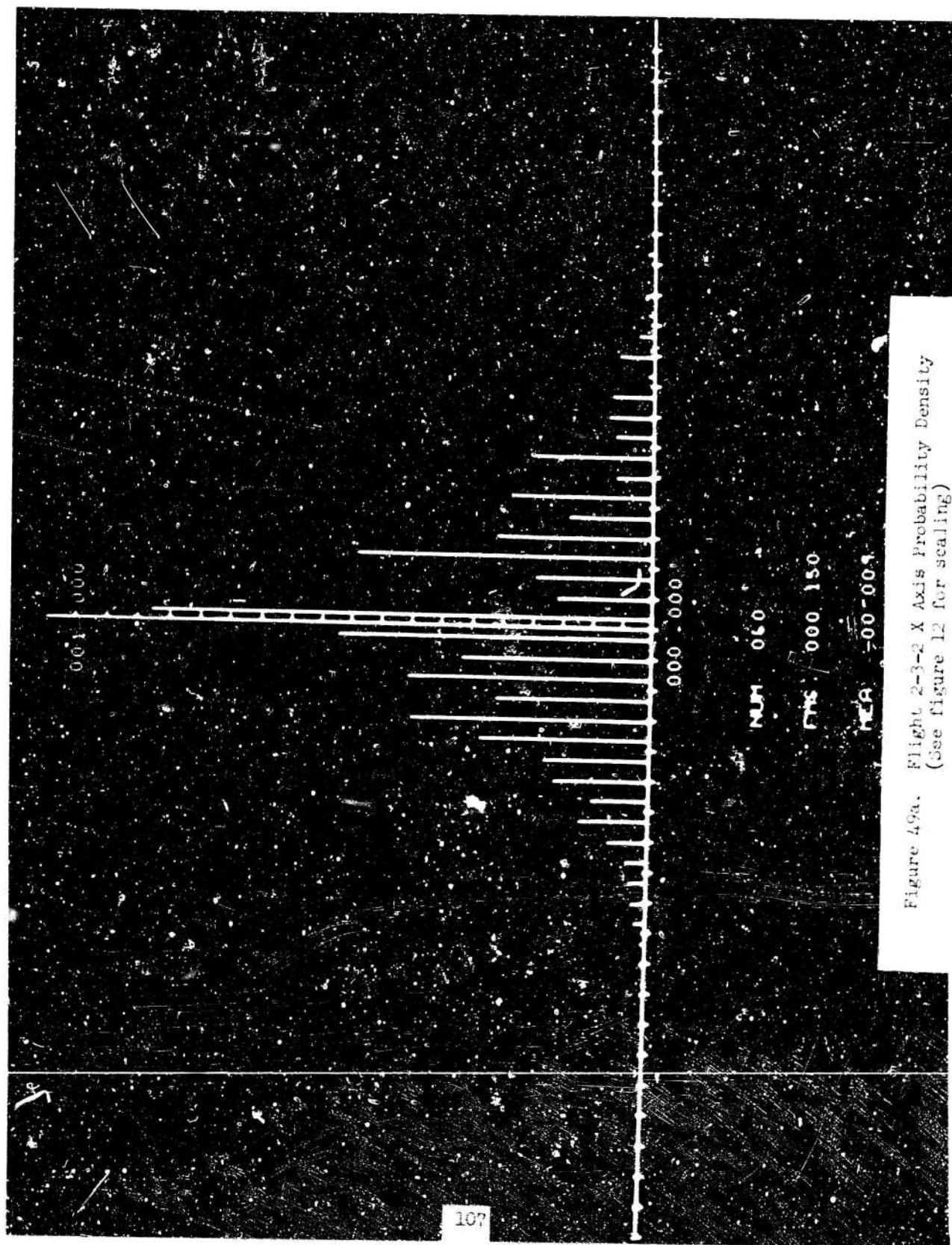


Figure 49a. Flight 2-3-2 X Axis Probability Density
(See figure 12 for scaling)

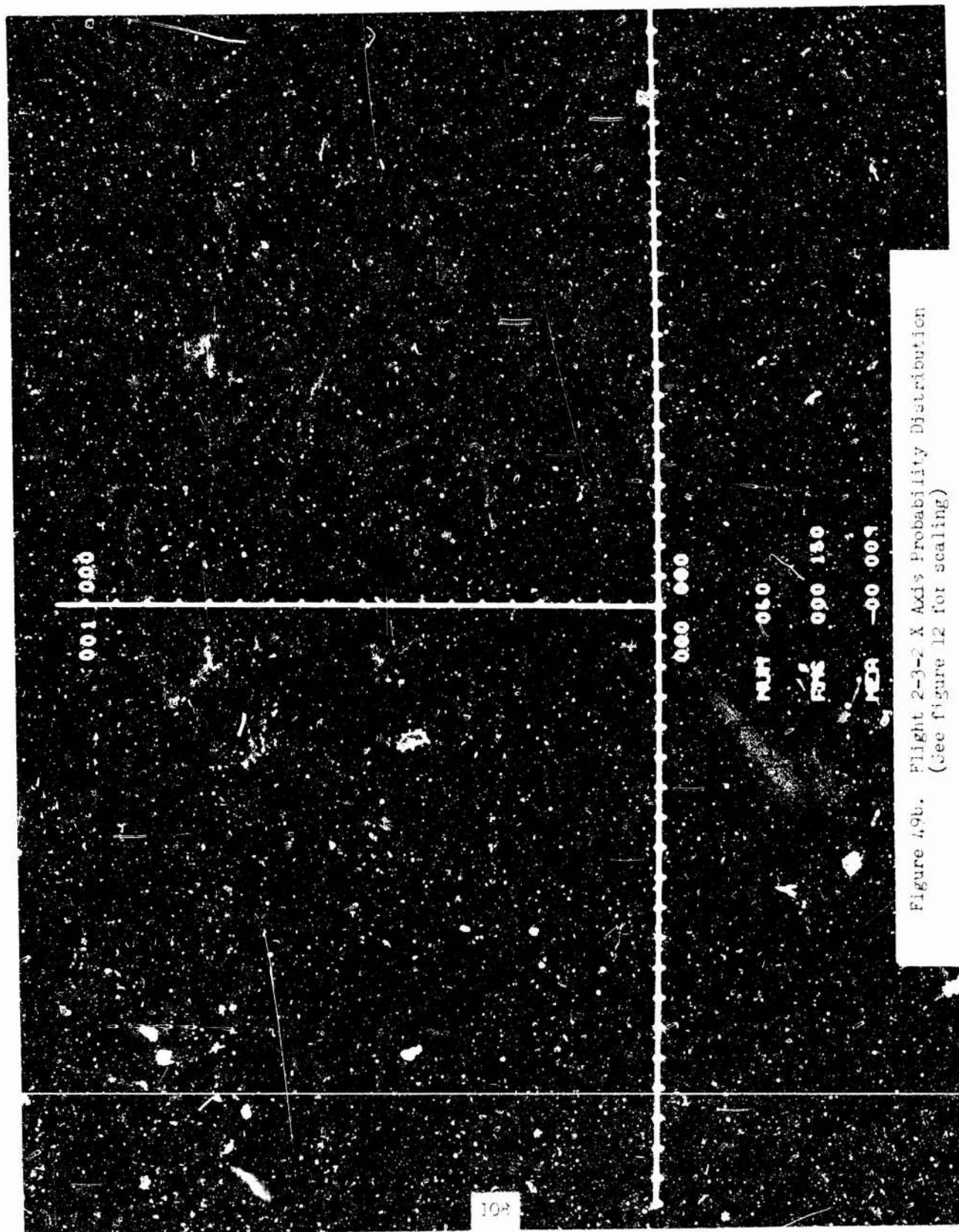
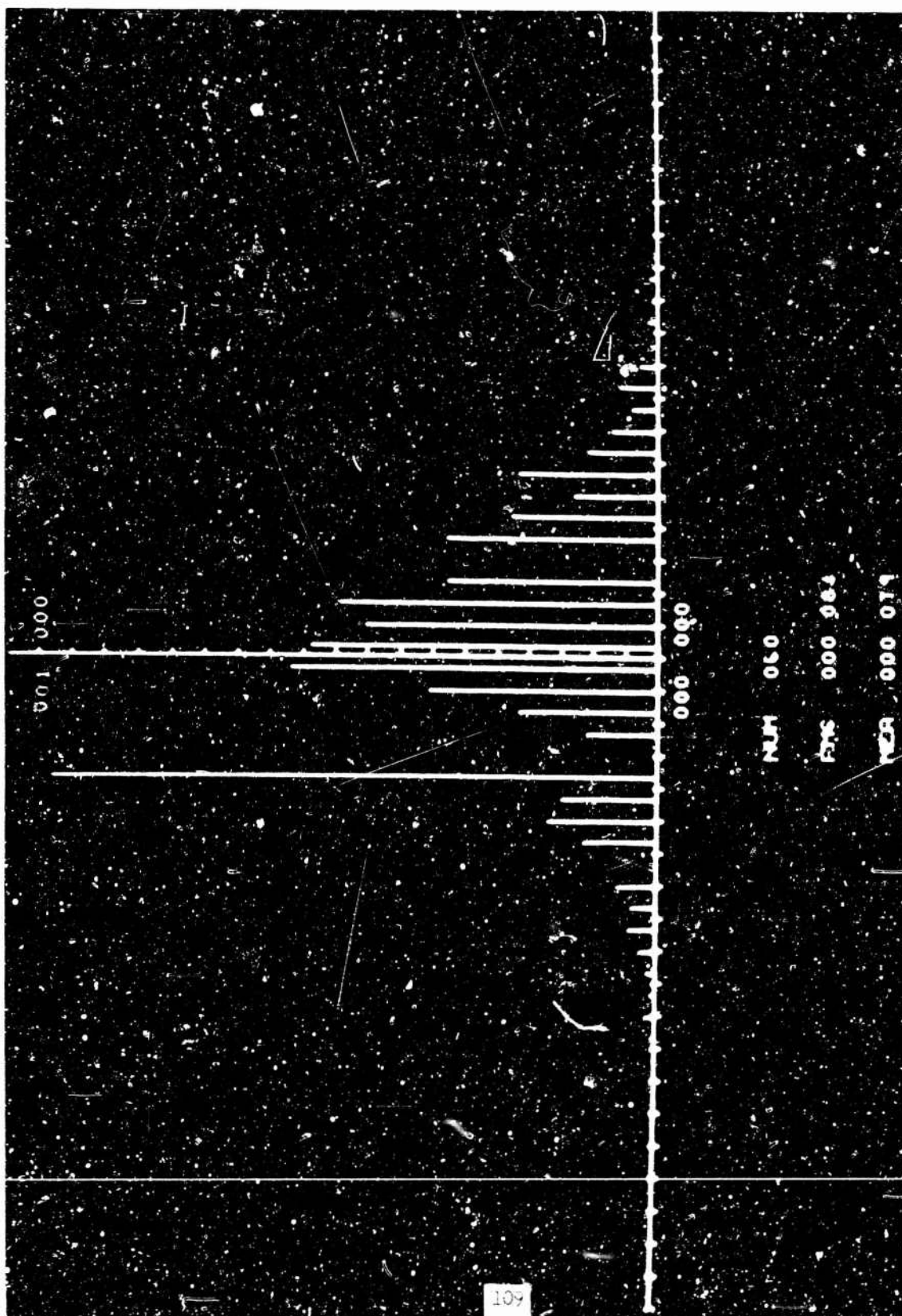


Figure 4.9b. Flight 2-3-2 X Axis Probability Distribution
(See figure 12 for scaling)



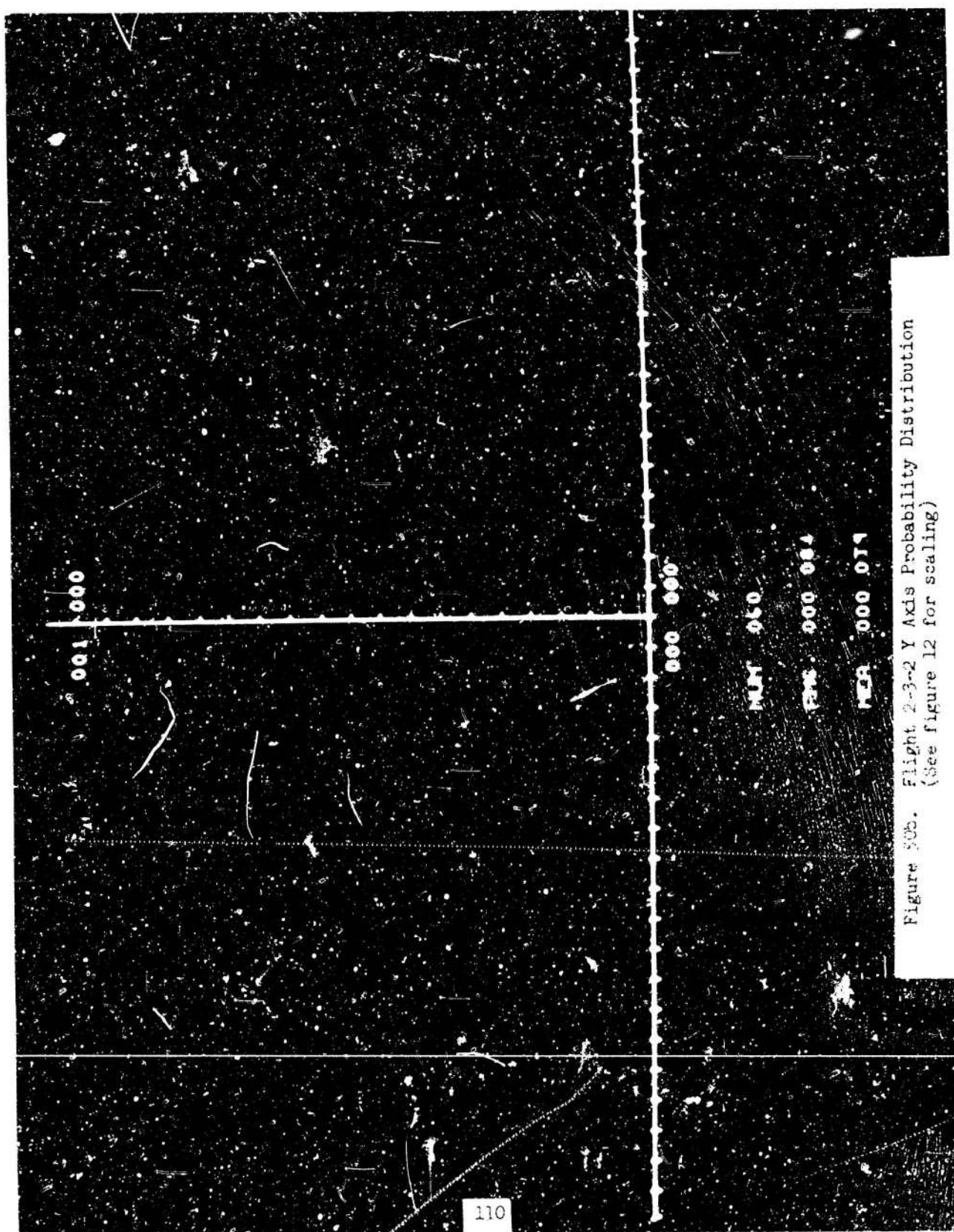


Figure 50b. Flight 2-3-2 Y Axis Probability Distribution
(See figure 12 for scaling)

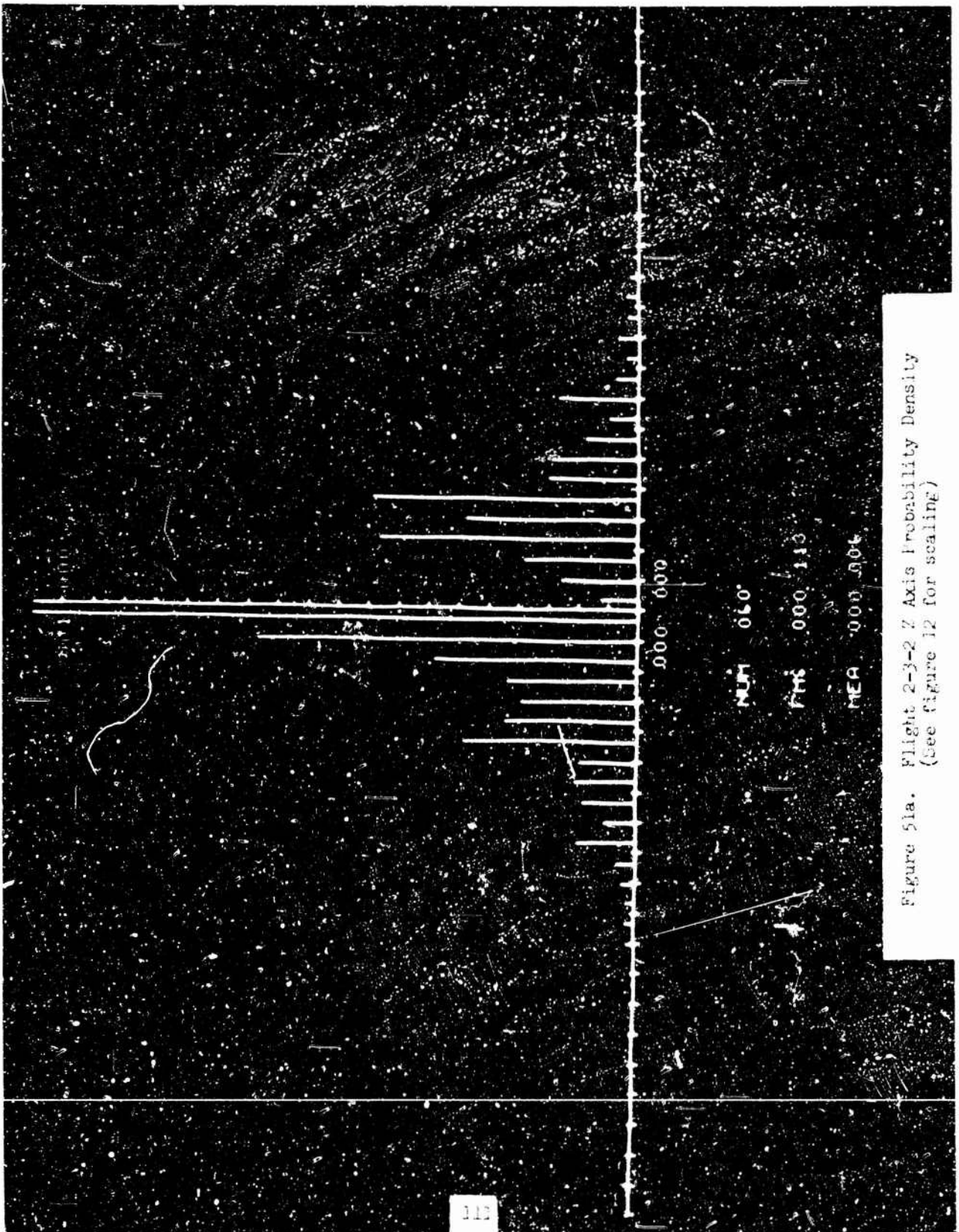


Figure 51a. Flight 2-3-2 Z Axis Probability Density
(See figure 12 for scaling)

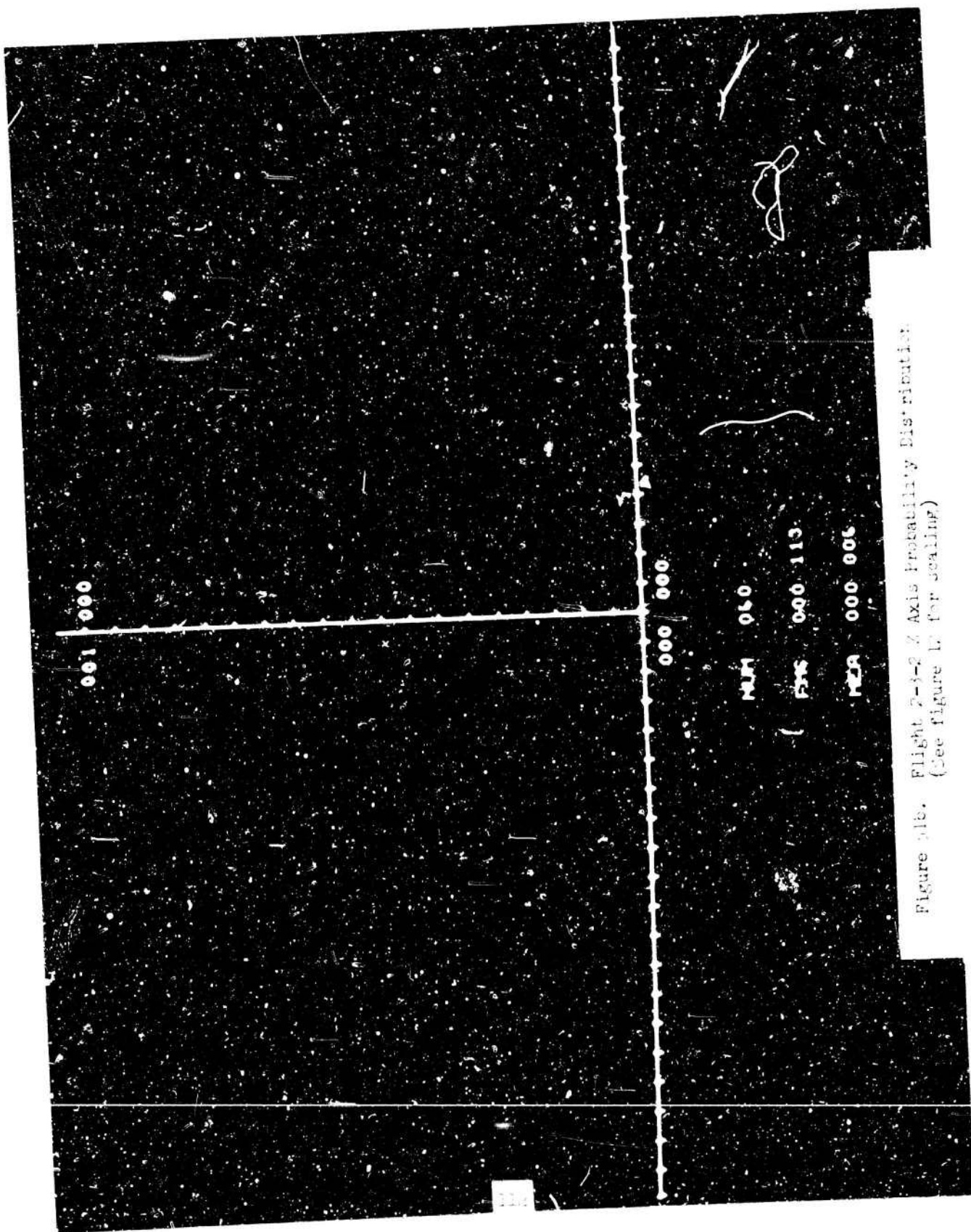


Figure 913. Flight 7-3-2 Z Axis Probability Distribution
(See figure 12 for scaling)

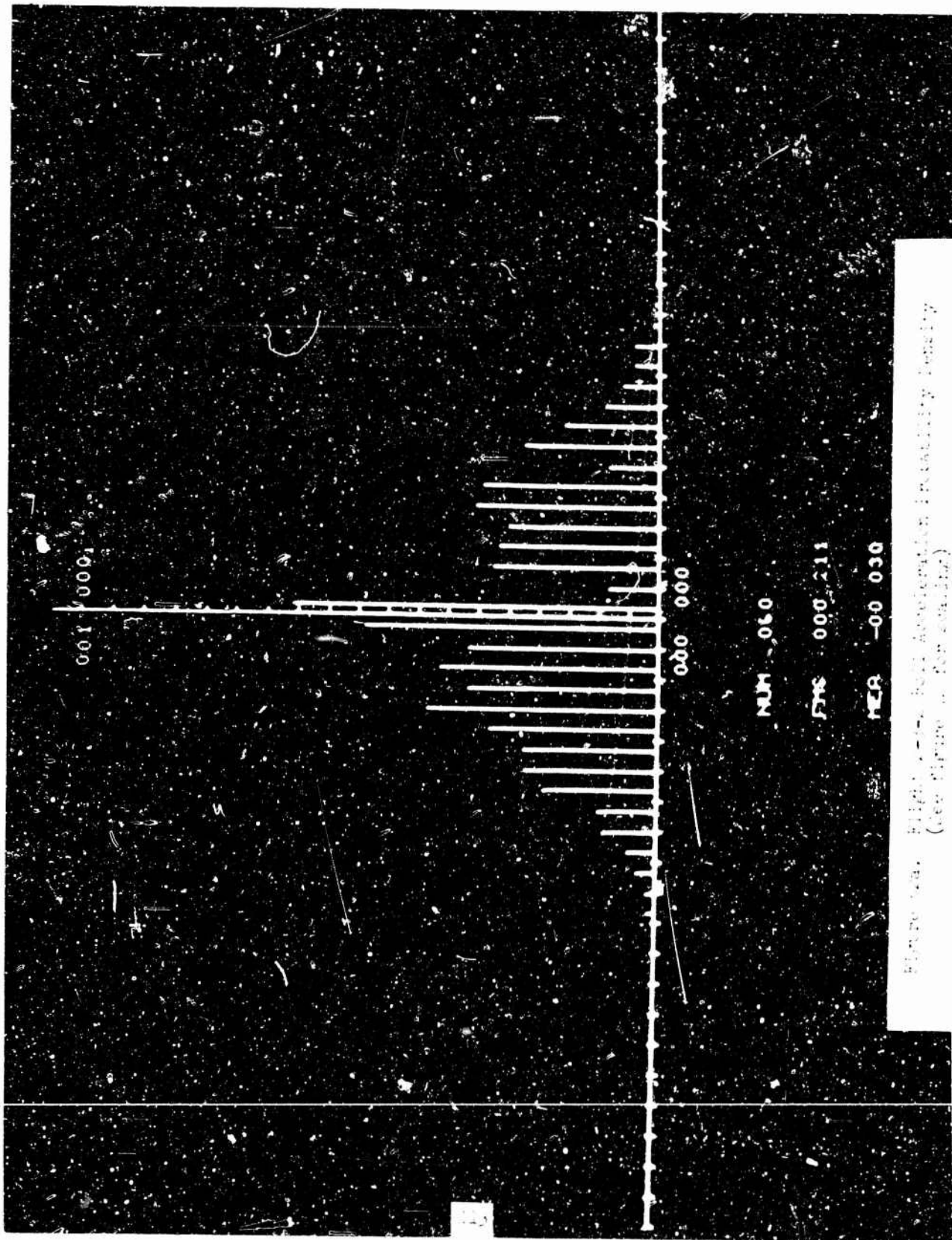


Photo 104. High-speed film developed in Kodak D-19
(see film in box 104)

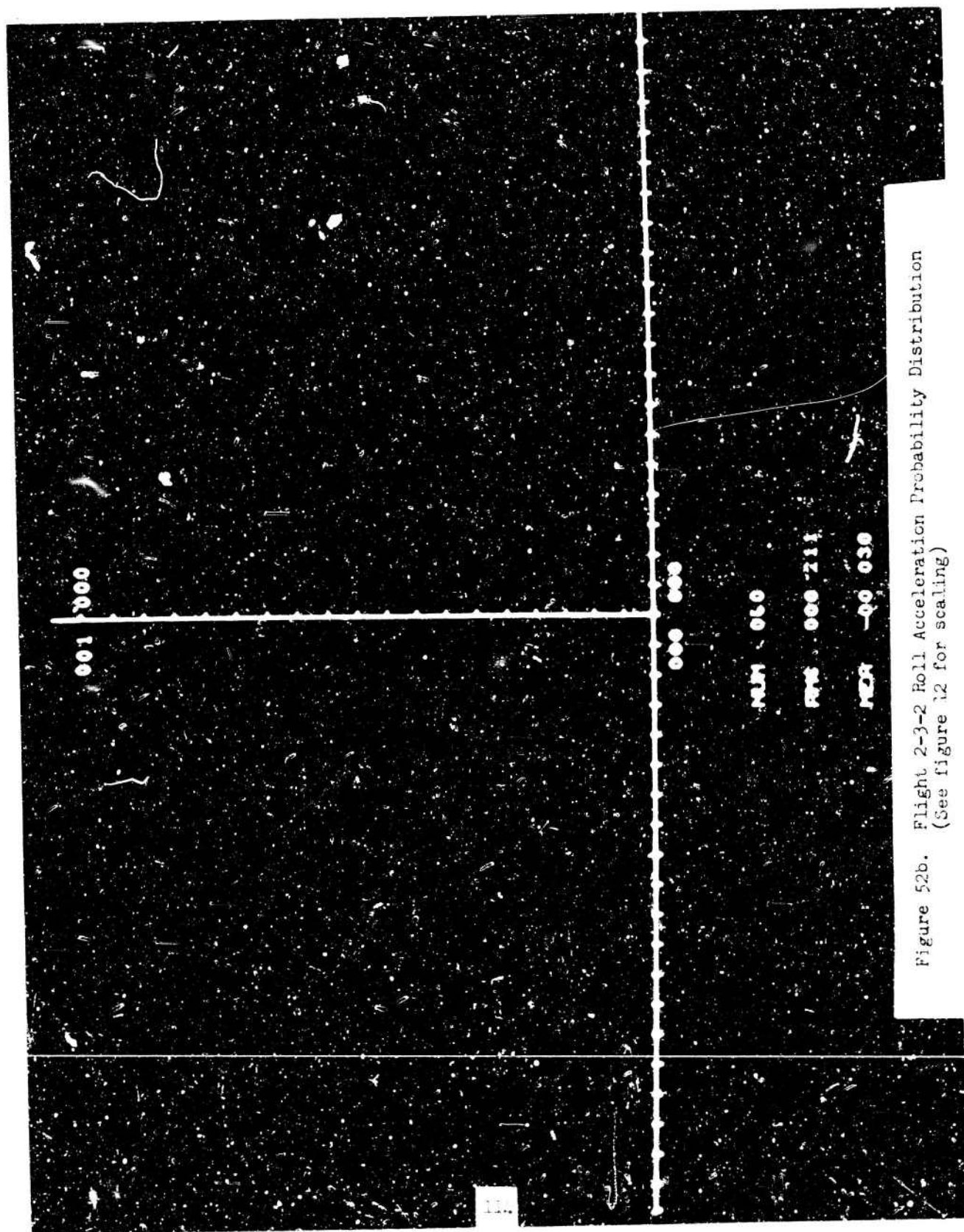


Figure 52b. Flight 2-3-2 Roll Acceleration Probability Distribution
(See figure 12 for scaling)

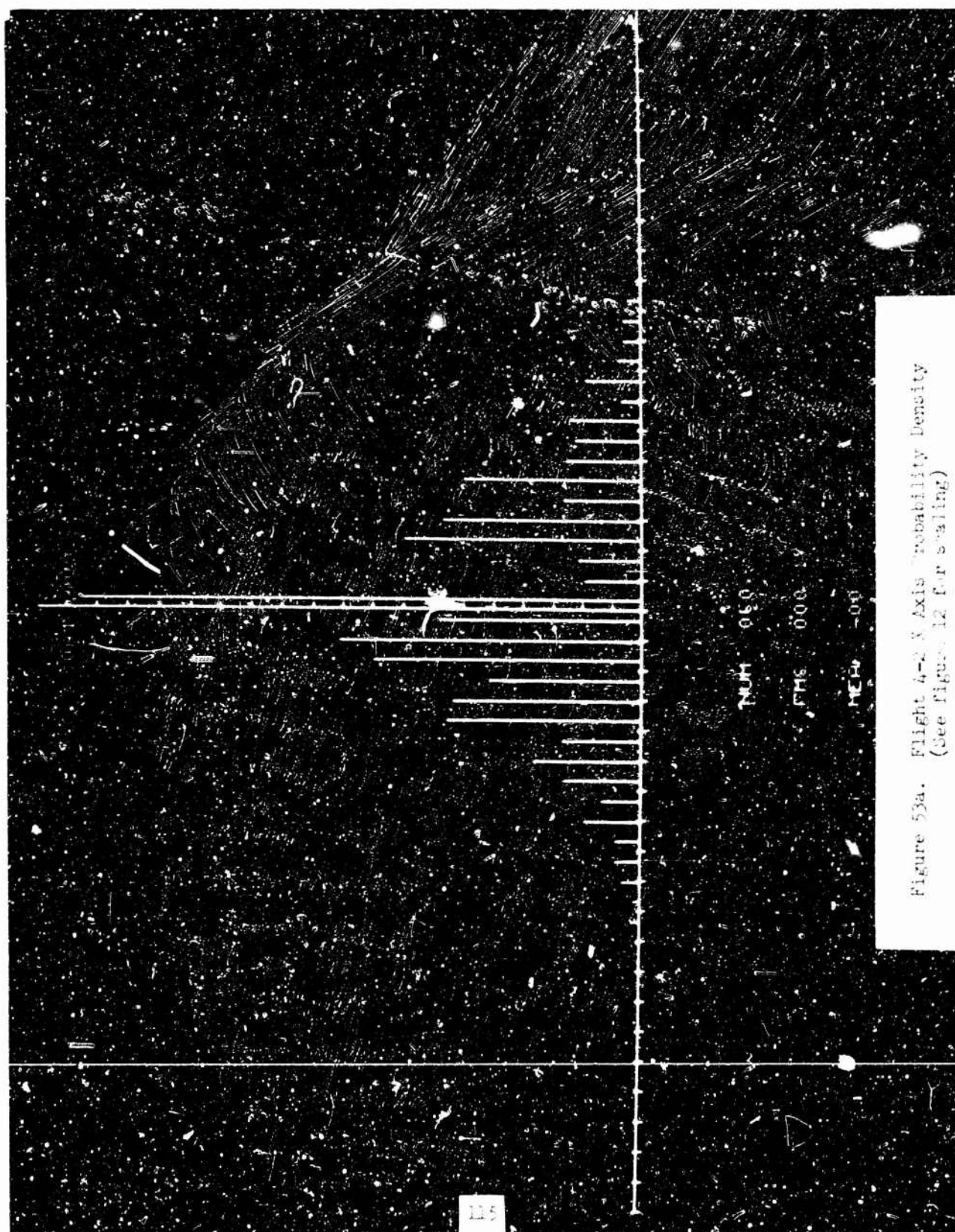


Figure 53a. Flight 4-2 X Axis Probability Density
(See figure 12 for scaling)

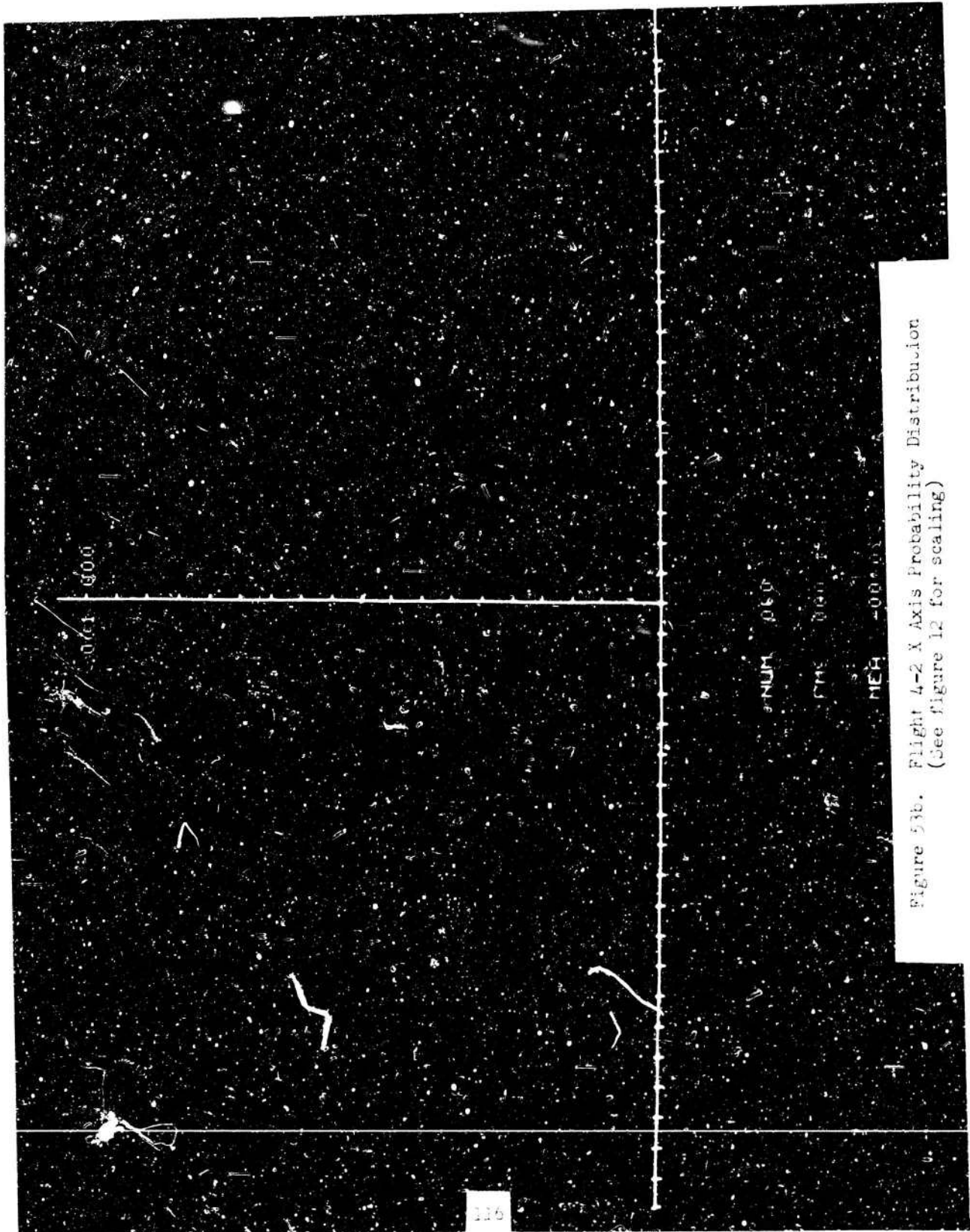


Figure 53b. Flight 4-2 X Axis Probability Distribution
(See figure 12 for scaling)

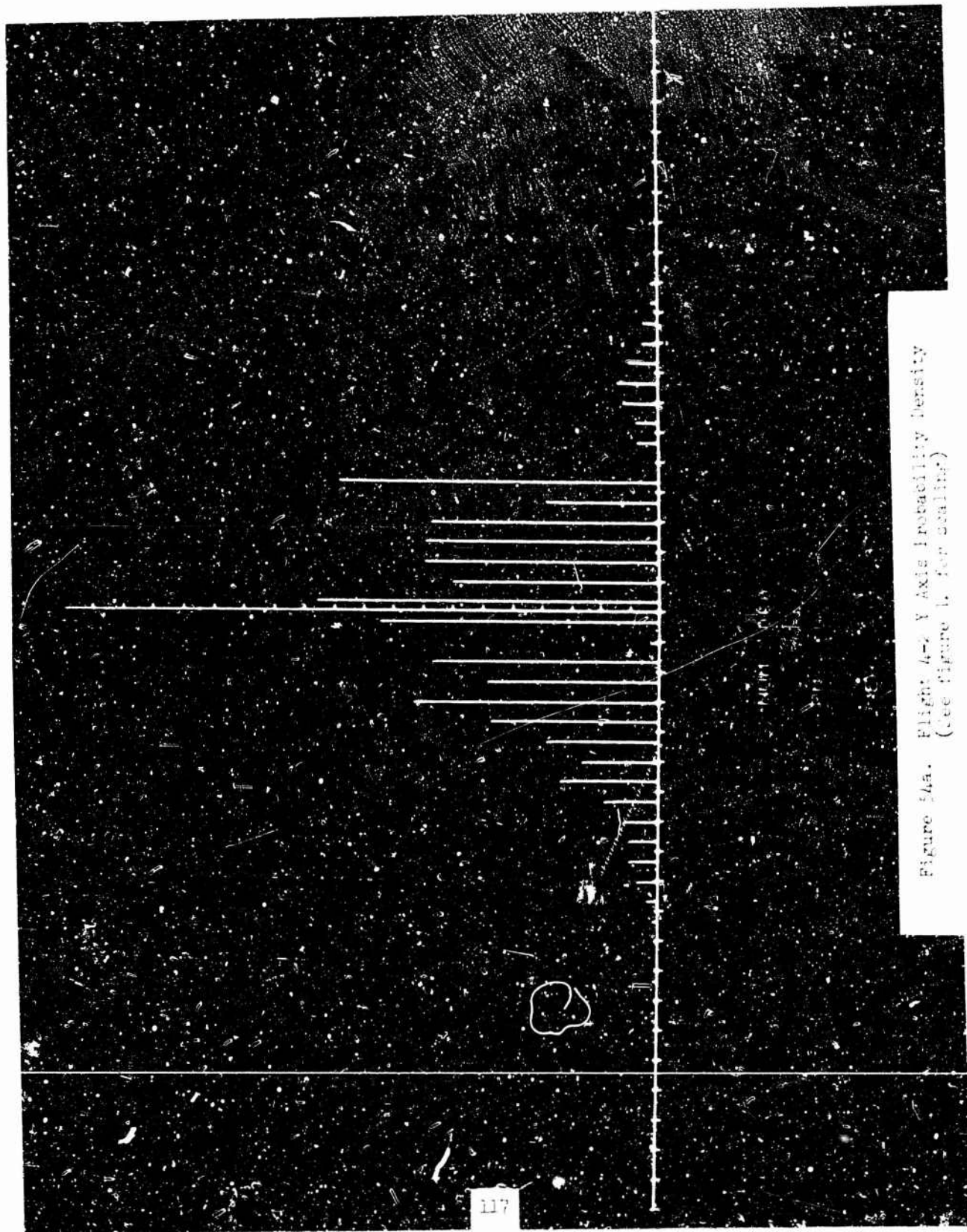


Figure 4a. Flight 4-2 Y Axis Probability Density
(See Figure 1. for Scaling)

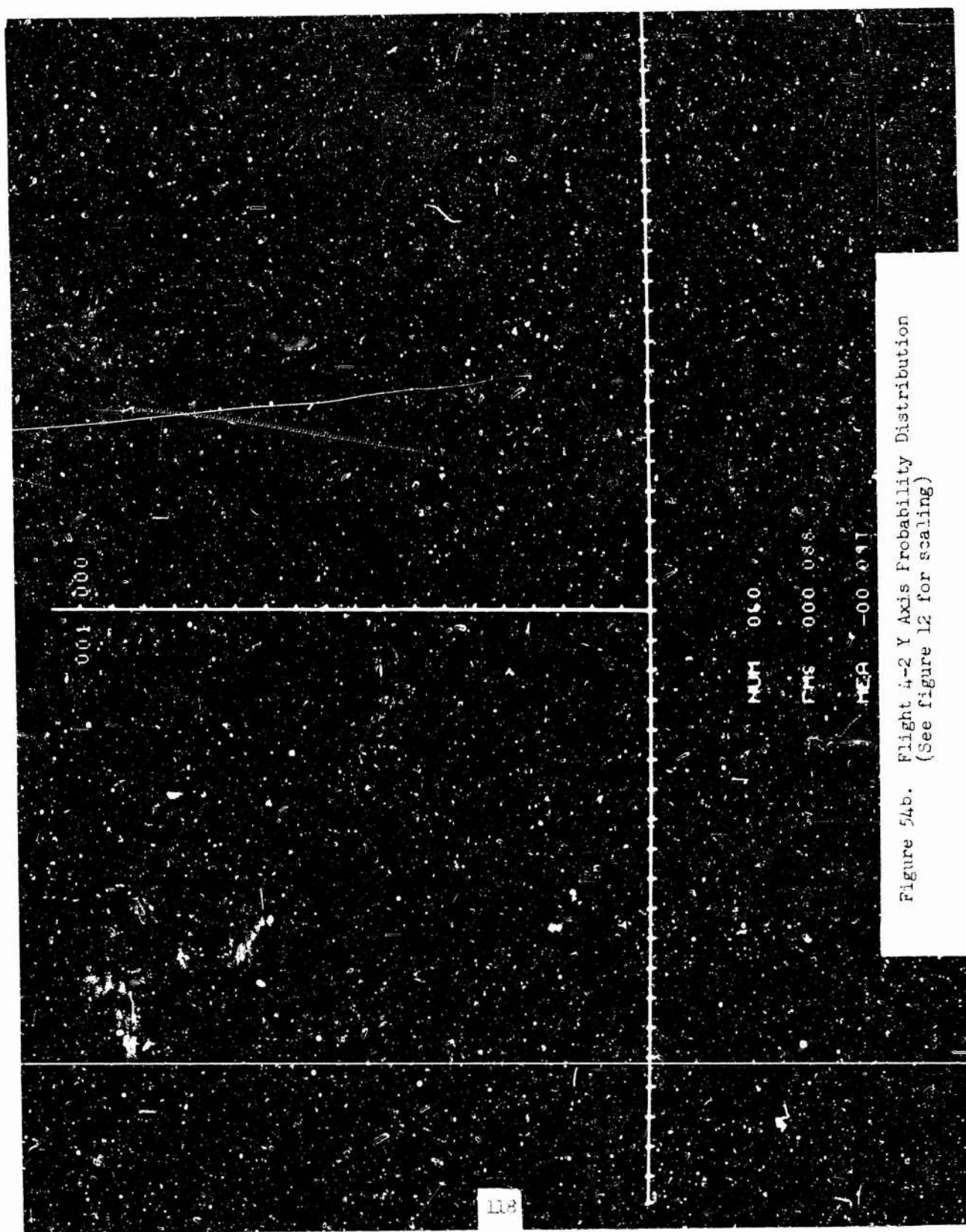


Figure 54b. Flight 4-2 Y Axis Probability Distribution
(See figure 12 for scaling)

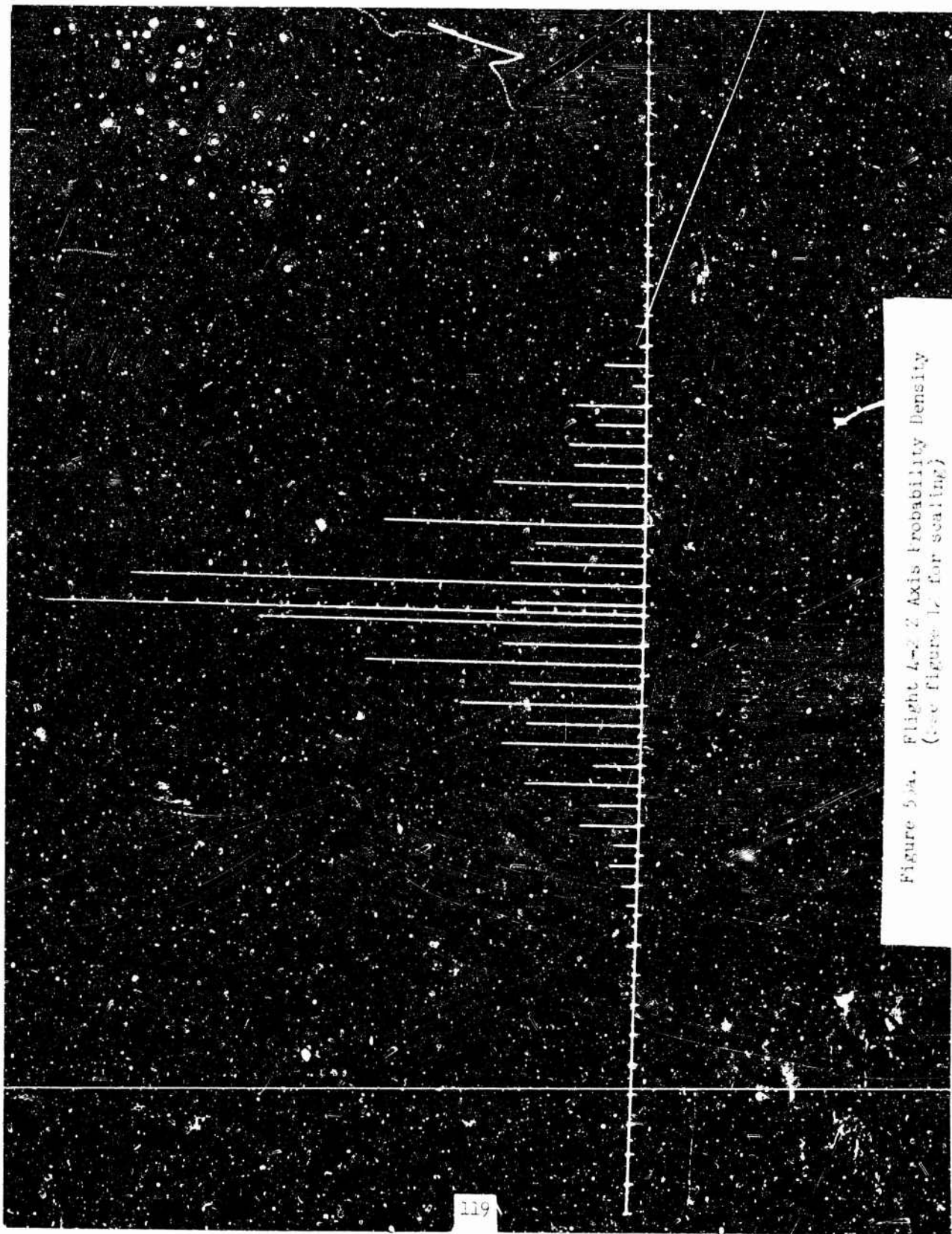


Figure 5-5a. Flight 4-2 2 Axis Probability Density
(see figure 1-2 for scaling)

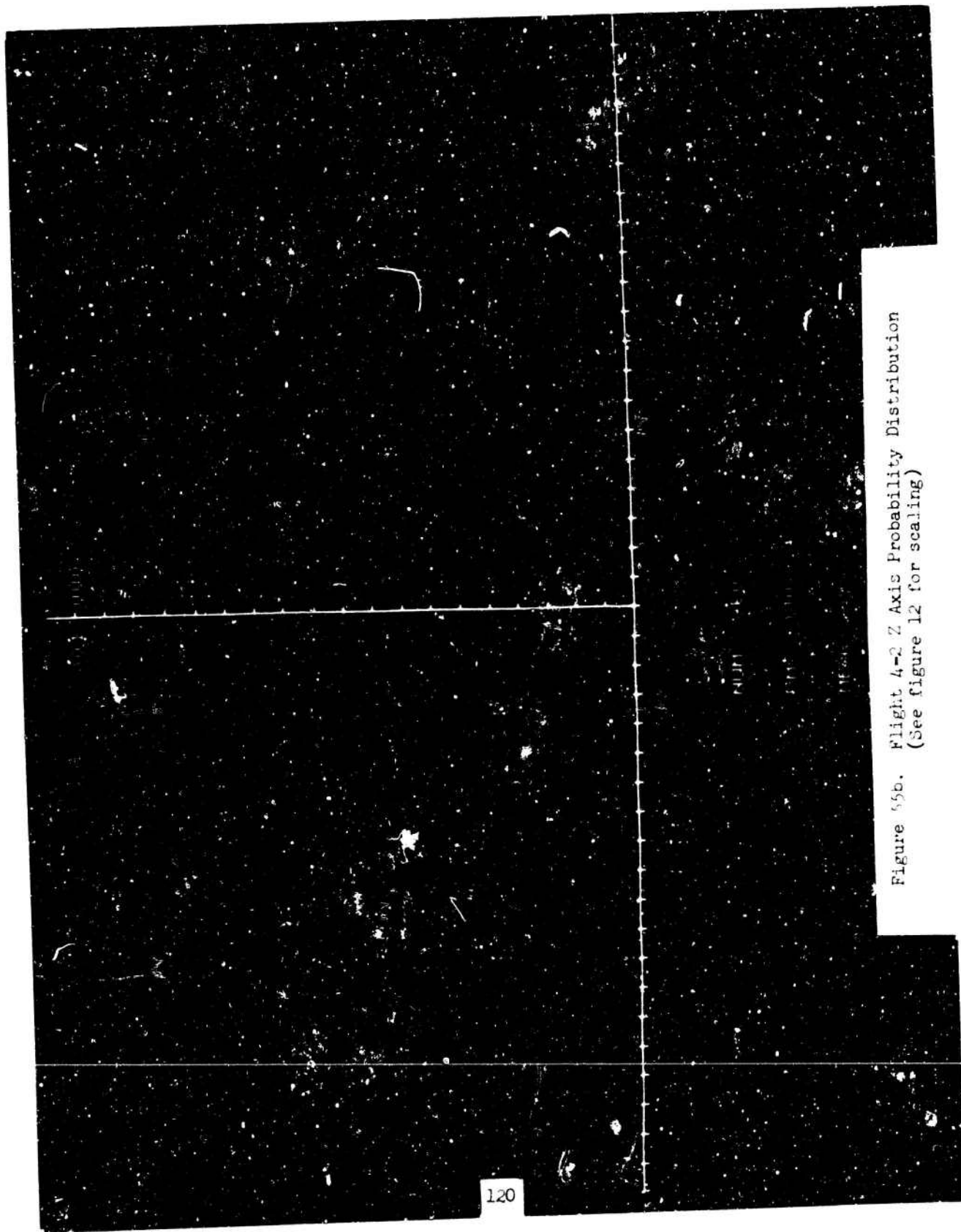


Figure 55b. Flight 4-2 Z Axis Probability Distribution
(See figure 12 for scaling)

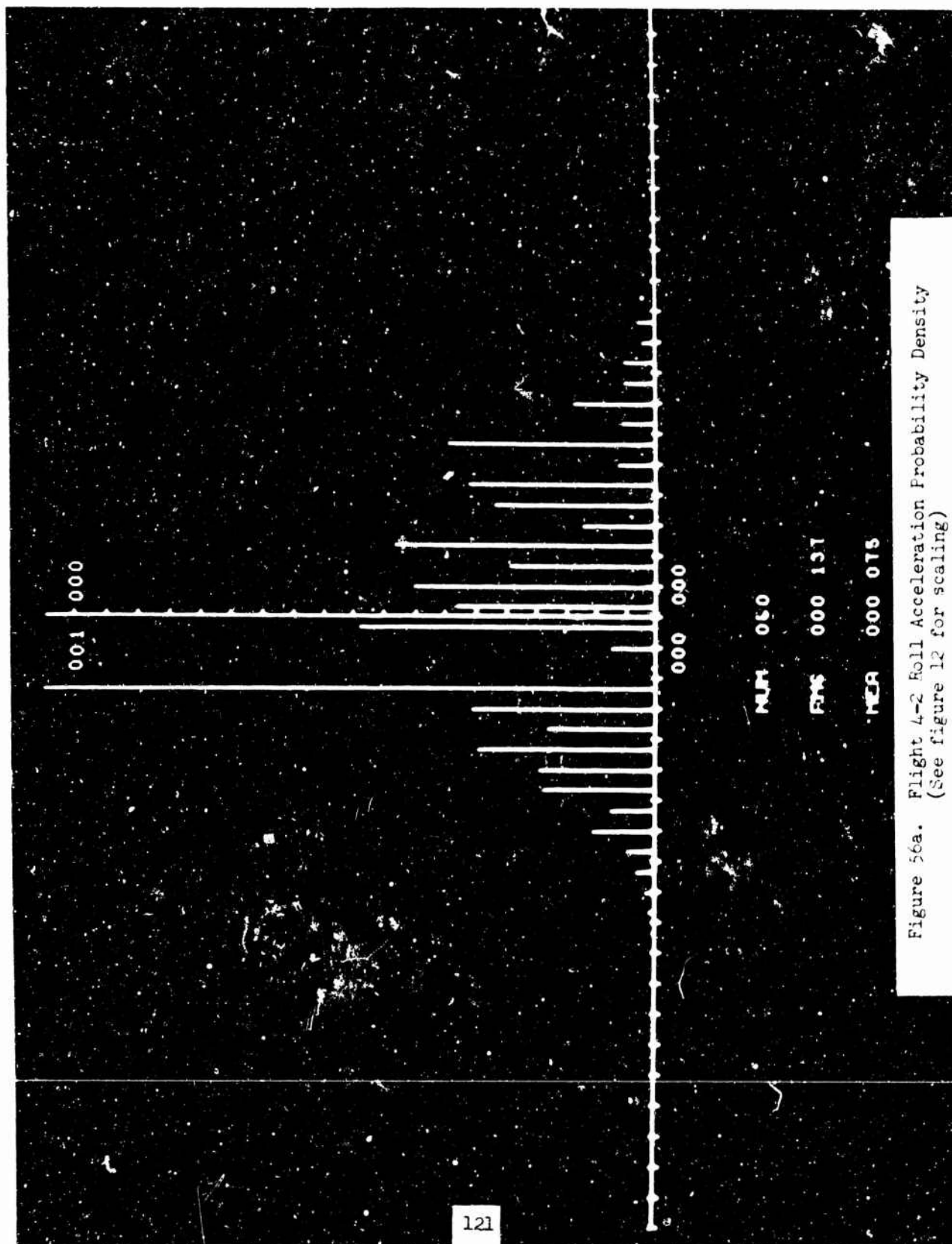


Figure 56a. Flight 4-2 Roll Acceleration Probability Density
(See figure 12 for scaling)

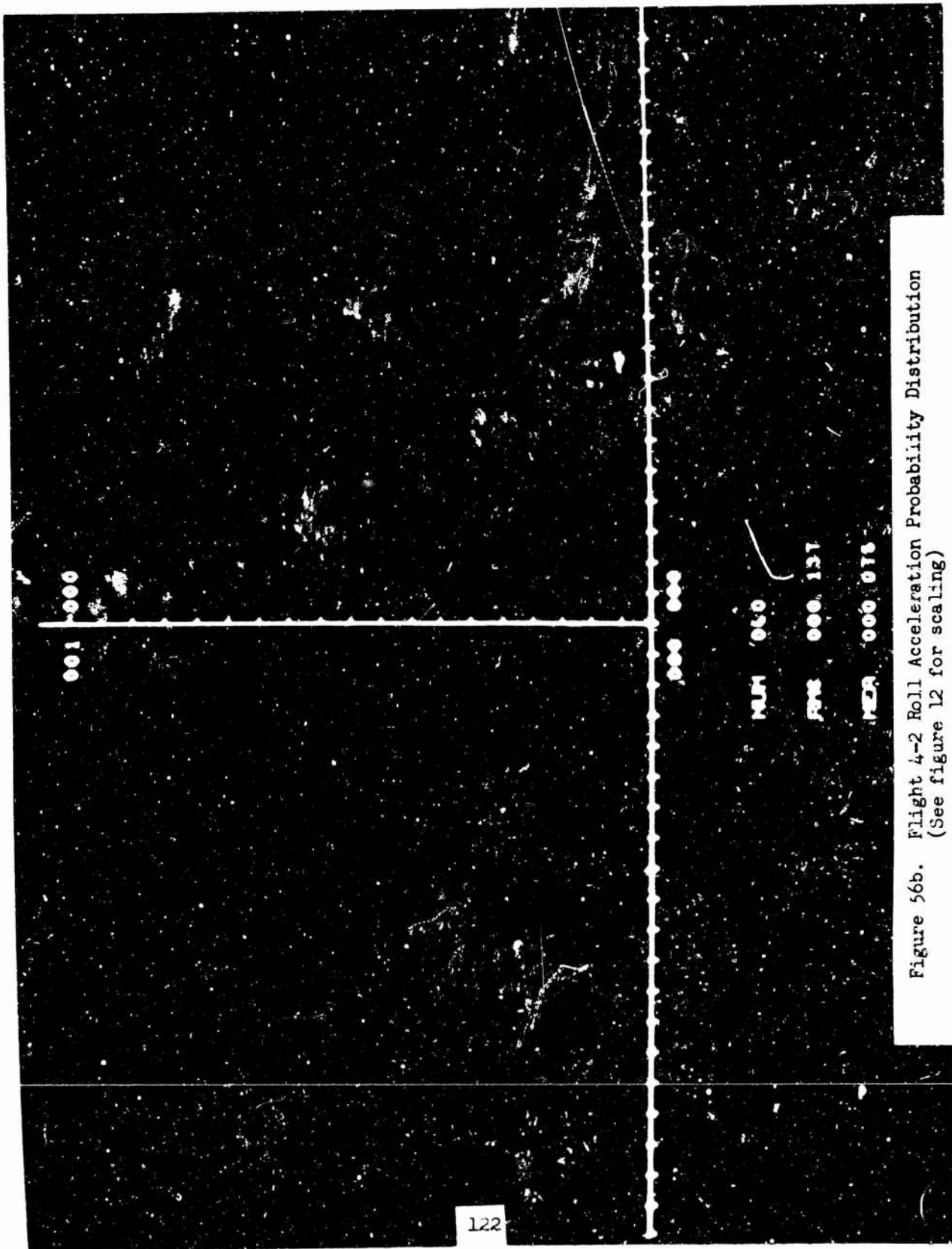


Figure 56b. Flight 4-2 Roll Acceleration Probability Distribution
(See figure 12 for scaling)

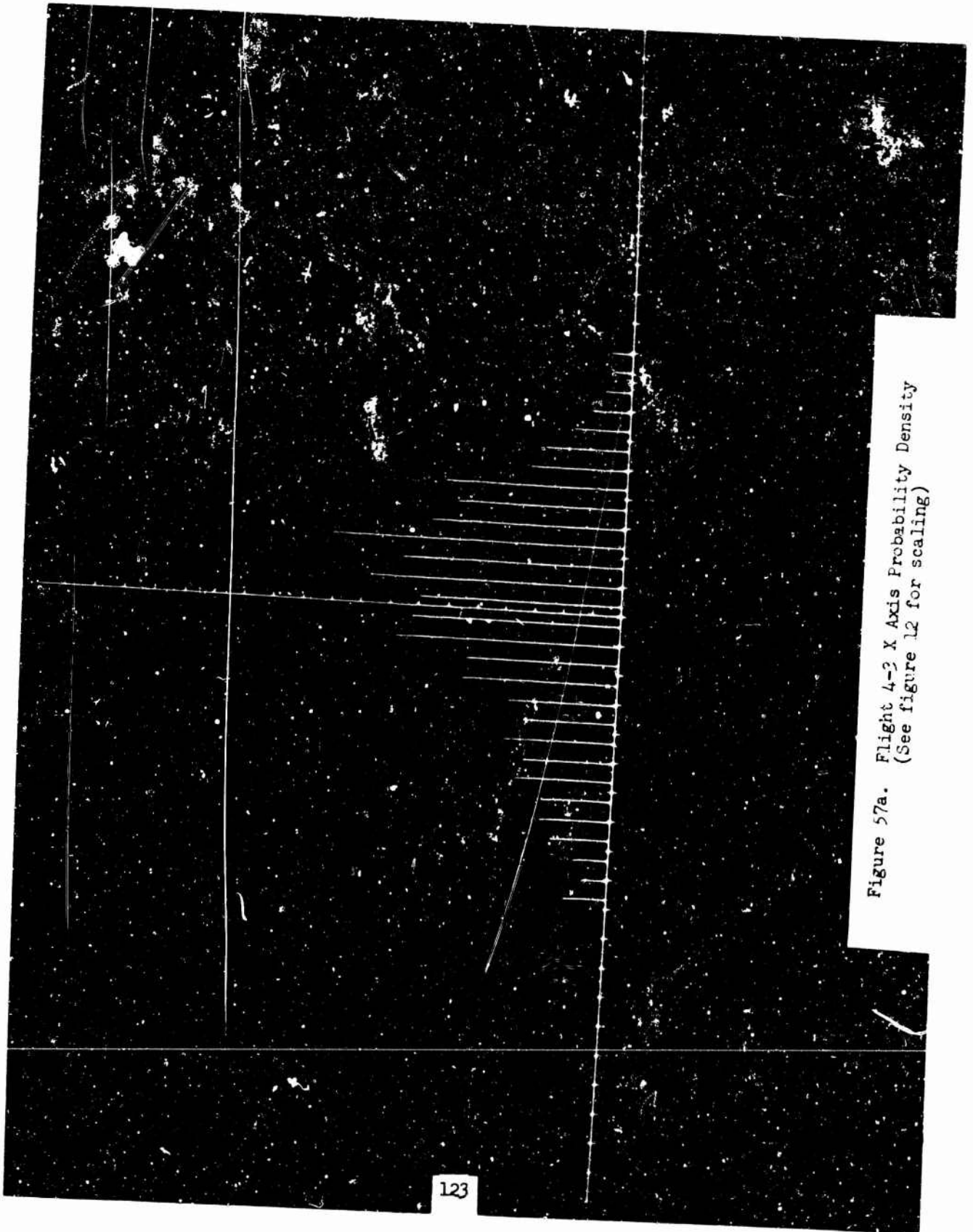


Figure 57a. Flight 4-3 X Axis Probability Density
(See figure 12 for scaling)

Figure 57b Flight 4-3 X Axis Probability Distribution
(See figure 12 for scaling)

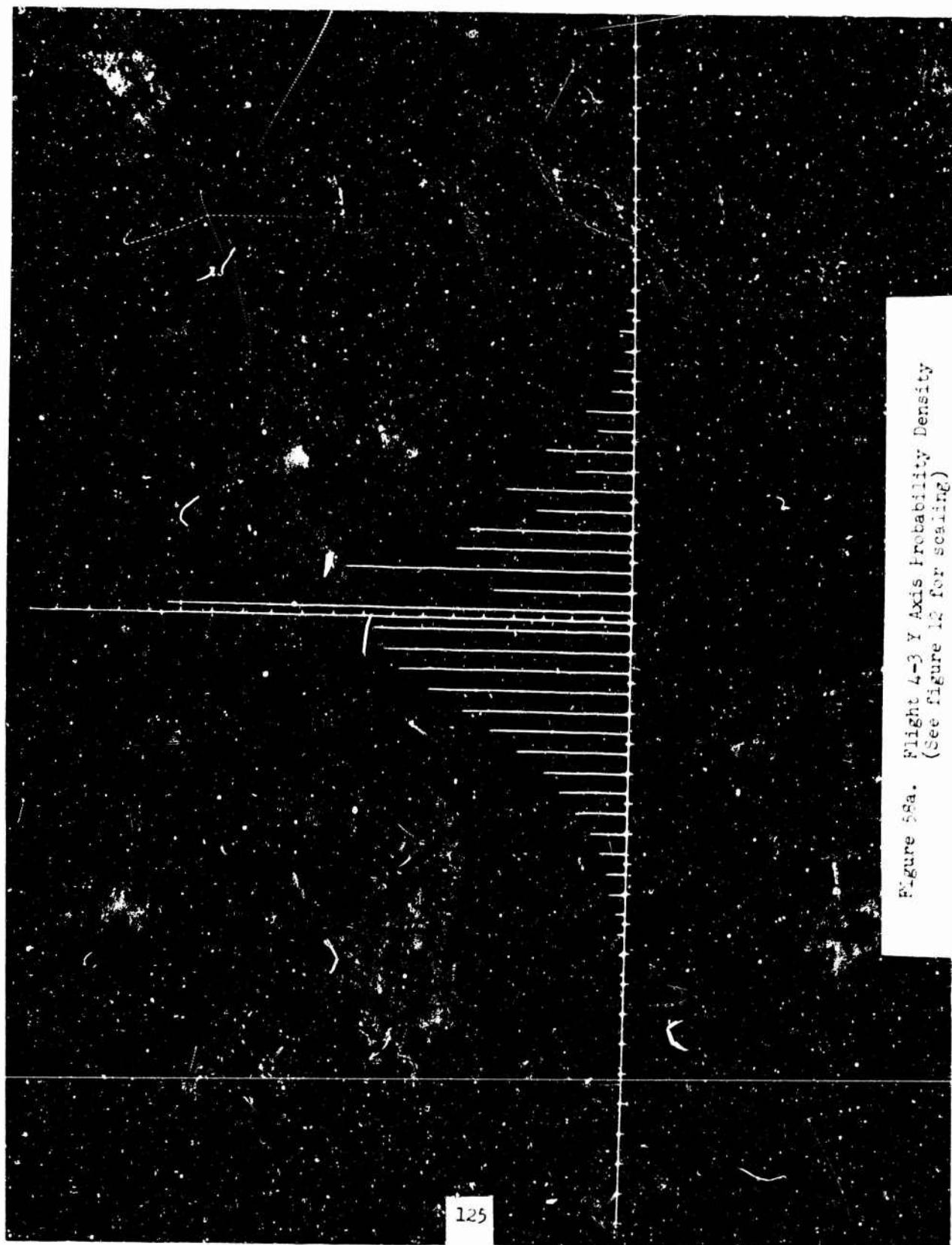


Figure 58a. Flight 4-3 Y Axis Probability Density
(See figure 12 for scaling)

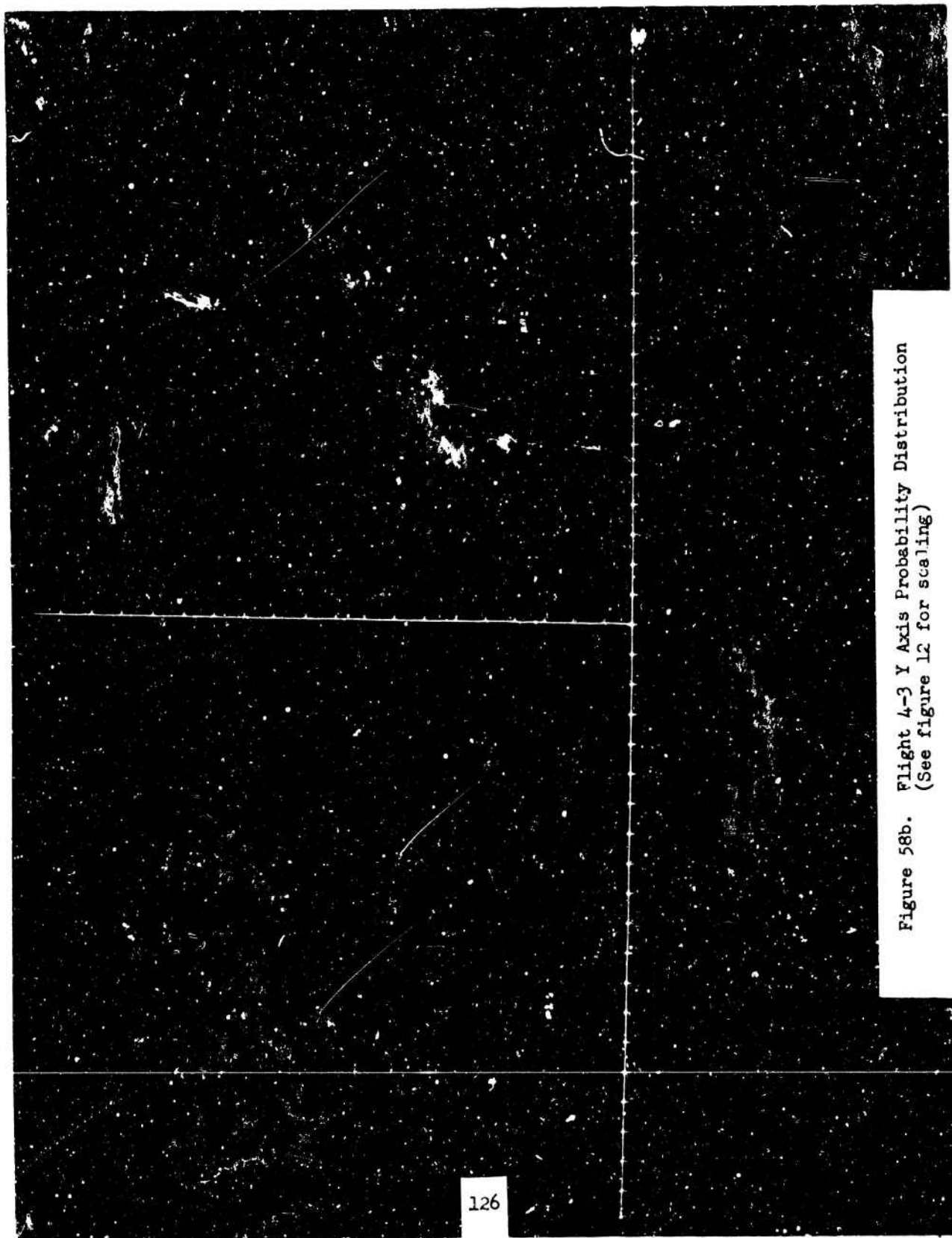


Figure 58b. Flight 4-3 Y Axis Probability Distribution
(See figure 12 for scaling)

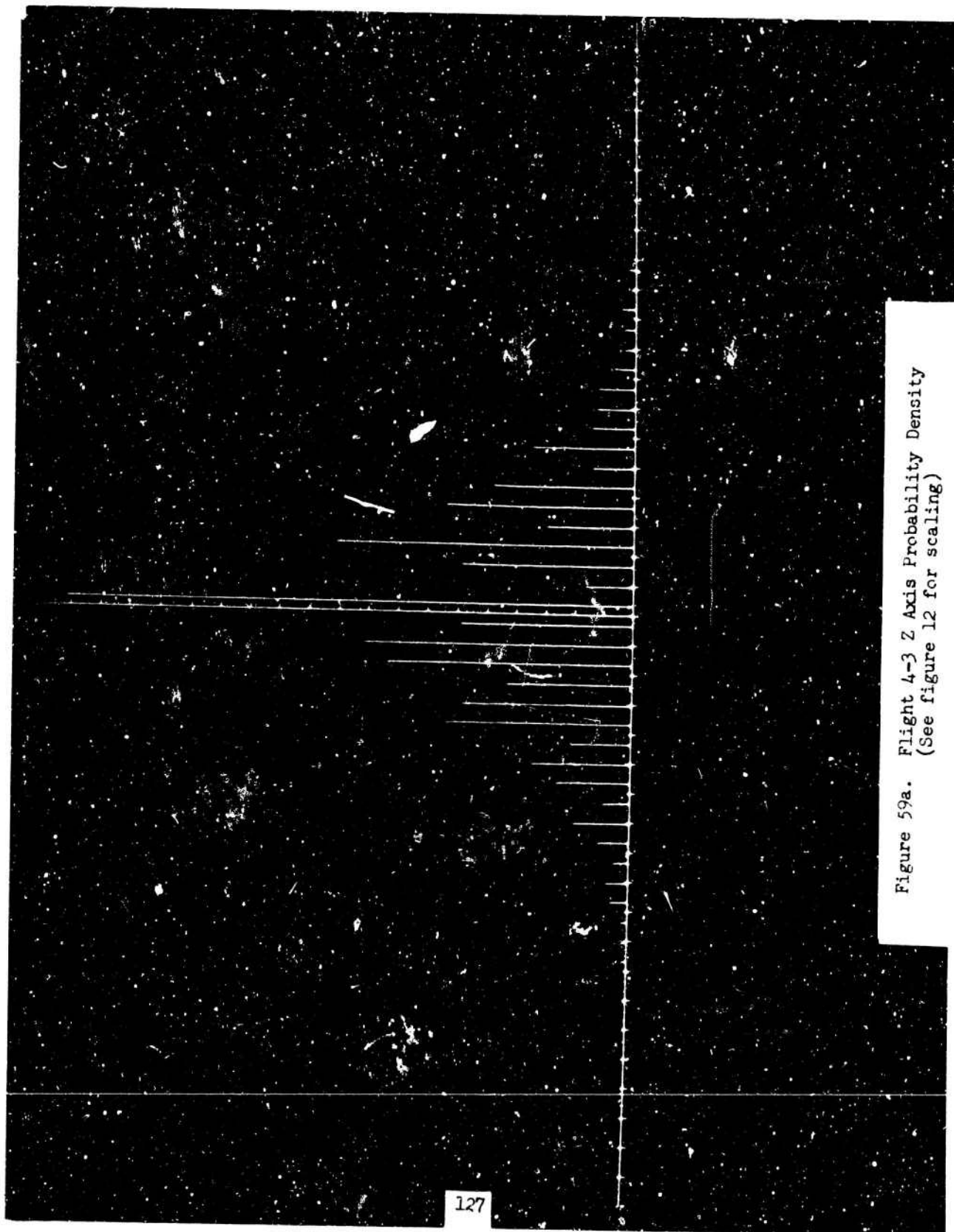


Figure 59a. Flight 4-3 Z Axis Probability Density
(See figure 12 for scaling)

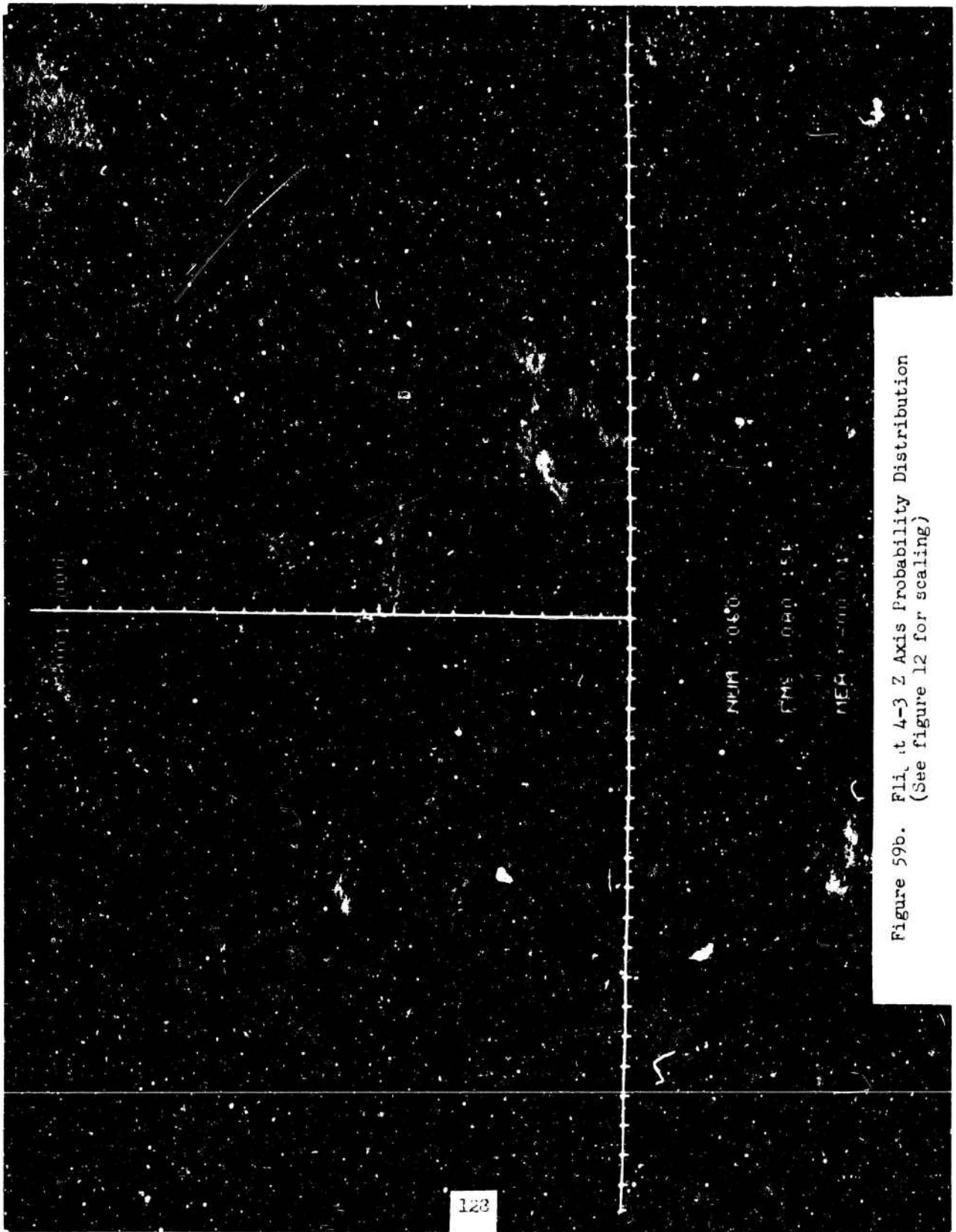
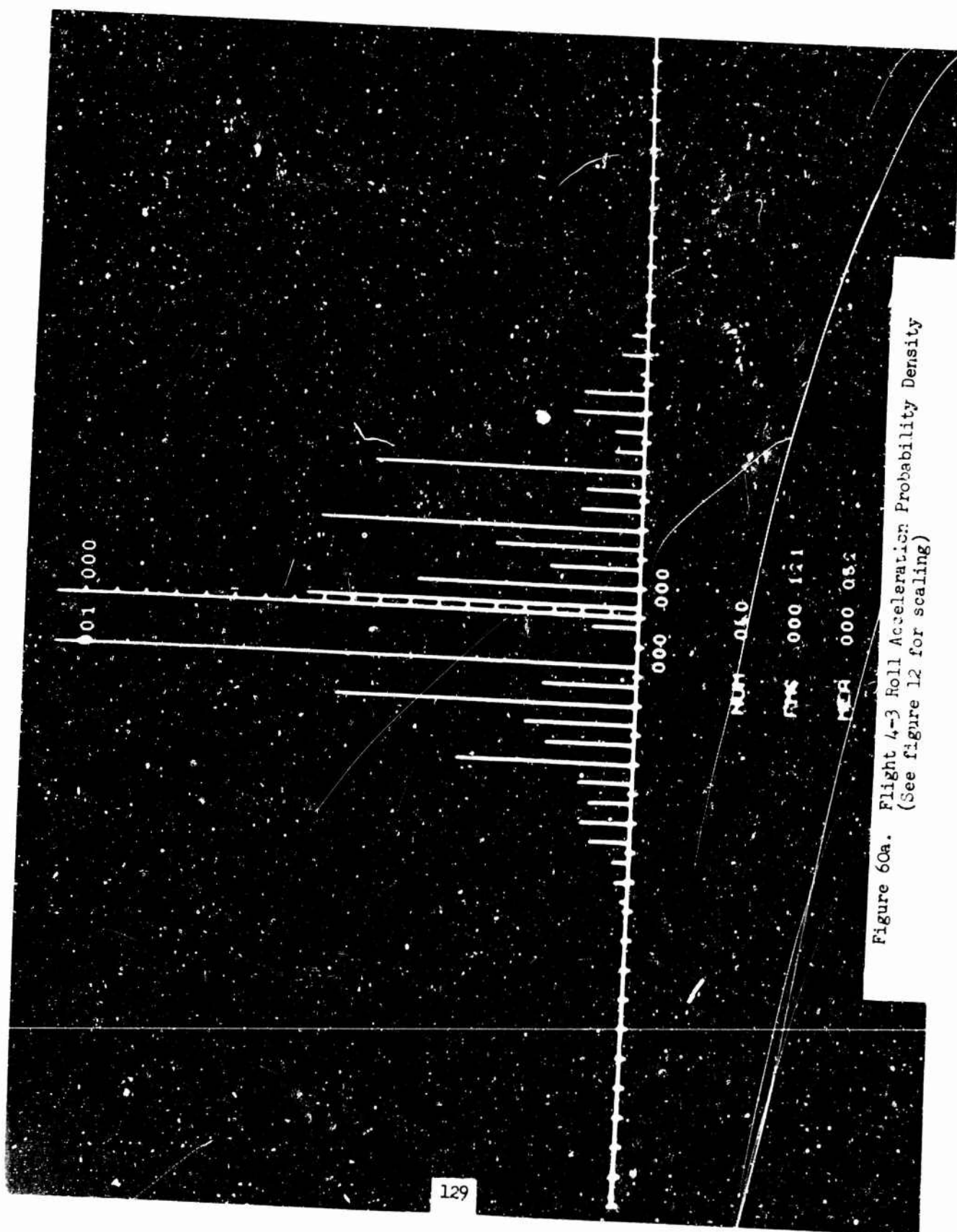


Figure 59b. Plot of 4-3 Z Axis Probability Distribution
(See figure 12 for scaling)



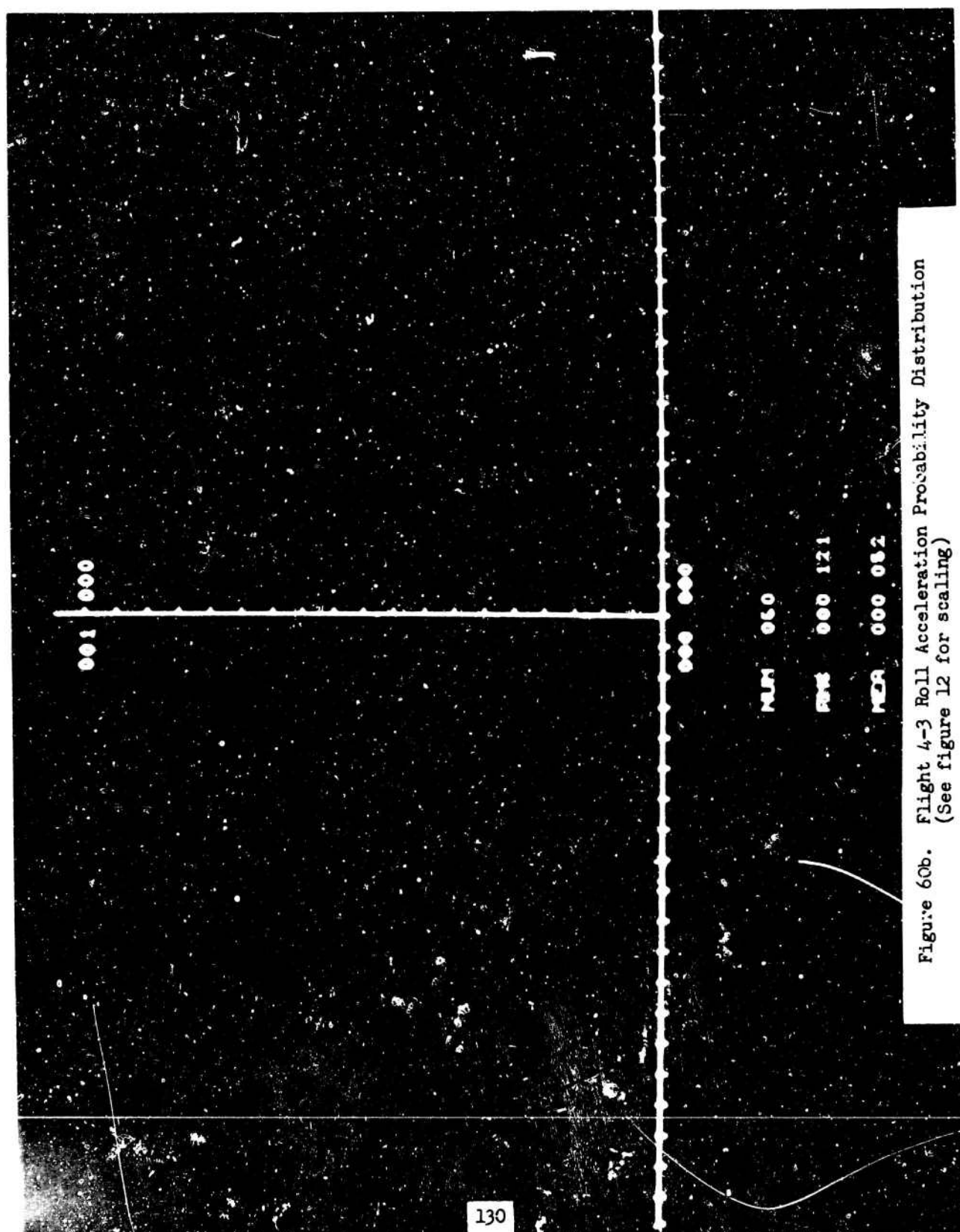


Figure 6Ob. Flight 4-3 Roll Acceleration Probability Distribution
(See figure 12 for scaling)

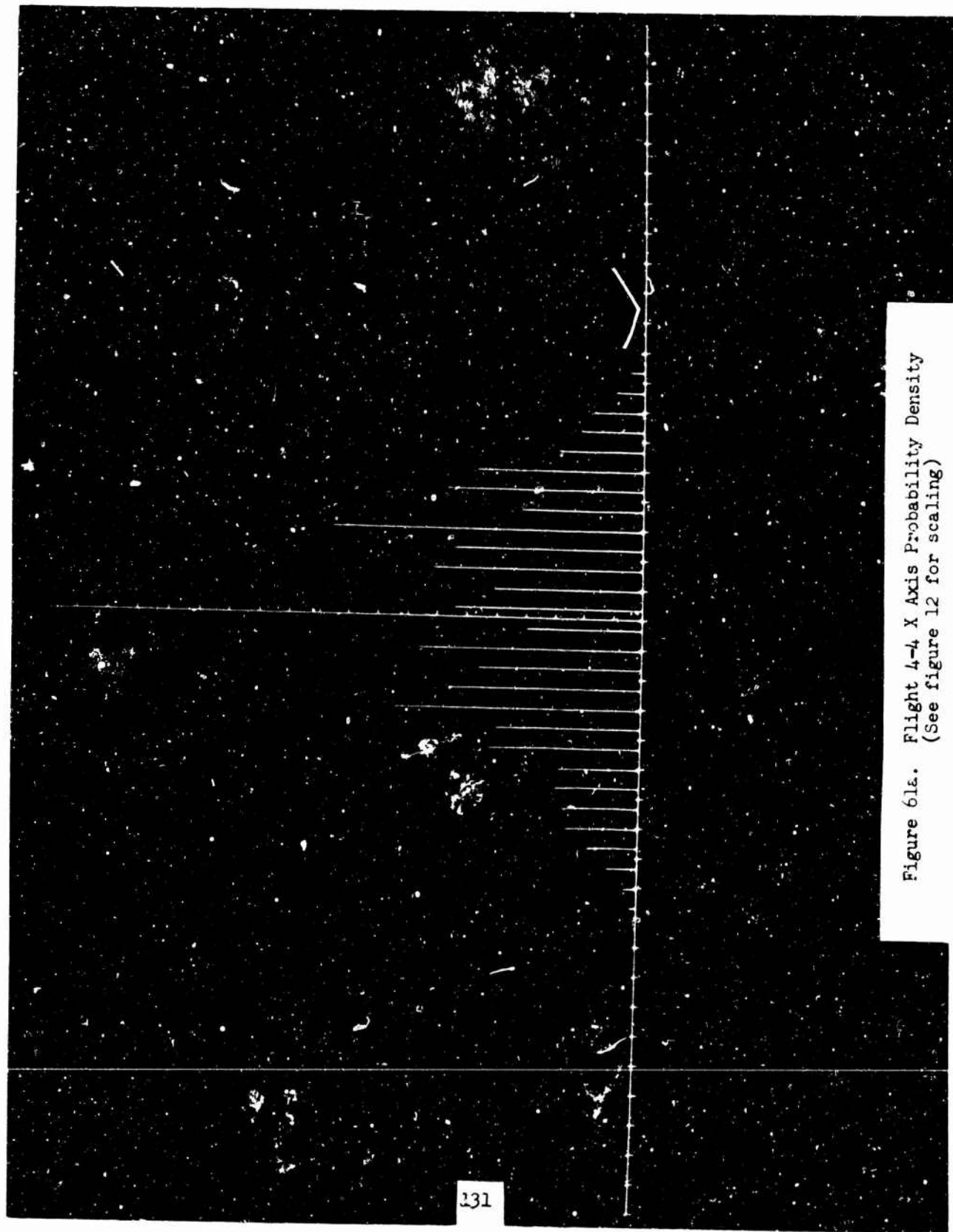


Figure 61a. Flight 4-4 X Axis Probability Density
(See figure 12 for scaling)

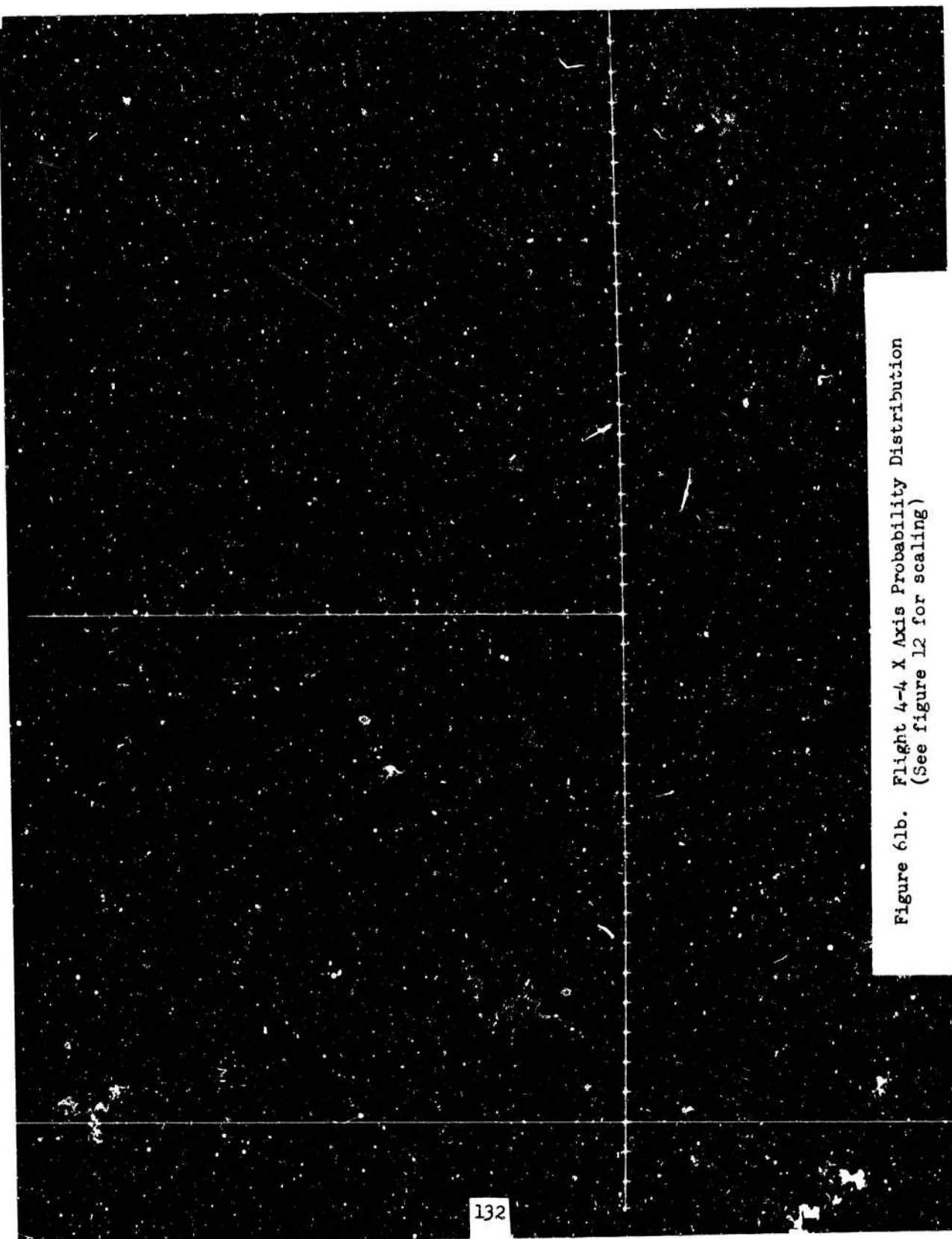


Figure 6lb. Flight 4-4 X Axis Probability Distribution
(See figure 12 for scaling)

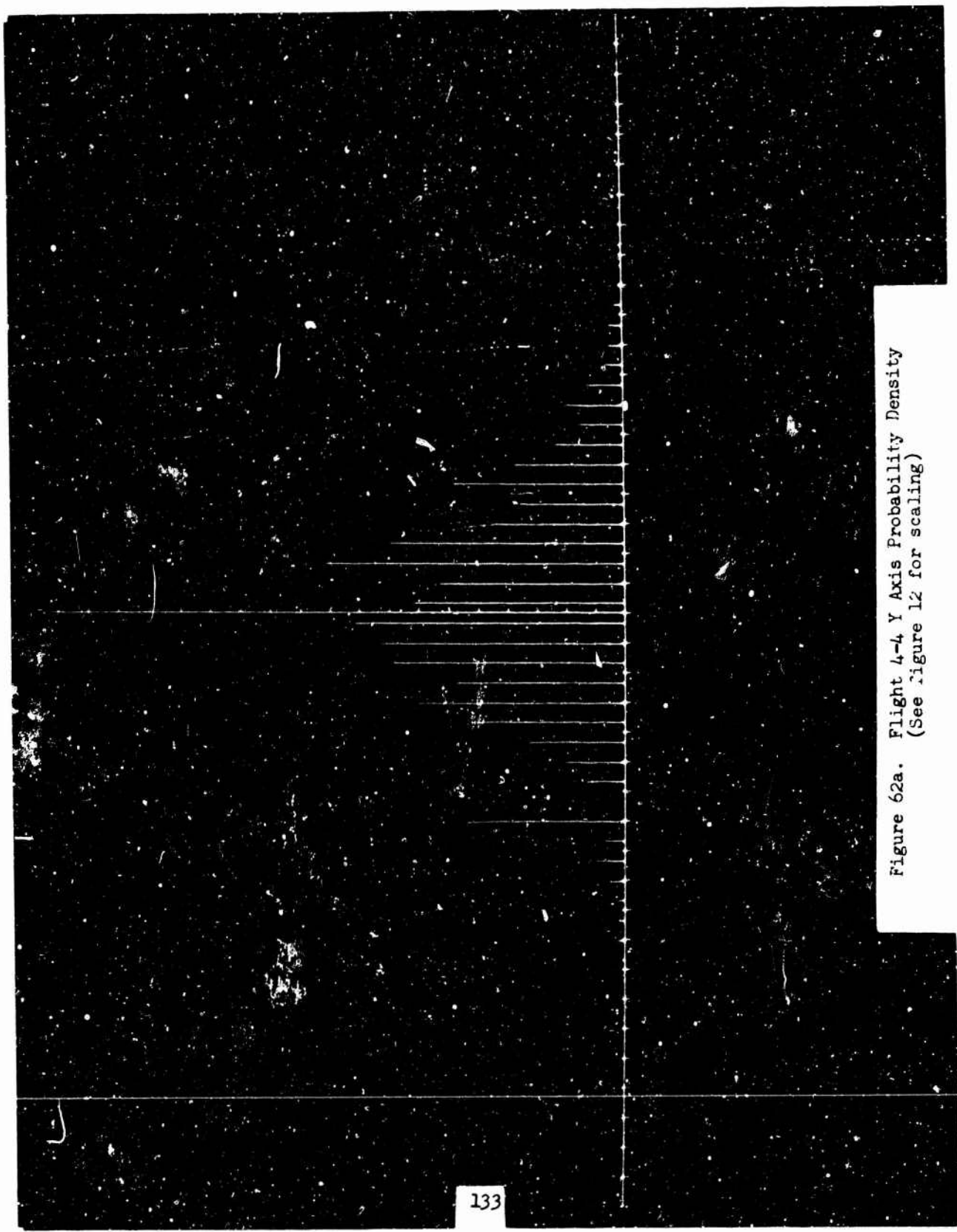


Figure 62a. Flight 4-4 Y Axis Probability Density
(See Figure 12 for scaling)

Figure 62b. Flight 4-4 Y Axis Probability Distribution
(See figure 12 for scaling)

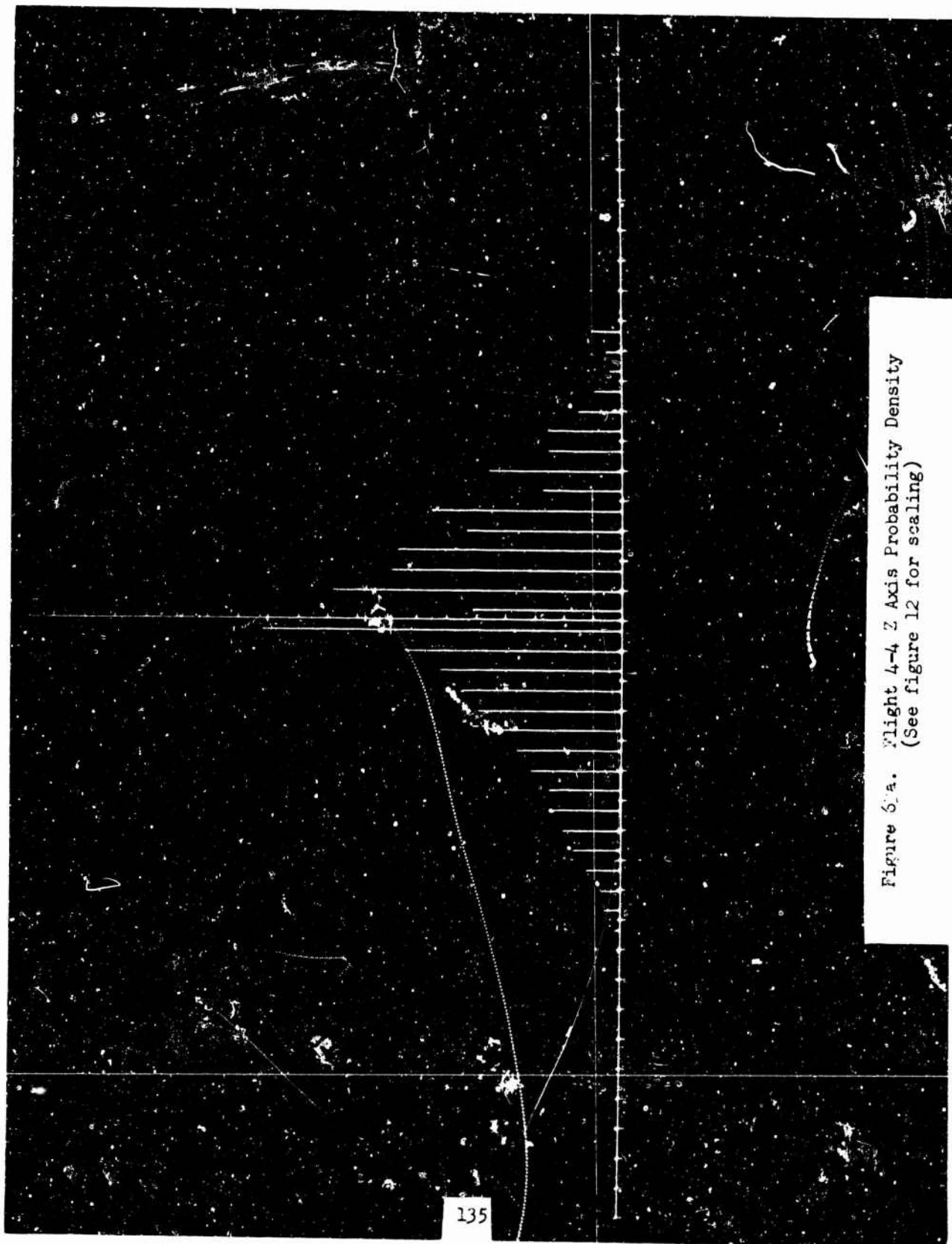


Figure 6a. Flight 4-4 Z Axis Probability Density
(See figure 12 for scaling)

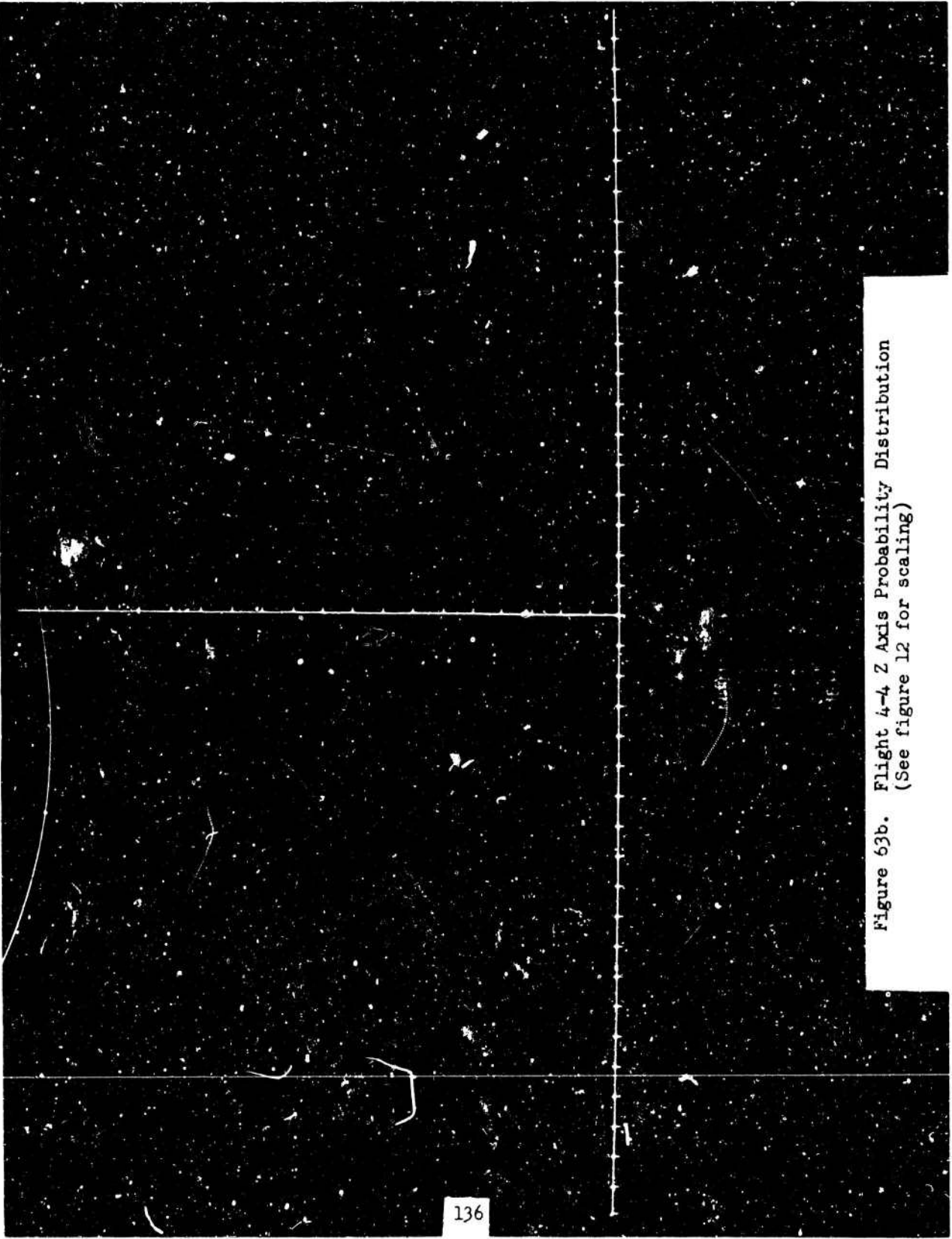


Figure 63b. Flight 4-4 Z Axis Probability Distribution
(See figure 12 for scaling)

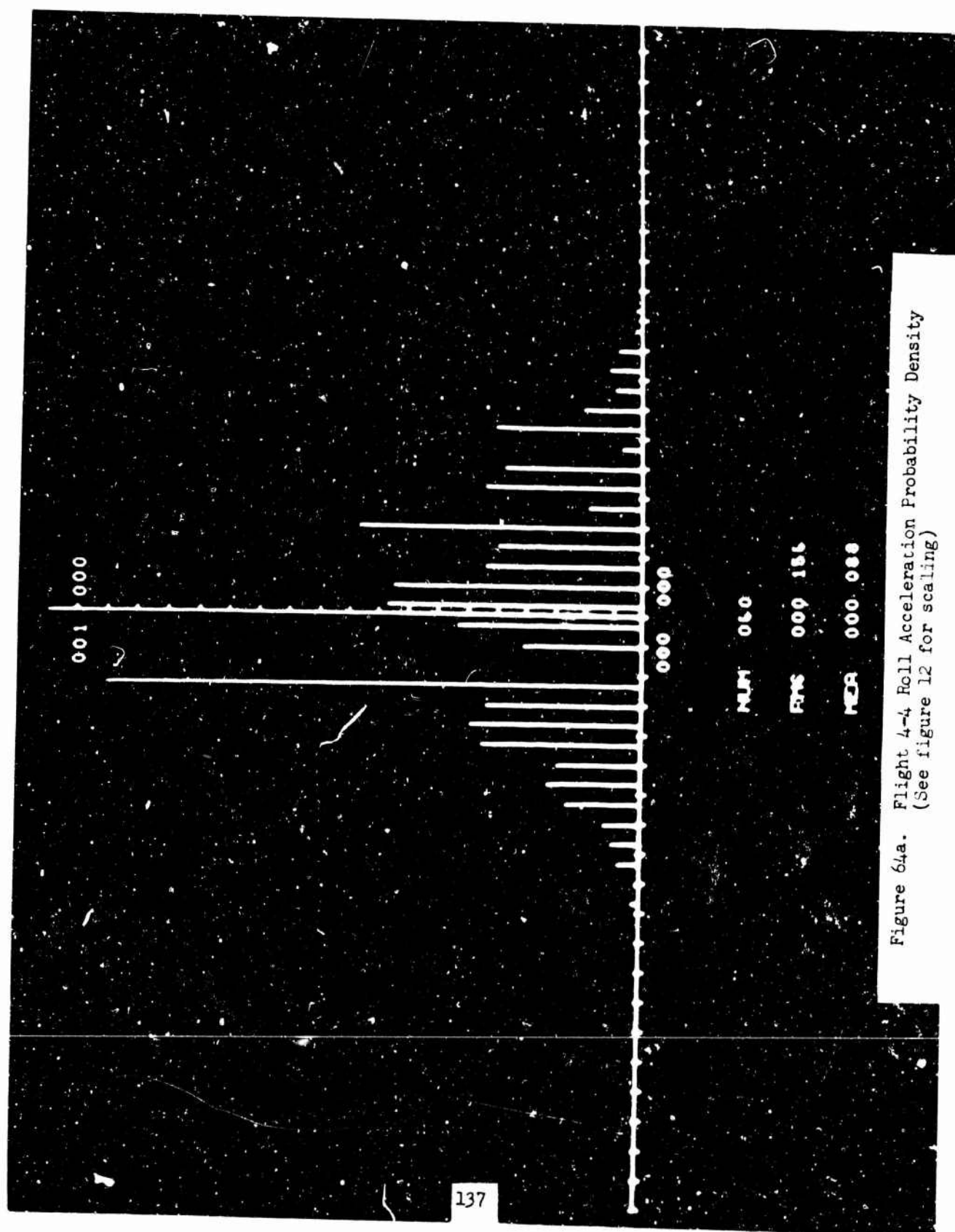


Figure 64a. Flight 4-4 Roll Acceleration Probability Density
(See figure 12 for scaling)

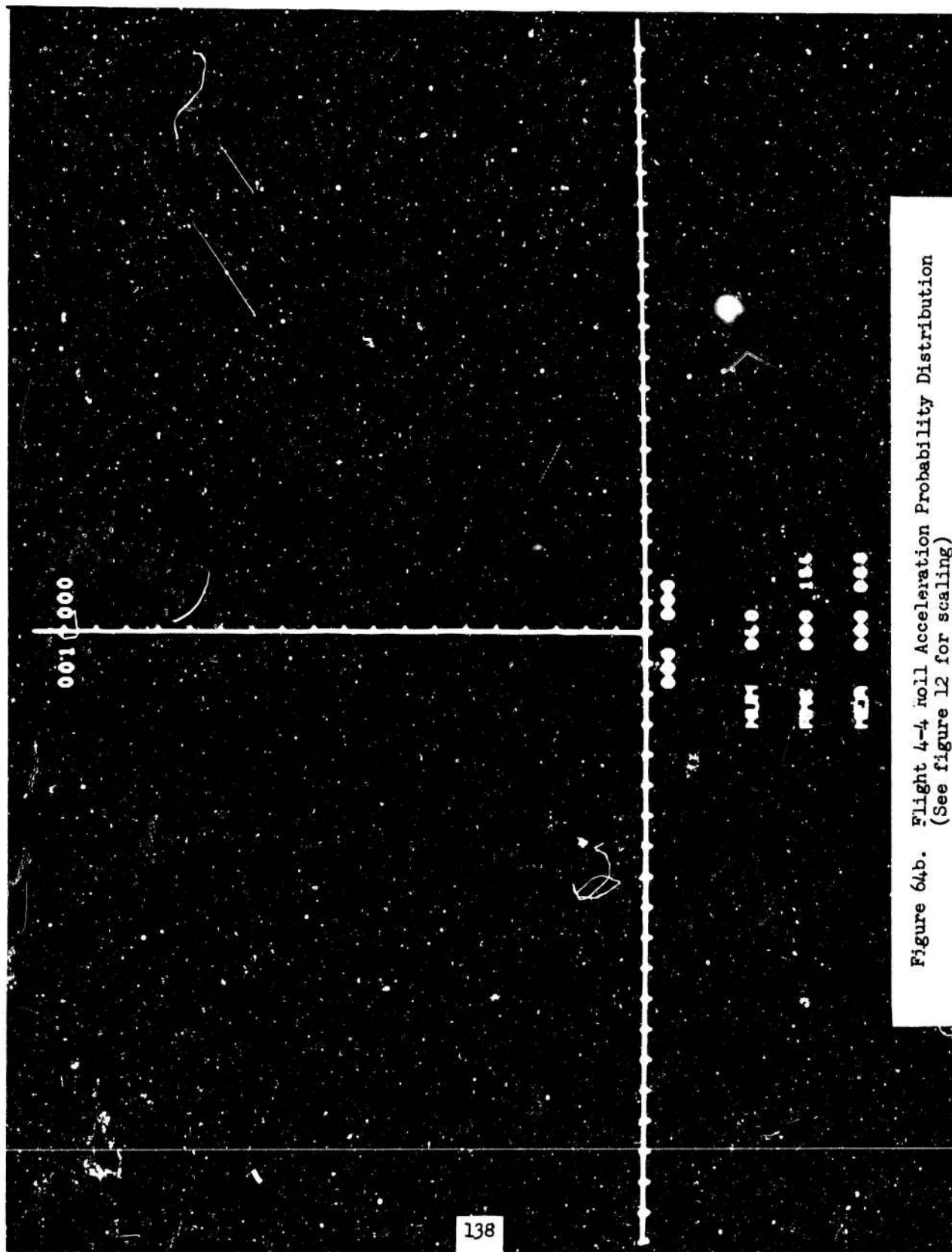


Figure 64b. Flight 4-4 roll Acceleration Probability Distribution
(See figure 12 for scaling)

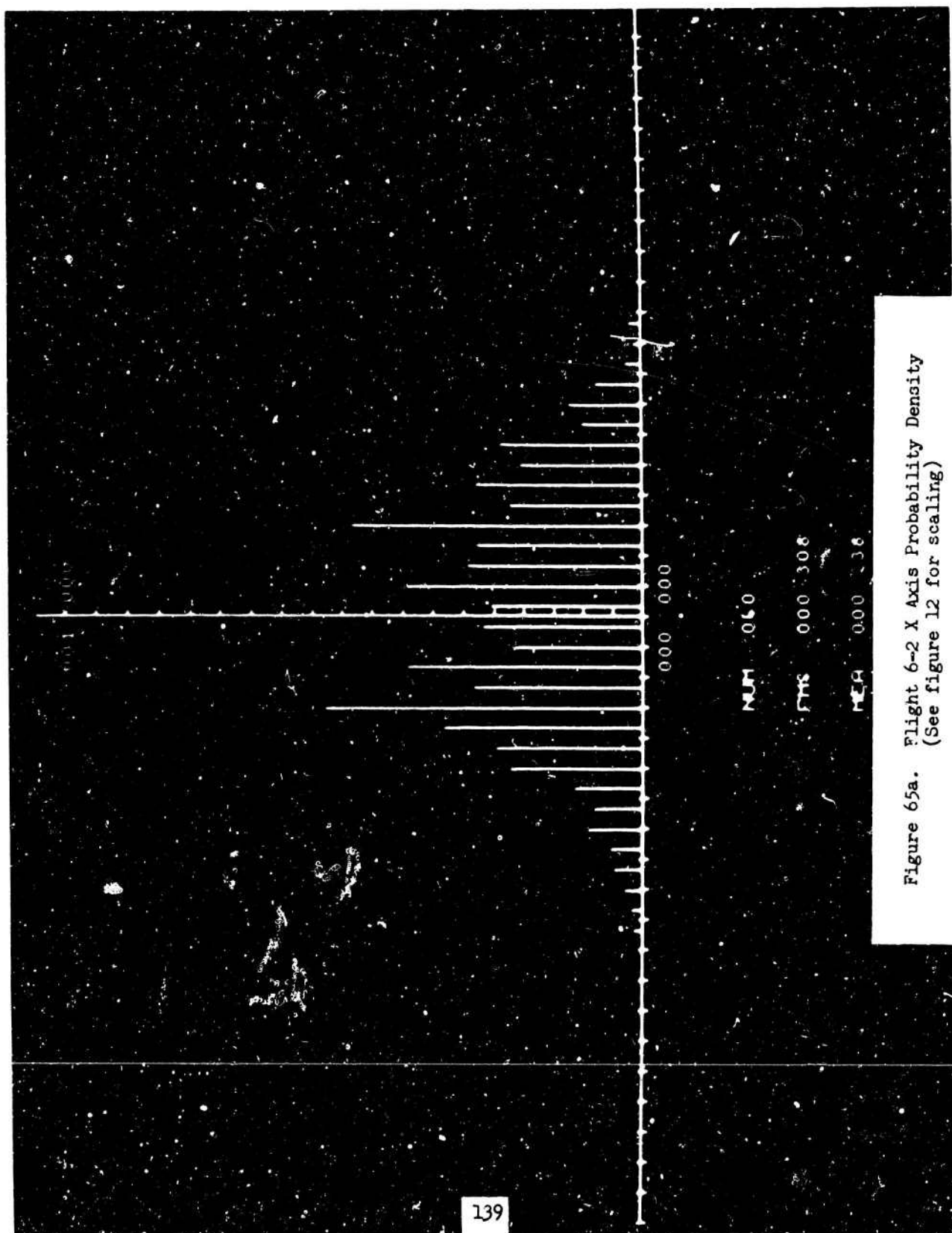


Figure 65a. Flight 6-2 X Axis Probability Density
(See figure 12 for scaling)

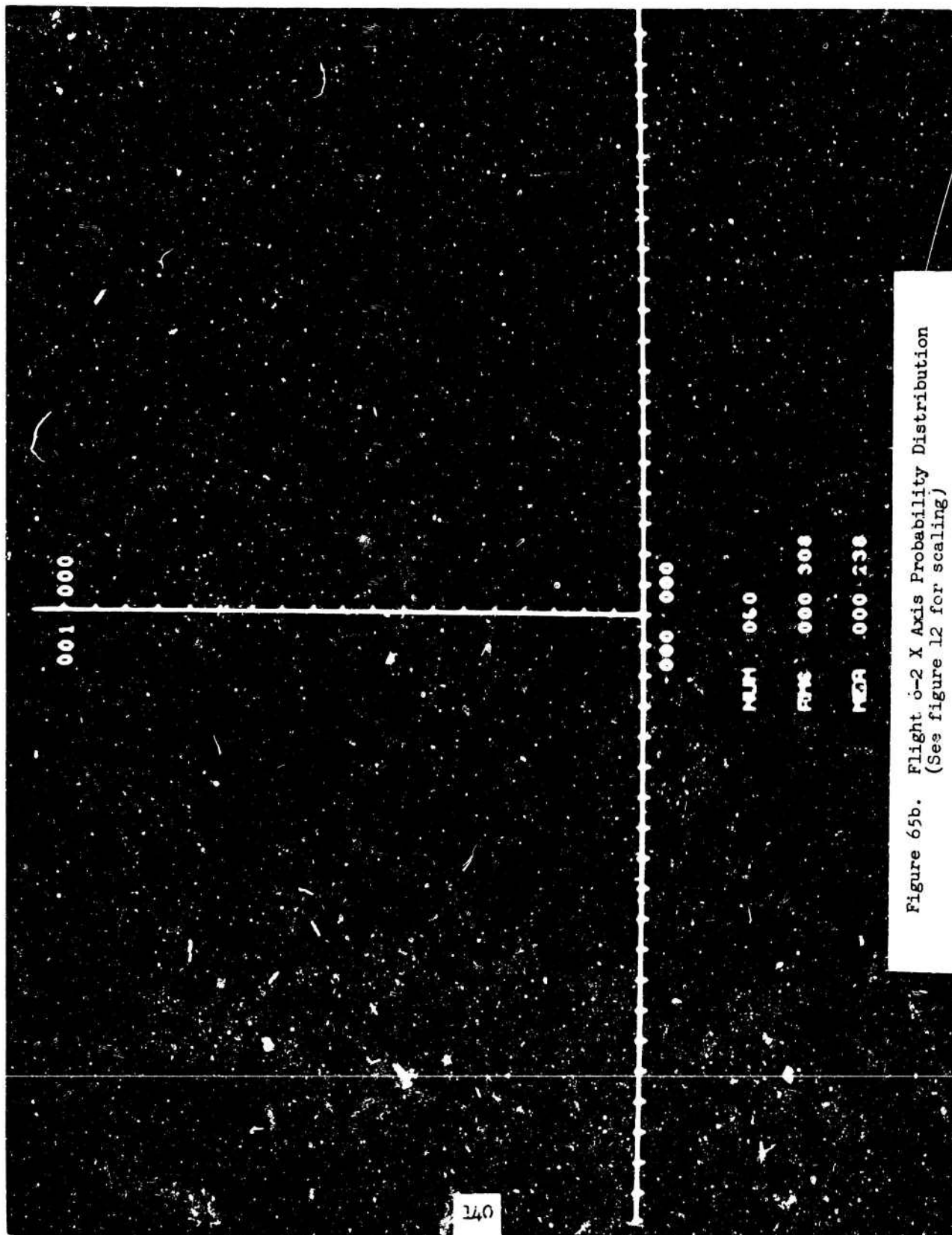


Figure 65b. Flight 6-2 X Axis Probability Distribution
(See figure 12 for scaling)

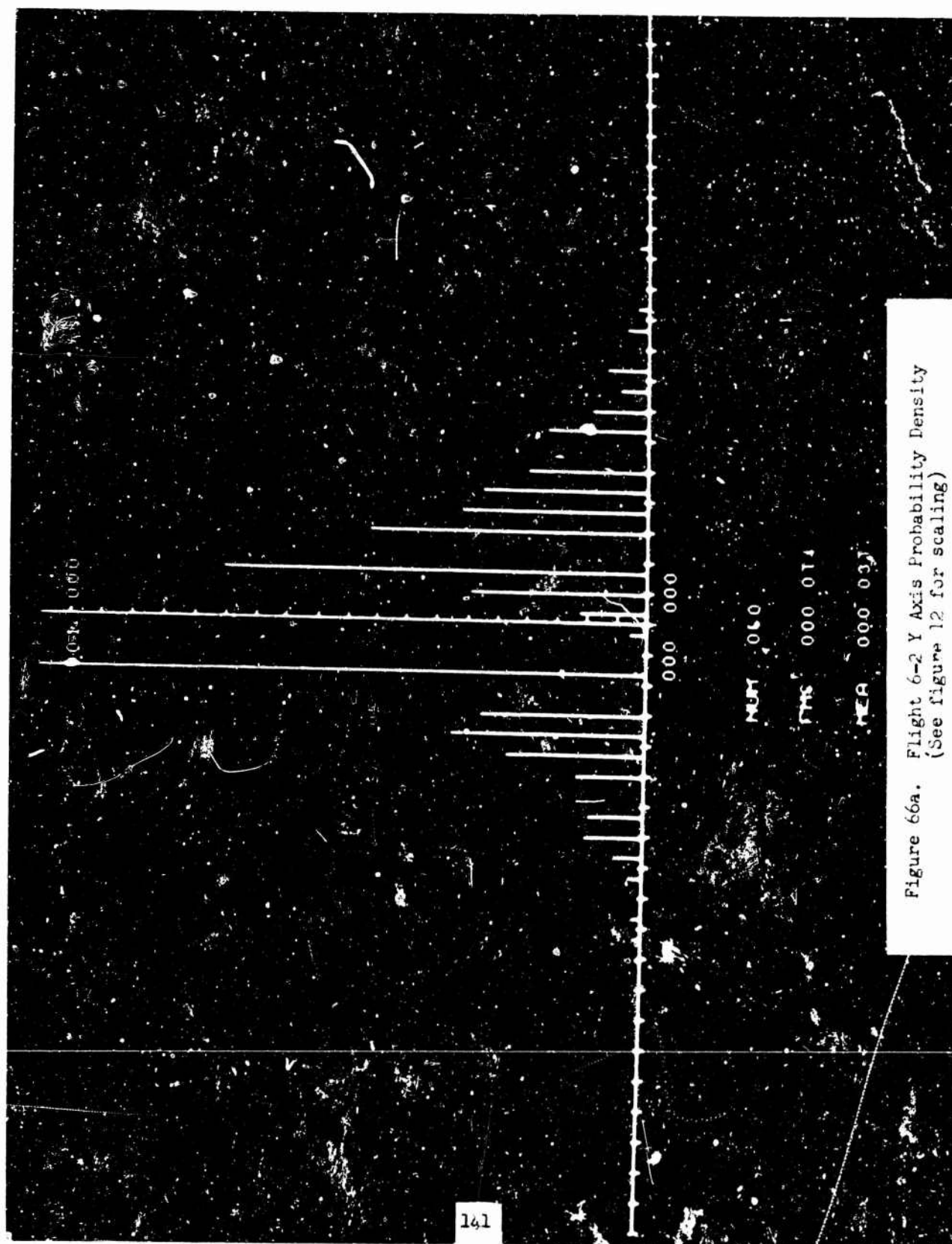


Figure 66a. Flight 6-2 Y Axis Probability Density
(See figure 12 for scaling)

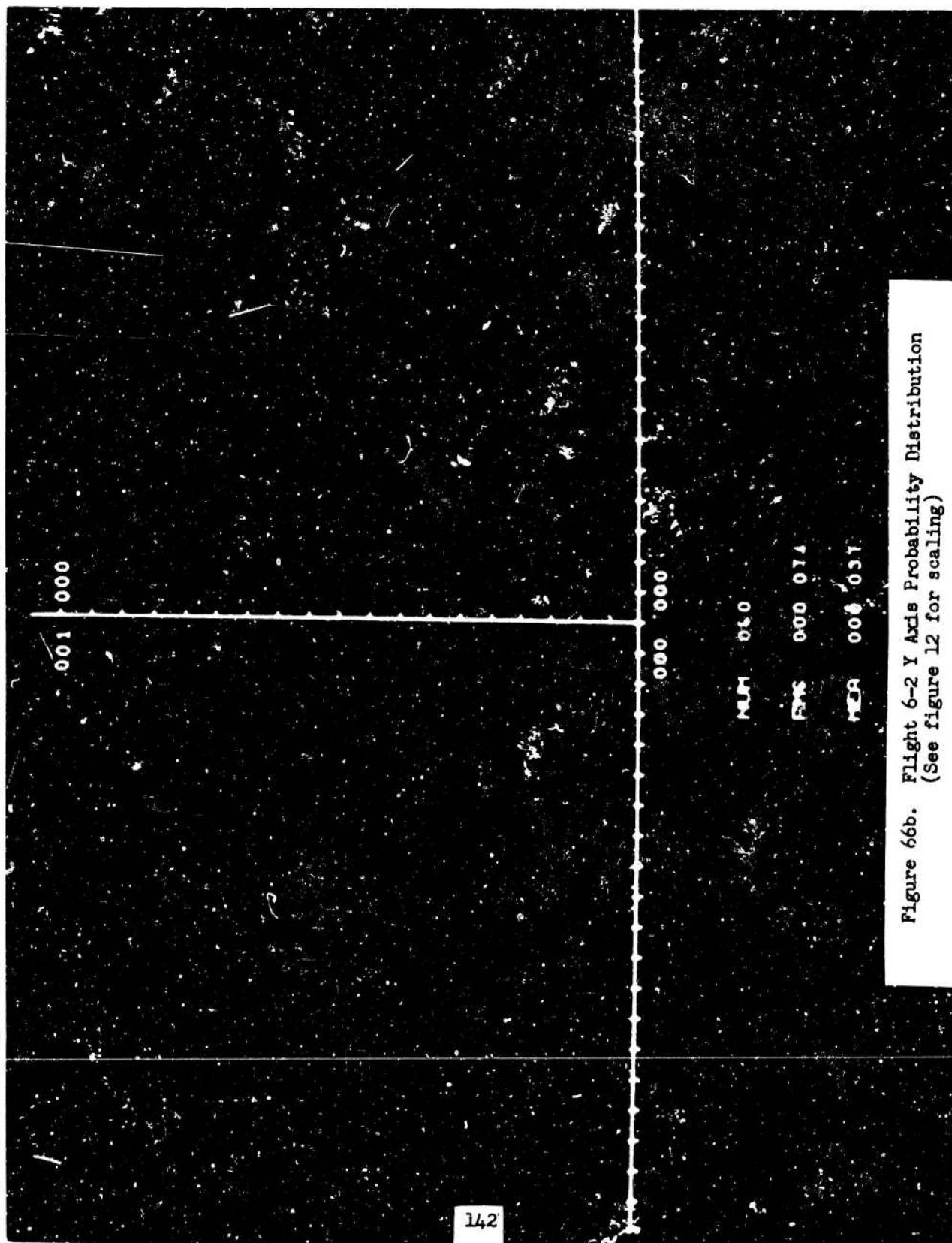


Figure 66b. Flight 6-2 Y Axis Probability Distribution
(See figure 12 for scaling)

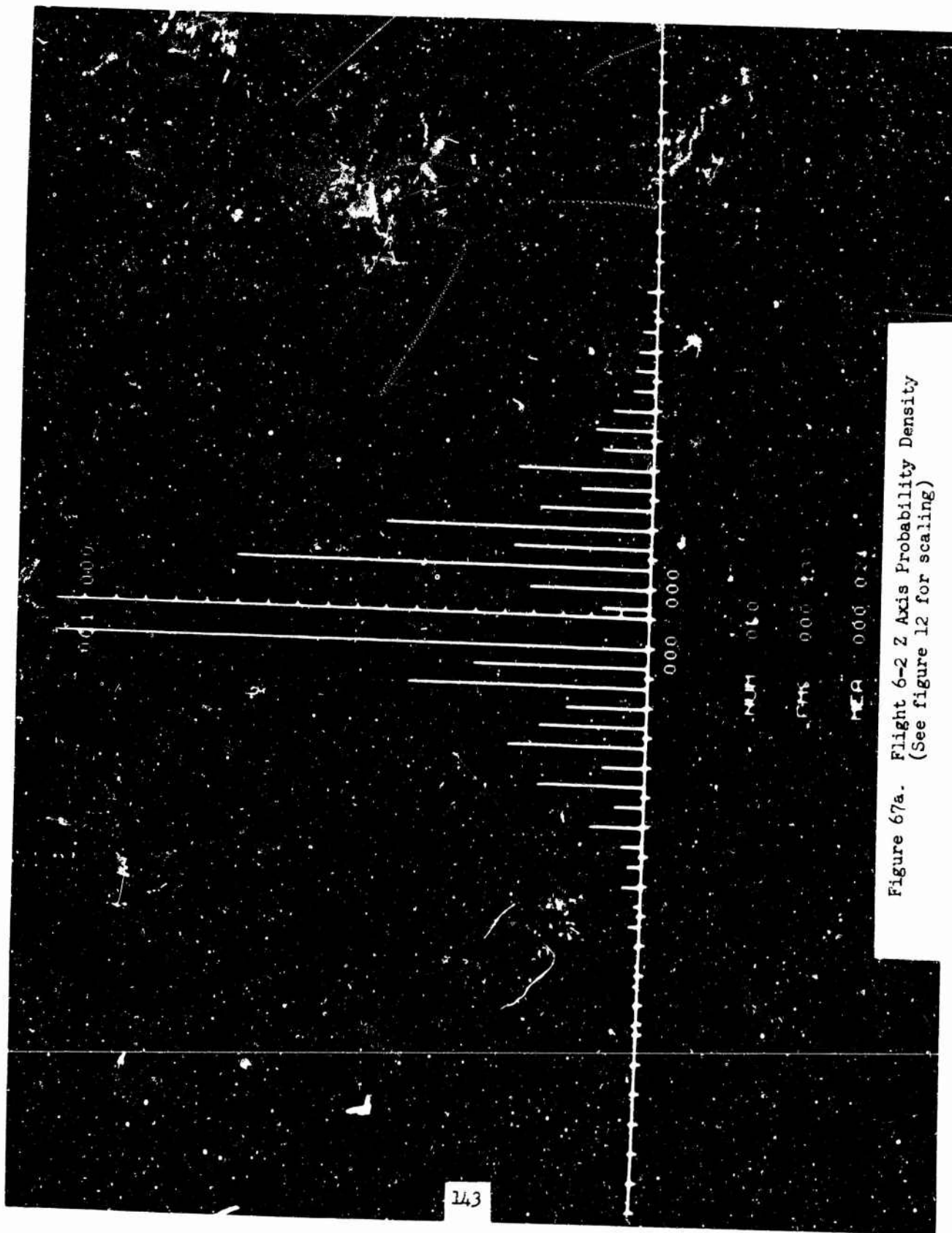
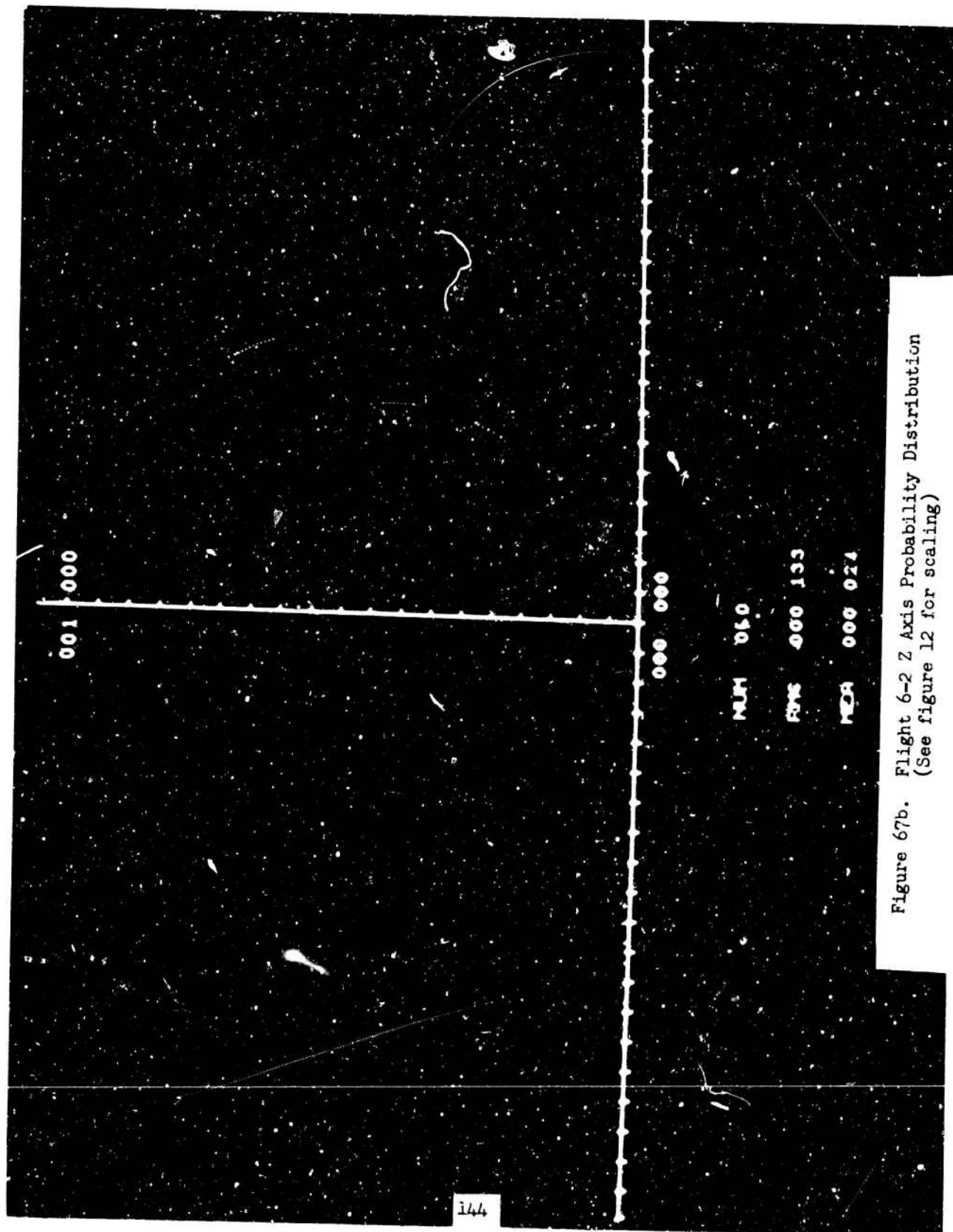


Figure 67a. Flight 6-2 Z Axis Probability Density
(See figure 12 for scaling)



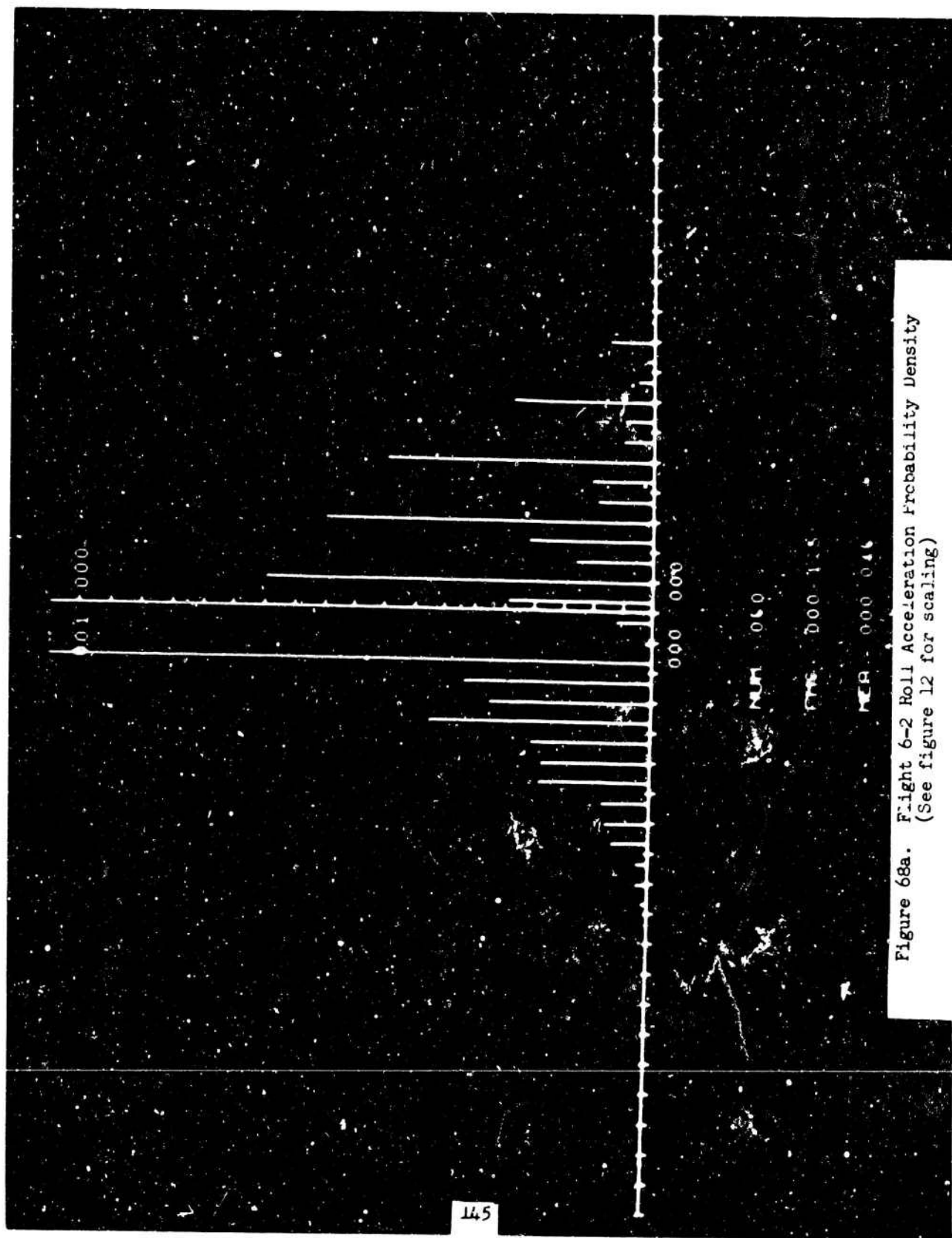


Figure 68a. Flight 6-2 Roll Acceleration Probability Density
(See figure 12 for scaling)

001 000

000 000

MLM 060

PM 000 128

WCA 000 046

Figure 68b. Flight 6-2 Roll Acceleration Probability Distribution
(See figure 12 for scaling)

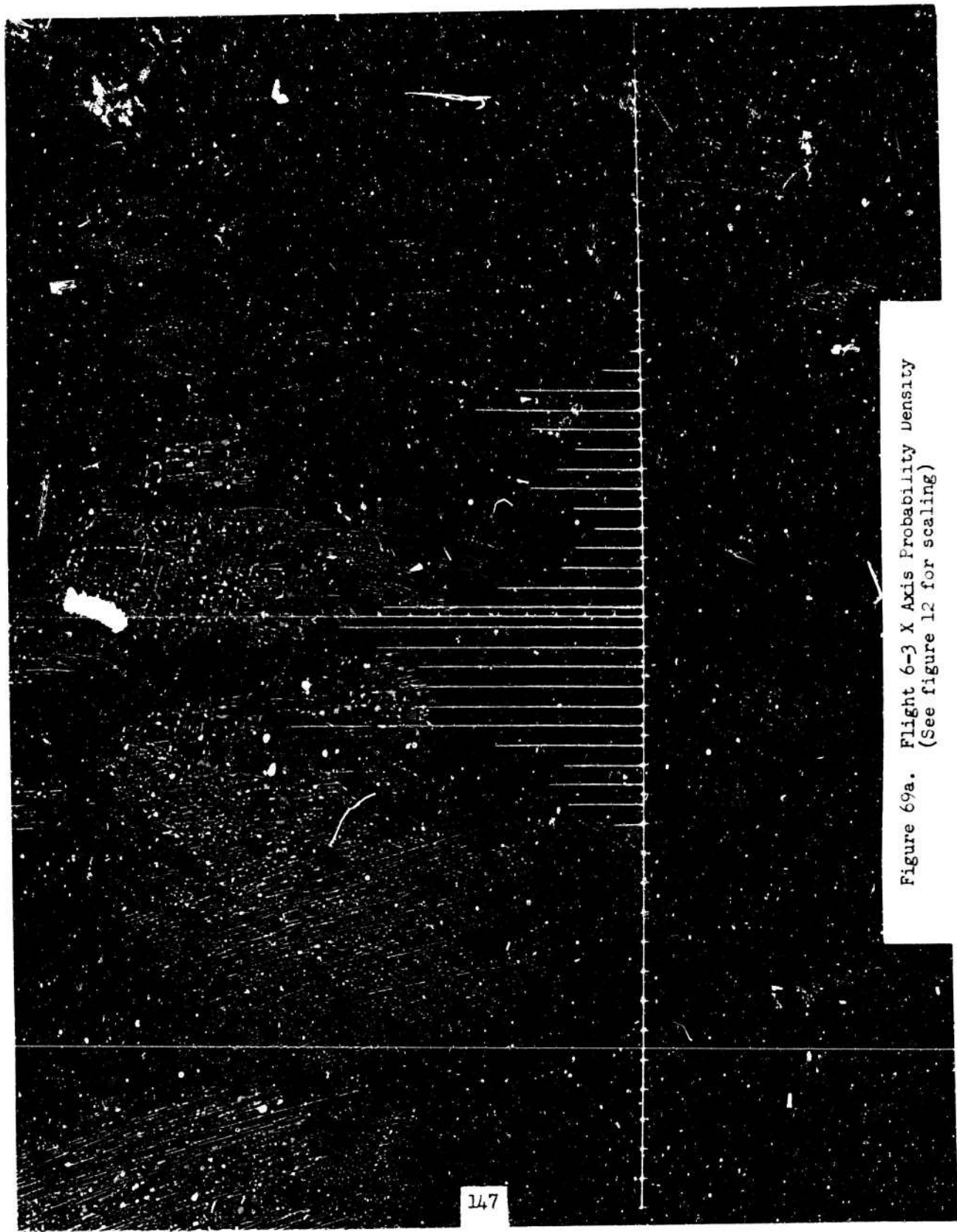


Figure 69a. Flight 6-3 X Axis Probability Density
(See figure 12 for scaling)

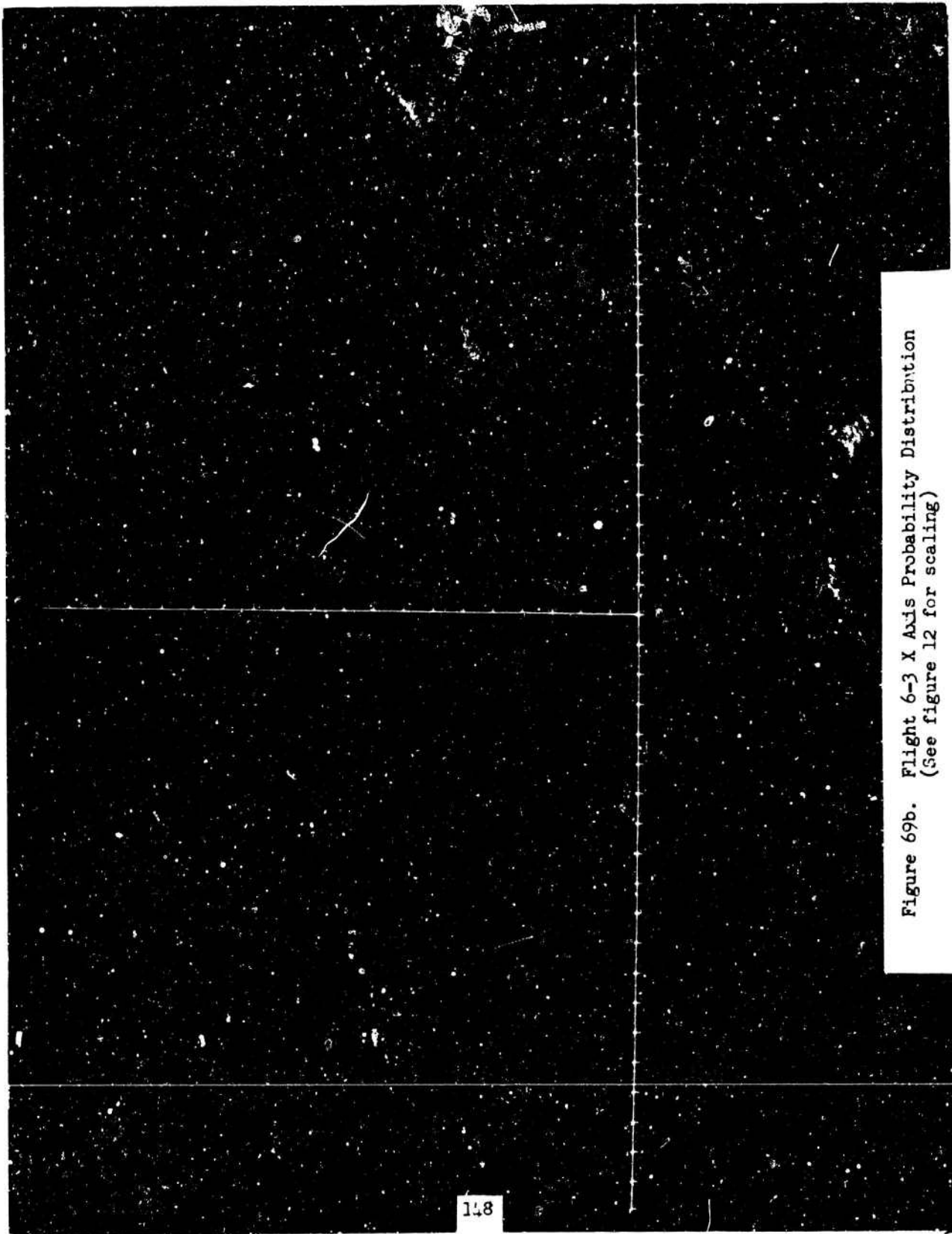


Figure 69b. Flight 6-3 X Axis Probability Distribution
(See figure 12 for scaling)

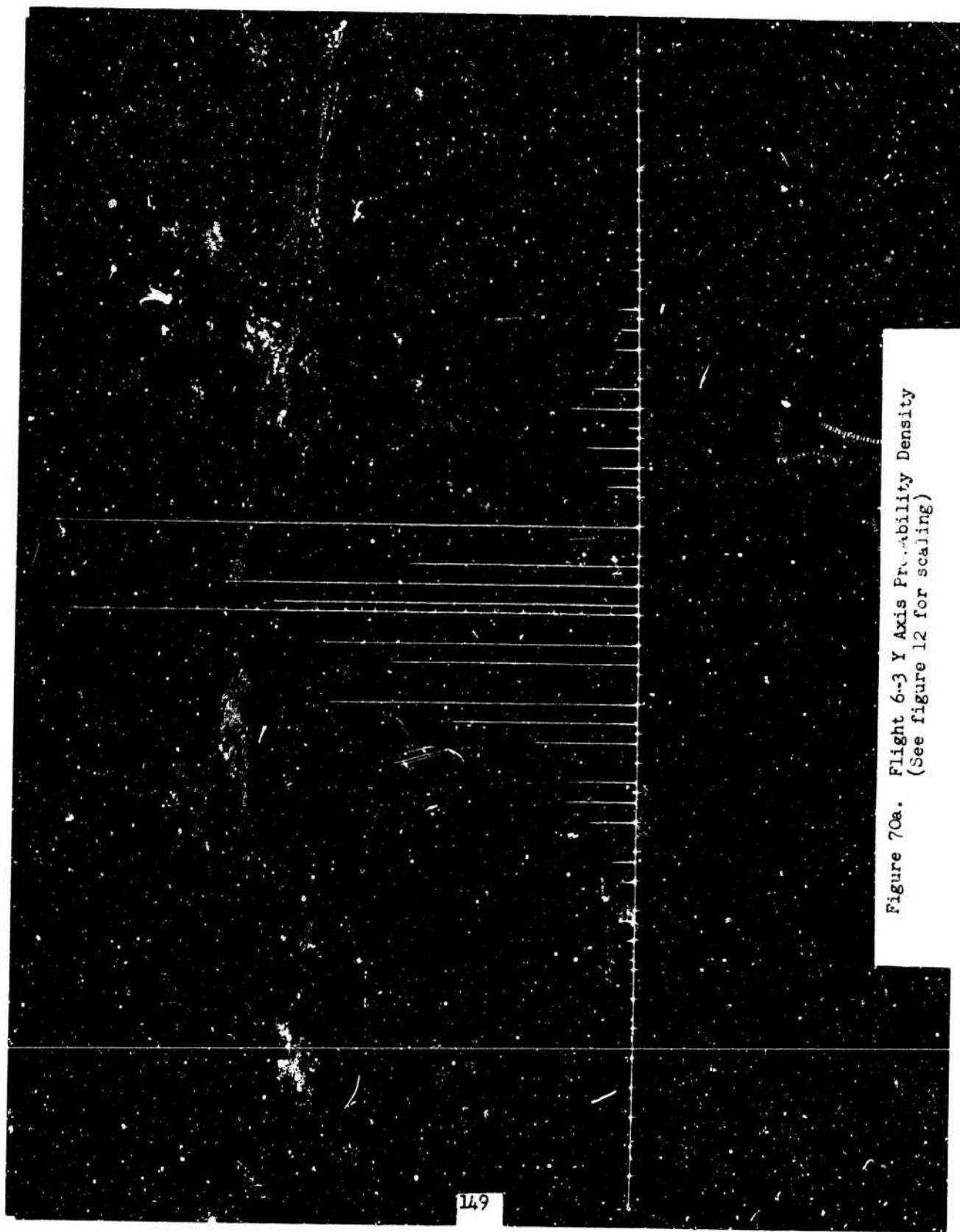


Figure 70a. Flight 6-3 Y Axis Probability Density
(See figure 12 for scaling)

Figure 70b. Flight 6-3 Y Axis Probability Distribution
(See figure 12 for scaling)

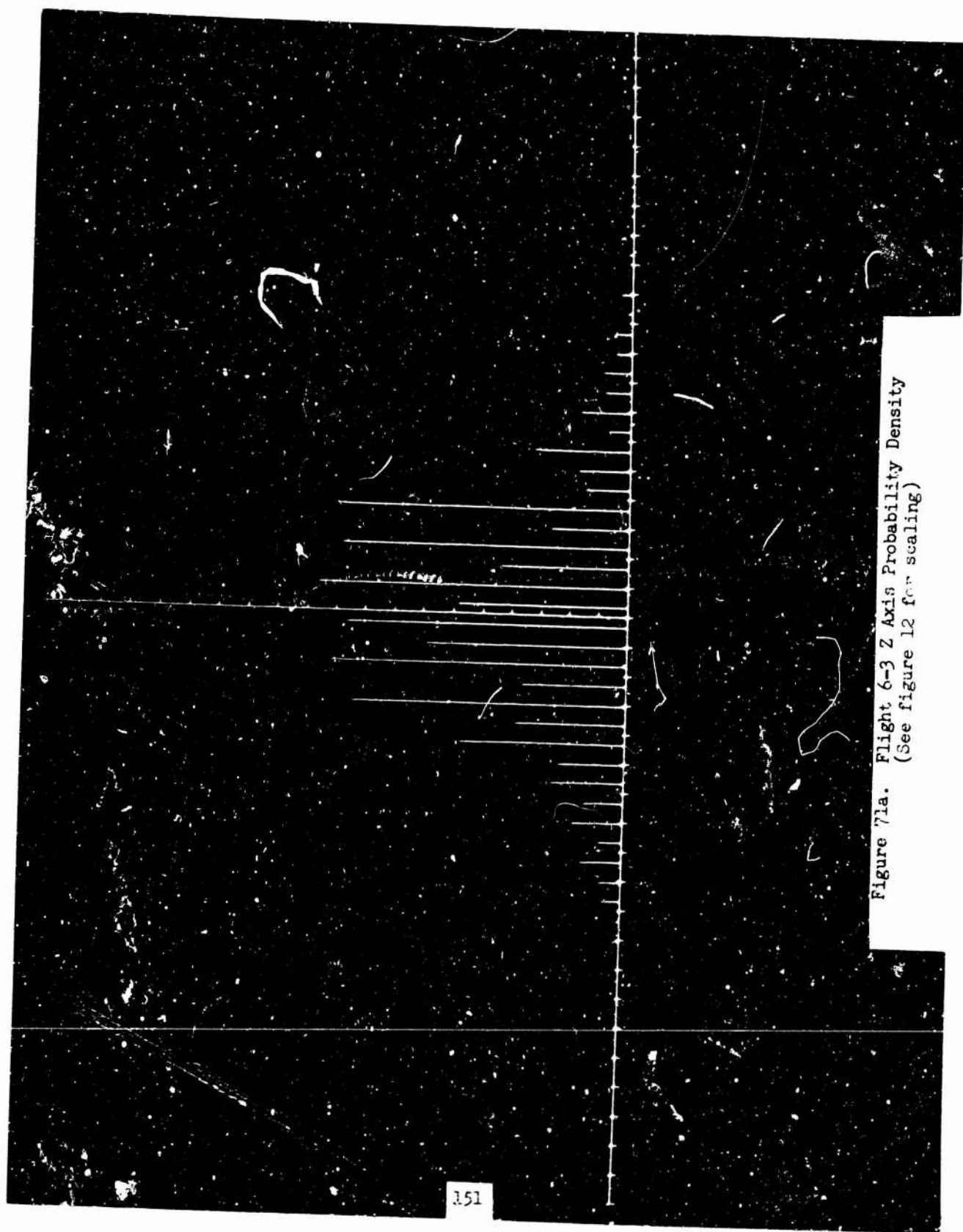
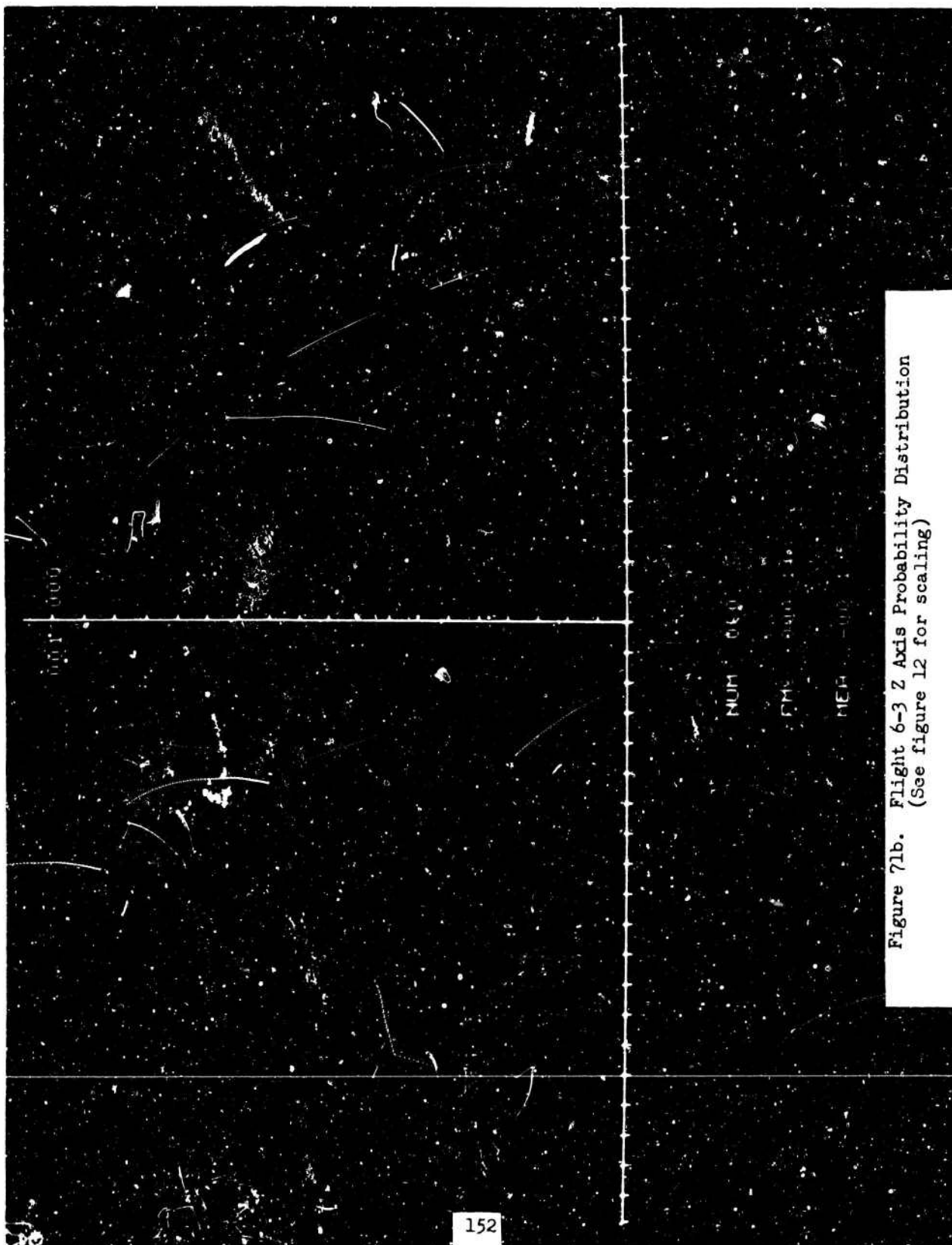


Figure 71a. Flight 6-3 Z Axis Probability Density
(See figure 12 for scaling)



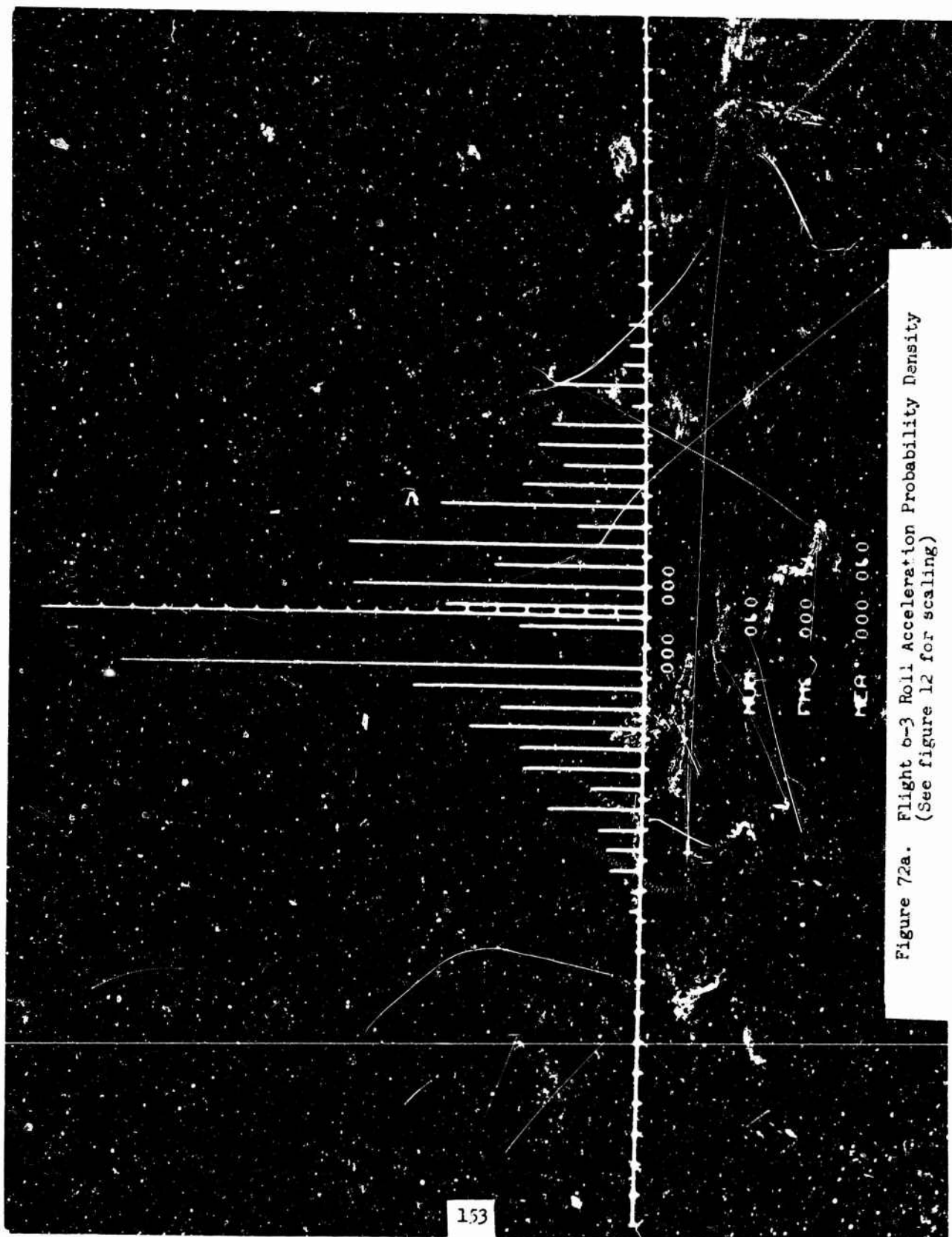


Figure 72a. Flight 6-3 Roll Acceleration Probability Density
(See figure 12 for scaling)

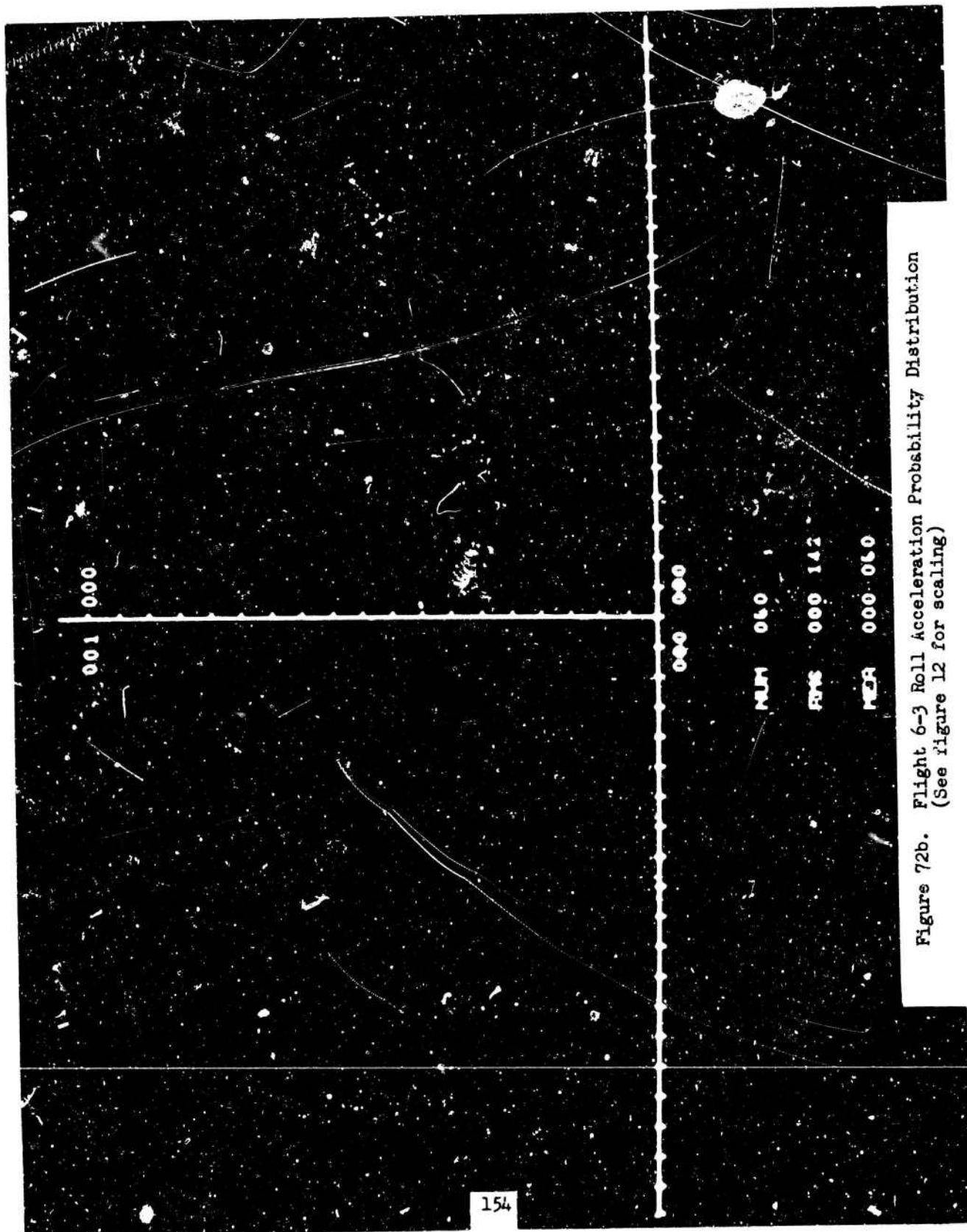


Figure 72b. Flight 6-3 Roll Acceleration Probability Distribution
(See Figure 12 for scaling)

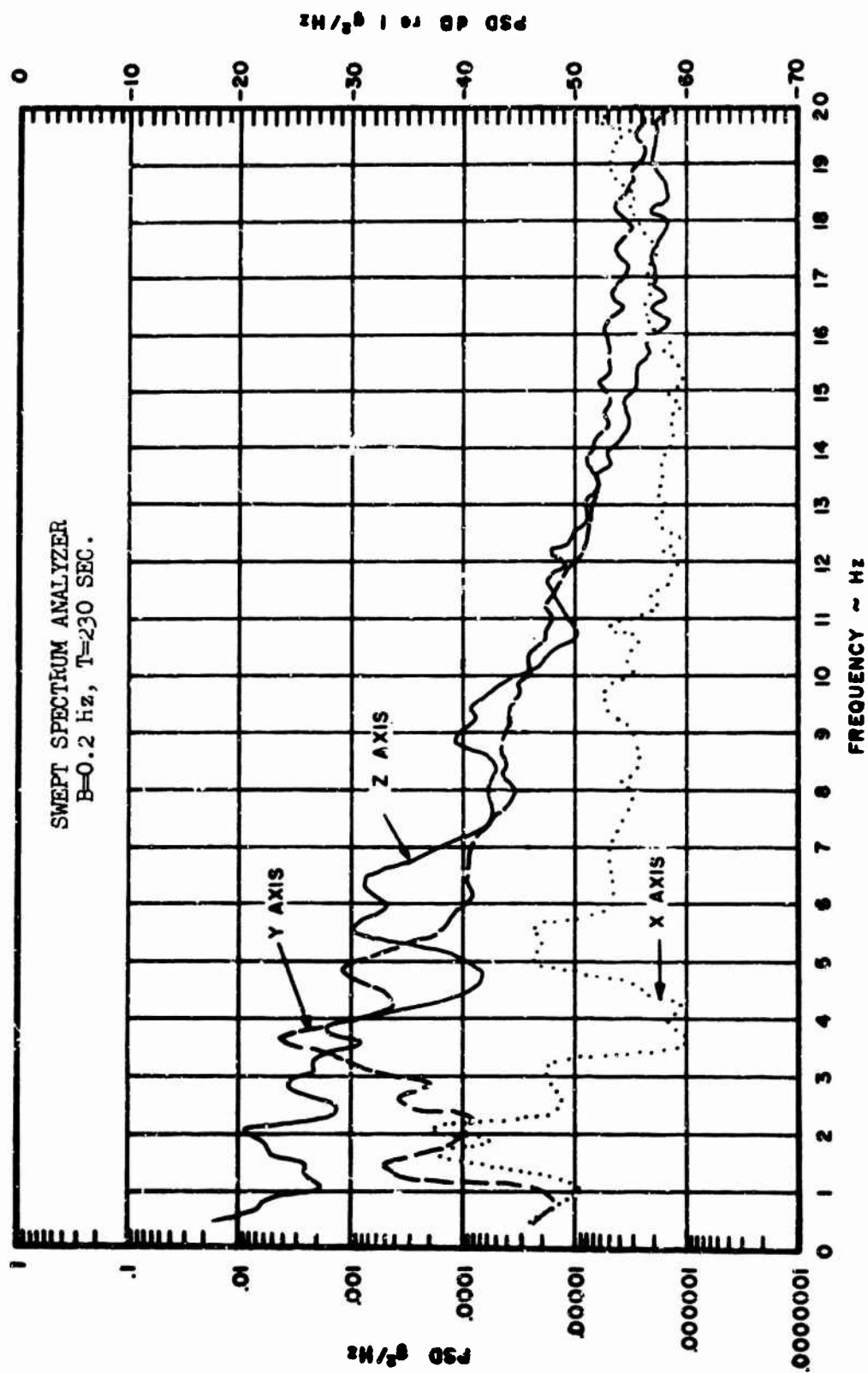


Figure 73a. Flight 1-1-1 X, Y and Z Axes PSD

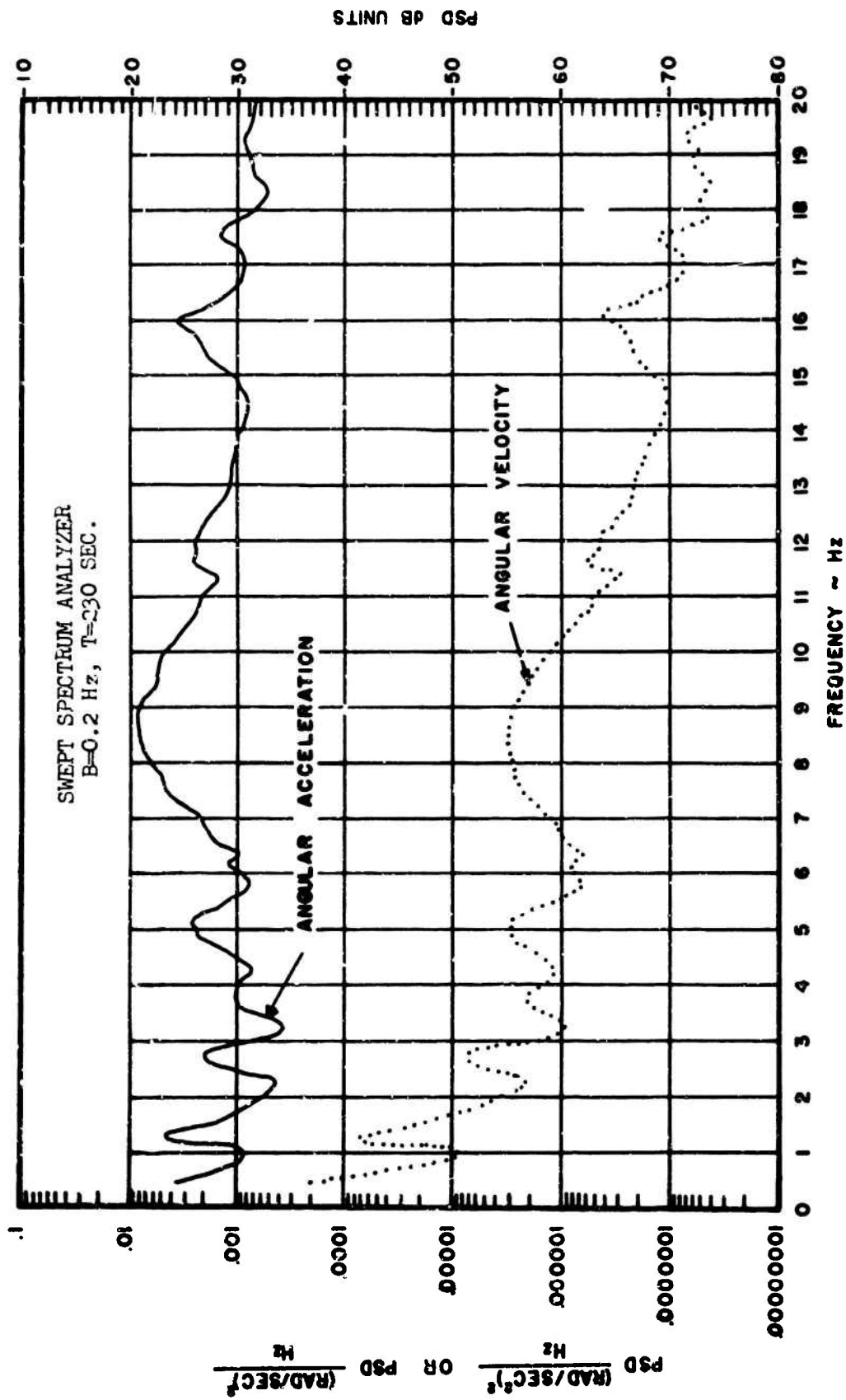


Figure 73b. Flight 1-1-1 Roll Axis PSD

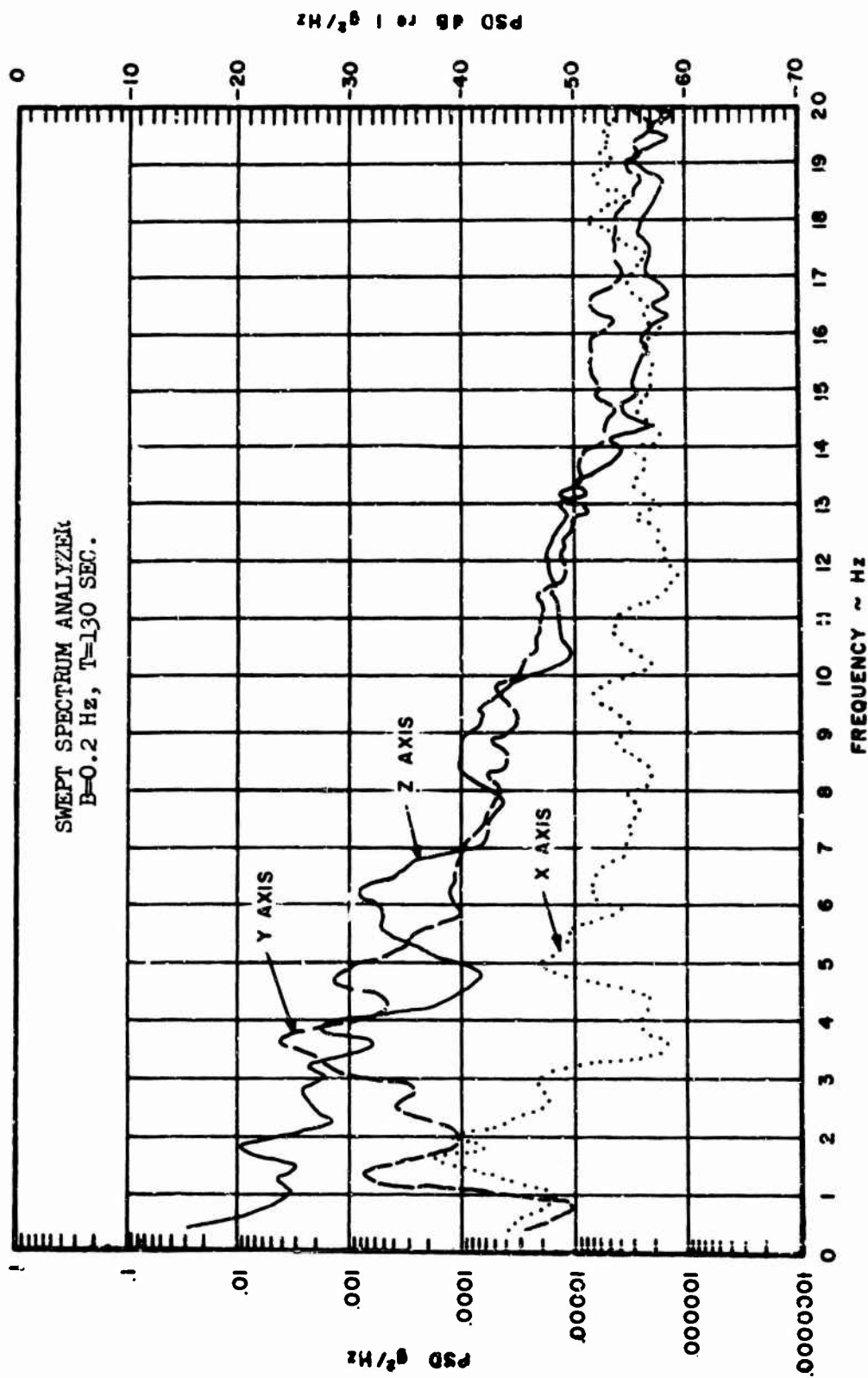


Figure 74a. Flight 1-1-2 X, Y and Z Axes PSD

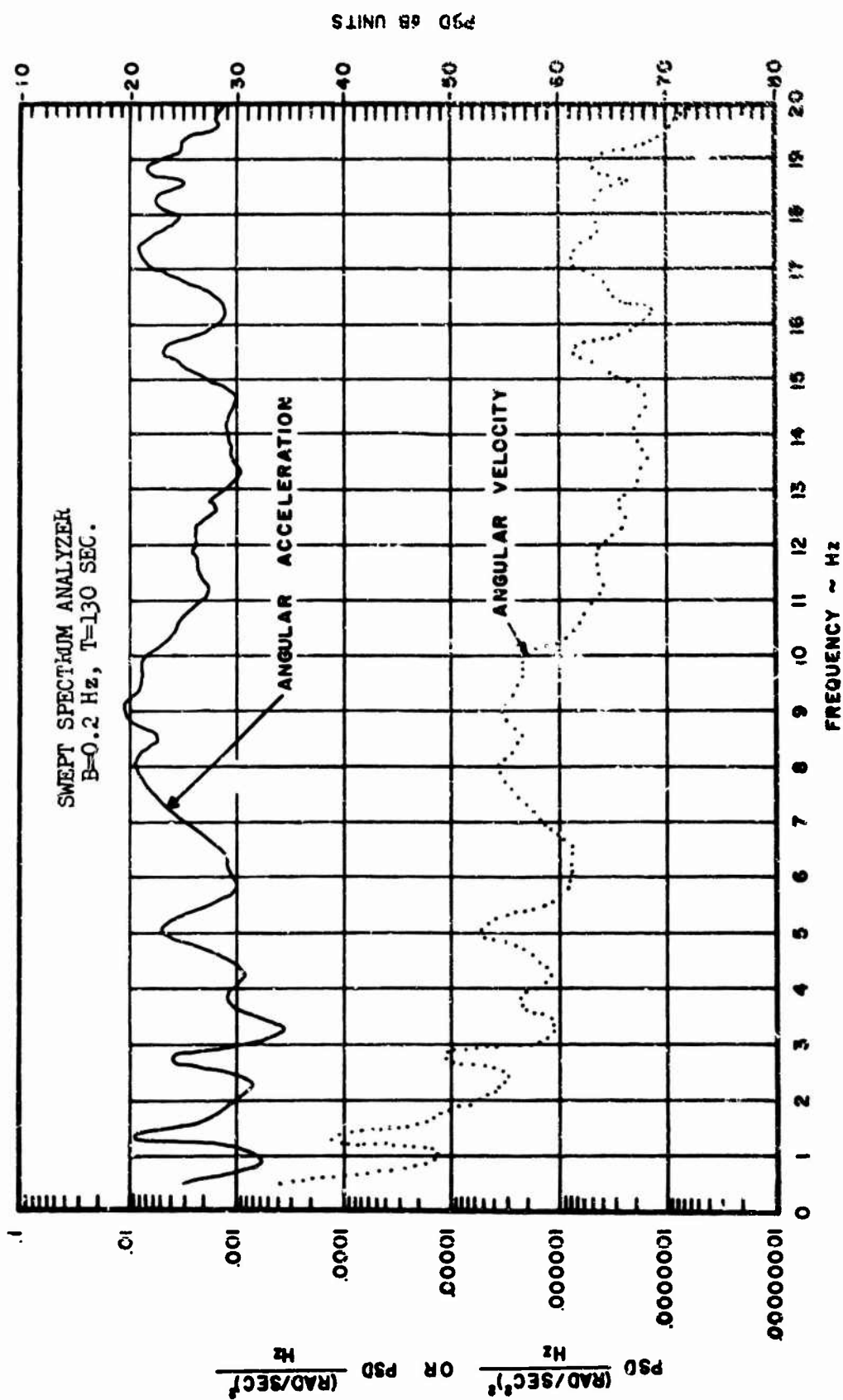


Figure 74b. Flight 1-1-2 Roll Axis PSD

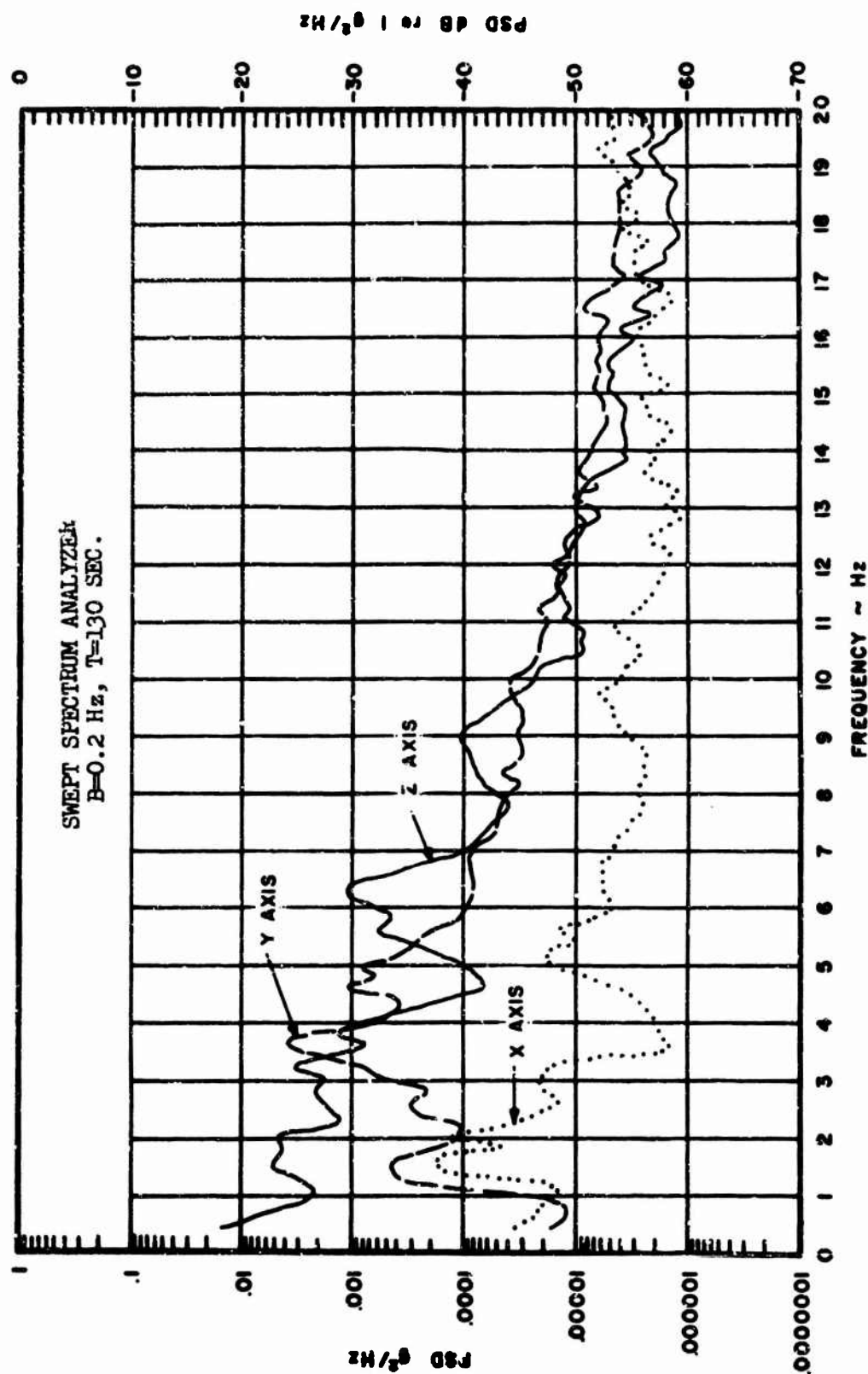


Figure 75a. Flight 1-1-3 X, Y and Z Axes PSD

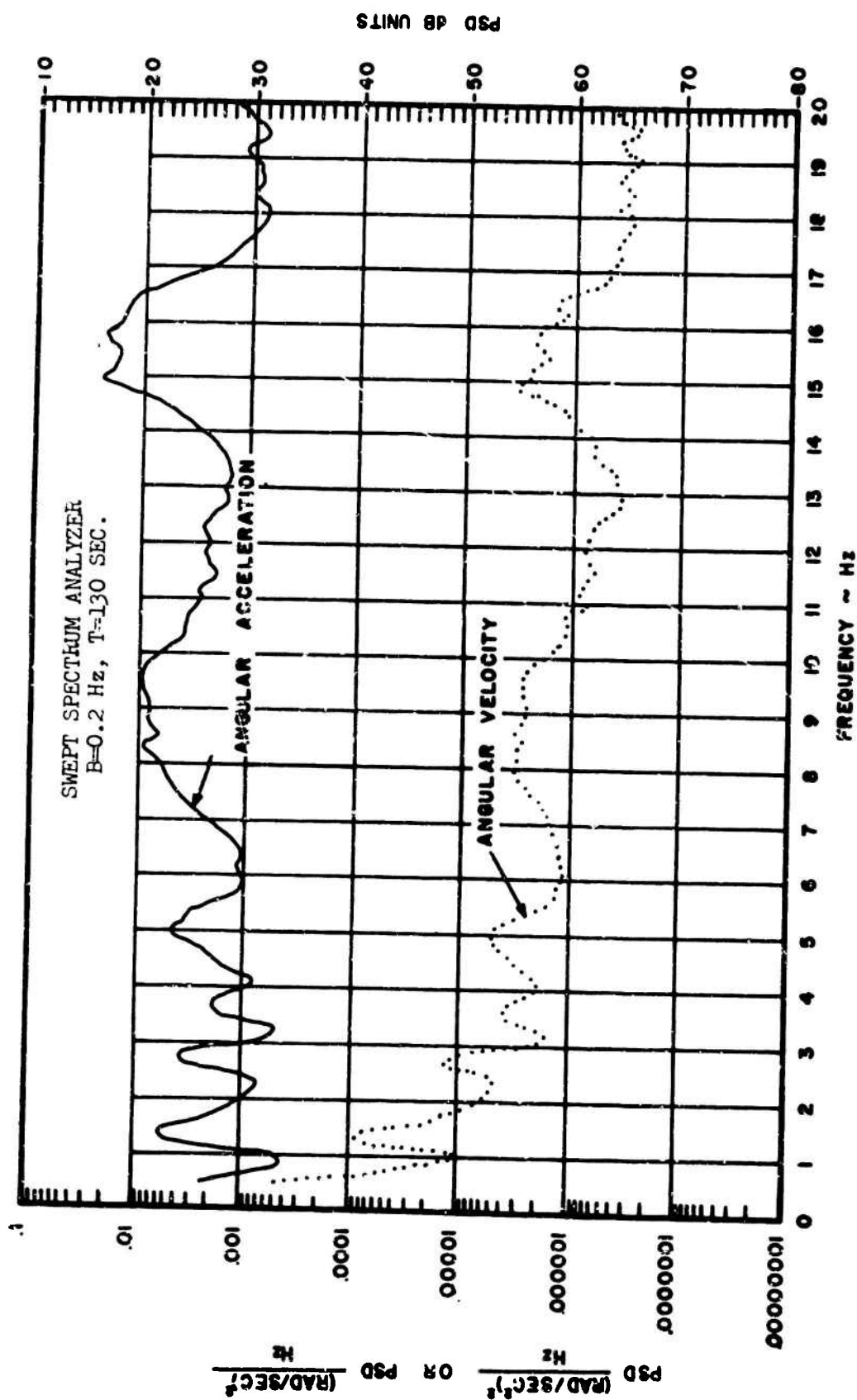


Figure 75b. Flight 1-1-3 Roll Axis PSD

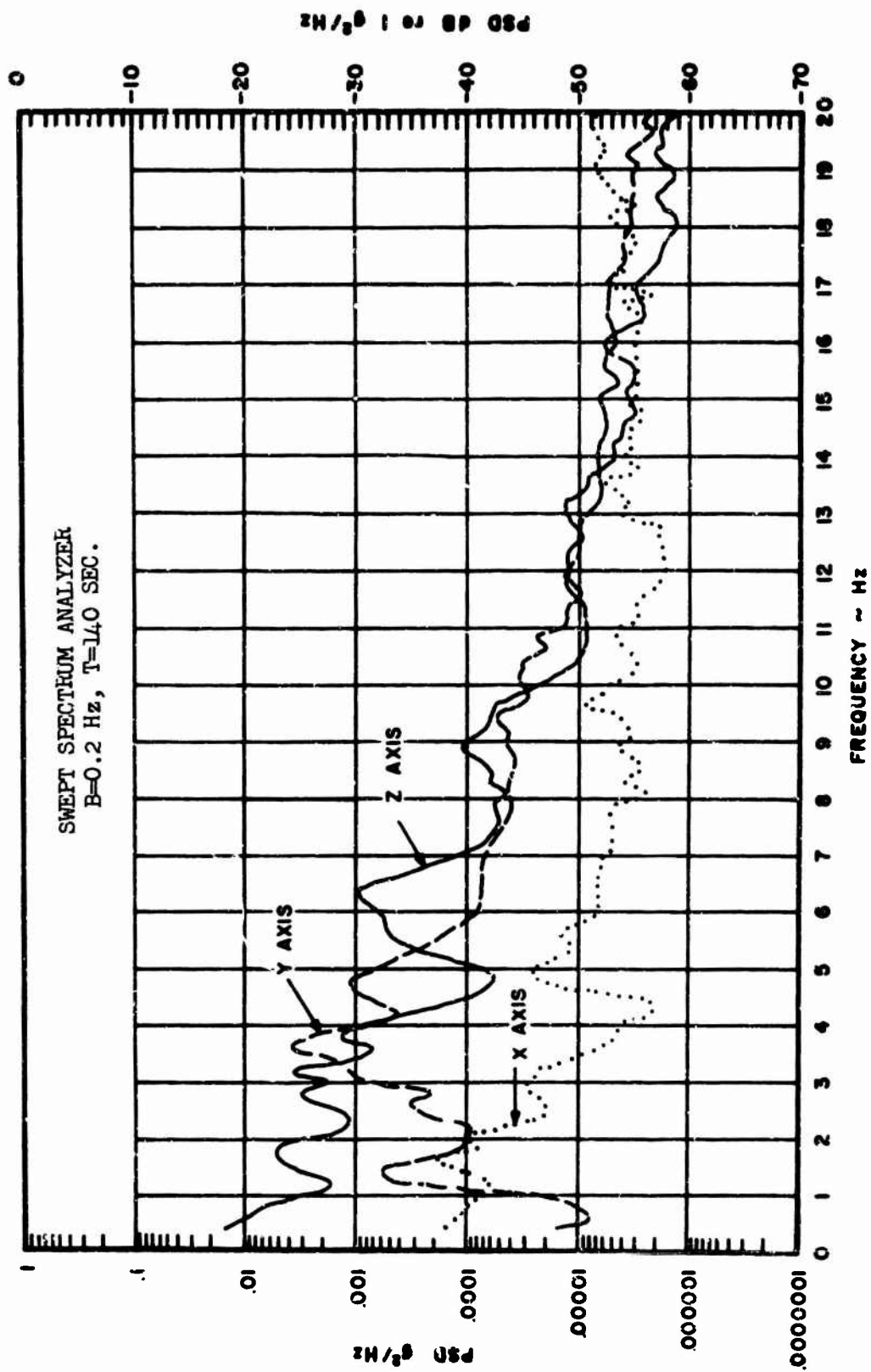


Figure 76a. Flight 1-2-1 X, Y and Z Axes PSD

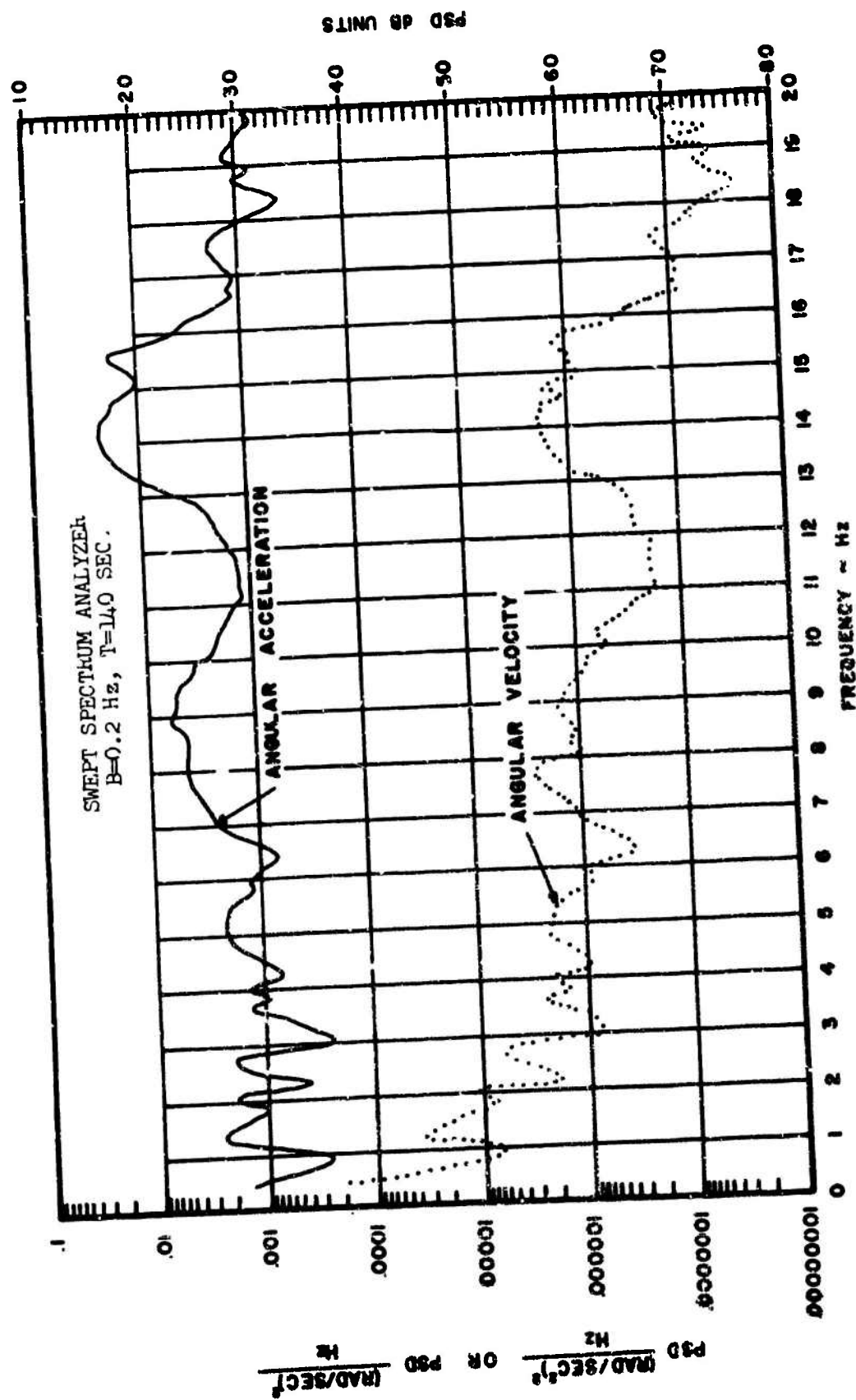


Figure 76b. Flight 1-2-1 Roll Axis PSD

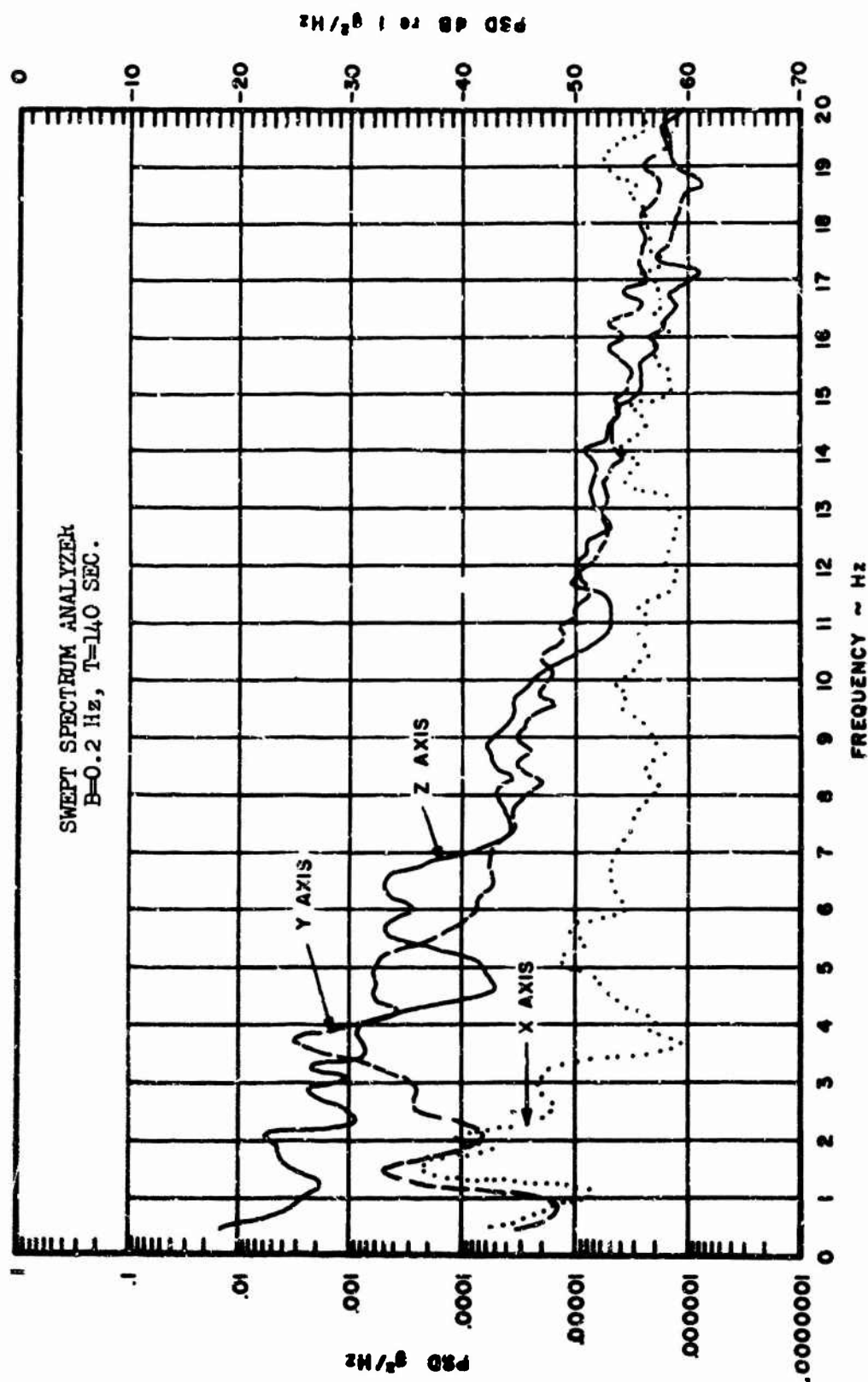


Figure 7/a. Flight 1-2-2 X, Y and Z Axes PSD

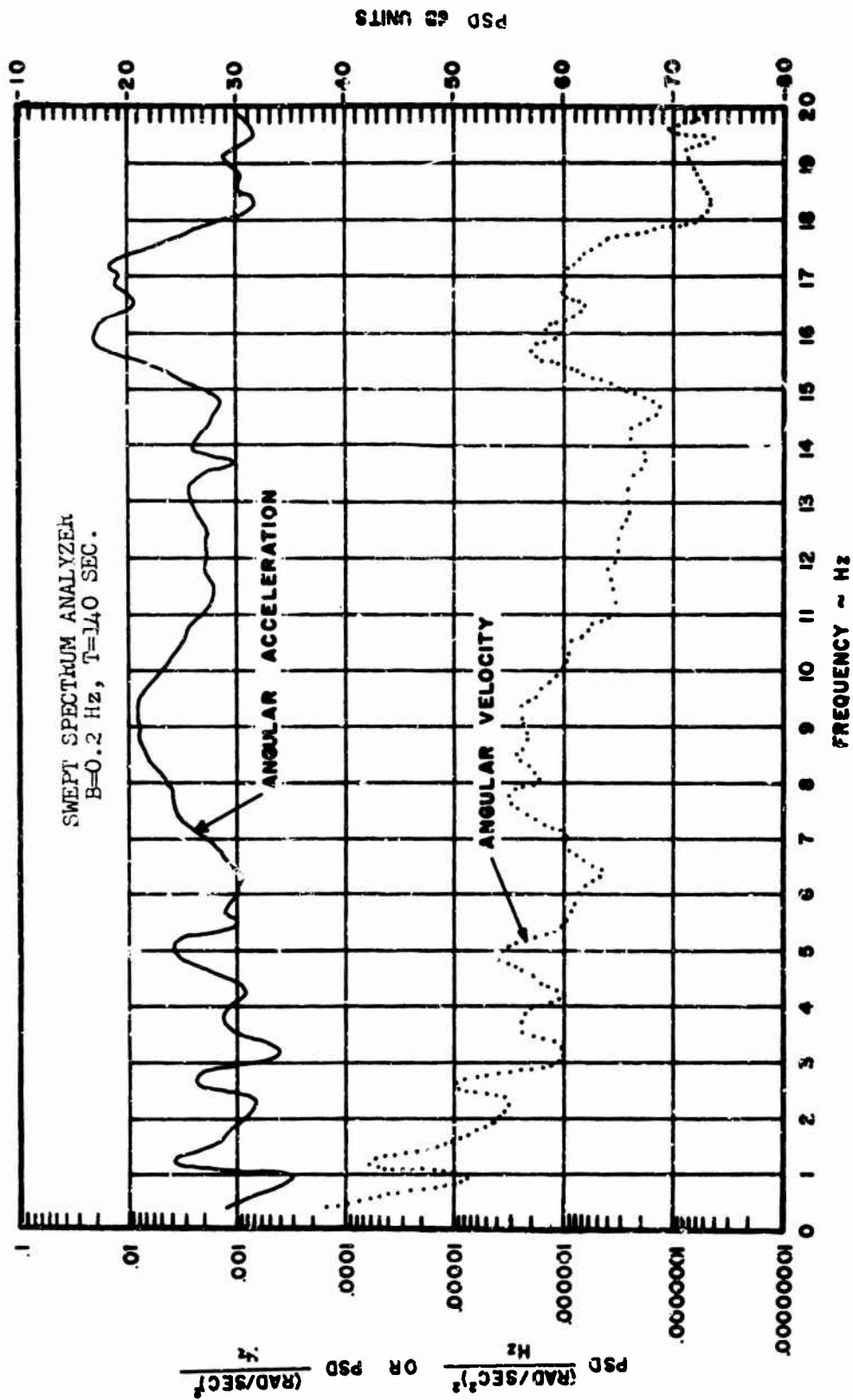


Figure 77b. Flight 1-2-2 Roll Axis PSD

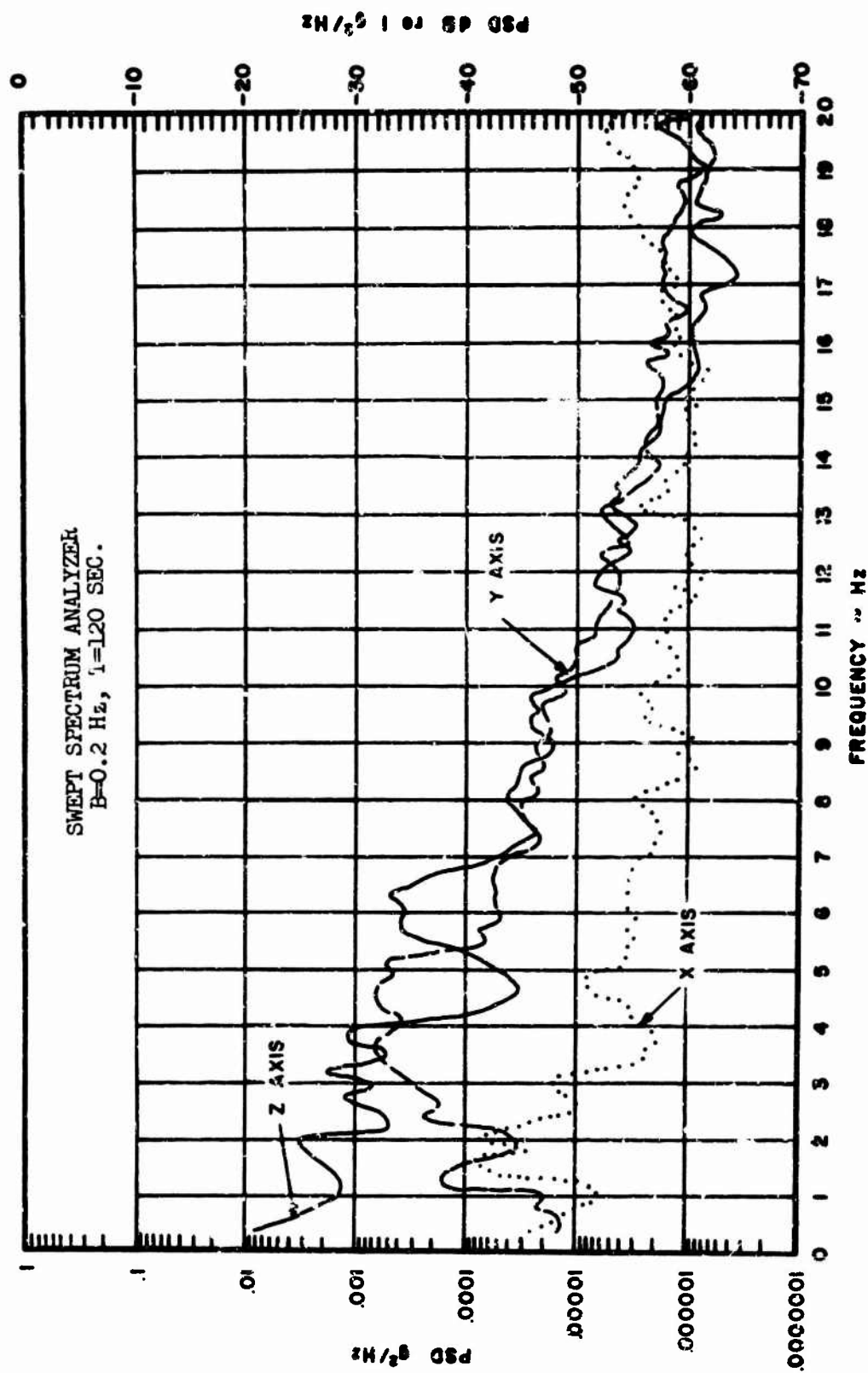


Figure 78a. Flight 1-2-3 X, Y and Z Axes PSD

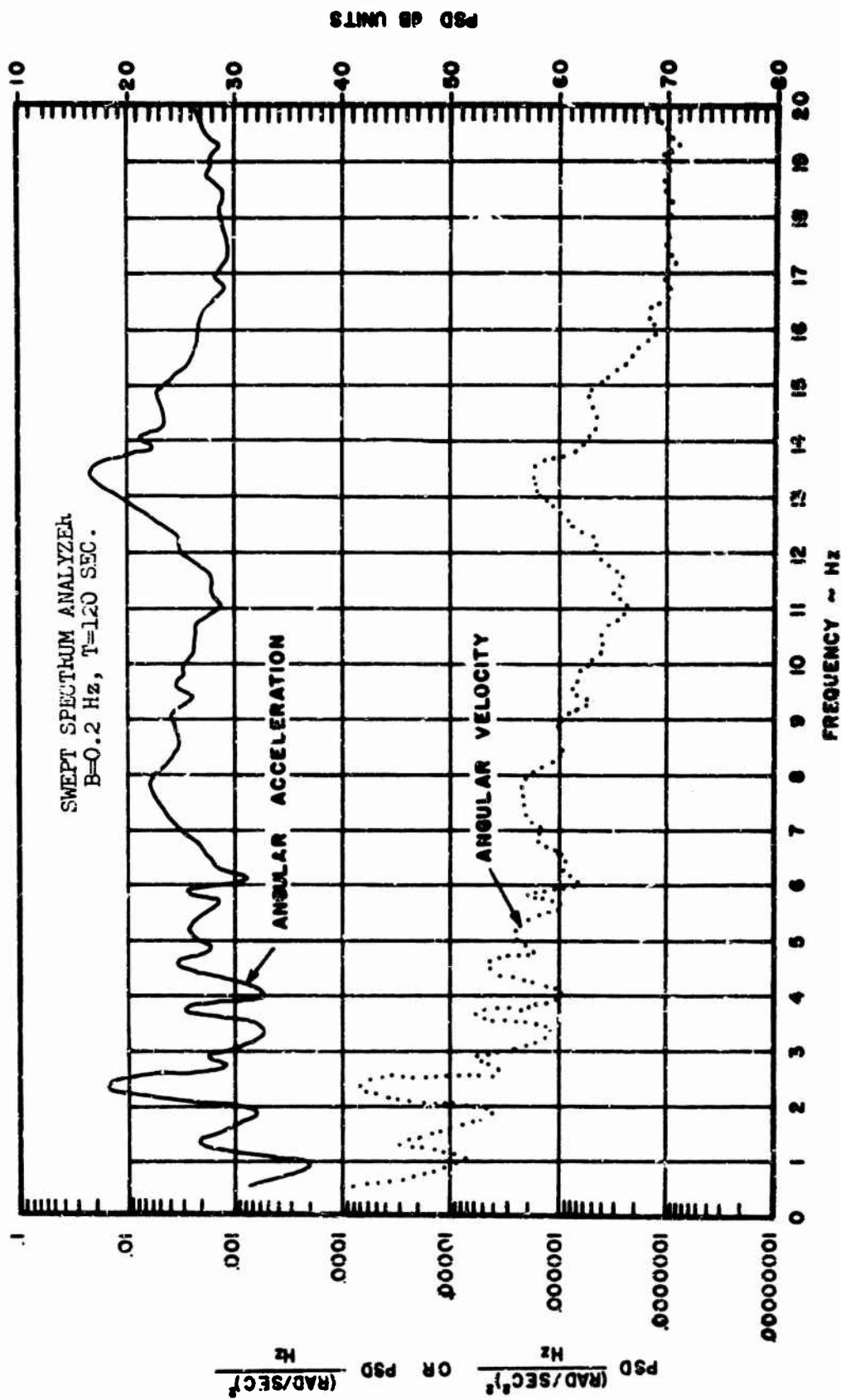


Figure 78b. Flight 1-2-3 Roll Axis PSD

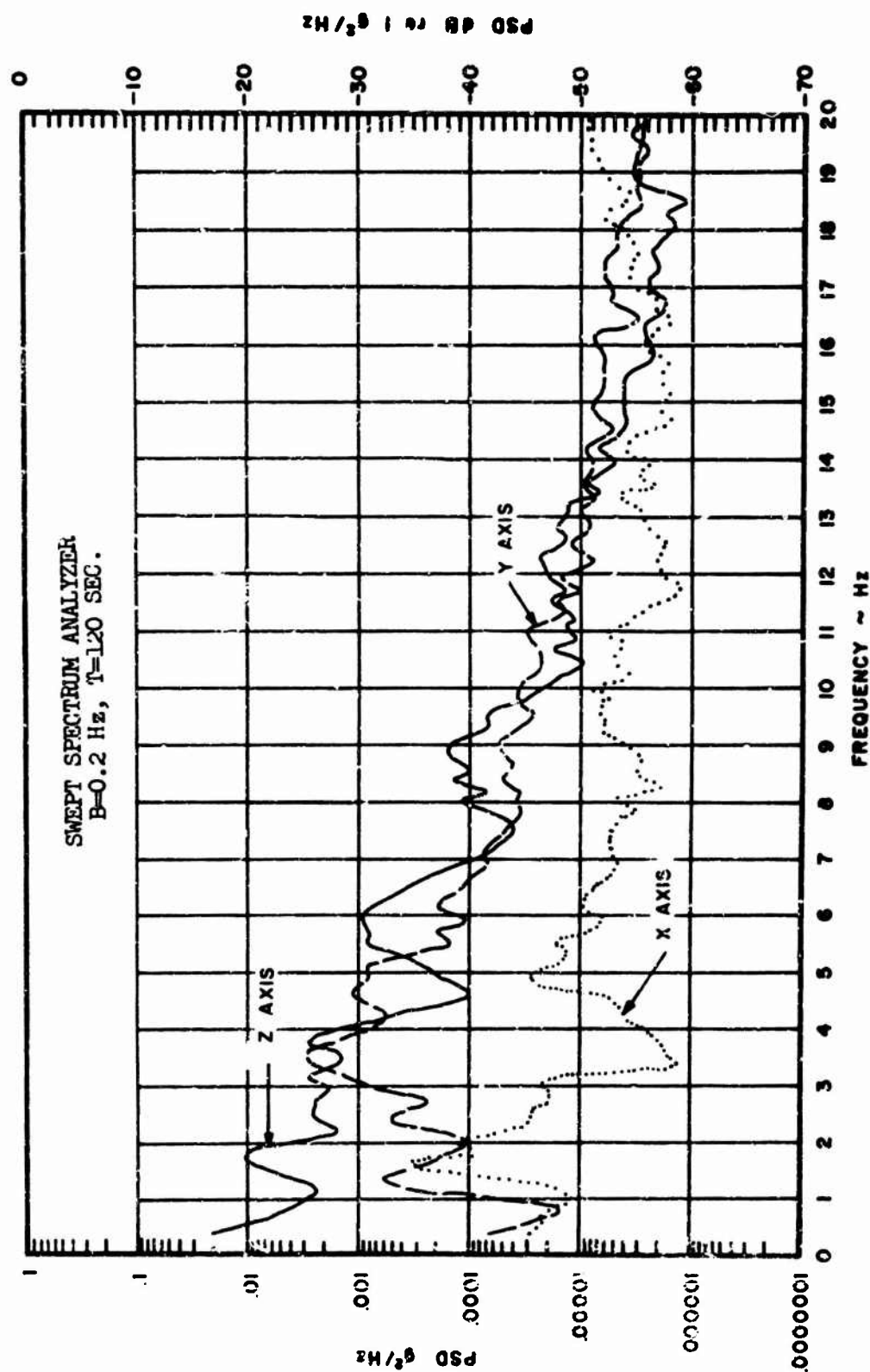


Figure 79a. Flight 2-1 X, Y and Z Axes PSD

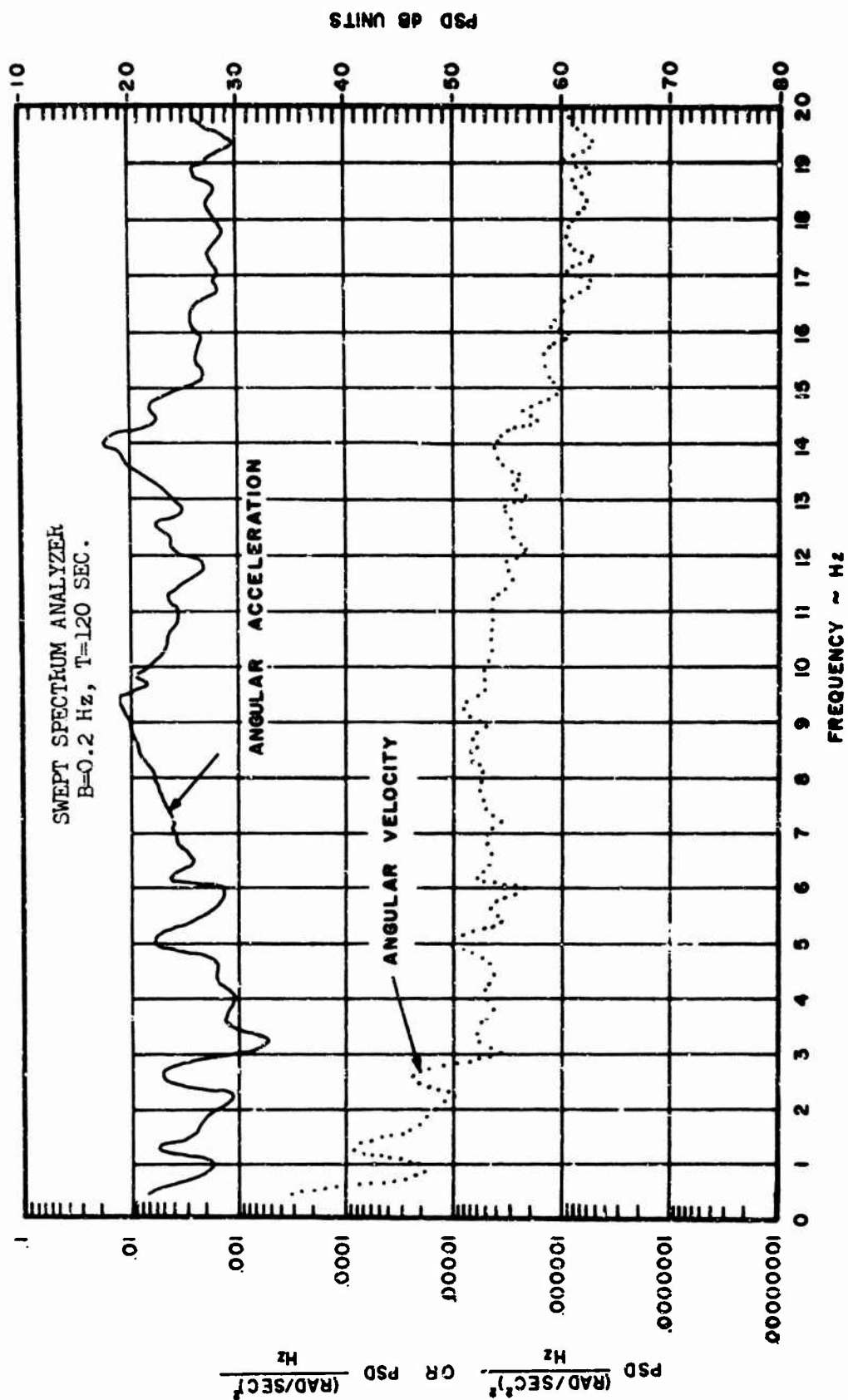


Figure 79b. Flight 2-1 Roll Axis PSD

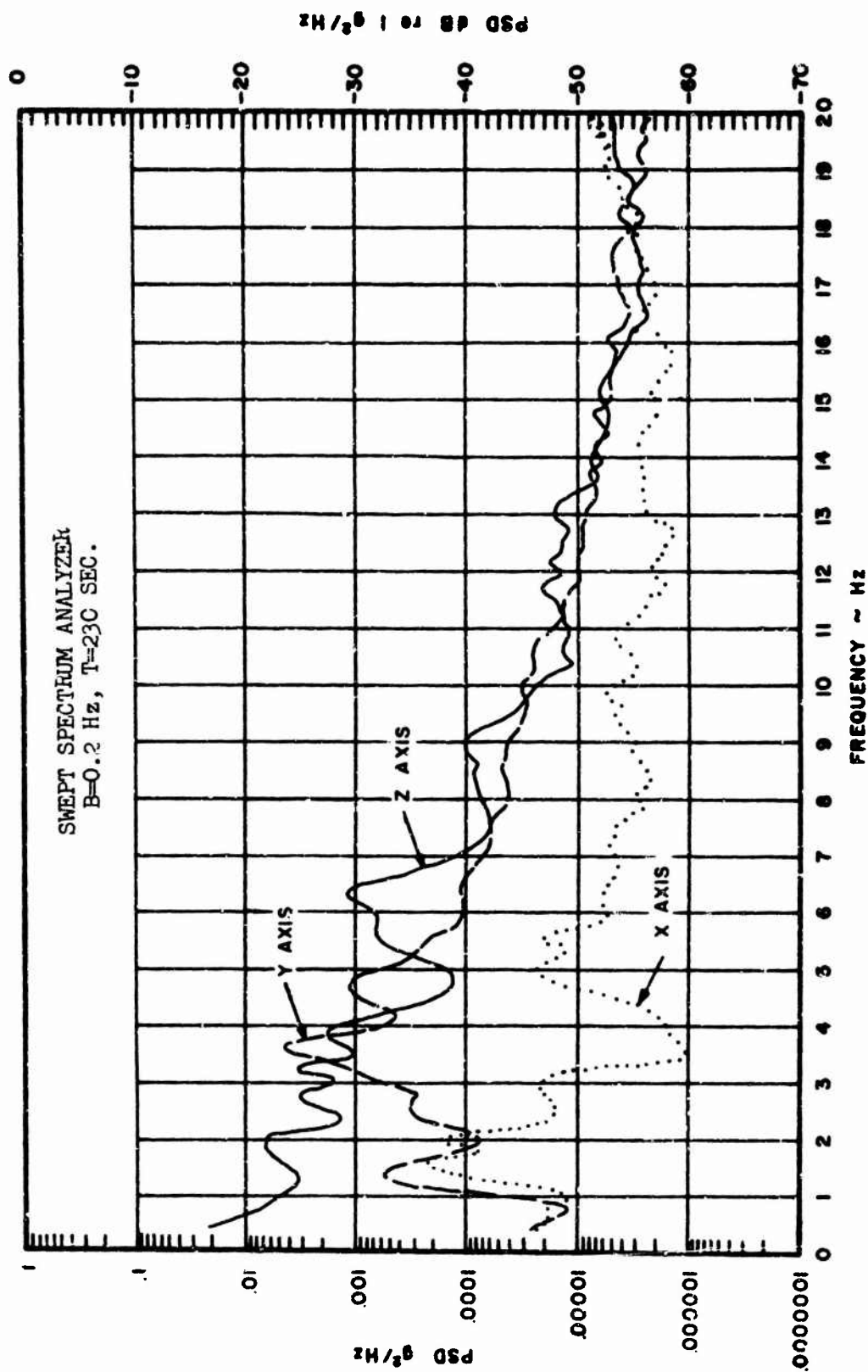


Figure 80a. Flight 2-2 X, Y and Z Axes PSD

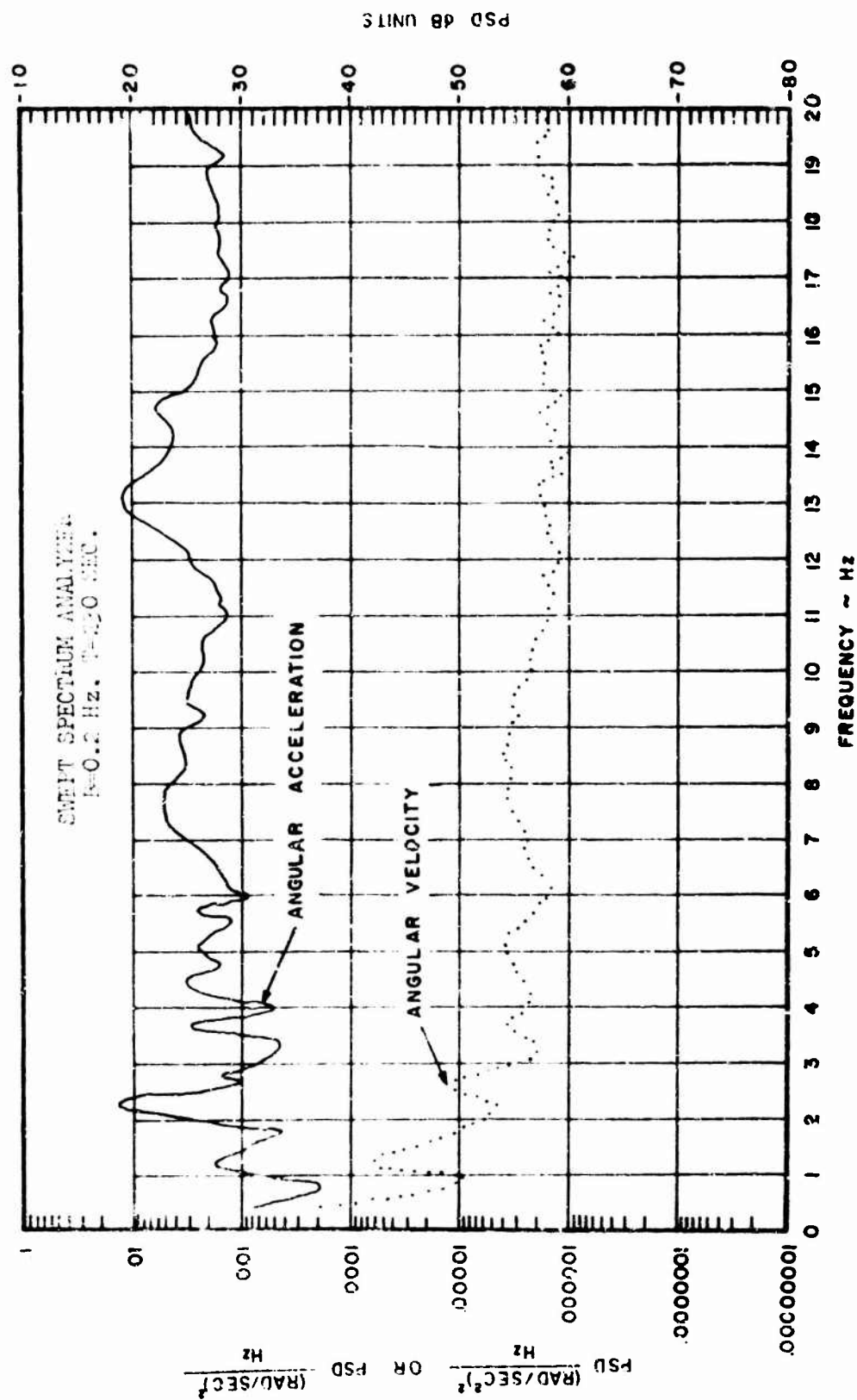


Figure 80b. Flight 2-2 Roll Axis PSD

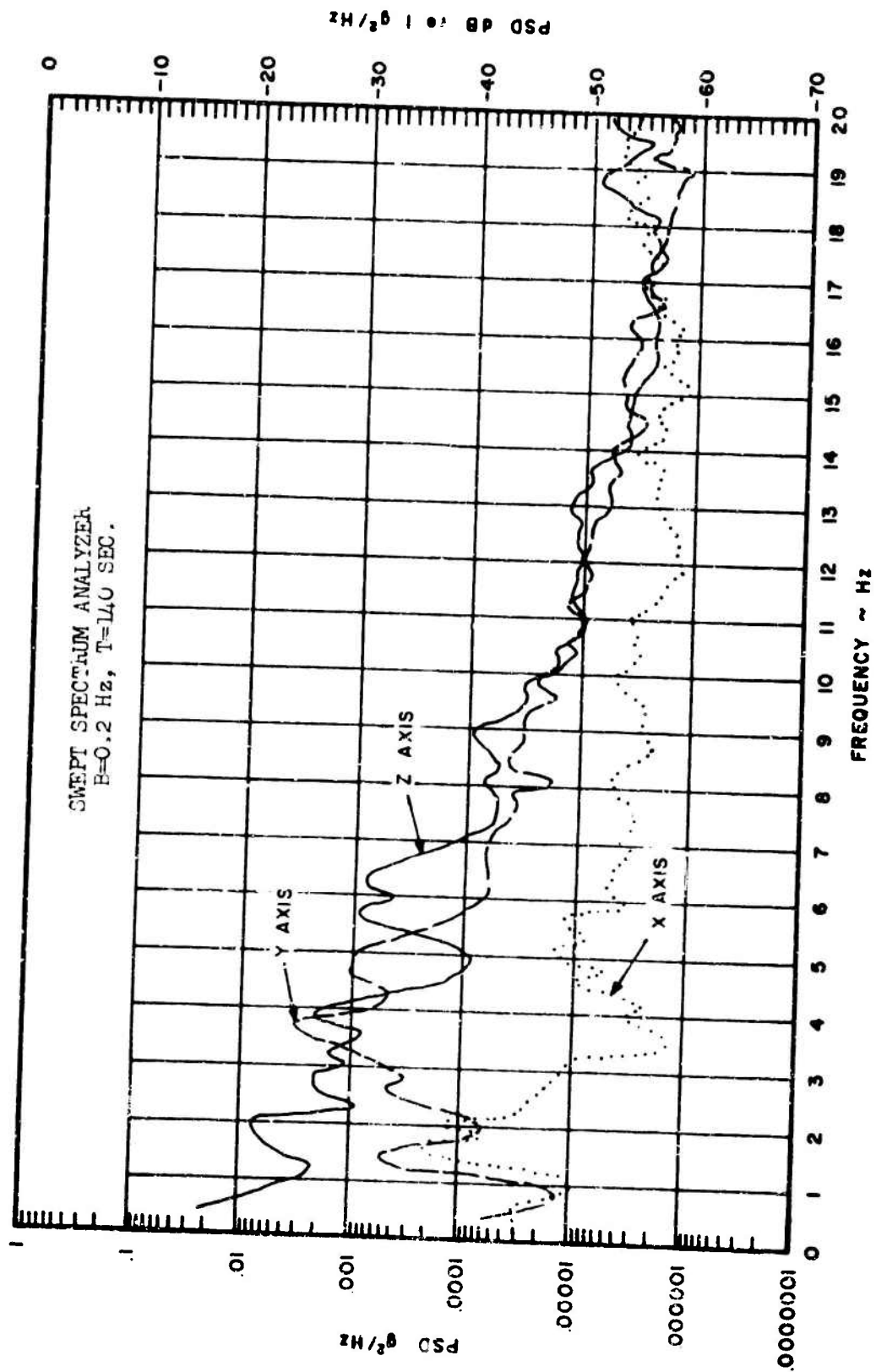


Figure 81a. Flight 2-3-1 X, Y and Z Axes PSD

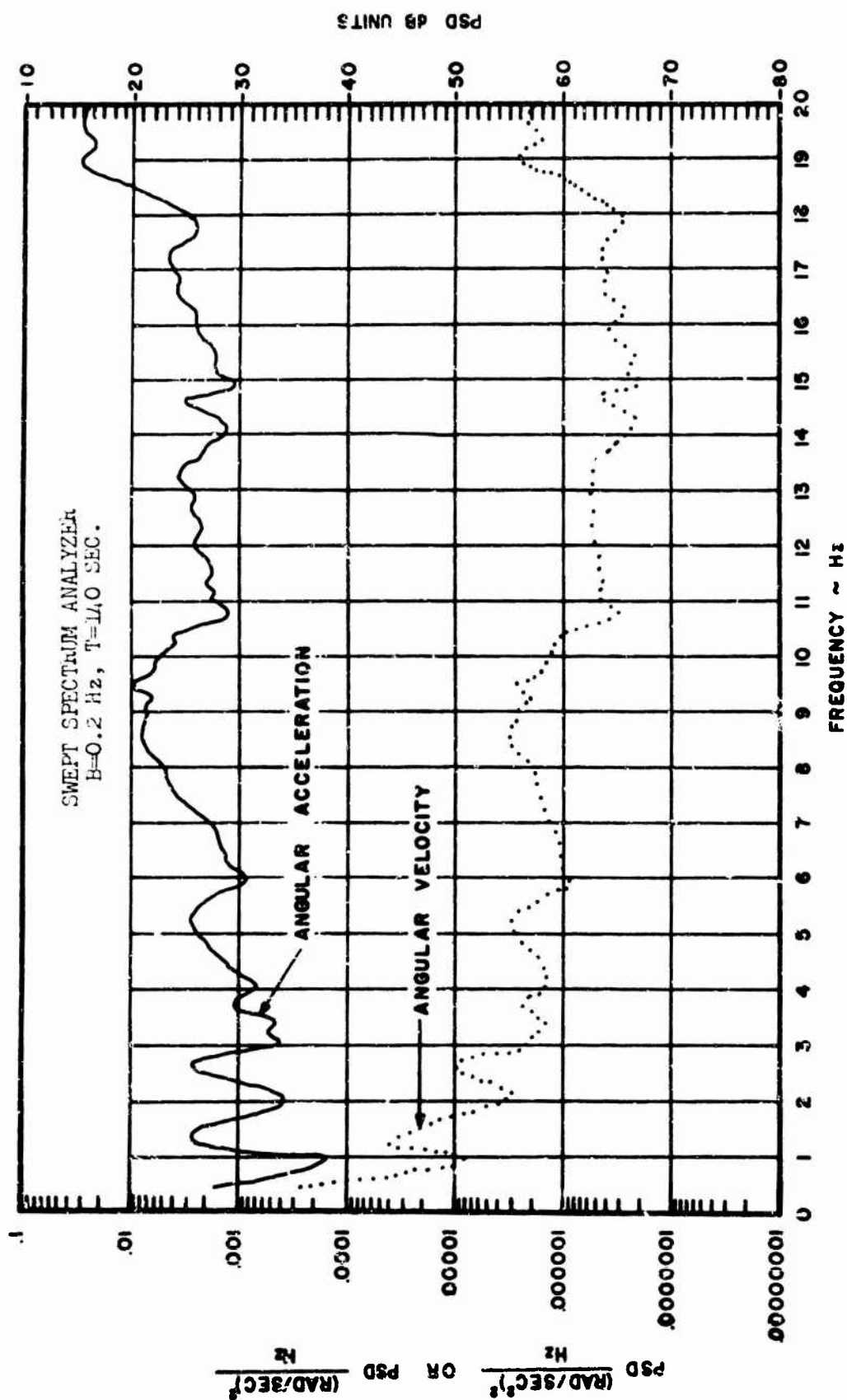


Figure 8lb. Flight 2-3-1 Roll Axis PSD

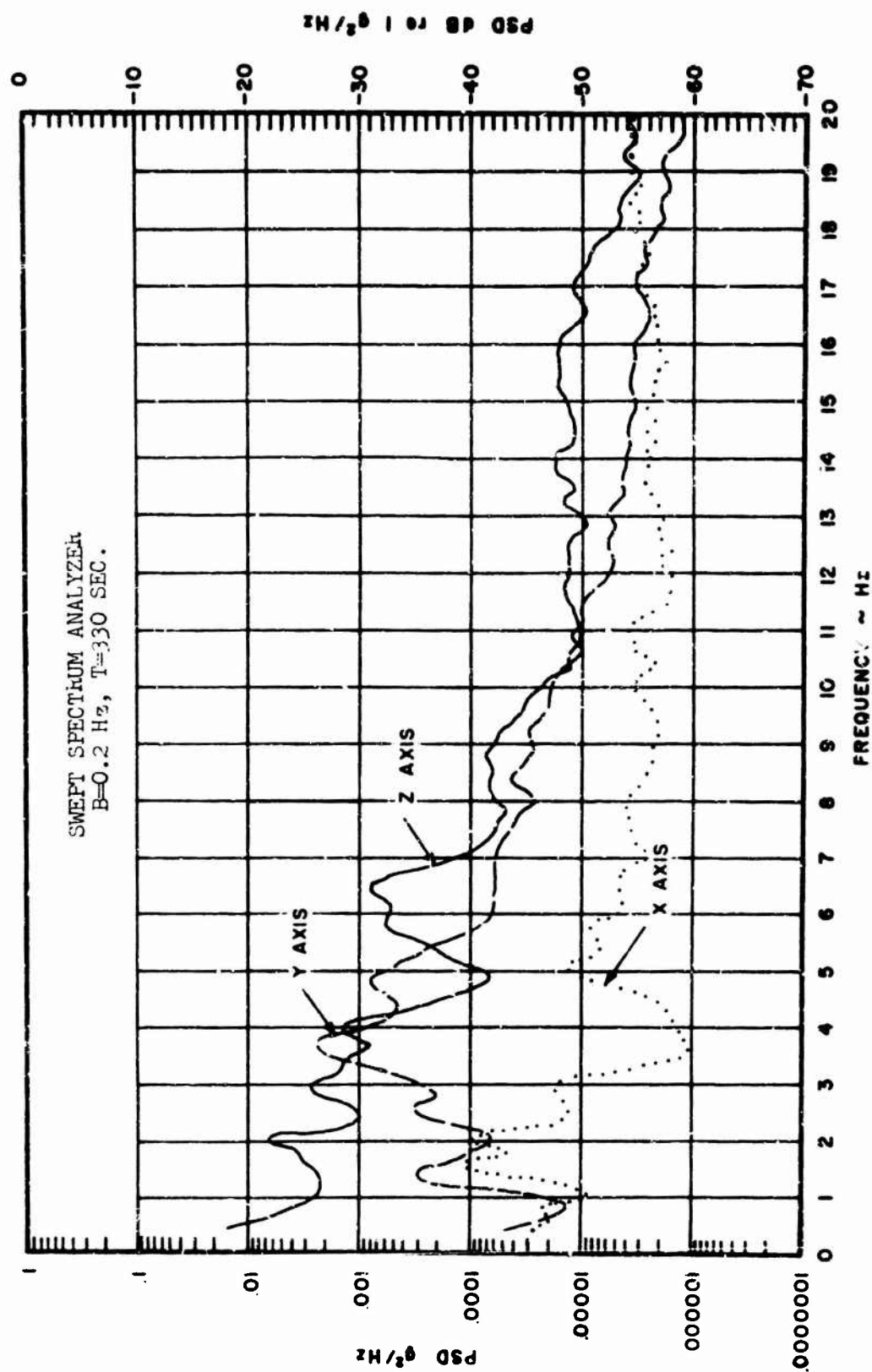


Figure 82a. Flight 2-3-2 X, Y and Z Axes PSD

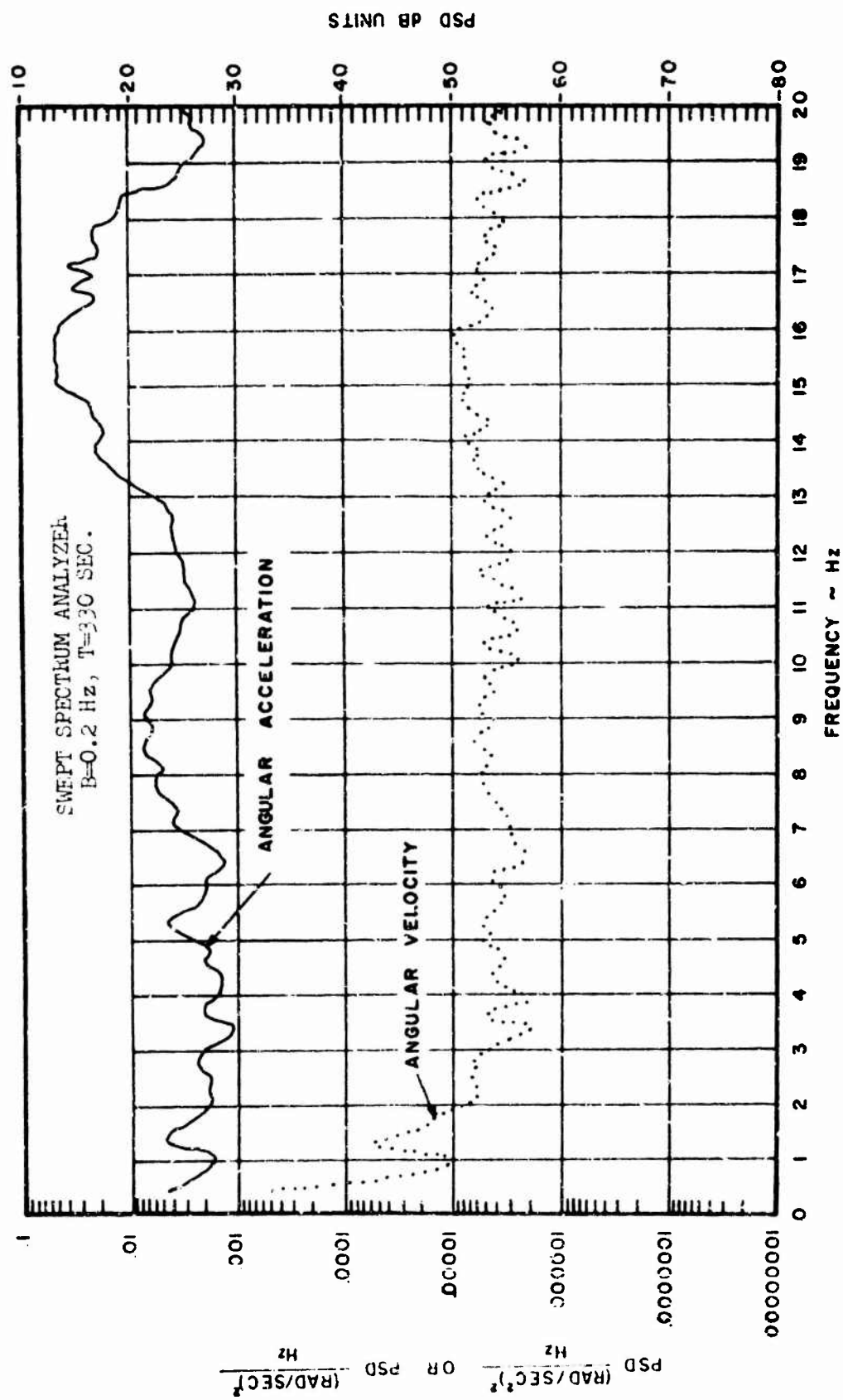


Figure 82b. Flight 2-3-2 Roll Axis PSD

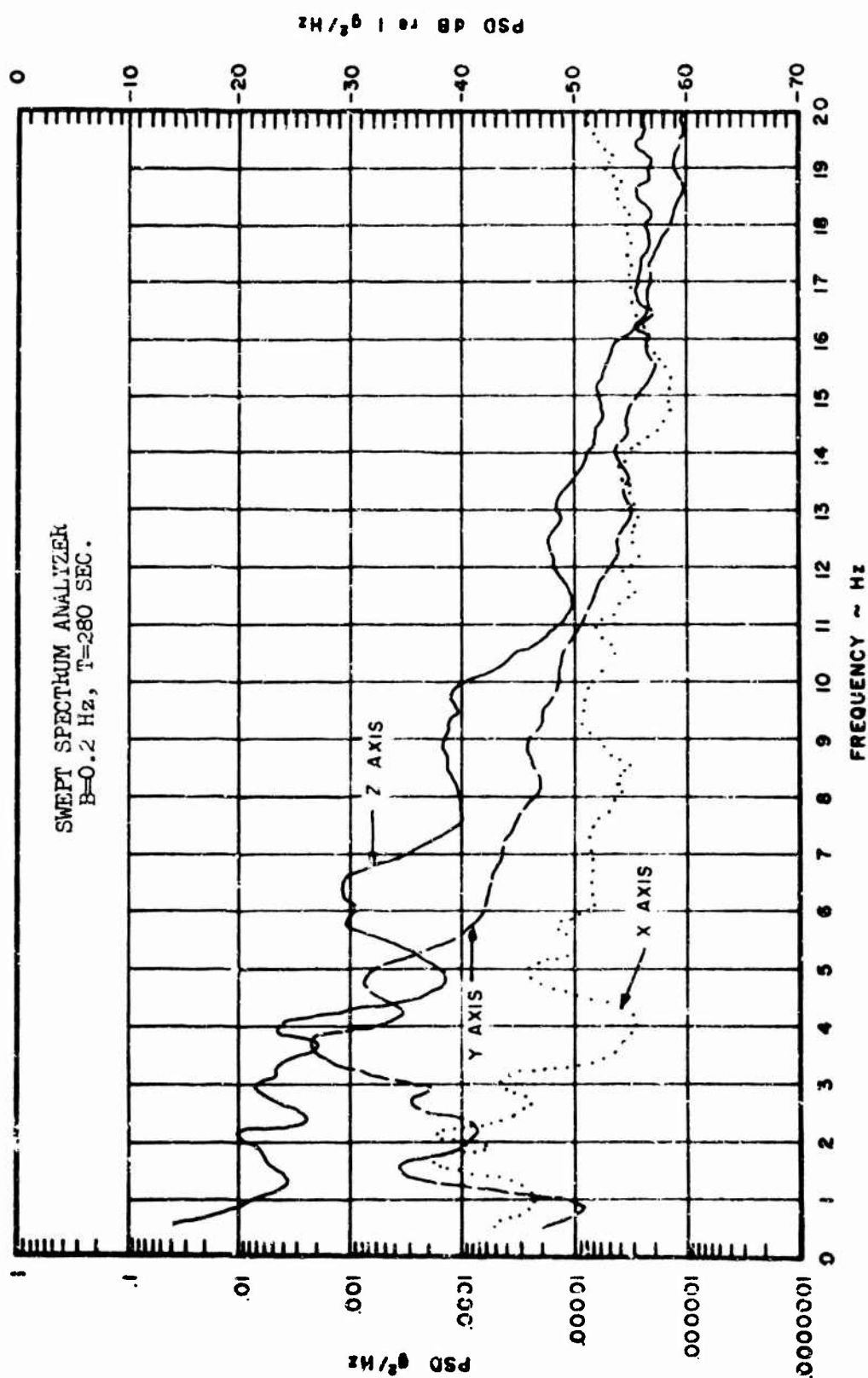


Figure 33a. Flight 4-2 X, Y and Z Axes PSD

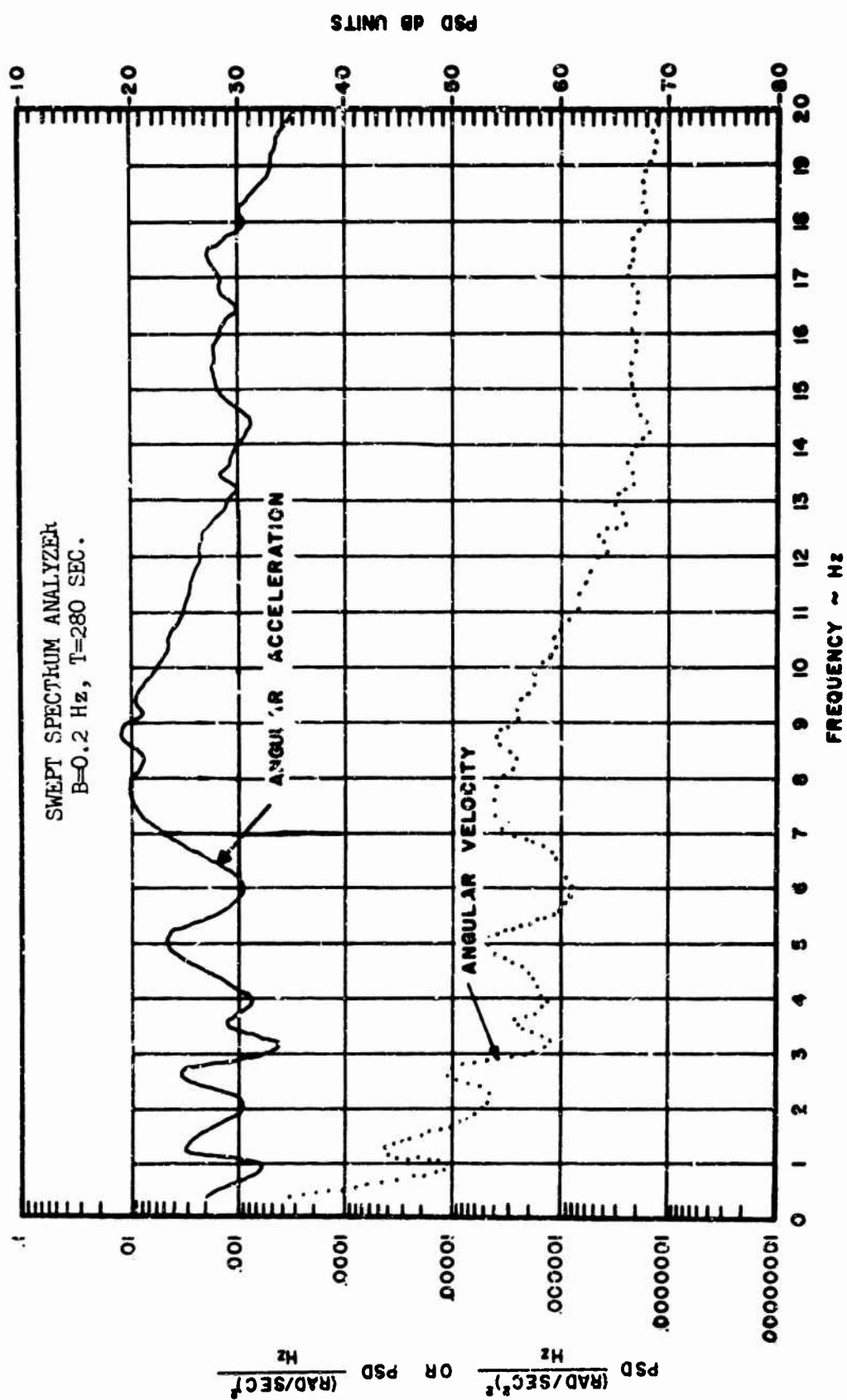


Figure 83b. Flight 4-2 Roll Axis PSD

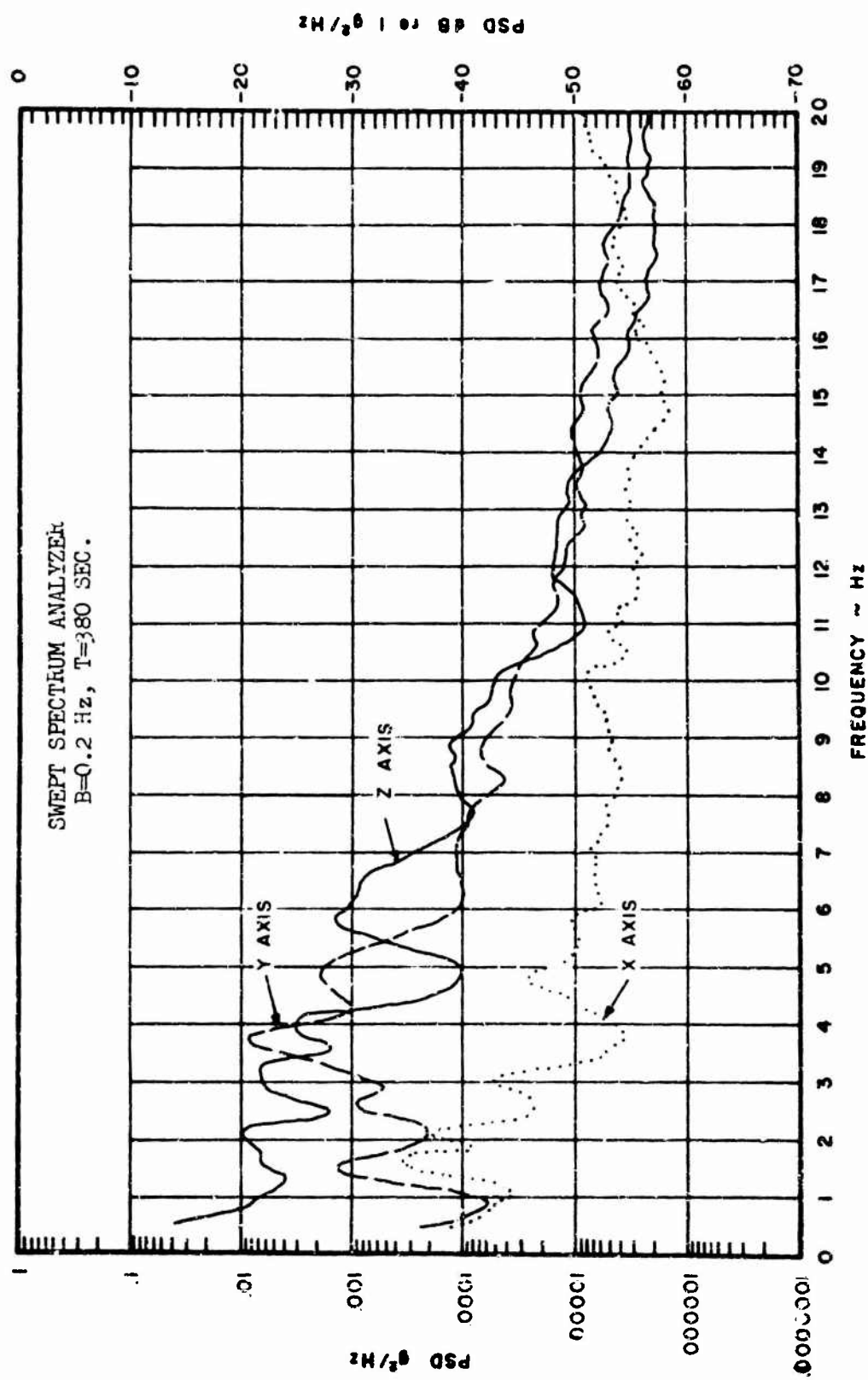


Figure 84a. Flight 4-3 X, Y and Z Axes PSD

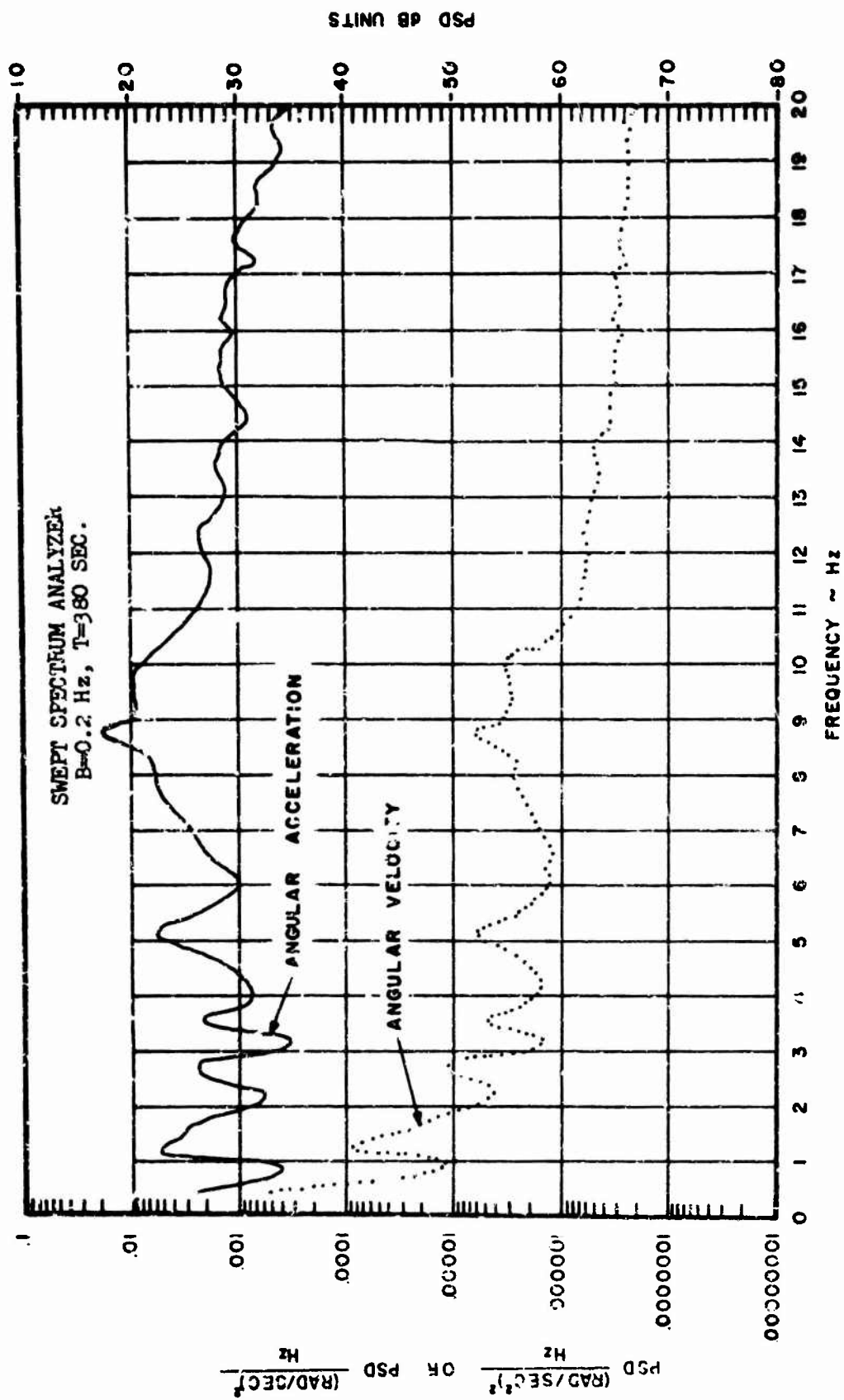


Figure 84b. Flight 4-3 Roll Axis PSD

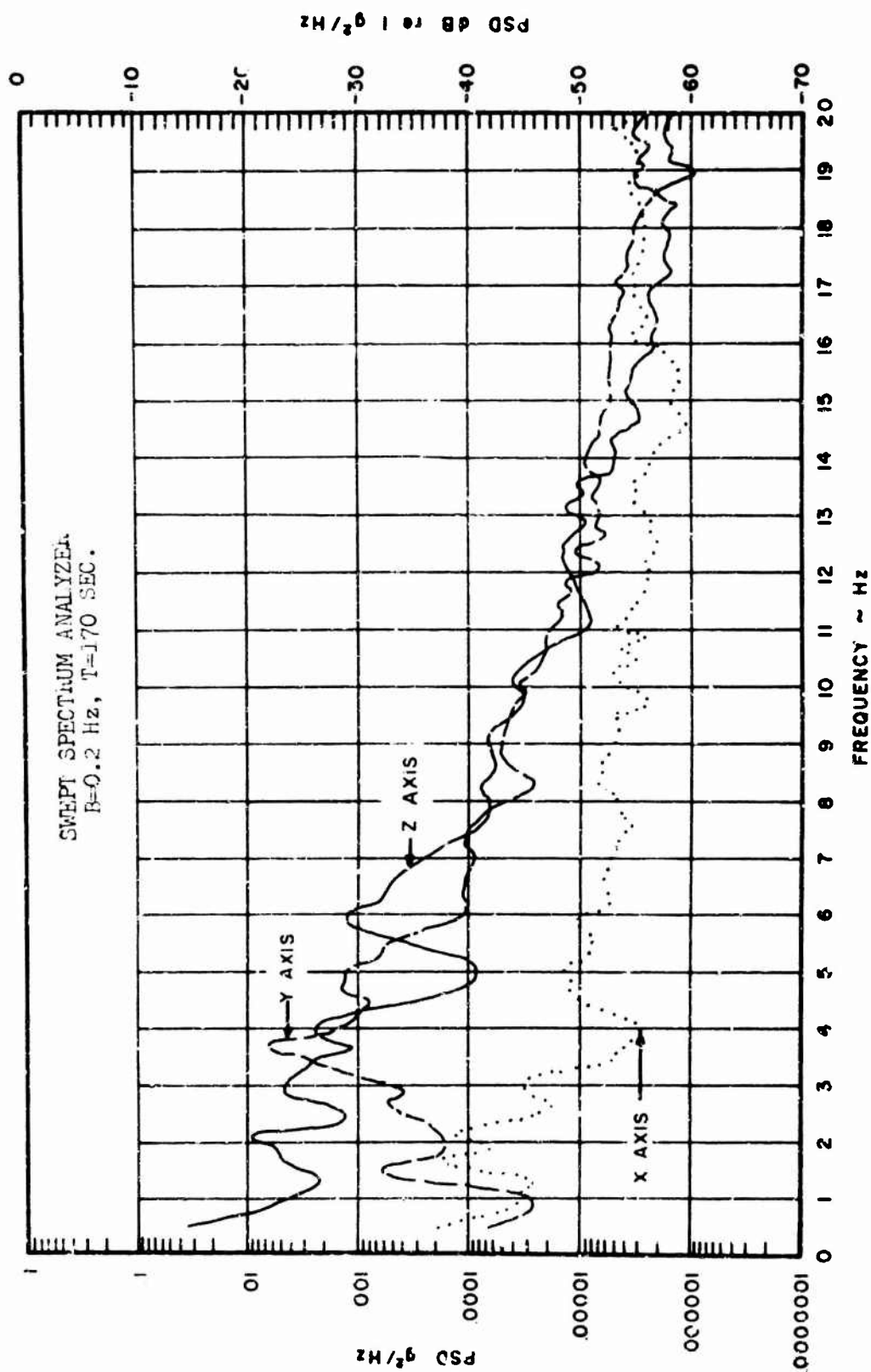


Figure 85a. Flight 4-4 X, Y and Z Axes PSD

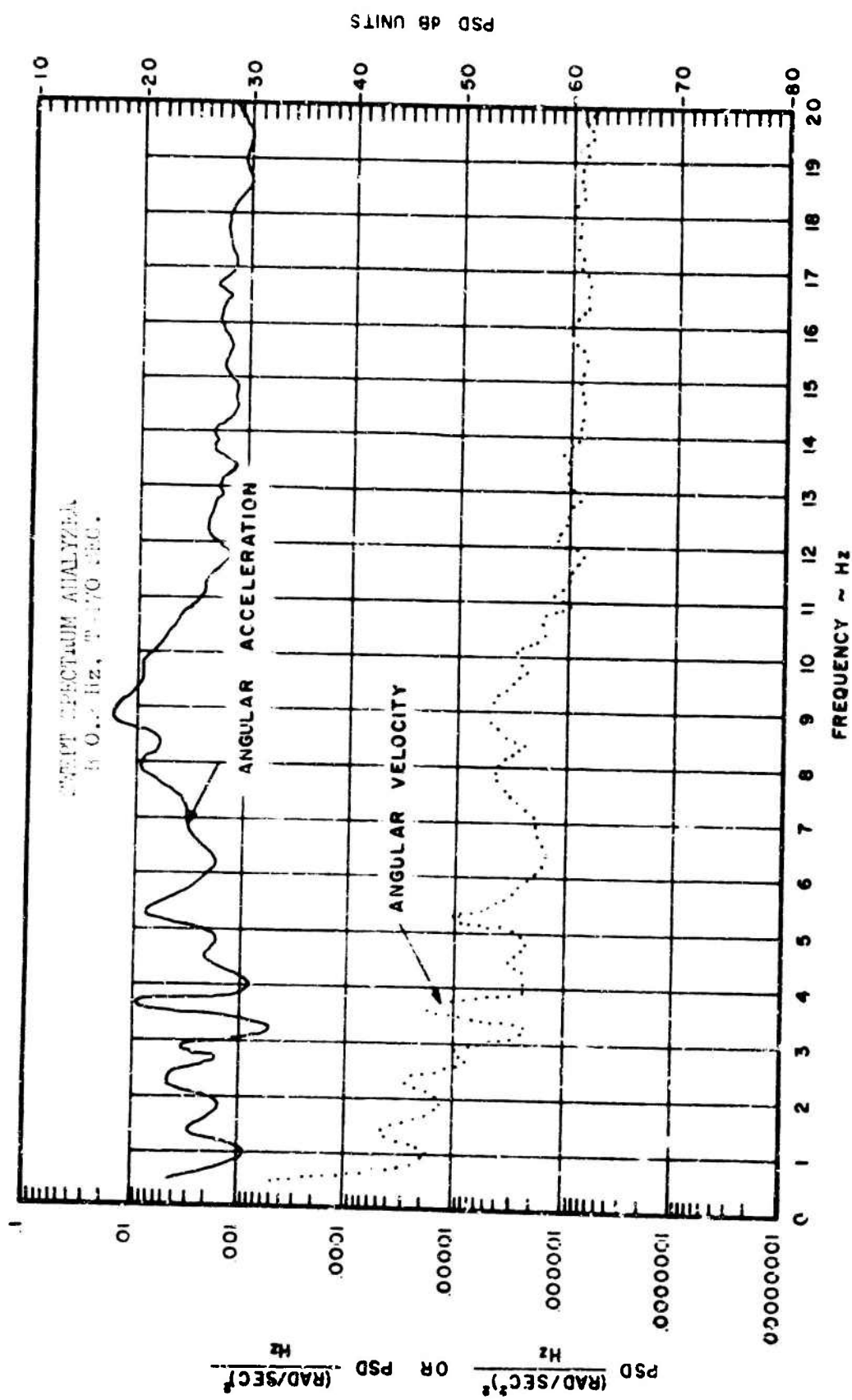


Figure 85h. Flight 4-4 Roll Axis PSD

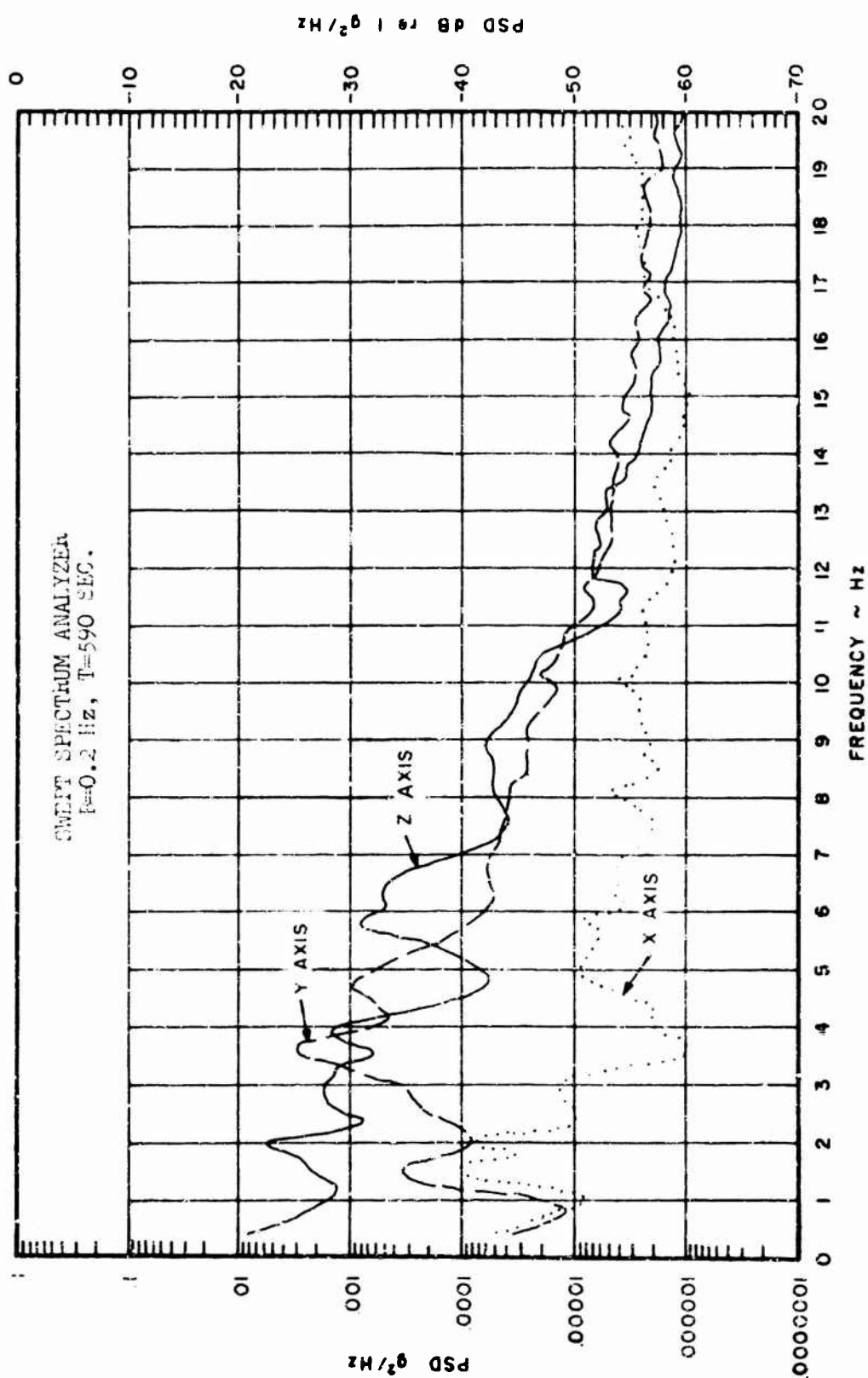


Figure 804. Flight 6-2 X, Y and Z Axes PSD

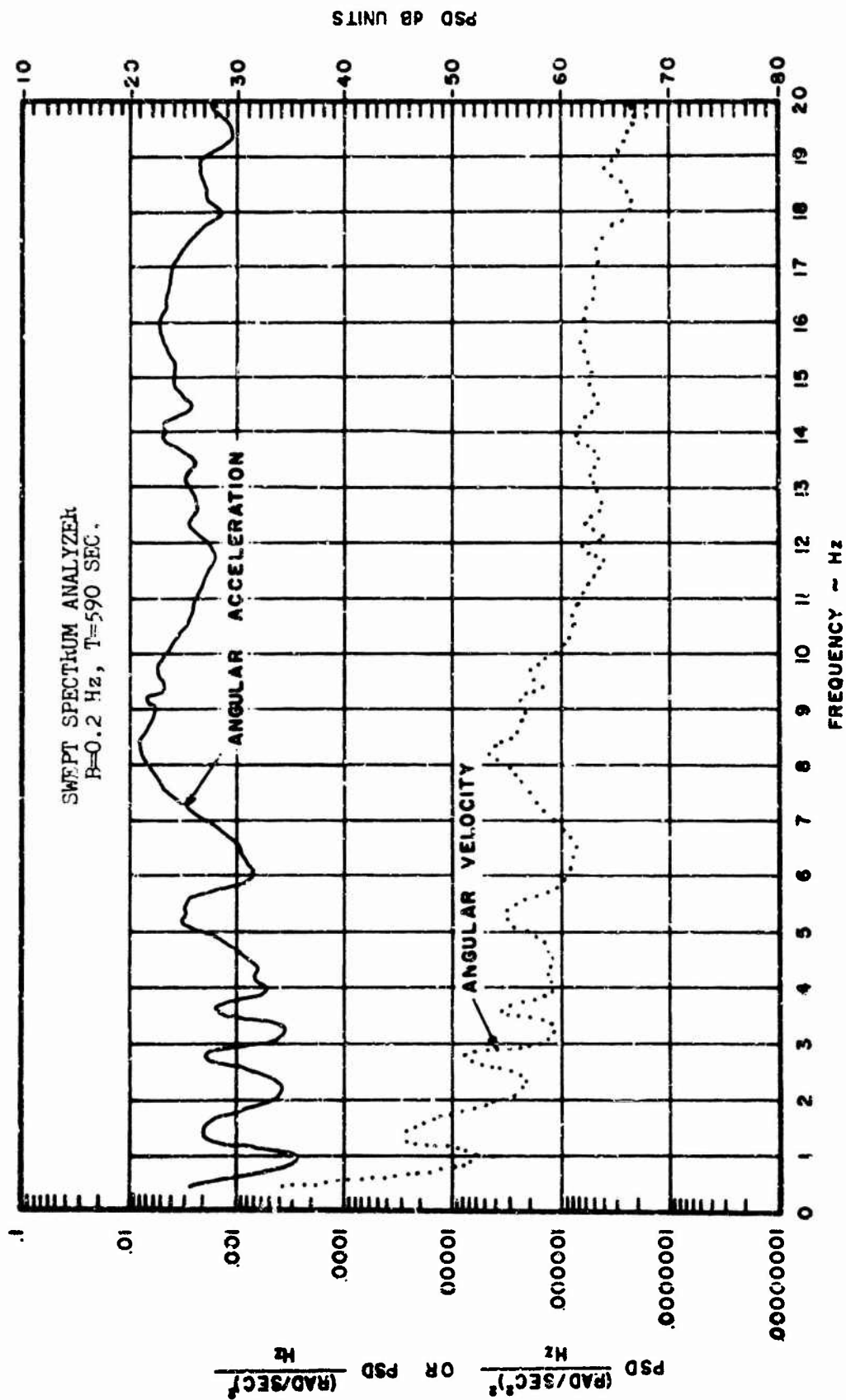


Figure 86b. Flight 6-2 Roll Axis PSD

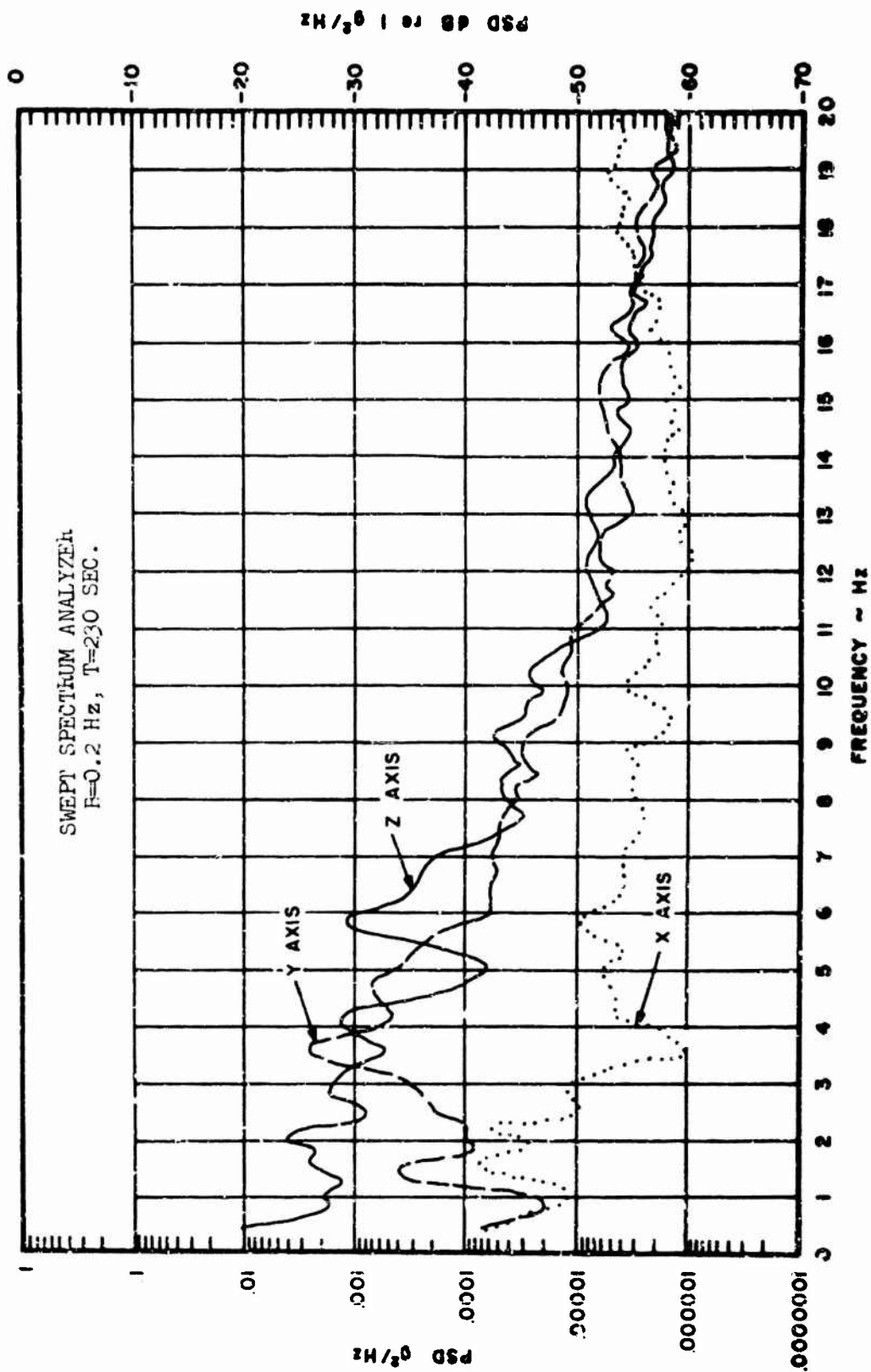


Figure 87a. Flight 6-3 X, Y and Z Axes PSD

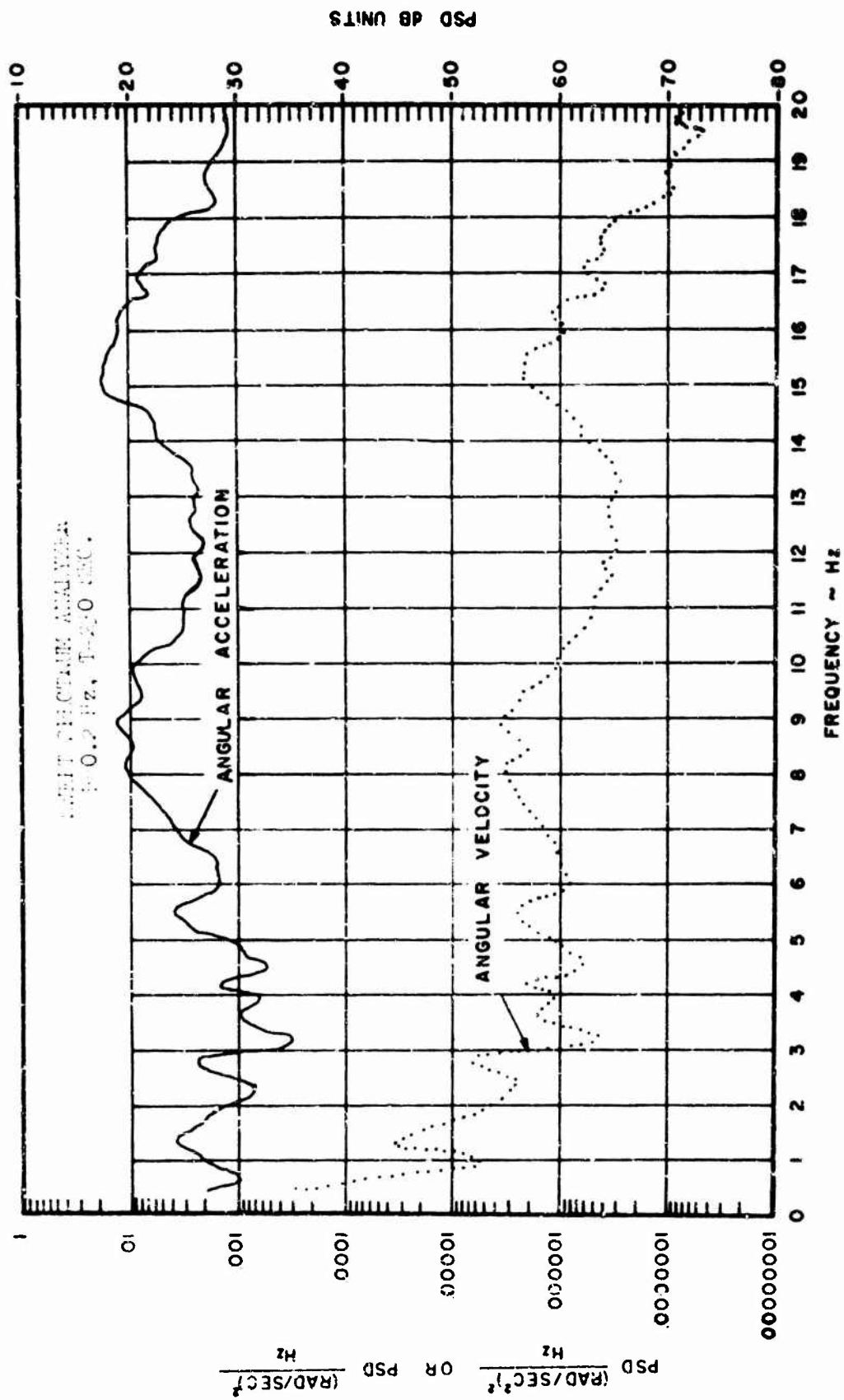


Figure 87b. Flight 6-3 Roll Axis PSD

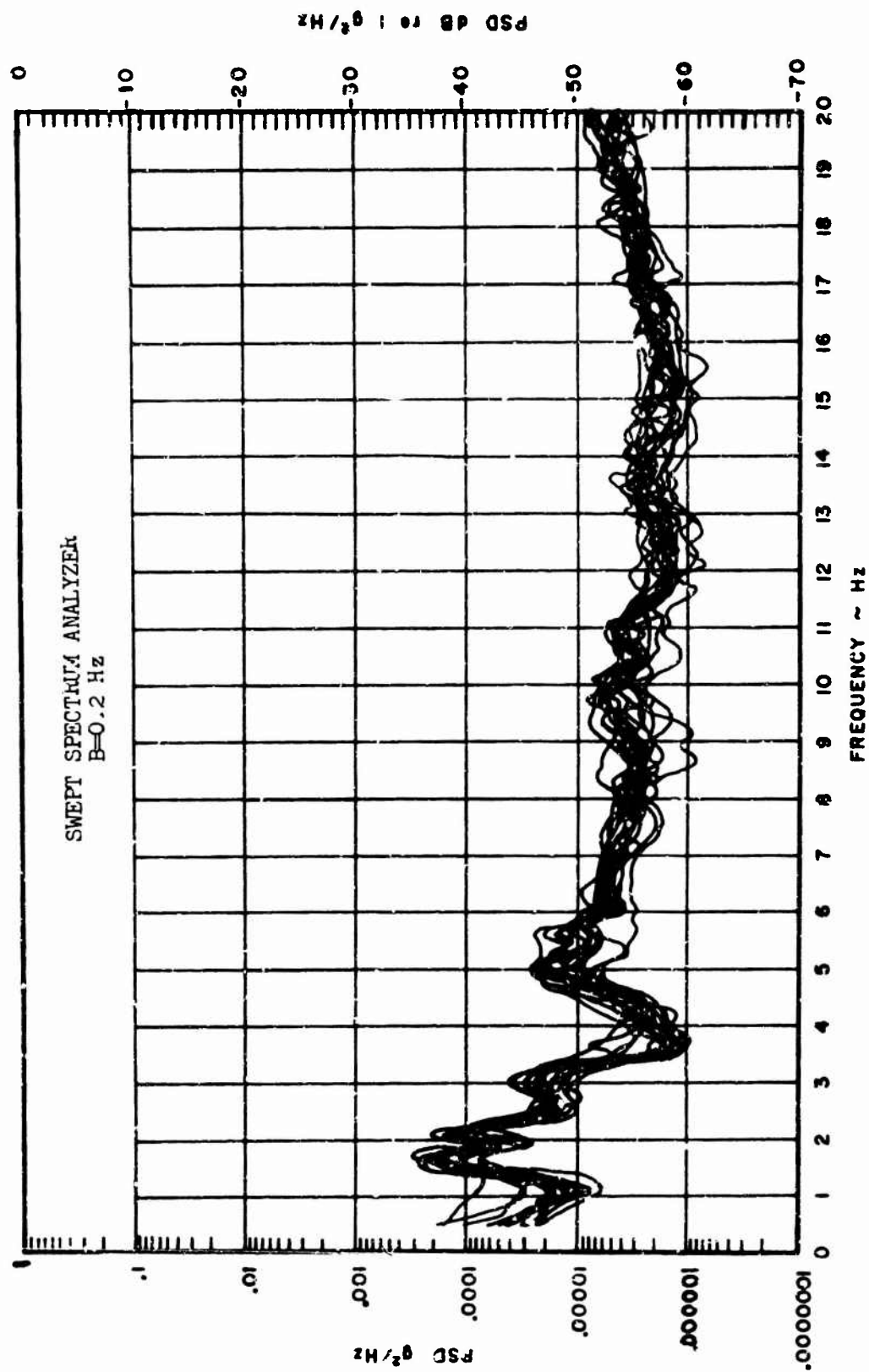


Figure 88. Composite X Axis PSD's

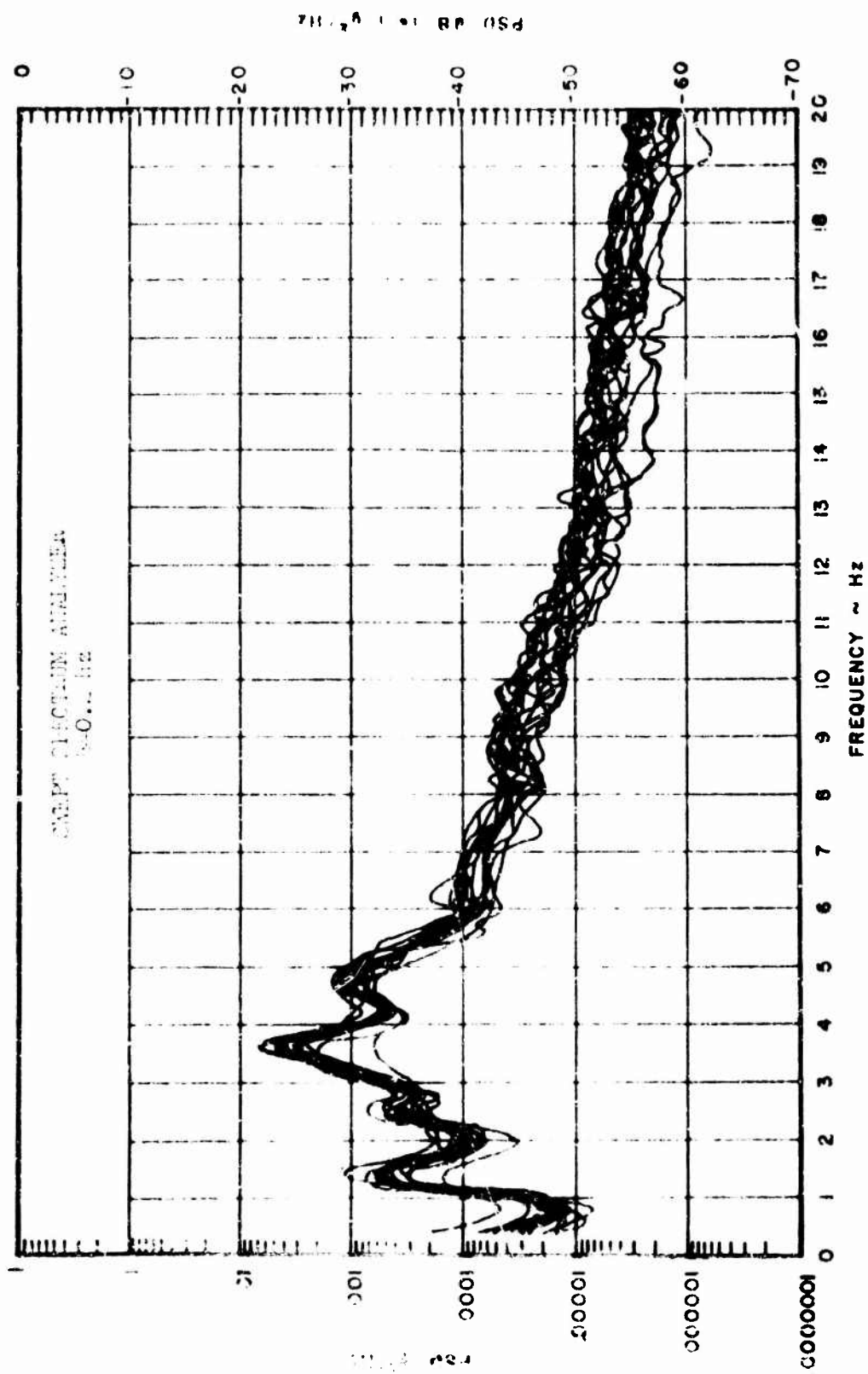


Figure 89. Composite Y Axis PSD's

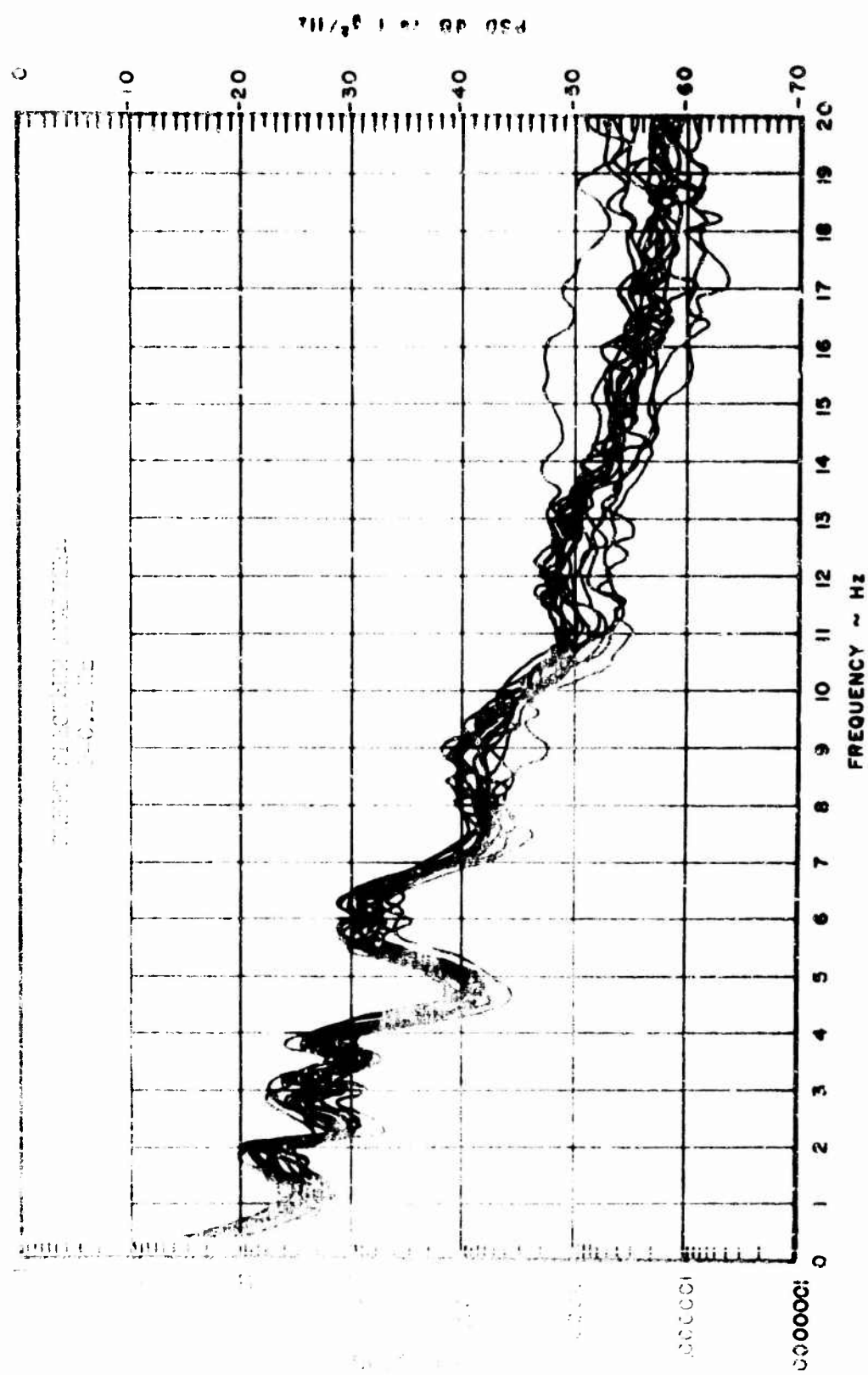


Figure 90. Composite 1-axis plots

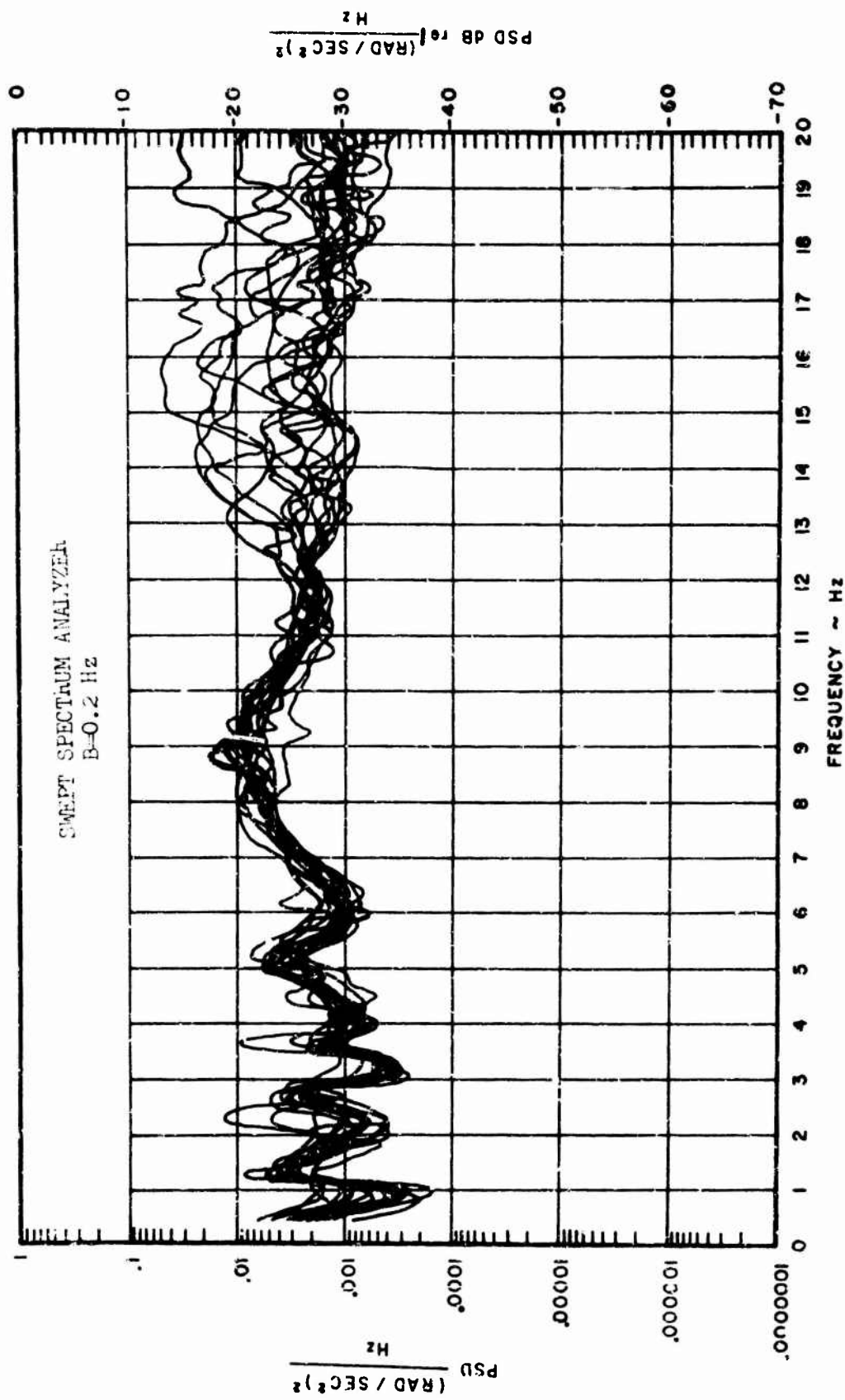


Figure 91. Composite Roll Axis Acceleration PSD's

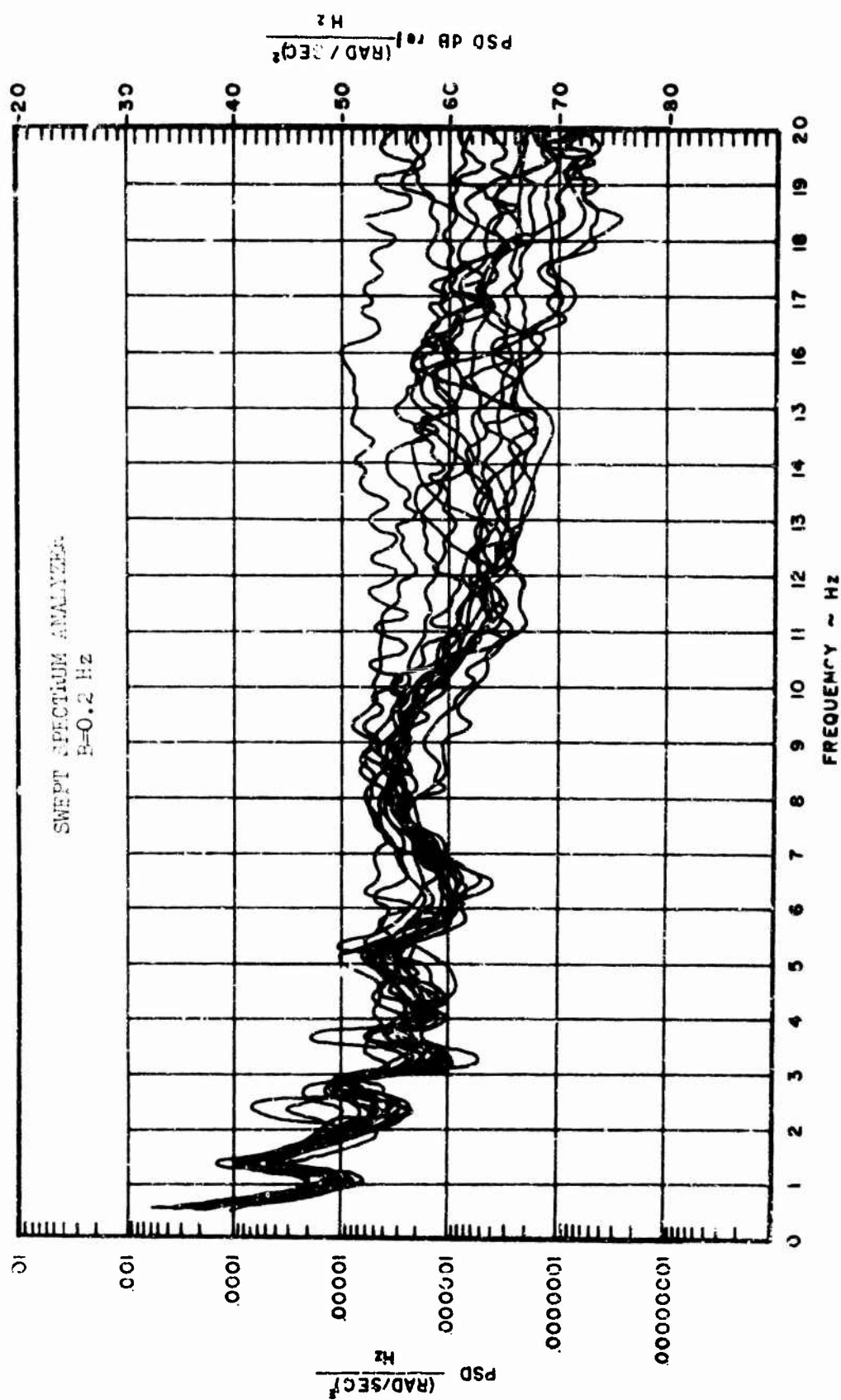


Figure 92. Composite Roll Axis Velocity PSD's

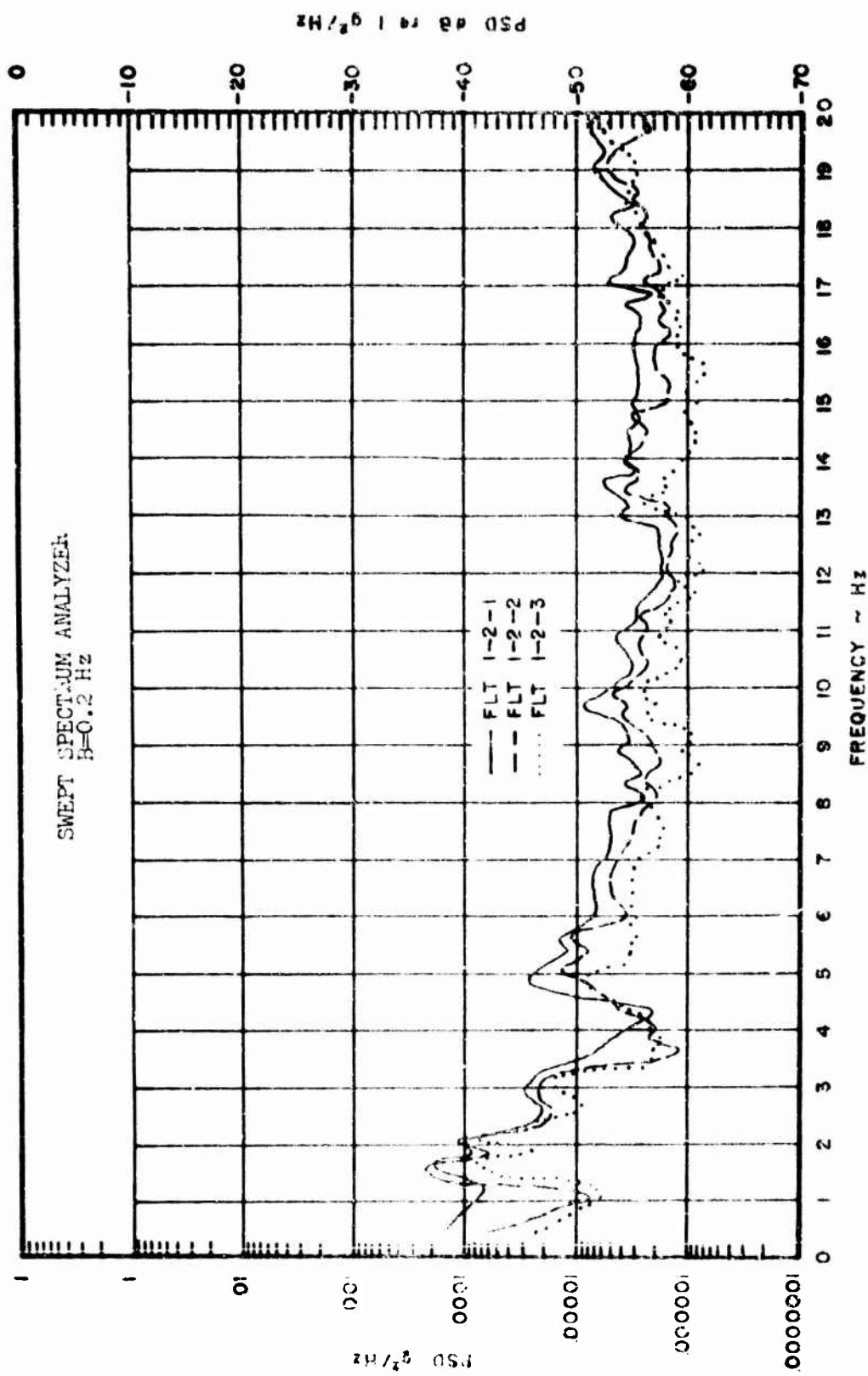


Figure 93. Flight 1-2 Variation in X Axis PSD

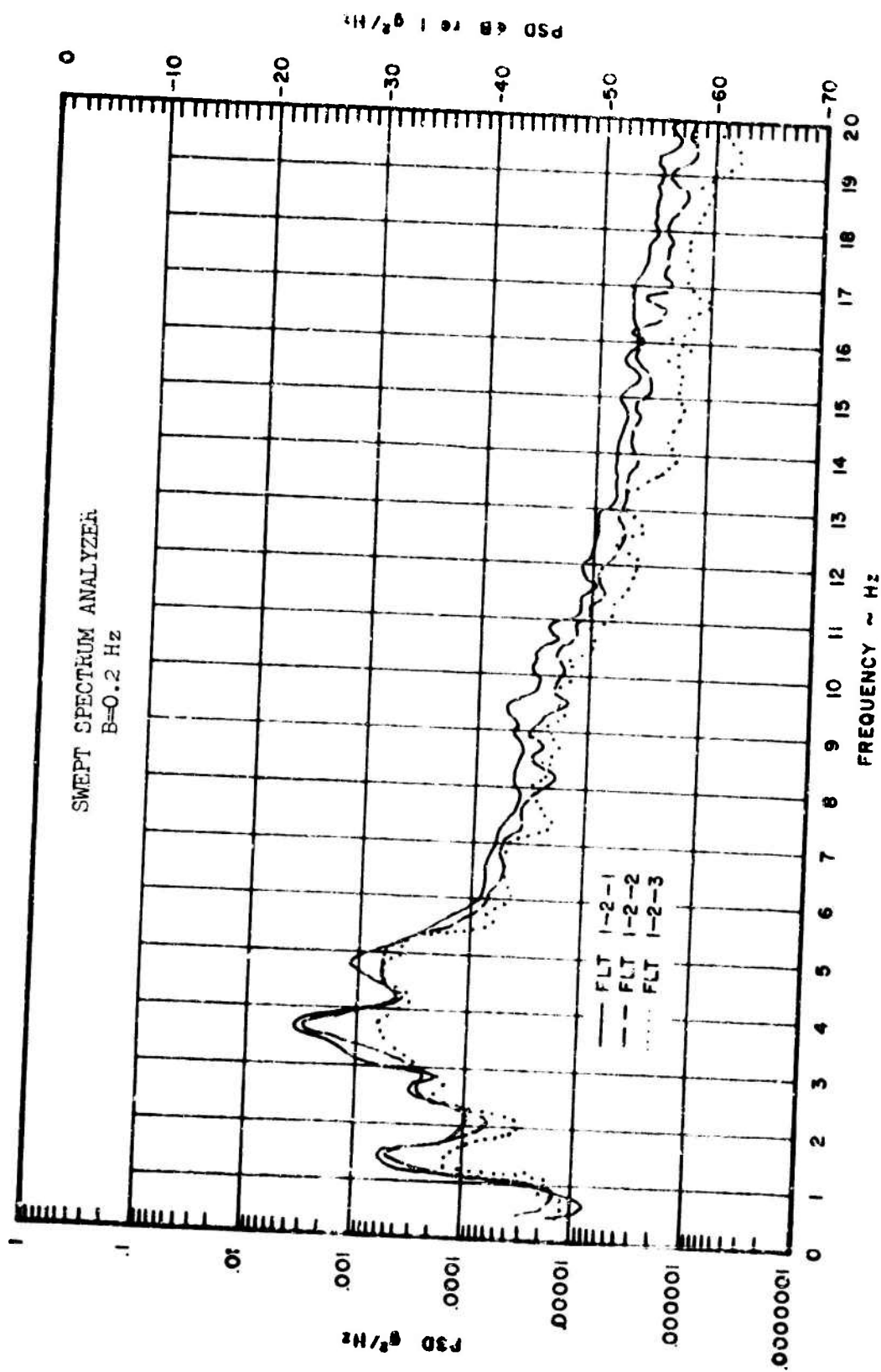


Figure 2... Flight 1-2 Variation in Y Axis PSD

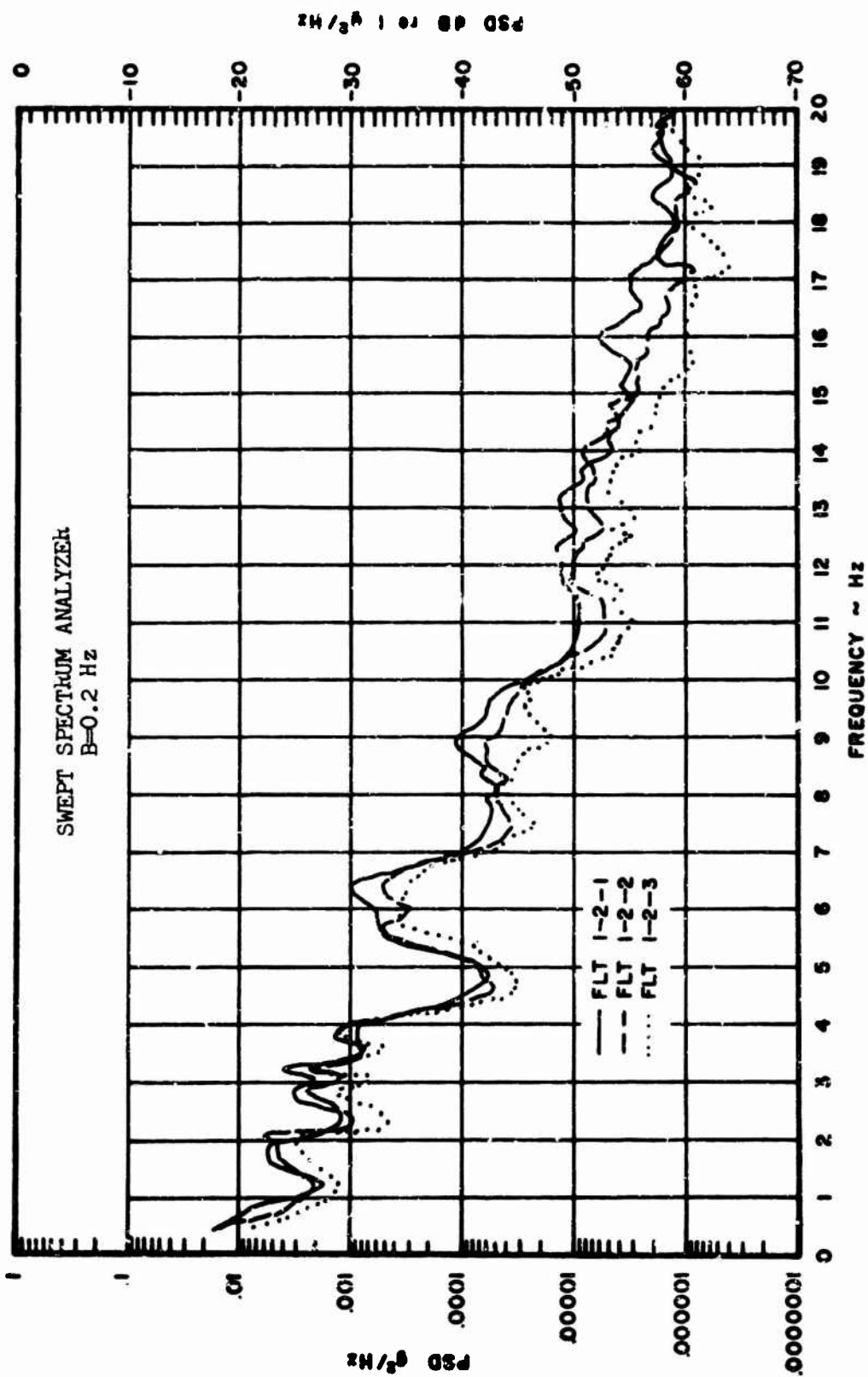


Figure 95. Flight 1-2 Variation in Z Axis PSD

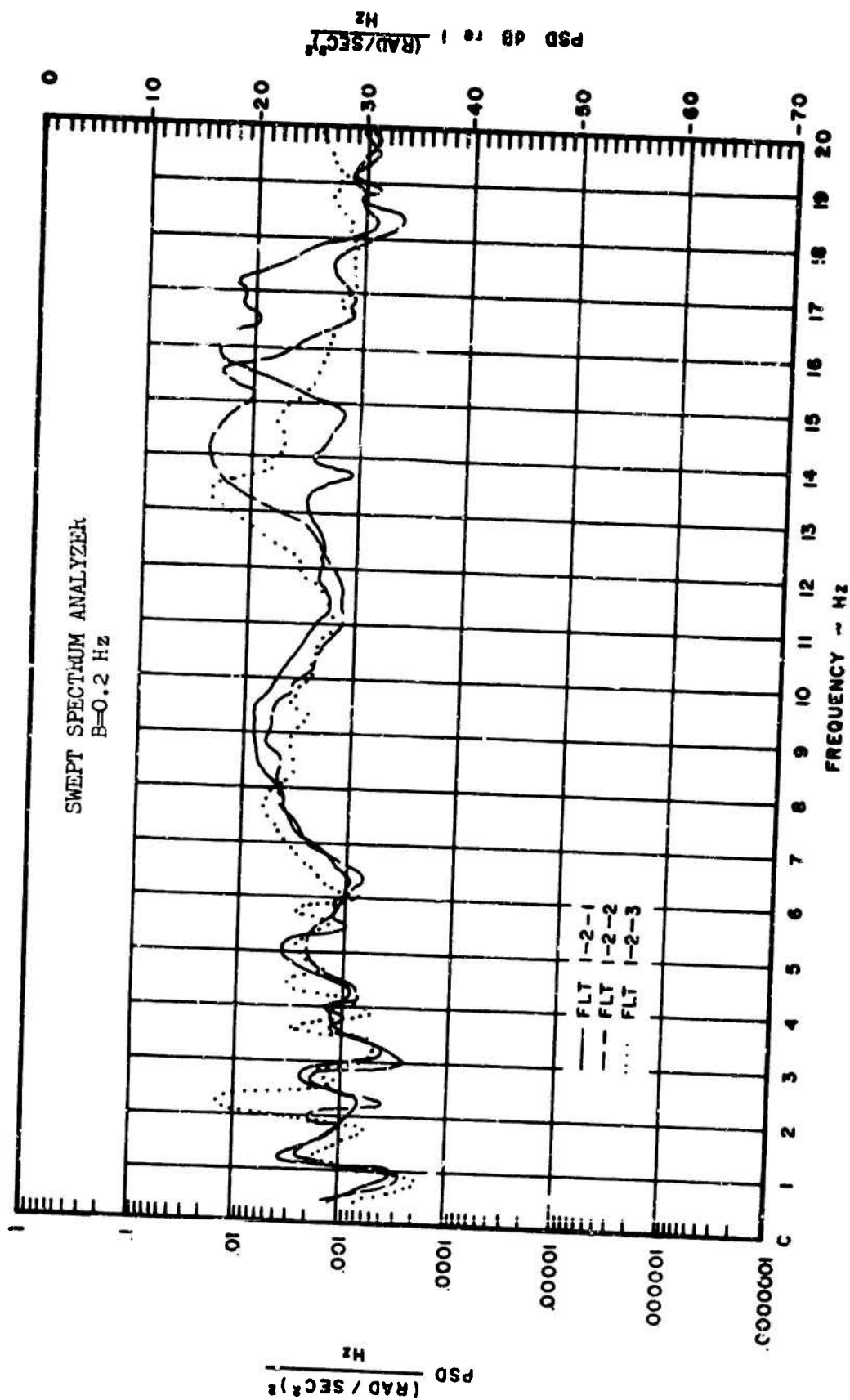


Figure 96. Flight 1-2 Variation in Roll Axis Acceleration PSD

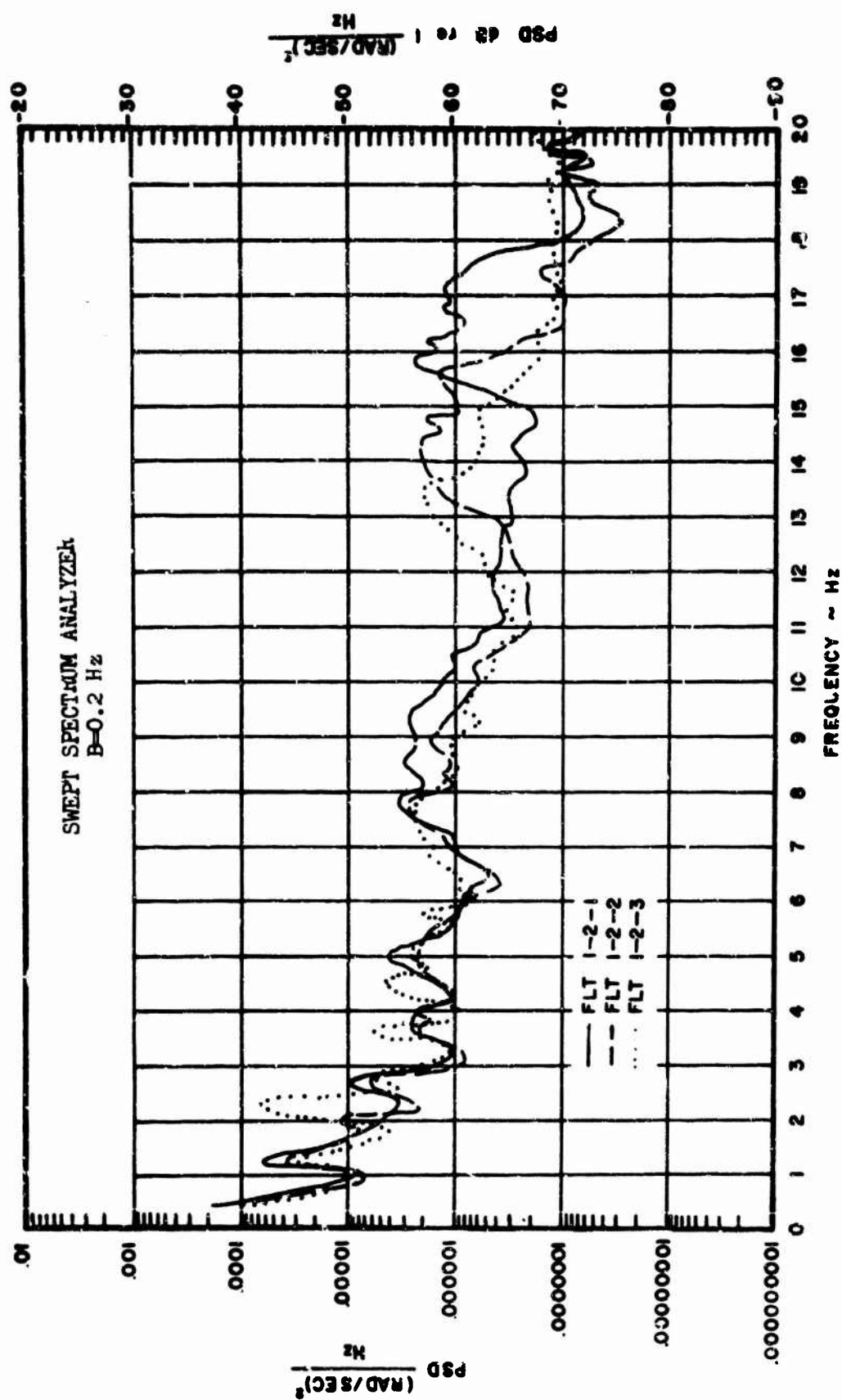


Figure 97. Flight 1-2 Variation in Roll Axis Velocity PSD

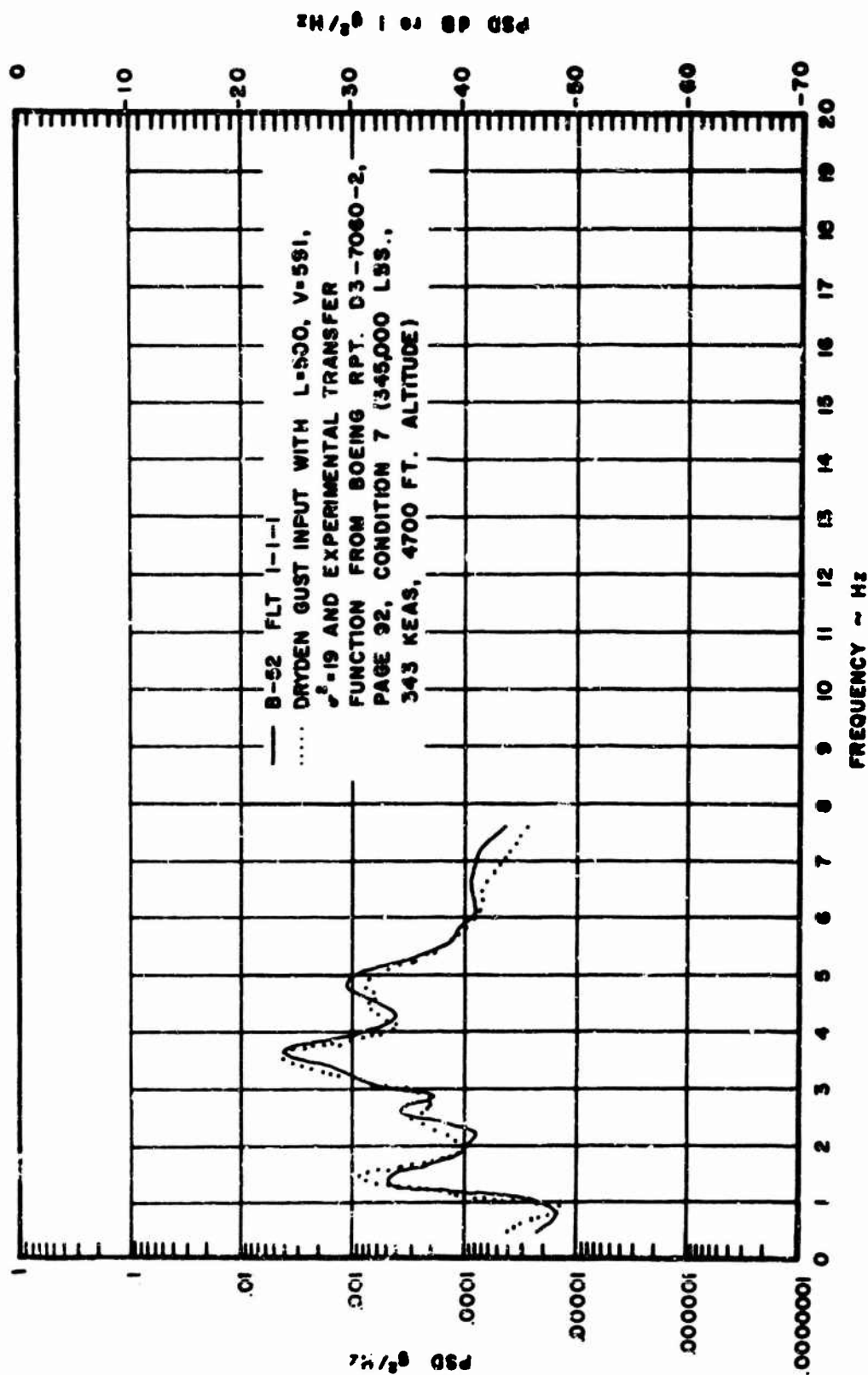


Figure 98. Comparison of Experimental - Hypothetical Y Axis PSD's

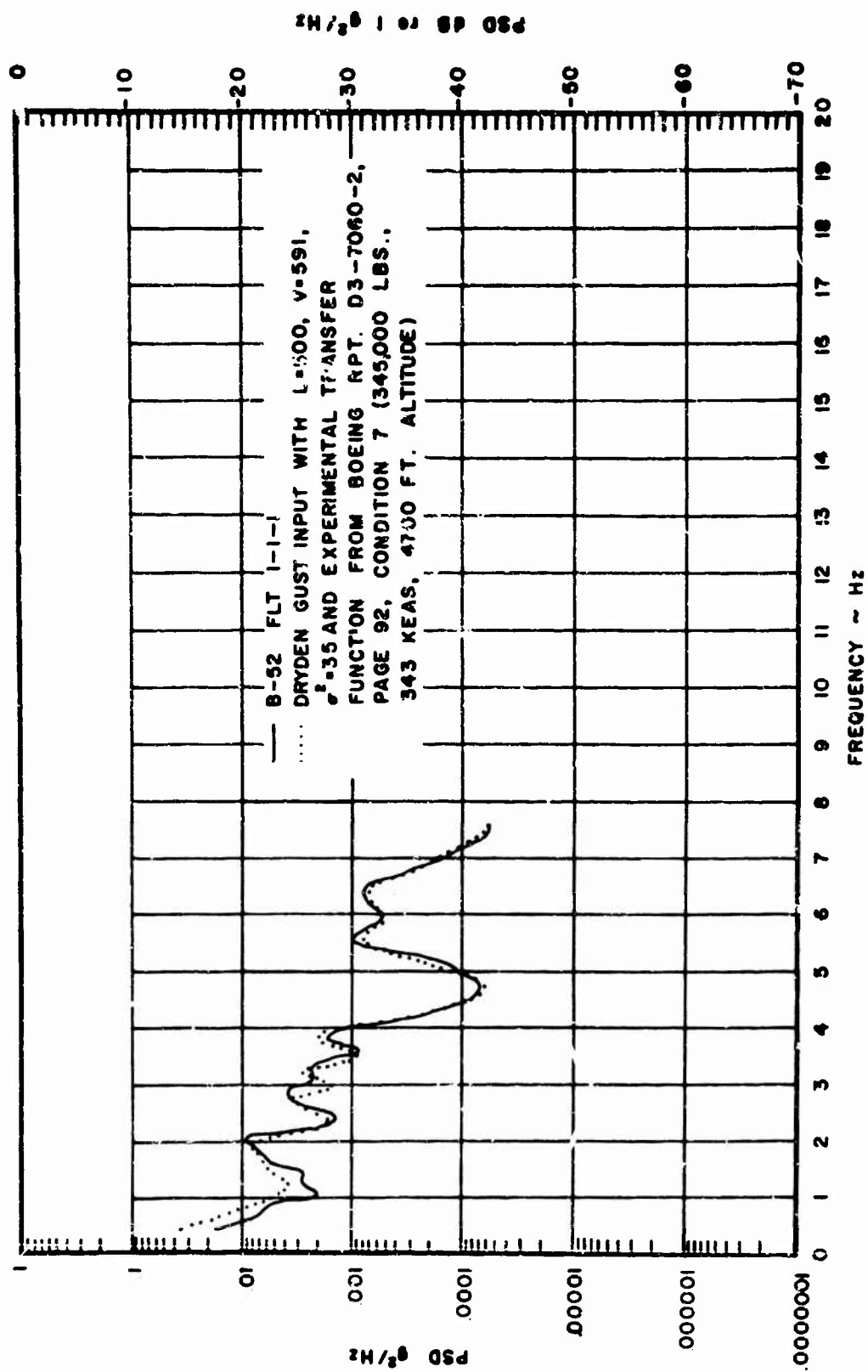


Figure 99. Comparison of Experimental - Hypothetical Z Axis FSD's

SECTION VI

REFERENCES

1. Houbolt, J. C., Steiner, R., and Pratt, K. G., Dynamic Response of Airplanes to Atmospheric Turbulence Including Flight Data on Input and Response, NASA TR-R-199, Langley Research Center, Hampton, Virginia, 1964.
2. Bendat, J. S., and Piersol, A. G., Measurement and Analysis of Random Data, John Wiley & Sons, Inc., 1966.
3. Gilley, T. A. and Cast, R. D., B-52 C-F Dynamic Response and Loads Survey (Volume II), Boeing D3-7060-2, The Boeing Company, Airplane Division, Wichita, Kansas, 1966.
4. Speakman, J. D., Bonfili, H. F., Hille, H. K. and Cole, J. N., Crew Exposure in the F-4C Aircraft During Low-Altitude, High-Speed Flight, AMRL TR 70-99, Aerospace Medical Research Laboratory, Wright-Patterson Air Force Base, Ohio, January 1971.